Zintl Anions, Polychalcogenides and Chalcogenometalates via Solvothermal Syntheses

Dissertation

zur Erlangung des Doktorgrades (Dr. rer. nat.)

der

Mathematisch–Naturwissenschaftlichen Fakultät

der

Rheinischen Friedrich–Wilhelms–Universität Bonn

vorgelegt von

Dominik Offermanns

aus

Troisdorf

Bonn, 2023

Angefertigt mit Genehmigung der Mathematisch-Naturwissenschaftlichen Fakultät der

Rheinischen-Friedrich-Wilhelms-Universität Bonn

„Da ist das Ding!"

Oliver Kahn, 2001

Table of Content

Abstract

The focus of this work is on the synthesis and structural investigation of polychalcogenides and *Zintl* phases. Therefore, mainly ammonothermal syntheses under mild or supercritical conditions were used. Additionally, some experiments in ethylene diamine as solvent were performed. A prerequisite for this work is the solubility if the alkaline earth metals and the lanthanides Eu and Yb in liquid ammonia due to the formation of blue electride solutions similar as it is known for the dissolution of alkaline metals. Beside binary compounds with anions containing only chalcogen atoms, it was successfully tried to link the polychalcogenides via arsenic or coinage metals to ternary compounds with more complex anionic structures or higher dimensional polyanions. Structural motifs of binary compounds in this work reach from simple anions such as $(Se_2)^{2-}$ dumbbells in $[Eu(NH_3)_8]_2(Se_2)_2(Se_3)$ to very complex anions as $(Te_{20})^{8-}$ in $[Yb(NH_3)_8]_4(Te_{20})(Te_3)\cdot 2NH_3$.

Reactions of lanthanindes with sulfur in liquid ammonia led to the formation of $[Ln(NH_3)_9]_2(S_5)_3\cdot 2NH_3$ (Ln = Eu or Sm), $[Er(NH_3)_8]_2(S_5)_2(S_6)\cdot 3NH_3$ and $[Yb(NH_3)_8]_2(S_5)_2(S_4)\cdot 4NH_3$ with slightly different chain lengths among the polysulfides. It was possible to synthesize the compounds $[Eu(NH_3)_8][Cu(S_4)_2]\cdot NH_3$ and $[Er(NH_3)_8][Cu(S_4)_2]\cdot NH_3$, containing molecular thiometallates by insertion of copper to the reaction of Eu or Er with sulfur in liquid ammonia. Analog to the thiocuprates, the selenoargentate $[Ag(Se_4)_2]^{3+}$ in $[Eu(NH_3)_9][Ag(Se_4)_2]\cdot NH_3$ could be obtained.

The fact that gold is soluble in electride solutions made it possible to synthesize the four chalcogenidoaurates(III) $[Yb(NH_3)_8](AuSe_5S_7)\cdot NH_3$, $[Yb(NH_3)_8](AuS_4Se_6)$, $[Ca(en)_4](AuTe_5)_2$ and $[Yb(NH_3)_8](AuSe_4)_3$. The dimensionality of the complex chalcogenidoaurate(III) anions reaches from one- to three-dimensional. The $[Yb(NH_3)_8]^{3+}$ complex in $[Yb(NH_3)_8](AuSe_4)_3$ shows an almost perfect cubic coordination, which has been mentioned so far only once in literature for the uranium(IV) complex $[U(SCN)_8]^{4-}$.

The molecular chalcogenidoarsenate(III) anions containing compounds $[Ca(en)_4]_2(As_4Te_6)$, $[Sr(en)_4]_2(As_4Te_6)$, $[Eu(en)_4]_2(As_4Se_6)$, $[Ca(en)_4](As_2Se_6)$ and $[Ca(en)_4]_2(As_2Se_7O)$ could be isolated from ethylene diamine. Their structures can all be derived from the simple salt structure types of Li_2O or CsCl, respectively. The one-dimensional infinite selenidoarsenate(III) anion $^1_\infty[AsSe_2]^-$, in $[M(en)_3(H_2O)_2](As_2Se_4)$ with M = Ca or Sr, was isolated from ethylene diamine likewise. It shows a new conformation as *zwölfer* chain with very short As-Se and Se-Se interactions leading to a plausible description of an almost linear selenium chain with attached As-Se dumbbells.

Zusammenfassung

Der Fokus dieser Arbeit liegt auf der Synthese und der strukturellen Untersuchung von Polychalkogeniden und *Zintl* Phasen. Dafür wurde größtenteils die Ammonothermalsynthese unter milden oder superkritischen Bedingungen genutzt. Zusätzlich wurden Experimente in Ethylendiamin als Lösungsmittel durchgeführt. Grundlage der Experimente ist die Löslichkeit der Erdalkalimetalle, sowie die der Lanthanide Eu und Yb in flüssigem Ammoniak unter der Bildung von Elektridlösungen, wie es von den Alkalimetallen bekannt ist. Neben binären Verbindungen, welche lediglich Chalkogenatome in den Anionen enthalten, wurde erfolgreich versucht, mit der Hilfe von Arsen oder Münzmetallen, Polychalkogenide zu ternären Verbindungen mit komplexeren molekularen Anionen oder mehrdimensionalen Polyanionen zu verbinden. Strukturmotive der binären Verbindungen reichen von einfachen Anionen, wie $(Se_2)^{2-}$ Hanteln in $[Eu(NH_3)_8]_2(Se_2)_2(Se_3)$ bis zu sehr komplexen Anionen wie $(Te_{20})^{8-}$ in $[Yb(NH_3)_8]_4(Te_{20})(Te_3)\cdot 2NH_3$.

Reaktionen von Lanthaniden mit Schwefel in flüssigem Ammoniak führte zur Bildung von $[Ln(NH_3)_9]_2(S_5)_3\cdot 2NH_3$ (Ln = Eu or Sm), $[Er(NH_3)_8]_2(S_5)_2(S_6)\cdot 3NH_3$ und $[Yb(NH_3)_8]_2(S_5)_2(S_4)\cdot 4NH_3$ mit leicht verschiedenen Kettenlängen der Polysulfide. Es war möglich, die Verbindungen $[Eu(NH_3)_8][Cu(S_4)_2]\cdot NH_3$ und $[Er(NH_3)_8][Cu(S_4)_2]\cdot NH_3$ zu synthetisieren, welche durch die Zugabe von Kupfer in die Reaktion von Eu oder Er mit Schwefel in flüssigem Ammoniak molekulare Thiometallate enthalten. Analog zu den Thiocupraten, konnte das Selenoargentat $[Ag(Se_4)_2]^{3+}$ in $[Eu(NH_3)_9][Ag(Se_4)_2]\cdot NH_3$ synthetisiert werden.

Die Tatsache, dass Gold in Elektridlösungen löslich ist ermöglichte es, die Chalkogenidoaurate(III) in $[Yb(NH_3)_8](AuSe_5S_7)\cdot NH_3$, $[Yb(NH_3)_8](AuS_4Se_6)$, $[Ca(en)_4](AuTe_5)_2$ and $[Yb(NH_3)_8](AuSe_4)_3$ zu synthetisieren. Die Dimensionalität der Chalkogenidoaurat(III)-Anionen reicht von ein- bis dreidimensional. Der $[Yb(NH_3)_8]^{3+}$-Komplex in $[Yb(NH_3)_8](AuSe_4)_3$ weist eine fast perfekt kubische Koordination auf, welche in dieser Form erst einmal in der Literatur für den Uran(V)-Komplex $[U(SCN)_8]^{4-}$ beschrieben ist. Die molekularen Chalkogenidoarsenat(III)-Anionen in $[Ca(en)_4]_2(As_4Te_6)$, $[Sr(en)_4]_2(As_4Te_6)$, $[Eu(en)_4]_2(As_4Se_6)$, $[Ca(en)_4](As_2Se_6)$ and $[Ca(en)_4]_2(As_2Se_7O)$ konnten aus Ethylendiamin isoliert werden. Die Strukturen lassen sich von den einfach Salzstrukturtypen Li_2O und $CsCl$ abgeleiten. Das eindimensional-unendliche Selenoarsenat(III)-Anion ${}^{1}_{\infty}[AsSe_2]^-$ in $[M(en)_3(H_2O)_2](As_2Se_4)$ mit M = Ca or Sr konnte ebenfalls aus Ethylendiamin isoliert werden. Die Kette weist eine neue Konformation als *zwölfer*-Kette auf mit sehr kurzen As-Se und Se-

Se Bindungen, welche zu einer möglichen Beschreibung des Anions als fast lineare Selenkette mit benachbarten As-Se Hanteln führt.

1. Introduction

1.1 Zintl ions

This thesis aims at the structural variety of polychalcogenides of the heavier chalcogens sulfur, selenium and tellurium. The word "chalcogen" is derived from the Greek words *khalkós* and *genēs*, which mean "ore forming", and describes the group 16 elements. All compounds presented in this thesis contain either pure polychalcogenides or polychalcogenides linked by arsenic or coinage metals. Polychalcogenides are of great interest in the last decades, shown by a huge number of publications on this topic. Their properties make them attractive for a wide range of applications, from thermoelectric energy converters [1], seminconductors [2] in solid state devices, to color-giving pigments, containing $(S_6)^{2-}$ units [3].

Polychalcogenides frequently obey the *Zintl* valence rules and therefore they can be described as *Zintl* ions. *Zintl* phases were named after *Eduard Zintl* (1898-1941). *Zintl* was interested in the observation of the green colored solution of sodium and lead in liquid ammonia made by *A. Joannis* in 1891 [4]. With his skills in electrochemistry, he was able to do a potentiometric titration of lead iodide by a solution of sodium in liquid ammonia, whereby the green solution was formed. The outcome of the experiment was, that the solution must contain charged particles. As composition of the formed compound, he postulated Na_4Pb_9 [5], which can be understood to be composed of a lead polyanion $(Pb_9)^{4-}$ with homonuclear bonds and solvated sodium ions $[Na(NH_3)_x]^+$ as counterions. As consequence, *Zintl* carried out the same experiment with elements of the main groups 3-7, resulting in the formation of salts with polyanions for the elements of the main groups 4-7 and with the formation of insoluble alloy-like structures for the elements of main group 3 [6]. This line of classification between the main groups 3 and 4 was posthumously named 'Zintl line' by *Fritz Laves* after *Eduard Zintl* [7]. In Figure 1, the representation of the 'Zintl line' from *Laves* original publication is shown. In 1963 *Wilhelm*

Figure 1: '*Zintl* line' between the 3 and 4 main group. Taken from the original publication of *F. Laves* 1941.

Klemm supplemented the work of *Zintl*. He worked out that the anionic substructure in binary *Zintl* phases is similar to the structure of the element with the same number of valence electrons. This rule is known as '*Zintl-Klemm-Bussmann*-concept' [8]. In accordance with this concept, the structure of the binary *Zintl* phase NaTl can be explained. The formally negatively charged Tl atoms are iso-valence-electronic to carbon. Therefore, the anionic framework of Tl atoms adopts the diamond structure. But this basic example is somewhat problematic, since Tl is placed on the left side of the *Zintl* line. However, this is the exception that proves the rule. In the following year, *Herbert Schäfer* extended the *Zintl-Klemm-Bussmann*-concept with the (8-N)-rule. N is equal to the number of valence electrons plus the electrons donated by the less electronegative metal [9]. With this extension, the concept was no longer restricted to isosterism to elemental structures with the same number of valence electrons, but also bonding was taken into account.

Ternary Zintl phases can either build structures, which are comparable with the binary phases like KSnAs[10], where [AsSn]$^-$ adopts the layered structure of grey arsenic, or they can build complex anionic frameworks as in $Na_6Ga_2Se_6$ [11]. Here, $[Ga_2Se_6]^{6-}$ forms a molecular edge-sharing double-tetrahedron, with negatively charged Ga atoms and a valence of four. The two bridging Se atoms have a valence of two and are neutral. The four terminal Se atoms are monovalent and carry one negative charge. Ternary *Zintl* phases, where the two more electronegative elements have a small difference in their electronegativities, show the tendency to form structures similar to binary *Zintl* phases. Whereas, ternary *Zintl* phases, with the two more electronegative elements having a small difference in their electronegativities, show the tendency to form complex anionic frameworks.

The synthesis method, reduction in liquid ammonia, often used by *Zintl*, leads to the formation of ammoniates. Ammoniates are not stable with respect to decomposition into alloys and the loss of ammonia above the boiling point of ammonia, due to the high content of ammonia within the crystal structure. Therefore, crystals of ammoniates have to be handled under low temperatures for examination. The examination and characterization of ammoniates was described as 'impossible' by *Kummer* and *Diehl* in 1970[12]. In 1993 *Kottke* and *Stalke* published an experimental setup for crystal handling at low temperatures[13]. They handled the crystals in a cold inert oil, which was additionally cooled by a cold inert gas stream. The use of the described setup made it possible for *Korber* to isolate and characterize a single crystal of $[Li(NH_3)_4][Pb_9]\cdot NH_3$[14], containing the Pb_9^{4-} ion described by *Zintl*. The setup to select and mount suitable single crystals was extensively used for the experimental work of this thesis and is described and schematically shown in chapter 2.1.4. If the solvent NH_3 is exchanged by an

aliphatic amine, such as ethylene diamine, the complex setup to mount single crystals is not necessary. Crystals of *Zintl* salts with cations complexed by aliphatic amines are usually stable at room temperature. Therefore, they can be handled under inert gas conditions. Today, a large variety of solvents/ligands to stabilize the cations in *Zintl* salts is used e.g. aliphatic amines[15], crown ethers[16] or cryptants[17].

In the following chapters, *Zintl* salts will be presented, that either contain only chalcogen atoms or polychalcogenides linked by arsenic or a coinage metal to complex polyanions. A short overview on the actual knowledge about each kind of polyanion is given ahead of the respective chapter. All *Zintl* salts of this thesis were synthesized in liquid ammonia or in ethylene diamine. As cations the alkaline earth metals Ca, Sr, Ba and the lanthanides Eu, Sm, Er and Yt were used.

1.2 Solvothermal synthesis in ammonia and ethylene diamine

Solvothermal or ammonothermal synthesis is of increasing interest in research in the last decades. The term solvothermal synthesis has not a fixed definition. The definitions reach from more general ones as the one from *Birappa* and *Yoshimura* 'any heterogeneous chemical reaction in the presence of a solvent (whether aqueous or non-aqueous) above room temperature and at pressure greater than 1 atm in a closed system' [18] to more specific ones, where the temperature has to be above the boiling point of the respective solvent [19] [20].

Ammonia and ethylene diamine are less protic and polar than water. The major difference between water and ammonia/ethylene diamine as solvents is their dielectric constants (ε_r). For water ε_r amounts to 80.3 and for ammonia/ethylene diamine ε_r amounts to 15.0 [21]. Therefore, salt-like compounds are dissolved better in water than in ammonia or ethylene diamine. This often results in crystals with a disappointing quality, twinning or even in amorphous solids, caused by the inhibited nucleation and crystal growth. To overcome this problem supercritical conditions ($T_c(NH_3)$= 405.7 K and $p_c(NH_3)$= 113.59 bar)[22] can be used. Above these critical parameters, ammonia is in the supercritical state, a homogeneous fluid, where the liquid and the gaseous state cannot be distinguished. In this state, the dielectric constants are much higher resulting in increasing solubility of salt-like compounds. The first experiments under supercritical conditions in ammonothermal syntheses were done by *Juza* and *Jacobs* 1966 in the synthesis of the binary amines $Be(NH_2)_2$ and $Mg(NH_2)_2$ [23]. Today the ammonothermal synthesis under supercritical conditions is used for the high quality synthesis of the wide band gap semiconductors GaN and AlN [24]. In Figure 2, a phase diagram of ammonia is shown. The little, green marked area shows the conditions used in this thesis for ammonothermal synthesis under supercritical conditions. For solvothermal syntheses in ethylene diamine no supercritical conditions were used.

The used reaction vessels were thick-walled glass ampules. The density of the supercritical state can be adjusted by modifying the used reaction temperatures or the filling degree of the ampoules. A change of the density in the supercritical state has a direct influence on the dielectric constant and therefore on the solubility of salt-like compounds.
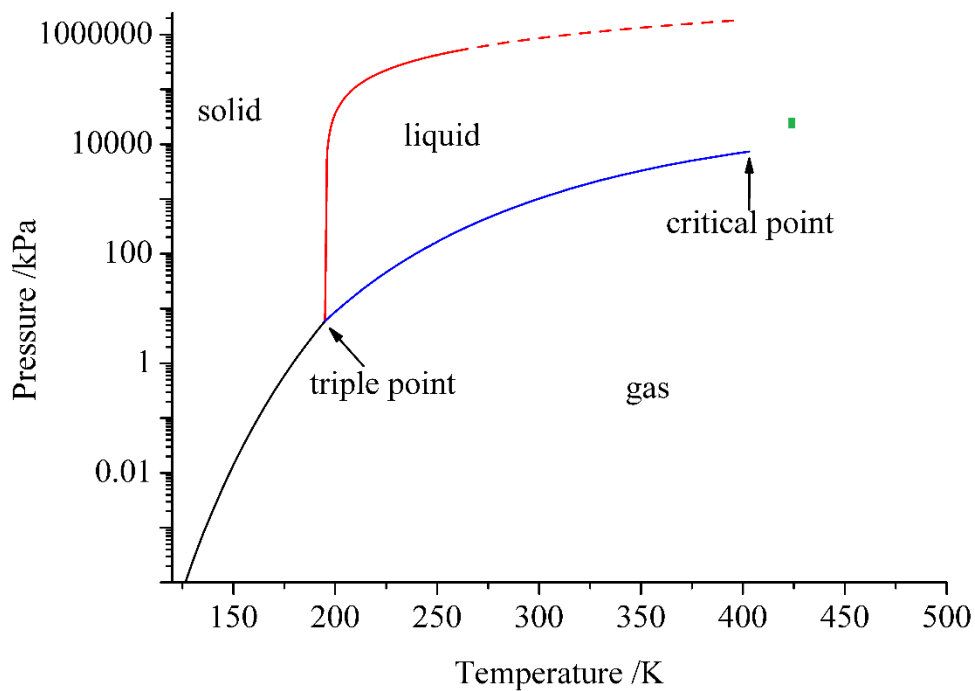
Figure 2: Pressure/temperature phase diagram of ammonia. The dashed line is extrapolated. The green-marked area shows the experimental parameters used for supercritical ammonothermal synthesis in this thesis. The figure was taken from the reference [25] with some modifications.

2. Experimental part

2.1 Recovery of gold from collected gold scraps

For a contribution to enhance sustainability, the gold used for experiments was recycled from gold scraps of previous experiments. The collected gold scraps were dissolved in *aqua regia* after they were dried under vacuum. The resulting solution was heated up and filtered after cooling down to room temperature. The filtrate was heated and diluted with hydrochloric acid until no more nitrous gases were emitted. The pH value of the solution was adjusted to 4-5 with the help of ammonium chloride and aqueous ammonia (25%). At the end, gaseous SO_2 was feeded into the solution to reduce the gold. The precipitated gold was filtered off and dried.

2.2 Preparative methods

2.2.1 Working under inert gas atmosphere: Schlenk line

For working under inert gas atmosphere and for working under reduced pressures, a Schlenk line was used. The connected vacuum pump was a rotary vane pump achieving a vacuum of at least 10^{-2} mbar. The pressure inside the Schlenk line was controlled with a pressure gauge (Combitron CM 300, Leybold, Cologne). Argon was used as inert gas in the Schlenk line. The used Argon gas was purified and had the specification 4.6 (Ar $\geq$ 99.996 %, $O_2 \leq$ 6 ppm, $N_2 \leq$ 20 ppm, $H_2O \leq$ 5 ppm, Praxair, Düsseldorf). The inert gas was purified and dried by routing the gas through four drying towers filled with silica gel, potassium hydroxide pellets, molecular sieve (3 Å) and phosphorus pentoxide. Behind the drying towers, the inert gas was routed through a furnace heated to 650 °C containing a titanium sponge to remove the residual oxygen and nitrogen. The vacuum pump was protected from volatile compounds by a cooling trap, which was cooled with liquid nitrogen.

All glass vessels were connected to the Schlenk line via ground glass joints. Ampoules and glass vessels were heated under reduced pressure on the Schlenk line with a hot air gun before charging with chemicals. Ampoules were charged with chemicals in an argon countercurrent flow.

2.2.2 Working under inert gas atmosphere: glove box

Some of the preparative work with air sensitive compounds was performed in a glove box (Labmaster 130, MBraun, Garching). The inert gas used in the glove box was argon 4.6. For purification of the inert gas, a molecular sieve (400 pm) and a BTS catalyst was used. The content of water and oxygen inside the glove box was usually between 1 and 10 ppm. The glove box contained a precision scale (BP61S, Sartorius AG, Göttingen) and a microscope (MZ6, Leica Microsystems GmbH, Wetzlar).

2.2.3 Condensation of liquid ammonia and ammonothermal synthesis

Gaseous ammonia was condensed in a cooling trap with the help of an ethanol/dry ice bath (- 72°C). The cooling trap was filled with a piece of elemental sodium to remove water from the liquid ammonia. The solution in the cooling trap achieved the blue color of solvated electrons. If the solution did not achieve the blue color the cooling trap had to be cleaned and filled with fresh sodium. Via ground joints, thick-walled glass ampoules (wall thickness = 2.2 mm, inner diameter = 5.6 mm) were connected to the *Schlenk* line with the cooling trap, where the liquid ammonia was stored (Figure 3). To guarantee a good ablation after filling, capillaries are drawn by heating the ampoules at a suitable point with a burner. After evacuating of the ampoule, ammonia was condensed from the cooling trap into the ampoule. Therefore, the ampoule was cooled with liquid nitrogen or a mixture of ethanol and dry ice and the cooling of the trap was removed. The degree of filling for the ampoules was around 30-50 %. To handle the fluctuating pressures within the system, two pressure relief valves filled with mercury were installed. The ampoules were molten off in dynamic vacuum by closing the drawn capillaries with a burner after freezing the liquid ammonia with liquid nitrogen. After being molten off,

the ampoules were annealed for three minutes to remove all tensions from the glass. Ideally molten off ampoules can resist a pressure of approximately 39 bar.

Low temperature ammonothermal syntheses at room temperature or at 55°C were done in the thick-walled glass ampoules without applying any counter-pressure. The expected pressure inside the ampoules was determined by their filling degree and with the help of the respective tables in the "NIST Chemistry WebBook, SRD 69" [26]. For a filling degree of 33% the expected pressures at room temperature and at 55 °C amount to 10 and 23 bar, respectively.
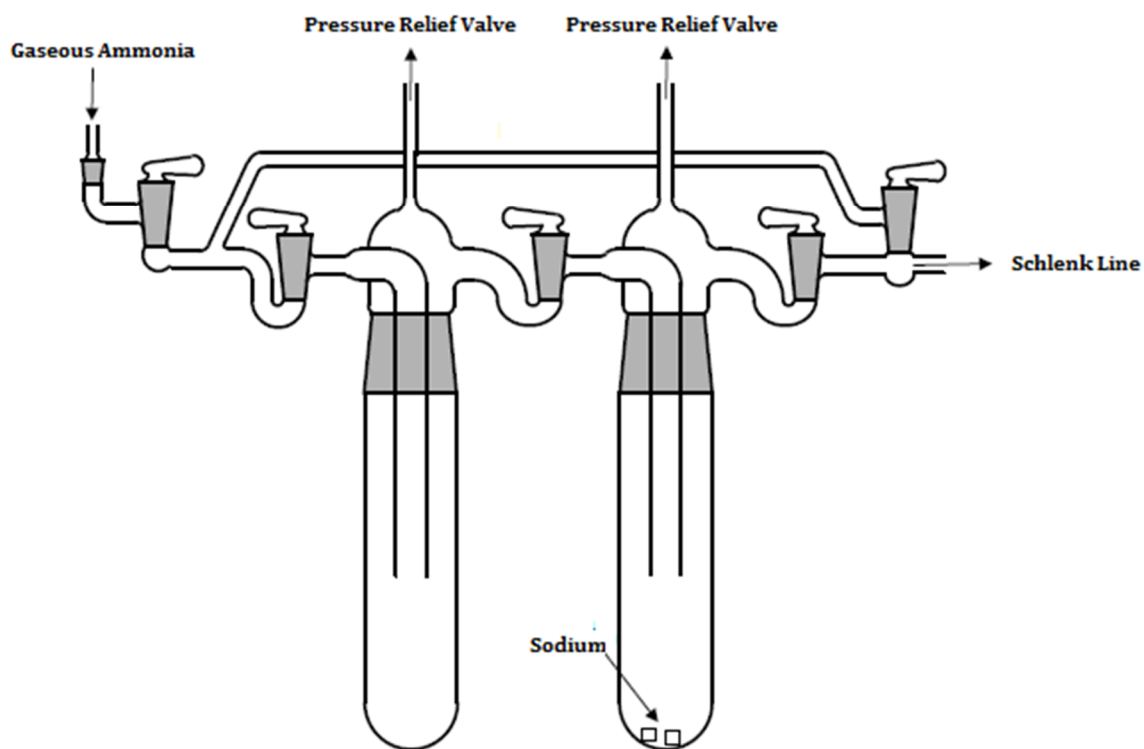
Figure 3: Schematic setup for storage and condensation of ammonia.

2.2.4 Working with steel autoclaves

For ammonothermal syntheses under supercritical conditions, higher temperatures and pressures are needed. The resulting pressures are higher than the bursting pressure of the used thick-walled glass ampoules. Therefore, steel autoclaves and dry ice for establishing a sufficient counter-pressure were used. In Figure 4, a schematic drawing of a used steel autoclave is shown. For a filling degree of about 50 % the expected pressure at the applied temperature of 150 °C amounts to 165 bar. For the calculation of an appropriate amount of dry ice, the volume of the autoclave minus the volume of the ampoules had to be determined. With the volume and the necessary pressure the amount of dry ice was determined with the help of the "NIST Chemistry WebBook, SRD 69" [26]. The dry ice was weighed in and the autoclave was quickly sealed with a wrench to avoid the loss of volatile CO_2. By twisting the screw cap tight, a conic steel stamp was pressed against the walls of the autoclave. This method for keeping autoclaves tight is called "cold sealing". For getting the autoclave cold sealed high forces are needed. Therefore, the wrench is connected to a 1.5 m long lever. With the long lever and the force of two people, the torque can be estimated to reach up to 1500 Nm.
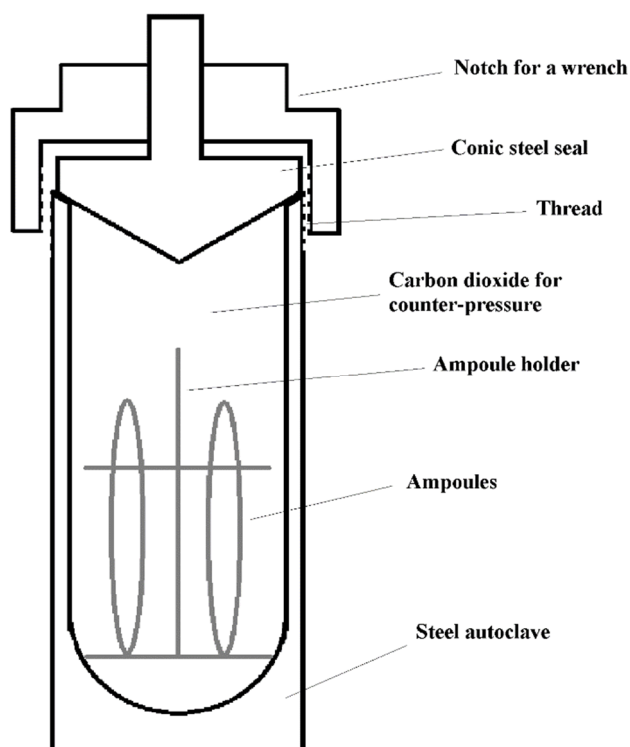
Figure 4: Schematic drawing of the used steel autoclave for ammonothermal syntheses under supercritical conditions.

Labels in figure: Notch for a wrench; Conic steel seal; Thread; Carbon dioxide for counter-pressure; Ampoule holder; Ampoules; Steel autoclave

2.2.5 Working in ethylenediamine as solvent

Ethylenediamine was distilled under inert gas atmosphere over CaH_2 for removing oxygen and water. After purification it was stored in a *Schlenk* flask. For syntheses, ethylenediamine was extracted from the *Schlenk* flask in an argon countercurrent with a syringe, which was purged with argon before. Via ground joints, thick-walled glass ampoules were connected to the *Schlenk* line and were filled with 1 mL ethylenediamine in an argon countercurrent. The ampoules were molten off in dynamic vacuum after freezing the ethylenediamine with a mixture of dry ice and ethanol. The sealed ampoules were stored at either 55°C or 170°C in a furnace for solvothermal reactions.

2.2.6 Crystal handling at low temperatures

Crystals that were grown in liquid ammonia are often temperature sensitive and need a special treatment during the handling to avoid decomposition. In Figure 5, the used experimental setup for the low temperature crystal manipulation is shown. It is a modified setup of the one described first by *Kottke* and *Stalke* [13]. Before the ampoules were opened with a glass cutter, they were frozen in liquid nitrogen for solidifying the ammonia inside the ampoules. The crystals and the frozen ammonia were scraped out of the ampoule into a concave glass bowl with perfluorinated oil. The perfluorinated oil with the sample was cooled from above with a cooled nitrogen stream and from below with a dewar vessel, filled with liquid nitrogen. The perfluorinated oil is viscous at temperatures under -40 °C so that the crystals can be easily fixed on the x-ray amorphous sample holder. The crystals were permanently cooled during the measurement with a nitrogen stream to -150 °C.
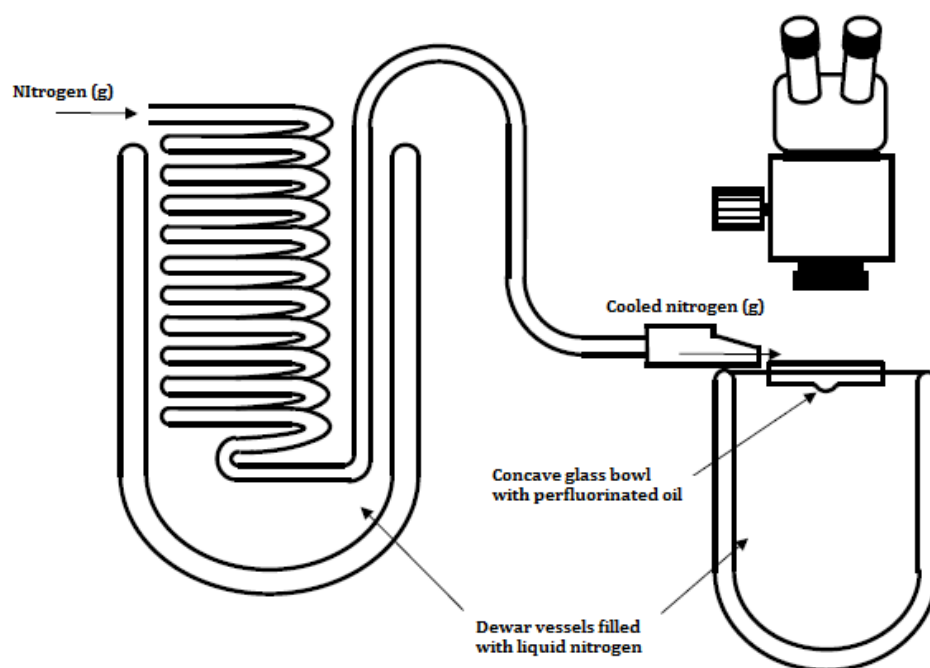
Figure 5: Schematic setup for mounting of single crystals under oxygen free conditions and at low temperatures.

2.3 Analytical methods

2.3.1 X-ray powder diffraction

The used powder diffractometer (STADI P, STOE, Darmstadt) contained a cobalt x-ray source (PANalytical, Almelo, Netherlands) and a curved germanium (111) monochromator. The used radiation was Co-K$_{\alpha 1}$ radiation with the wavelength $\lambda_{K\alpha 1}$ = 1.78896 Å. The measurements were performed in an angular range of 0 ° to 90 ° 2θ.

There were two types of sample carriers that can be placed on the diffractometer. One is a flat disc-like sample carrier where the sample was placed between two mylar foils. This type of sample carrier was used for air stable compounds. Air sensitive compounds were filled into glass capillaries (wall-thickness 0.01 mm, inner diameter 0.01 – 0.03 mm) inside the glove box. The diffractometer was controlled with the software Win XPOW [27] and the resulting powder diffractograms were analyzed with the computer program MATCH! [28].

2.3.2 X-ray single crystal diffraction

Crystals were selected in the glove box and filled into argon filled vessels or ampoules. The crystals were then transferred into perfluorinated oil (FOMBLIN Y HVAC 140/30, Solvay, Brussels, Belgium). From the oil, a selected single crystal is transferred to the goniometer head of the diffractometer. The crystals were cooled during the measurement with a nitrogen stream to 123 K (Oxford Cryosystems, Oxford, United Kingdom). The used diffractometer was a four cycle κ-CCD diffractometer (Bruker-Nonius, Delft, Netherlands) containing a molybdenum x-ray source. As monochromator for the resulting Mo-K$\bar{\alpha}$ radiation with the wave length λ = 0.71073 Å a graphite single crystal was used. The used detector was a CCD area detector with a diameter of 95 mm. The measurement was performed with the program "Collect" [29], cell determination was done with the program "PHI/CHI-Scans"[30] and for integration and scaling the program "hkl2000"[31] was used. The structure solution from the collected data and the structure refinement were performed with the programs "SHELXL"[32] and "PLATON"[33] in the user interface "WinGX"[34]. For visualization of the crystal structures the program Diamond 4 [35] was used.

2.3.3 Energy dispersive x-ray spectroscopy (EDX)

Energy dispersive x-ray spectroscopy was used for elemental analysis. This was especially necessary for compounds containing two or more elements that are difficult to differentiate by x-ray diffraction e.g. As and Se. The measurements were done with a scanning electron microscope (SU3800, Hitachi). For the quantitative EDX analyses, a x-ray detector (Octane Elect Super EDS, EDAX EDS System) was used additionally. Samples were fixed on an aluminium sample holder. The sample holder was laminated with a conducting graphite foil for keeping the sample from statically charging. The quantitative analysis was done with the computer software EDAX APEX Advanced (EDAX).

2.3.4 Continuous shape measures (CShM)

All compounds presented in this work contain metal cations coordinated by either ammine or ethylenediamine as ligands. For a better description of the formed coordination polyhedra, continuous shape measures were performed using the computer program SHAPE [36]. A continuous shape measure gives a quantification of the deviation of a given polyhedron to the respective ideal shaped polyhedron in percent. The principle is based on a distance function which gives the minimal distance between the given and the ideal polyhedron. For minimizing the distance function an algorithm of *M.Pinsky* and *D.Avnir* [37] is used. The distance function contains the position vectors $\overrightarrow{Q_k}$ of N atoms, the position vectors $\overrightarrow{P_k}$ of the ideal polyhedron and the vector of the geometrical center $\overrightarrow{Q_0}$ (Equation 1).

$$S(Q,P) = \min \frac{\sum_{k=1}^{N} \left|\overrightarrow{Q_k} - \overrightarrow{P_k}\right|^2}{\sum_{k=1}^{N} \left|\overrightarrow{Q_k} - \overrightarrow{Q_0}\right|^2} \times 100$$

Equation 1: Distance function used for continuous shape measures.

In Table 1, selected ideal shapes are listed, which were compared to the coordination polyhedra presented in this work below. The coordination polyhedra presented in this work all have either

the coordination number eight or nine. All abbreviations for the ideal shapes are adopted from the computer program SHAPE.

Table 1: Ideal shapes used for comparison and their abbreviations.

Abbreviation	Shape	Point group
OP-8 [38]	Octagon	D_{8h}
HPY-8 [38]	Heptagonal pyramid	C_{7v}
HBPY-8 [38]	Hexagonal bipyramid	D_{6h}
CU-8 [38]	Cube	O_h
SAPR-8 [38]	Square antiprism	D_{4d}
TDD-8 [38]	Triangular dodecahedron	D_{2d}
BTPR-8 [38]	Bicapped trigonal prism	C_{2v}
EP-9 [39]	Enneagon	D_{9h}
OPY-9 [39]	Octagonal pyramid	C_{8v}
HBPY-9 [39]	Heptagonal bypiramid	D_{7h}
JTC-9 [39]	Trivacant cuboctahedron	C_{3v}
CCU-9 [39]	Capped cube	C_{4v}
CSAPR-9 [39]	Capped square antiprism	C_{4v}
TCTPR-9 [39]	Tricapped trigonal prism	D_{3h}

2.4 Product syntheses

The syntheses, performed in the course of this thesis were all similar. Therefore, representative synthetic procedures are described in the following two sections. The descriptions of the respective synthetic work is followed by a table, in which the performed synthesis for each product is summarized (Table 2). The different synthetic routes are abbreviated by the numbers *1 – 5*.

2.4.1 Ammonothermal syntheses at r.t. (*1*), 55 °C (*2*) and 150 °C (*3*)

For the syntheses in liquid ammonia, thick-walled glass ampoules (wall thickness = 2.2 mm, inner diameter = 5.6 mm) were prepared. Via ground joints they were connected to a *Schlenk* line, evacuated to a residual pressure of at least 10^{-2} mbar and heated with a hot air gun to remove all residues of humidity from the ampoule. The dry and evacuated ampoules were transferred to the glove box. All educts were weighed on a precision scale inside glove box and transferred to the ampoules via long funnels. The filled ampoules were connected to the *Schlenk* line described in chapter 2.2.3. Before condensing the ammonia into the ampoule, a capillary was drawn by heating the ampoule at a suitable point. Therefore, one sealing cap was opened in a counter current of argon to release the rising pressure caused by expansion of the argon protecting gas inside the ampoule caused by external heating. Capillaries were drawn to guarantee a good ablation, which is important to keep the pressure resistance of the ampoules as high as possible. After the capillaries were drawn, the dry ammonia was condensed inside the ampoule in static vacuum. For condensation, the ampoule was cooled with a mixture of dry ice and ethanol (-72 °C). If a filling degree of about 50% was reached, the ampoule was frozen with liquid nitrogen. Thereafter the ampoules were sealed in dynamic vacuum by closing the drawn capillaries with an oxygen/natural gas burner. To avoid tension inside the walls of the glass ampoules they were annealed for a few minutes. The ampoules were placed in PE bottles for bursting protection.

For the syntheses under mild ammonothermal conditions the ampoules were stored either at room temperature (*1*) or in a drying cabinet at 55 °C (*2*). The reaction times for these conditions were not fixed. The ampoules were visually analyzed with a microscope for crystal growth and inspected every couple of days.

For ammonothermal syntheses under supercritical conditions (*3*), steel autoclaves were used, since the thick-walled glass ampoules could not resist the high pressures generated by the elevated temperatures. The used steel autoclaves are described in chapter 2.2.4. As reaction temperature, 150 °C was chosen (T_c(NH$_3$) = 133.5 °C). The resulting pressure inside the ampoule at 150 °C was calculated with the help of the "NIST Chemistry WebBook, SRD 69". Therefore, the filling degree was measured and the density of ammonia in the ampoule was calculated. With this density, the pressure could be calculated. To prevent the ampoules from bursting, dry ice was loaded to the autoclaves to create counter-pressure. For the calculation of an appropriate amount of dry ice, the volume of the autoclave minus the volume of the ampoules had to be determined. This was done by filling the autoclaves, with ampoules inside, with water and determining the volume of needed water. With the information of the volume and the necessary pressure, the amount of dry ice could be calculated. Various experiences showed that it worked better if the counter-pressure was higher than the internal pressure of the ampoule. It was found that an amount of dry ice, generating a counter-pressure of 225 bar, worked well. The autoclave was fixed with a vise and filled with the ampoule. The dry ice was weighed in and the autoclave was quickly sealed with a wrench to avoid the loss of volatile CO_2. By twisting the screw cap tight, a conic steel stamp was pressed against the walls of the autoclave. For heating the autoclave a drying cabinet was used, which was connected to a control element of a furnace. The drying cabinet was heated up with a rate of 30 °C/h to 150 °C. The temperature of 150 °C was hold for different periods, but at least for 120 h. After that, the autoclave was cooled down to room temperature with a rate of 5 °C/h. The used temperature profile is depicted in Figure 6 as temperature vs. time diagram. For opening, the autoclave was fixed with a vise and opened with a wrench.
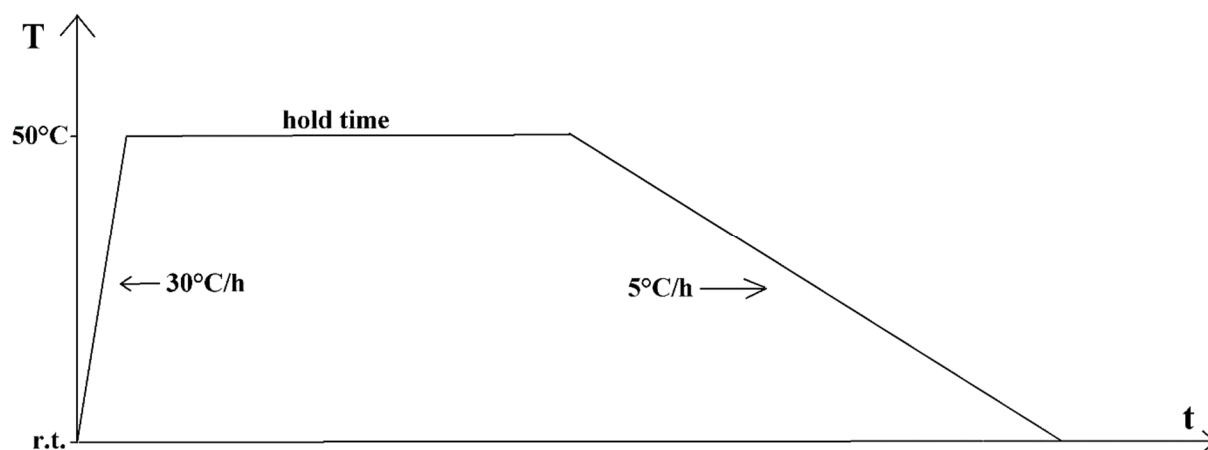
Figure 6: Temperature profile used for ammonothermal syntheses under supercritical conditions.

2.4.2 Solvothermal syntheses in ethylene diamine at 55 °C (*4*) and 170 °C (*5*)

For the syntheses in ethylene diamine, identical thick-walled glass ampoules (wall thickness = 2.2 mm, inner diameter = 5.6 mm) as for the ammonothermal syntheses were prepared and the synthetic procedure is the same with a few exceptions. The ethylene diamine was not condensed into the ampoules, it was injected with a syringe in an argon countercurrent. Therefore, a syringe with a long cannula was used, which was flushed multiple times with argon before using. Before the ampoule was sealed in dynamic vacuum, it was closed with a sealing cap and frozen with a dry ice/ethanol mixture. For removing tensions inside the glass ampoules they were annealed for a few minutes after they were molten off. The ampoules were placed in PE bottles as bursting protection. For the reactions the ampoules were placed either in a drying cabinet, which was heated up to 55 °C (*4*) or 170 °C (*5*). The reaction times were not fixed. The ampoules were visually analyzed with a light microscope if some crystal growth could be observed every couple of days.

Compound	Amount of starting materials	Molar ratio	Reaction type (hold time)	Product appearance	Yield (estimated)
$[Eu(NH_3)_9]_2(S_5)_3 \cdot 2NH_3$	10.0 mg Eu (0.066 mmol) 16.9 mg S (0.530 mmol)	1Eu:8S	*1* or *2* or *3* (200 h)	Yellow-orange, trapezoid habitus	Main product (95%), only crystalline phase
$[Sm(NH_3)_9]_2(S_5)_3 \cdot 2NH_3$	10.0 mg Sm (0.067 mmol) 17.1 mg S (0.536 mmol)	1Sm:8S	*3* (200 h)	Yellow-orange, parallelogram-shaped	Main product (95%), only crystalline phase
$[Er(NH_3)_8]_2(S_5)_2(S_6) \cdot 3NH_3$	10.0 mg Er (0.060 mmol) 15.3 mg S (0.480 mmol)	1Er:8S	*3* (200 h)	Yellow-orange, block-shaped	Main product (95%), only crystalline phase
$[Yb(NH_3)_8]_2(S_5)_2(S_6) \cdot 3NH_3$	20.0 mg Au (0.102 mmol) 3.3 mg S (0.102 mmol) 59.2 mg Yb_2Se_3 (0.102 mmol)	$1Au:1S:1Yb_2Se_3$	*3* (120 h)	Orange, block-shaped	Side product (20%), second phase present
$[Yb(NH_3)_8]_2(S_5)_2(S_4) \cdot 4NH_3$	10.0 mg Yb (0.058 mmol) 14.8 mg S (0.464 mmol)	1Yb:8S	*2*	Yellow, block-shaped	Main product (95%), only crystalline phase
$[Yb(NH_3)_7(S_2O_3)]_2(S_6) \cdot NH_3$	10.0 mg Yb (0.058 mmol) 14.8 mg S (0.464 mmol) Leak during ablation	1Yb:8S	*2*	Red, block-shaped	Side product (30%)

Compound	Amount of starting materials	Molar ratio	Reaction type (hold time)	Product appearance	Yield (estimated)
$[Eu(NH_3)_9]_2(Se_2)_2(Se_3)$	47.7 mg Eu (0.314 mmol) 198.8 mg Se (2.512 mmol)	1Eu:8Se	**3** (200 h)	Dark-red	Main product (80%), only crystalline phase
$[Sr(en)_4](Te_3)$	9.0 mg Sr (0.101 mmol) 103.0 mg Te (0.808 mmol)	1Sr:8Te	**5**	Dark-red to black, needle-shaped	Side product (40%), only crystalline phase
$[Eu(NH_3)_9]_2(Te_4)_3$	25.0 mg EuTe (0.089mmol) 25.0 mg Te (0.157 mmol)	1EuTe:1.76Te	**3** (168 h)	Dark-red to black, platelet-shaped	Main product (90%), only crystalline phase
$[Ba(NH_3)_8](Te_4)$	10.5 mg Ba (0.076 mmol) 19.4 mg Te (0.152 mmol) 30.0 mg Au (0.152 mmol)	1Ba:2Au:2Te	**3** (120 h)	Black, platy habitus	Side product (25%), only crystalline phase
$[Ca(en)_4](Te_4) \cdot 0.5en$	10.0 mg Ca (0.250 mmol) 18.7 mg As (0.250 mmol) 31.8 mg Te (0.250 mmol)	1Ca:1As:1Te	**5**	Black, platy habitus	Side product (30%), only crystalline phase
$[Yb(NH_3)_8]_4(Te_{20})(Te_3)_2 \cdot 2NH_3$	15.0 mg Yb (0.087 mmol) 5.5 mg Cu (0.087 mmol) 88.5 mg Te (0.696 mmol)	1Yb:1Cu:8Te	**3** (216 h)	Black, platy habitus	(50%), only crystalline phase

Compound	Amount of starting materials	Molar ratio	Reaction type (hold time)	Product appearance	Yield (estimated)
$[Eu(en)_4](Te_6)$	15.5 mg Eu (0.101 mmol) 103.0 mg Te (0.808 mmol)	1Eu:8Te	5	Black, platy habitus	Main product (90%), only crystalline phase
$[Ca(en)_4]_2(As_4Te_6)$	10.0 mg Ca (0.250 mmol) 37.4 mg As (0.500 mmol) 254.7 mg Te (2.000 mmol)	1Ca:2As:8Te	5	Dark-red, block-shaped	(50%), only crystalline phase
$[Sr(en)_4]_2(As_4Te_6)$	20.0 mg Sr (0.220 mmol) 16.5 mg As (0.220 mmol) 28.1 mg Te (0.220 mmol)	1Sr:1As:1Te	5	Dark-red, block-shaped	Side product (30%), only crystalline phase
$[Eu(en)_4]_2(As_4Se_6)$	20.0 mg Eu (0.130 mmol) 9.7 mg As (0.130 mmol) 10.3 mg Se (0.130 mmol)	1Eu:1As:1Se	5	Orange, block-shaped	Side product (30%), only crystalline phase
$[Ca(en)_4](As_2Se_6)$	10.0 mg Ca (0.250 mmol) 37.4 mg As (0.500 mmol) 157.6 mg Se (2.000 mmol)	1Ca:2As:8Se	4	Red, block-shaped	Main product (80%), only crystalline phase
$[Ca(en)_4]_2(As_2Se_7O)$	10.0 mg Ca (0.250 mmol) 37.4 mg As (0.500 mmol) 157.6 mg Se (2.000 mmol)	1Ca:2As:8Se	5	Red, platy habitus	Main product (80%), only crystalline phase

Compound	Amount of starting materials	Molar ratio	Reaction type (hold time)	Product appearance	Yield (estimated)
[Ca(en)$_3$(H$_2$O)$_2$]As$_2$Se$_4$	10.0 mg Ca (0.250 mmol) 18.7 mg As (0.250 mmol) 78.8 mg Se (1.000 mmol)	1Ca:1As:4Se	5	Yellow-orange, hexagonal rods	(50%), only crystalline phase
[Sr(en)$_3$(H$_2$O)$_2$]As$_2$Se$_4$	10.0 mg Sr (0.110 mmol) 8.2 mg As (0.110 mmol) 34.7 mg Se (0.440 mmol)	1Sr:1As:4Se	5	Yellow-orange, hexagonal rods	Main product (80%), only crystalline phase
[Eu(NH$_3$)$_8$][Cu(S$_4$)$_2$]·NH$_3$	47.8 mg Eu (0.314 mmol) 20.0 mg Cu (0.314 mmol) 80.7 mg S (2.512 mmol)	1Eu:1Cu:8S	3 (200 h)	Orange, block-shaped	Main product (90%), only crystalline phase
[Er(NH$_3$)$_8$][Cu(S$_4$)$_2$]·NH$_3$	52.6 mg Er (0.314 mmol) 20.0 mg Cu (0.314 mmol) 80.7 mg S (2.512 mmol)	1Er:1Cu:8S	3 (140 h)	Yellow, block-shaped	Main product (90%), only crystalline phase
[Eu(NH$_3$)$_9$][Ag(Se$_4$)$_2$]·2NH$_3$	20.0 mg Ag (0.190 mmol) 28.2 mg Eu (0.190 mmol) 117.1 mg Se (1.52 mmol)	1Eu:1Ag:8Se	3 (200 h)	Dark-red, block-shaped	Main product (80%), only crystalline phase
[Yb(NH$_3$)$_8$](AuSe$_5$S$_7$)·NH$_3$	20.0 mg Au (0.102 mmol) 3.3 mg S (0.102 mmol) 59.2 mg Yb$_2$Se$_3$ (0.102 mmol)	1Au:1S:1Yb$_2$Se$_3$	3 (120 h)	Black, columnar habit	Main product (70%), second phase present

Compound	Amount of starting materials	Molar ratio	Reaction type (hold time)	Product appearance	Yield (estimated)
$[Yb(NH_3)_8](AuS_4Se_6)$	20.0 mg Au (0.100 mmol) 17.6 mg Yb (0.100 mmol) 32.1 mg Se (0.400 mmol) 13.0 mg S (0.400 mmol)	1Yb:1Au:4Se:4S	*3* (216 h)	Black, rod-shaped	Main product (70%), second phase present
$[Ca(en)_4](AuTe_5)_2$	4.0 mg Ca (0.100 mmol) 20.0 mg Au (0.100 mmol) 103.6 mg Te (0.800 mmol)	1Ca:1Au:8Te	*5*	Black, platy-shaped	Main product (80%), only crystalline phase
$[Yb(NH_3)_8](AuSe_4)_3$	30.0 mg Au (0.150 mmol) 8.8 mg Yb (0.050 mmol) 48.1 mg Se (0.600 mmol)	1Yb:3Au:12Se	*3* (196 h)	Black, golden luster, cubic crystal habit	Main product (90%), only crystalline phase

Table 2: Summary of all performed syntheses for the compounds presented in this thesis. The yield given in the table is a visually estimated quantity.

2.4.4 Content of oxygen and water in [Ca(en)$_4$]$_2$(As$_2$Se$_7$O) and [M(en)$_3$(H$_2$O)$_2$]As$_2$Se$_4$, M = Ca or Sr

The analysis and examination of the crystal structures of the three compounds, [Ca(en)$_4$]$_2$(As$_2$Se$_7$O), [M(en)$_3$(H$_2$O)$_2$]As$_2$Se$_4$ and [Sr(en)$_3$(H$_2$O)$_2$]As$_2$Se$_4$, lead to the result that they all contain oxygen. Nothing obvious leading to the oxygen content happened during the syntheses, so the educts were checked for purity. Two possible sources for oxygen were found, the used arsenic and the used ethylene diamine. A powder diffraction pattern of the used arsenic shows arsenic oxide as second phase beside arsenic, which was quantified to 26.1 % from the comparison of the diffraction intensities with the program MATCH!. The other identified source for oxygen is the used solvent ethylene diamine, which was not completely dry. For quantification of the amount of water in the solvent, a *Karl-Fischer* [40] titration was performed with salicylic acid as buffer. The determination gave an amount of water of 0.36 %.

The contamination by arsenic oxide was removed by washing the contaminated arsenic with ammonia solution. Afterwards the purity was proved by X-ray powder diffraction. Both powder diffraction patterns are included in the appendix. After the removal of arsenic oxide, the syntheses were repeated and led to identical results. Hence, the small amount of water in the used ethylene diamine leads to the oxygen and water content in the three title compounds.

The *Karl-Fischer* titration gave an amount of water of 0.36 %. For the used amounts of educts, the amount of water present in the solvent is sufficient for a conversion of 42.2% to the product with the composition [Ca(en)$_3$(H$_2$O)$_2$]As$_2$Se$_4$ of 95.9%, to the product with the composition [Ca(en)$_3$(H$_2$O)$_2$]As$_2$Se$_4$ and to a quantitative conversion to the product with the composition [Ca(en)$_4$]$_2$(As$_2$Se$_7$O).

3. Results and Discussion

3.1 Compounds containing oligomeric Q_n^{2-} units or polymeric chalcogenides

Sulfur and its heavier homologues selenium and tellurium have all the tendency to form homonuclear covalent bonds, as present in their elemental structures. Elemental sulfur mainly appears as octasulfur in three polymorphs, that all contain S_8 rings [41]. Beside S_8 rings, also other rings are known up to S_{20} [42]. Selenium appears either as Se_8 rings (red selenium) as found for sulfur or as infinite chains in its grey elemental form. Tellurium only forms infinite chains in its element structure [43]. Reduction of the chalcogens leads to bond cleavage for attaining the electron octet in polychalcogenides.

For all three chalcogenides, oligomeric Q_n^{2-} motifs are known. The simplest motif is the Q_2^{2-} dumbbell. This motif can be found for all three chalcogenides in binary compounds with alkali metals e.g. in A_2Q_2, with A = Na-Rb [44]. For S and Se oligomeric Q_n^{2-} motifs for n = 2-9 are known. These oligomeric anions are helical chains, with the negative charges located at the terminal chalcogen atoms. The spatial structure of these chains can be explained by the VSEPR theory (valence shell electron pair repulsion). According to the VSEPR theory, the Q atoms within the chain are of the type AX_2E_2 (A = central atom, X = binding electron pair between central atom and a ligand, E = lone pair of electrons on A), which results in a ψ^2-tetraheral arrangement with Q-Q-Q angles ranging between 100°-110°. Long chains with n > 5 only exist with large cations as $[PPh_4]^+$ in $[PPh_4]_2(S_7)$ [45] or as $[Rb(222\text{-crypt})]^+$ in $[Rb(222\text{-crypt})]_2(Se_6)$ [46]. The nonasulfide dianion and nonaselenide dianion are the largest oligomeric chains known for polysulfides and polyselenides, present in the structures of $[K_2(THF)](S_9)$ [47] and $[Sr(15\text{-crown-5})_2](Se_9)$ [48]. $(Te_n)^{2-}$ dianions are known for n = 2-6, 8, 12 and 13. The $(Te_{13})^{2-}$ unit was identified in the structure of Cs_2Te_{13} [49].

Beside the described polychalcogenides built up on regular $2e\text{-}2c$ bonds, Se and Te are able to form so called hypervalent bonds. Linear Q_3^{4-} units as occurring e.g. in $Ba_2Ag_4Se_5$ [50] are valence isoelectronic to I_3^- [51] or XeF_2 [52]. The linearity can be understood according to the VSEPR theory, since the central atoms of a Q_3^{4-} unit is an AX_2E_3 type atom, which leads so a linear arrangement. Hypervalency is explained by Pimentel [53], who expanded the theory of Rundle to of electron deficient compounds [54][55] according to the molecular orbital theory.

However, in Figure 7 two simplified molecular orbital schemes are shown, one for a Q_2^{2-} unit with a regular $2c$-$2e$ bond and one for a hypervalent Q_3^{4-} unit with a $3c$-$4e$ bond. For the $3c$-$4e$ bond an empty antibonding molecular Ψ_a^* (σ^*) orbital of a Q_2^{2-} unit acts as acceptor and a filled molecular orbital Ψ (p) of a Q^{2-} acts as donor, resulting in a filled, bonding molecular orbital Ψ_1, a filled non-bonding molecular orbital Ψ_2 and an empty anti-bonding molecular orbital Ψ_3. The non-bonding orbital Ψ_2 results from an anti-bonding interaction of the p-orbital of the donor with the σ-orbital of the acceptor and a bonding interaction between the p-orbital of the donor and the σ^*-orbital of the acceptor. In a Q_3^{4-} unit, only one filled binding molecular orbital is present for two bonds. Therefore, the bonds within a $3c$-$4e$ arrangement were often called 'half-bonds' and they are elongated in comparison to a $2c$-$2e$ bond, since their electron deficiency.
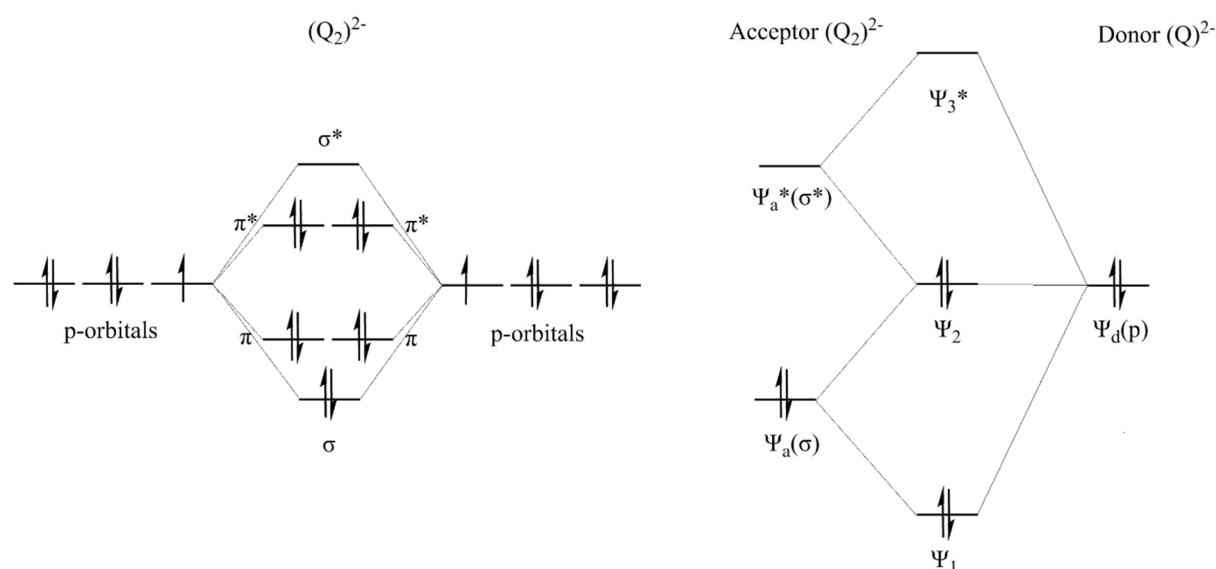
Figure 7: MO schemes of $(Q_2)^{2-}$ with a regular $2e$-$2c$ bond (left) and of hypervalent $(Q_3)^{4-}$ with a $4e$-$3c$ bond (right).

For tellurium, no Q_n^{4-} unit with n = 3 or 4 is currently known, but there are examples for n > 4 e.g. $(Te_5)^{4-}$ in Ba_2SnTe_5 [56] or $(Te_7)^{4-}$ in $[Ag(Te_7)]^{3-}$ [57]. The largest known Q_n^{4-} unit for tellurium is a $(Te_{15})^{4-}$ ion, identified in the structure of $[Zn(NH_3)_4]_2(Te_{15})$ [58] by *O. Kysliak*. For selenium, representatives of Q_n^{4-} ions with n = 4 or 5 were identified in the structures of $K_3CuNb_2Se_{12}$ [59] or Nb_2Se_9 [60], respectively. Another example for a discrete hypervalent anion is the $(Te_5)^{6-}$ anion as present in the structure of Ga_2Te_5 [61]. The cross-shaped $(Te_5)^{6-}$ anion contains a square planar coordinated central Te atom of the type AX_4E_2 carrying two negative

charges. Each other terminal Te atom carries one negative charge resulting in six negative charges for the whole anion.

Polytellurides expand the structural diversity of polychalcogenides by the formation of polymeric motifs. Due to the ability of forming electron deficient multicenter bonds, Te can occur as linear $^1_\infty[\text{Te}^-]$. These chains, with interatomic distances between 3.0 Å and 3.1 Å, are present in the structures of CuTe [62], TlTe [63] or $\text{Ca}_{0.66}\text{K}_4\text{Te}_3$ [64]. In many cases, these chains are subjected to *Peierls* distortion [65]. Thus, chains with alternating shorter (2.8 Å) and longer (3.5 Å) bonds are formed as present in K_5Te_3 [66], leading to a more appropriate description as $(\text{Te}_2)^{2-}$ dumbbells, which are connected via *van-der-Waals* interactions to $^1_\infty[\text{Te}_2^{2-}]$. Two additional Te atoms connected to a linear $^1_\infty[\text{Te}^-]$ chain lead to the formation of $^1_\infty[\text{Te}_3^{3-}]$ chains as present in the structure of TlTe [63] beside the linear $^1_\infty[\text{Te}^-]$ chains. However, there are more complicated motifs possible than linear. The $^1_\infty[\text{Te}_3^{2-}]$ chains in Tl_2Te_3 [67] are best described as polymerized $(\text{Te}_3)^{4-}$ units with short and long Te-Te bonds of 2.83 Å and of 3.04 Å. In LiTe$_3$[68] $(\text{Te}_3)^{4-}$ units are interconnected via (Te_3) units, as present in elemental tellurium, forming $^1_\infty[(\text{Te}_3^{2-})(\text{Te}_3)]$ chains.

Higher than one-dimensional polytelluride motifs were also identified. Layers built up of T-shaped fragments dominate the two-dimensional motifs. These layers can either be planar as in NbTe$_4$ [69] or corrugated as in CsTe$_4$ [70]. The layered structures can be seen as interacting $(\text{Te}_2)^{2-}$ units with Te-Te bond lengths varying between 2.80 Å and 3.40 Å within a layer. Two representatives of polytelluride frameworks are known. They are present in the structures of $\text{Cs}_4\text{Te}_{28}$ [49] and $[\text{K}(\text{H}_2\text{O})_6]\text{Te}_{36}\cdot\text{Sb}_{12}\text{O}_{18}$ [71].

3.1.1 [Ln(NH₃)₉]₂(S₅)₃ · 2NH₃, with Ln = Eu or Sm
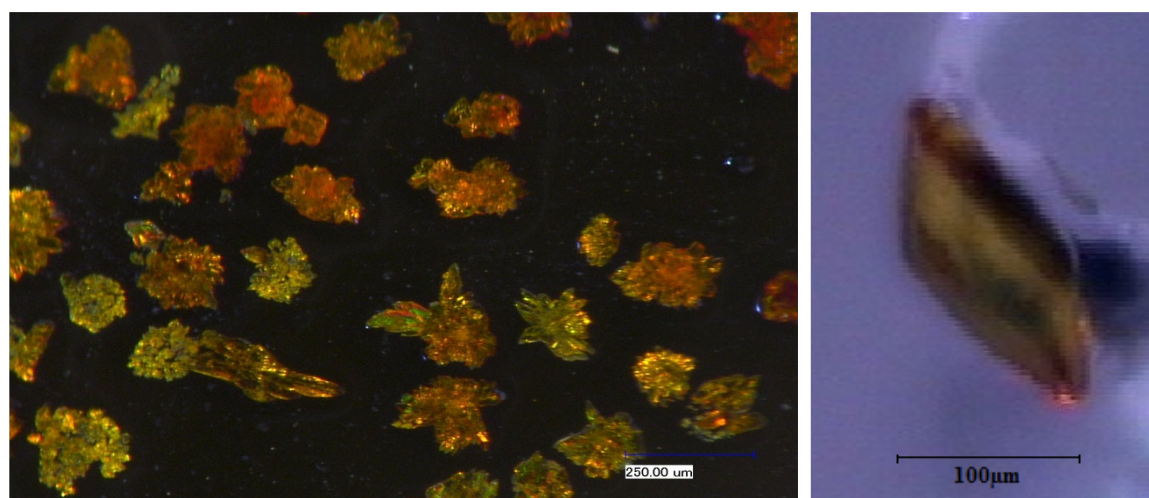
Figure 8: Crystal bulk of $[Eu(NH_3)_9]_2(S_5)_3 \cdot 2NH_3$ (left) and a single crystal of $[Sm(NH_3)_9]_2(S_5)_3 \cdot 2NH_3$ (right).

The crystals of $[Eu(NH_3)_9]_2(S_5)_3 \cdot 2NH_3$ and $[Sm(NH_3)_9]_2(S_5)_3 \cdot 2NH_3$ are both transparent and of orange-yellow color (Figure 8). The crystals of the europium compound have a trapezoid habitus und those of the samarium compound a parallelogram-shaped appearance. Both crystal structures are isotypic. They crystallize in the monoclinic space group $P2_1/n$ with the lattice constants $a = 10.9036(4)$ Å, $b = 15.0138(4)$ Å, $c = 13.5679(4)$ Å and $\beta = 94.586(1)$ ° for the europium compound and $a = 10.8879(3)$ Å, $b = 15.0272(4)$ Å, $c = 13.5817(4)$ Å and $\beta = 94.512(1)$ ° for the samarium compound. Both compounds decompose at room temperature due to the loss of NH_3. The crystal structures contain homoleptic lanthanide ammine complexes and $(S_5)^{2-}$ chains, of which one chain is disordered.
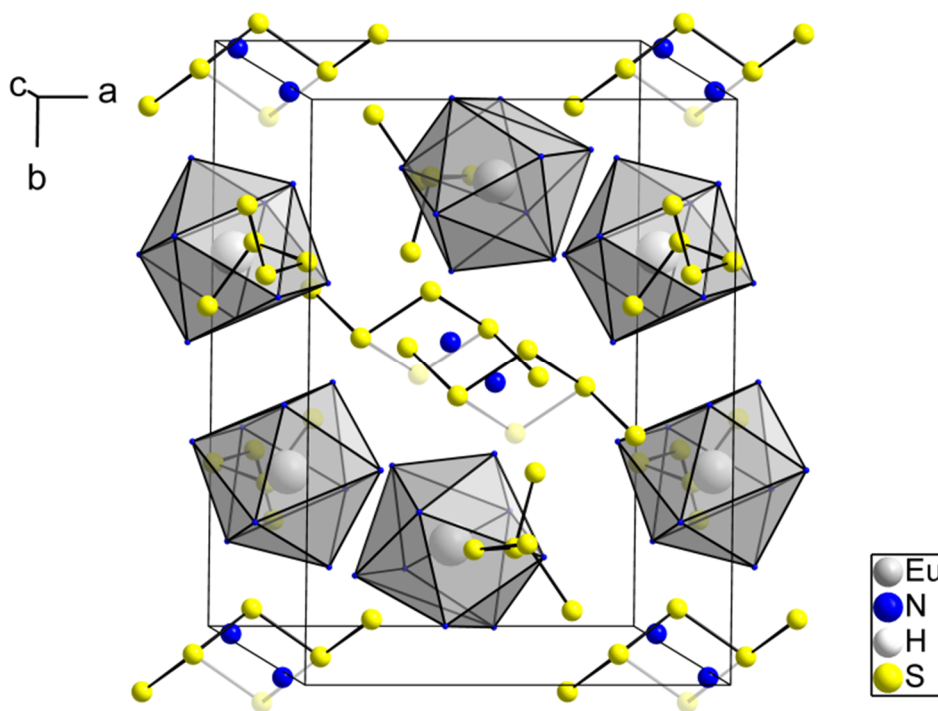
Figure 9: A view of the unit cell of the structure of $[Eu(NH_3)_8]_2(S_5)_3 \cdot 2NH_3$. The atoms are drawn as spheres with arbitrary radii. The hydrogen atoms bound to the N atoms of the ammonia ligands are omitted for clarity. The transparent atoms represent a disordering of 50%.

Samarium is insoluble in liquid ammonia at low temperatures. Solubility of elemental samarium in ammonia is however, given under supercritical conditions. Hence, $[Sm(NH_3)_9]_2(S_5)_3 \cdot 2NH_3$ can only be synthesized at high temperatures under supercritical conditions. In contrast, $[Eu(NH_3)_9]_2(S_5)_3 \cdot 2NH_3$ can be synthesized at room temperature, at 55°C and under supercritical conditions due to of the high solubility of europium in liquid ammonia even at lower temperatures. The temperature seems to have no influence on the formed product since the same product is formed at different temperatures. This statement holds only for the few measured crystals, because for one experimental approach only one crystal could be analyzed.
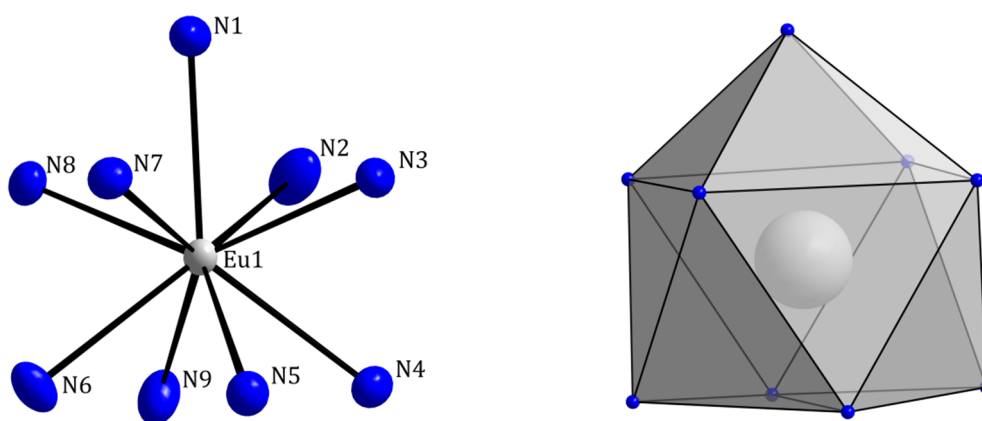
Figure 10: Coordination of Eu^{3+} in the structure of $[Eu(NH_3)_9]_2(S_5)_3 \cdot 2NH_3$. The displacement ellipsoids represent a probability of 50 %. The hydrogen atoms bound to the N atoms of the ammonia ligands are omitted for clarity.

Table 3: Results of the continuous shape measures of the EuN_9 and SmN_9 polyhedra in the structures of $[Eu(NH_3)_9]_2(S_5)_3 \cdot 2NH_3$ and $[Sm(NH_3)_9]_2(S_5)_3 \cdot 2NH_3$.

Ideal Shape	CShM / % (EuN$_9$ polyhedron)	CShM / % (SmN$_9$ polyhedron)
EP-9	37.470	37.433
OPY-9	22.400	22.375
HBPY-9	20.362	20.297
JTC-9	16.721	16.664
CCU-9	9.549	9.583
CSAPR-9	**0.111**	**0.115**
TCTPR-9	0.742	0.747

The metal ions Eu^{3+} and Sm^{3+} are surrounded by nine ammonia molecules forming homoleptic ammine complexes. The coordination polyhedron with the coordination number 9 of homoleptic ammine complexes can be typically described as distorted capped square-antiprism (C_{4v}) or as distorted threefold-capped triangular prism (D_{3h}) (Figure 10). The deviation from the ideal polyhedral shapes can be calculated by the method of continuous symmetry measures. The deviation of the $[Eu(NH_3)_9]^{3+}$ polyhedron from the ideal capped square-antiprism and the ideal threefold-capped triangular prism amounts to 0.111 % and 0.742 % or 0.115 % and 0.747 % for the $[Sm(NH_3)_9]^{3+}$ polyhedron, respectively (Table 3). The M^{III}-N distances range from 2.58 Å to 2.64 Å for $[Eu(NH_3)_9]^{3+}$ and from 2.59 Å to 2.65 Å for $[Sm(NH_3)_9]^{3+}$. The M^{III}-N

distances are according to their ionic radii ($r(Eu^{3+}) = 1.21$ Å and $r(Sm^{3+}) = 1.22$ Å) and therefore following the lanthanoid contraction. The distance between the "capping" ammine ligand N1 and the metal ions is the longest present in the coordination polyhedron. For homoleptic ammine complexes with Eu in the oxidation state +II as in $[Eu(NH_3)_8]I_2$, longer M-N bond lengths ranging from 2.72-2.82 Å are found [72].

The second building block in the structure is a polysufide chain. The (S_5) chain has formally a negative charge on each of the terminal sulfur atoms. Therefore the chain is twofold negatively charged. The distances between the sulfur atoms within the chain are similar to the distances present in the S_8 molecules. The angles between the sulfur atoms vary between 108°-110°. One of the two polysulfide chains shows a disorder (Figure 11). The disorder and the inversion centers located in the center of gravity of the disordered S_5-chains are mutually dependent on each other. In the structure refinement, the disorder can be solved by setting the site occupation factor of S1 to 50%. In addition to the surrounded metal ions and the (S_5)-chains, there are free ammonia molecules in the crystal structure. The positions of the hydrogen atoms of the free ammonia molecules in both structures could not be located from difference *Fourier* maps. The hydrogen atoms of the complexating ammonia molecules were placed on geometrically calculated positions and refined by a riding model.
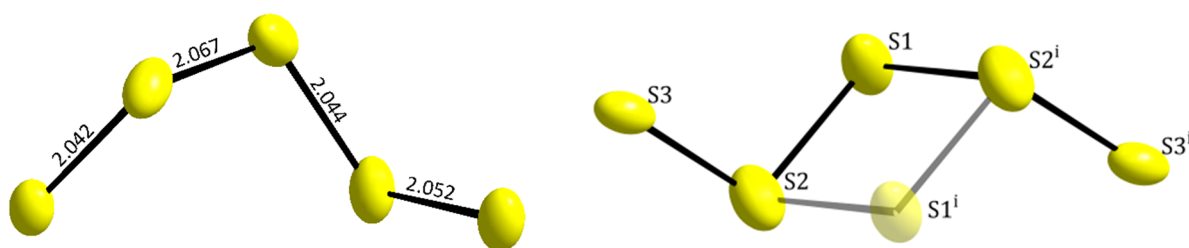
Figure 11: S_5 polysulfide chain (left) and the disordered polysulfide chain (right) in the structure of $[M(NH_3)_9]_2(S_5)_3 \cdot 2NH_3$. Bond lengths are given in Å. The displacement ellipsoids represent a probability of 50 %. The transparent atoms represent a disordering of 50%. The index *i* indicates the following symmetry operation: *-x*+1, *-y*+1, *-z*+2.

The disordered polysulfide chains are placed on special positions (½, ½, 0 and 0, 0, ½) in the unit cell with their centers of gravity. Accordingly, they are placed on the *Wyckhoff* position 2*b* with the site symmetry $\bar{1}$. These chains on the special positions are surrounded by six $[M(NH_3)_9]^{3+}$ complexes arranged in the form of distorted octahedra. Figure 13 shows that these

octahedra are interconnected via common edges along the crystallographic *a*-axis. The formed strands are linked via common edges forming a three dimensional network. Every M^{3+} belongs to three octahedra. The resulting composition can described as $(S_6)M_{6/3}$. Therefore, the disordered polysulfide chains and the europium ammine complexes build a Rutil-type structure. Whereas, the not disordered polysulfide chains are not surrounded by M^{3+} in a certain shape, thus they fill the voids in the crystal structure as well as the free ammonia molecules in the structure (Figure 12).
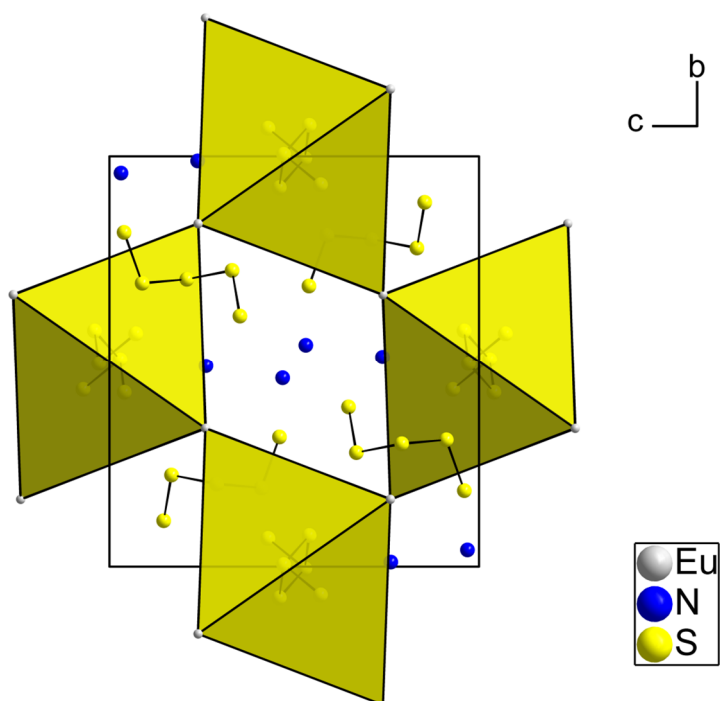
Figure 12: View of the unit of the structure of $[M(NH_3)_8]_2(S_5)_3 \cdot 2NH_3$ cell along the crystallographic *a*-axis. All atoms are drawn as spheres with arbitrary radii. The ligating ammonia molecules are omitted for clarity.
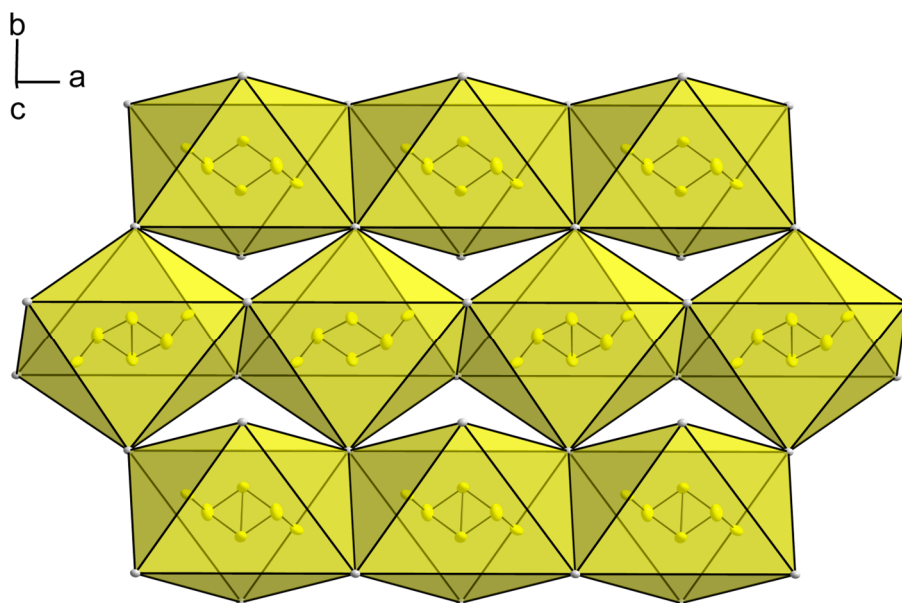
Figure 13: The strands of M_6 octahedra running along the crystallographic a-axis in the structure of $[M(NH_3)_9]_2(S_5)_3 \cdot 2NH_3$. The disordered $(S_5)^{2-}$ anions are located at the inversion centers in the octahedra made up of $[M(NH_3)_9]^{3+}$ units. The displacement ellipsoids show a probability of 50%.

3.1.2 [Ln(NH$_3$)$_8$]$_2$(S$_5$)$_2$(S$_6$) · 3NH$_3$, with Ln = Er or Yb
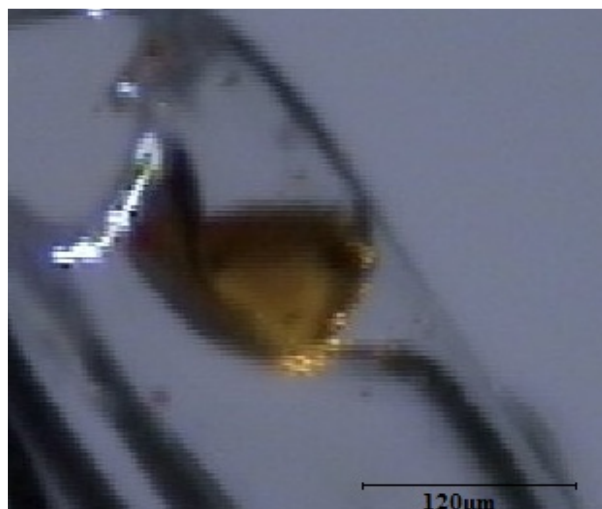
Figure 14: Single crystal of [Er(NH$_3$)$_8$]$_2$(S$_5$)$_2$(S$_6$) · 3NH$_3$.

The crystals with the composition [Er(NH$_3$)$_8$]$_2$(S$_5$)$_2$(S$_6$)·3NH$_3$ or [Yb(NH$_3$)$_8$]$_2$(S$_5$)$_2$(S$_6$)·3NH$_3$ are both block shaped. Both crystals are of an orange color, but those of the erbium containing compound are somewhat brighter in color than those of the ytterbium containing compound. The compounds are isotypic and crystallize in the monoclinic centrosymmetric space group $P2_1/c$ with the lattice parameters a = 15.1004(3) Å, b = 20.7552(5) Å, c = 13.9943(3) Å and β = 110.0490(10) ° for [Er(NH$_3$)$_8$]$_2$(S$_5$)$_2$(S$_6$)·3NH$_3$ and a = 15.0942(4) Å, b = 20.7195(9) Å, c = 14.0036(4) Å and β = 109.900(2)° for [Yb(NH$_3$)$_8$]$_2$(S$_5$)$_2$(S$_6$)·3NH$_3$, respectively. The unit cell contains 4 formula units. Er and Yb are in the formal oxidation state +III. The lanthanoid atoms are surrounded by eight ammine ligands forming homoleptic ammine complexes. There is no homoleptic erbium ammine complex known except the one presented in this work, whereas homoleptic ammine complexes for ytterbium have been described in the literature before. The resulting coordination polyhedra of the homoleptic ammine complexes are best described as square antiprisms. The deviation from a perfect square antiprism shape was calculated with the program SHAPE. A continuous shape measure of [Er(NH$_3$)$_8$]$^{3+}$ showed small deviations from the ideal square antiprism (D_{4d}) amounting to 0.244 % for Er2 and 0.421 % for Er1. For [Yb(NH$_3$)$_8$]$^{3+}$ deviations amount to 0.237 % for the coordination polyhedron of Yb1 and 0.353 % for Yb2 from the ideal square antiprism (D_{4d}) (Table 4). Compared to the cationic complexes [Sm(NH$_3$)$_9$]$^{3+}$ and [Eu(NH$_3$)$_9$]$^{3+}$, the central atoms have the coordination number eight with

M - N distances between 2.40 Å and 2.54 Å for M=Er and between 2.43 Å and 2.50 Å for M=Yb, respectively. The different coordination numbers can be explained by the differences of the ionic radii of the respective lanthanoids (Table 9 in chapter 3.1.3). Er^{3+} and Yb^{3+} have smaller ionic radii than Eu^{3+} or Sm^{3+}, thus the smaller coordination number is preferred. However, the Er-N distances cannot be compared with distances in the literature since homoleptic erbium ammine complexes have not been described so far. Though, the distances are similar to those found for $[Er(NH_3)_8]^{3+}$ in the structure of $[Er(NH_3)_8][Cu(S_4)_2]$ that will be discussed later in this work. The Yb-N distances are in the expected range for homoleptic ytterbium ammine complexes with ytterbium in the oxidation state +III. Similar Yb-N bond lengths are found in the structure of $[Yb(NH_3)_8][Ag(S_4)_2]\cdot2NH_3$ [73]. The positions of the hydrogen atoms of the ammine ligands were not found in the difference *Fourier* map. They were placed on geometrically calculated positions and refined using the riding model.
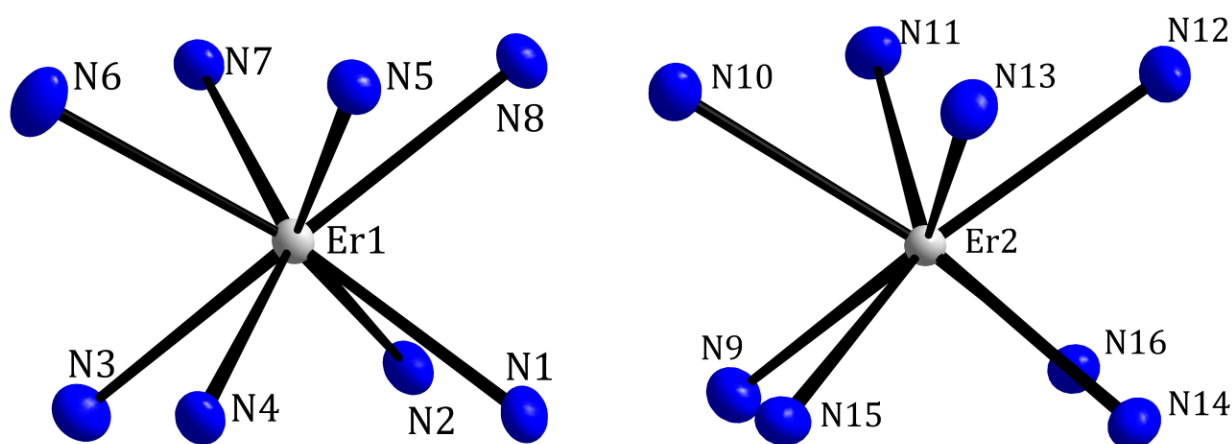
Figure 15: Coordination polyhedra of Er1 and Er2 in the structure of $[Er(NH_3)_8]_2(S_5)_2(S_6)\cdot3NH_3$. The displacement ellipsoids represent a probability of 50%. The hydrogen atoms bound to the N atoms of the ammonia ligands are omitted for clarity.
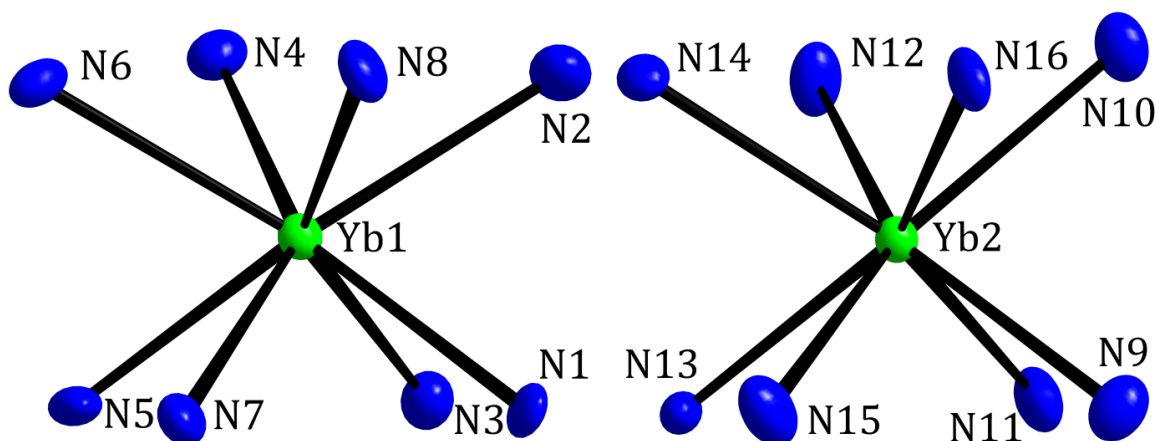
Figure 16: Coordination polyhedra of Yb1 and Yb2 in the structure of $[Yb(NH_3)_8]_2(S_5)_2(S_6) \cdot 3NH_3$. The displacement ellipsoids represent a probability of 50%. All hydrogen atoms bound to the N atoms of the ammine ligands are omitted for clarity.

Table 4: Results of the continuous shape measure of the ErN_8 and YbN_8 polyhedra in the structures of $[M(NH_3)_8]_2(S_5)_2(S_6) \cdot 3NH_3$, with M = Er or Yb.

Ideal Shape	CShM / % (Er(1)N$_8$ polyhedron)	CShM / % (Er(2)N$_8$ polyhedron)	CShM / % (Yb(1)N$_8$ polyhedron)	CShM / % (Yb(2)N$_8$ polyhedron)
OP-8	30.276	29.357	29.354	30.180
HPY-8	22.802	23.137	23.301	22.795
HBPY-8	15.858	17.043	16.924	16.193
CU-8	9.110	10.357	10.400	9.356
SAPR-8	**0.421**	**0.244**	**0.237**	**0.353**
TDD-8	1.667	2.164	2.279	1.809
BTPR-8	1.958	1.982	2.071	1.977

Beside two $[M(NH_3)_8]^{3+}$ cationic complexes the structure contains three independent polysulfide chains, two (S_5)-chains and one (S_6)-chain (Figure 17 and Figure 18). The asymmetric unit contains the full sum formula including three free ammonia molecules, which are not bound to the cations or the polysulfide chains. The positions of the hydrogen atoms of the free ammonia molecules were not found in the difference *Fourier* maps. Each of the three

polysulfide chains carries two negative charges located formally on the terminal sulfur atoms. The polysulfides form spiral chains with interatomic S-S distances ranging from 2.04 to 2.07 Å in $[Er(NH_3)_8]_2(S_5)_2(S_6) \cdot 3NH_3$ and from 2.04 to 2.09 Å in $[Yb(NH_3)_8]_2(S_5)_2(S_6) \cdot 3NH_3$ (Table 5 and Table 6), which is similar to the interatomic distances found in S_8 molecules. S-S-S angles within the chains ranging from 105 to 111 ° are typical for angles within polysulfide chains.
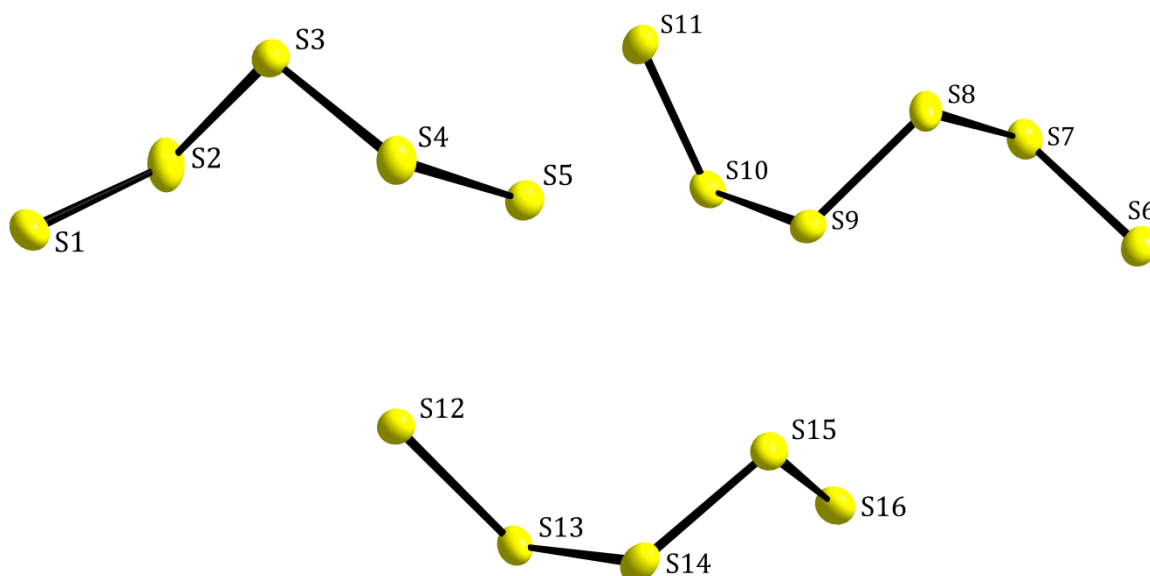
Figure 17: The three independent polysulfide chains in the structure of $[Er(NH_3)_8]_2(S_5)_2(S_6) \cdot 3NH_3$. The displacement ellipsoids represent a probability of 50%.

Table 5: Bond lengths of the three independent polysulfide chains in the structure of $[Er(NH_3)_8]_2(S_5)_2(S_6) \cdot 3NH_3$.

Atoms	Bond length/ Å	Atoms	Bond length/ Å	Atoms	Bond length/ Å
S1-S2	2.042(3)	S6-S7	2.035(3)	S12-S13	2.049(2)
S2-S3	2.051(3)	S7-S8	2.055(3)	S13-S14	2.056(3)
S3-S4	2.061(3)	S8-S9	2.074(2)	S14-S15	2.067(3)
S4-S5	2.059(2)	S9-S10	2.062(2)	S15-S16	2.051(3)
		S10-S11	2.044(2)		
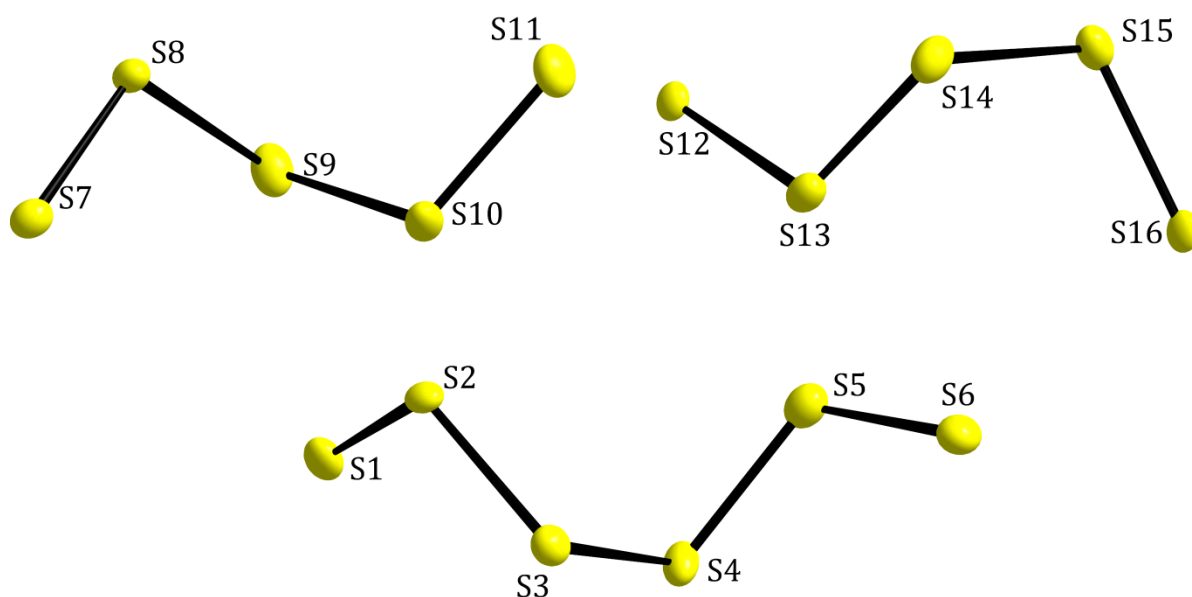
Figure 18: All independent polysulfide chains in the structure of $[Yb(NH_3)_8]_2(S_5)_2(S_6)\cdot 3NH_3$. The displacement ellipsoids represent a probability of 50%.

Table 6: Bond lengths of the three different polysulfide chains in the structure of $[Yb(NH_3)_8]_2(S_5)_2(S_6)\cdot 3NH_3$.

Atoms	Bond length/ Å	Atoms	Bond length/ Å	Atoms	Bond length/ Å
S1-S2	2.064(3)	S7-S8	2.077(3)	S12-S13	2.078(3)
S2-S3	2.080(3)	S8-S9	2.072(3)	S13-S14	2.066(3)
S3-S4	2.087(3)	S9-S10	2.068(3)	S14-S15	2.090(3)
S4-S5	2.069(3)	S10-S11	2.048(3)	S15-S16	2.092(3)
S5-S6	2.038(4)				

In Figure 19 and Figure 20 the unit cell of $[Er(NH_3)_8]_2(S_5)_2(S_6)\cdot 3NH_3$ is exemplarily shown from two different viewing directions. Neither the lanthanide ammine complexes nor the polysulfide chains are placed on special positions in the unit cell. All atoms are placed on the general *Wyckhoff* position 4*e*. The viewing direction along the crystallographic *b*-axis shows that the $[M(NH_3)_8]^{3+}$ complexes are apparently positioned in layers perpendicular to the

crystallographic *a*-axis. Voids between the complexes are filled with the polysulfide chains and the free ammonia molecules. Hydrogen bonds between the H atoms of the ammine ligands and the S atoms of the polysulfide chains stabilize the entire structure. All hydrogen bonds between the hydrogen atoms and the donating sulfur atoms shown in Figure 19 are bonds shorter than 2.90 Å. Therefore, all drawn hydrogen bonds have a reasonable influence on the structure, since all are shorter than the sum of the *van-der-Waals* radii of hydrogen and sulfur ($r_{vdW}(H) + r_{vdW}(S) = 3.00$ Å)
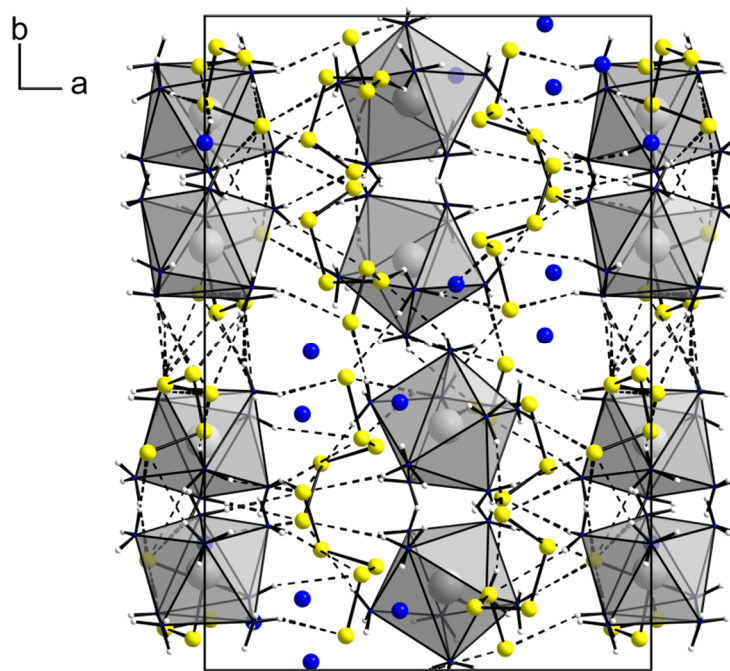
Figure 19: A view of the extended unit cell of the structure of $[Er(NH_3)_8]_2(S_5)_2(S_6)\cdot 3NH_3$ along the crystallographic *c*-axis. All atoms are drawn as spheres with arbitrary radii. Hydrogen bonds are drawn with dashed lines.
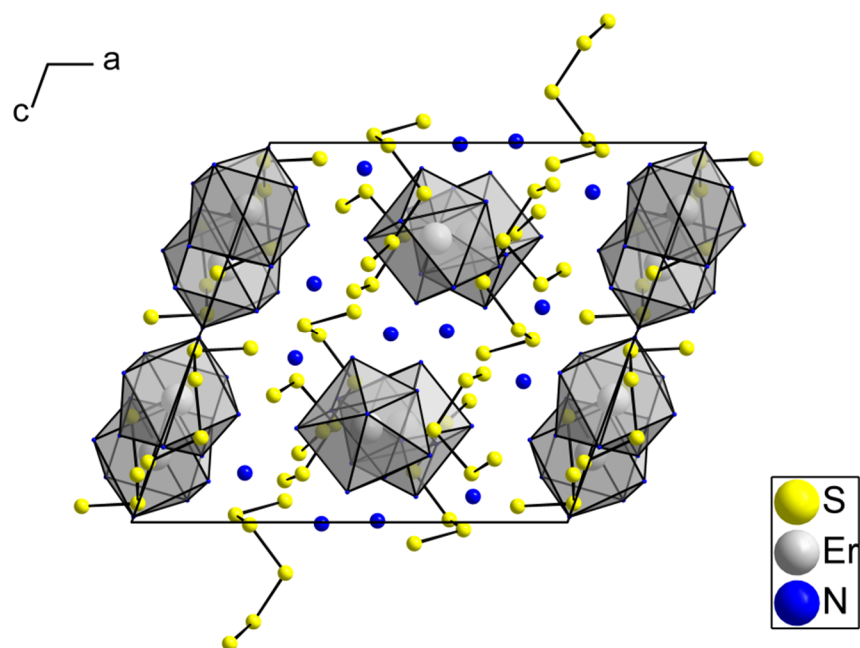
Figure 20: View of the extended unit cell of the structure of $[Er(NH_3)_8]_2(S_5)_2(S_6) \cdot 3NH_3$ along the crystallographic *b*-axis. All atoms are drawn as spheres with arbitrary radii. All hydrogen atoms of the ammonia molecules are omitted for clarity.

3.1.3 [Yb(NH₃)₈]₂(S₅)₂(S₄) · 4NH₃

$[Yb(NH_3)_8]_2(S_5)_2(S_4) \cdot 4NH_3$ forms in bright yellow block shaped crystals. They crystallize in the tetragonal space group $P4_12_12$ with the lattice parameters $a = 9.6150(2)$ Å and $c = 43.6485(10)$ Å. $P4_12_12$ is an acentric space group implying enantiomeric atoms arrangements with either a 4_1 screw axis or a 4_3 screw axis present in the structure. The analyzed crystal only consisted of the enantiomer with the 4_1 screw axis, indicated by an absolute structure parameter of 0.037(10), which is zero within the standard deviation. The unit cell contains 4 formula units and the asymmetric unit contains one half of a formula unit. The image of the 0kl plane (Figure 21) shows clearly separated reflections along the c*-axis, which legitimates the length of the c-axis of more than 40 Å.
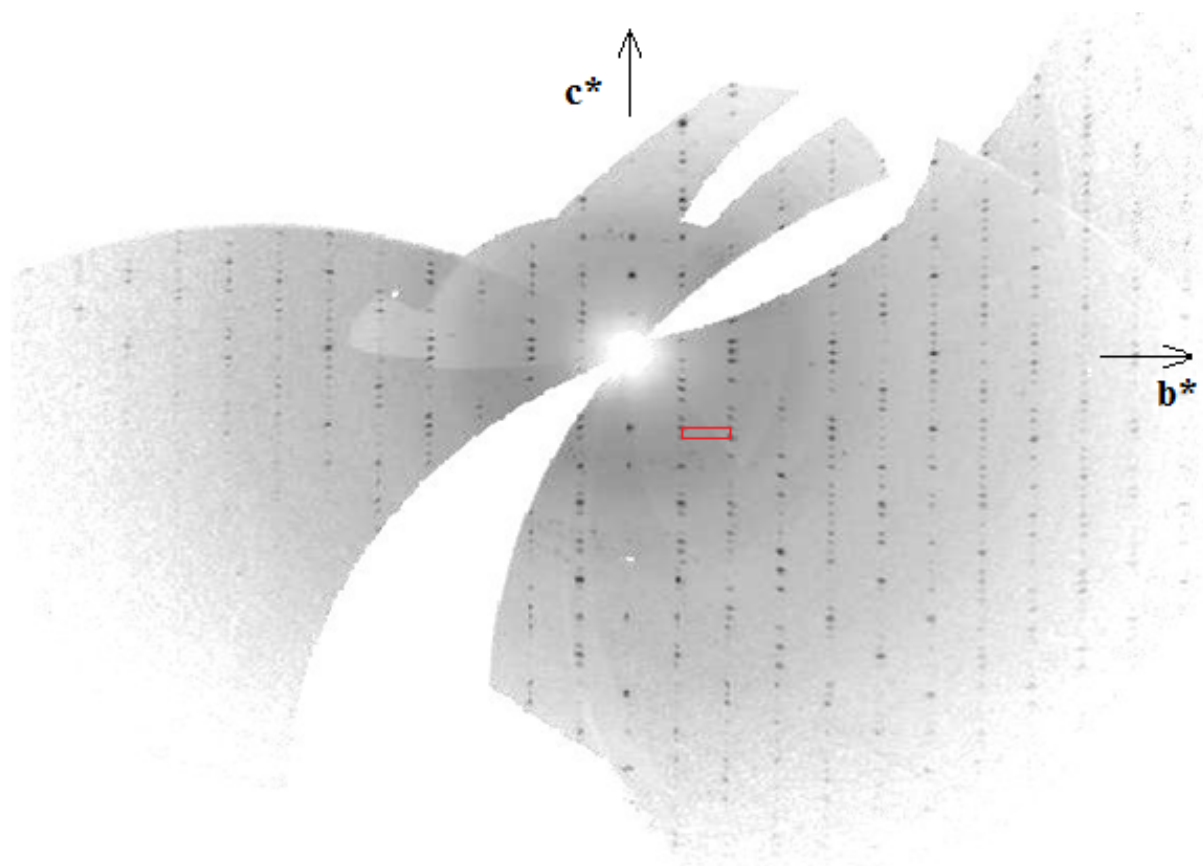
Figure 21: Reconstructed precession image of the 0kl plane of the investigated crystal of $[Yb(NH_3)_8]_2(S_5)_2(S_4) \cdot 2NH_3$. The reciprocal unit cell is shown in red.

The structure of $[Yb(NH_3)_8]_2(S_5)_2(S_4) \cdot 4NH_3$ contains 3 different building units. The first building unit is a homoleptic ammine complex with the central atom Yb^{3+}. Ytterbium is surrounded by 8 ammine ligands forming a polyhedron (Figure 22) that can be described as triangular dodecahedron (D_{2d}). A continuous shape measure gives a very small deviation of 0.139 % from an ideal triangular dodecahedron (D_{2d}) (Table 7). The positions of the hydrogen atoms of the ammine ligands were not found in the difference *Fourier* map. They were placed on geometrically calculated positions and refined by using the riding model. The Yb^{3+}-N distances range from 2.43 to 2.48 Å. This is significantly shorter as found for Yb^{2+} in the structure of $[Yb(NH_3)_8]I_2$, where the Yb^{2+}-N distances range from 2.61 to 2.75 Å [72].
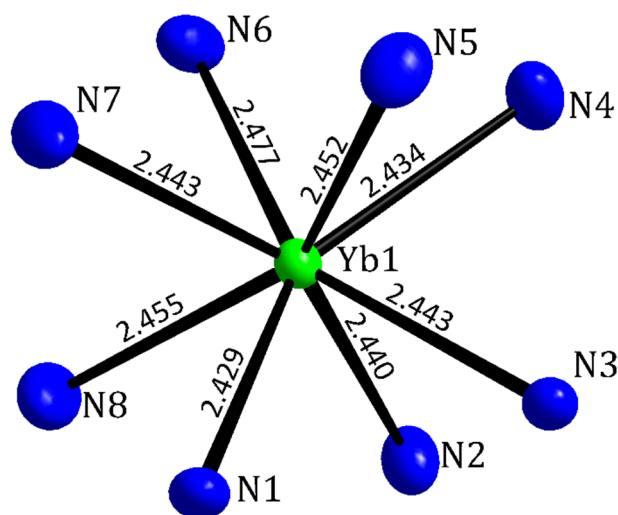
Figure 22: Coordination of Yb^{3+} in the structure of $[Yb(NH_3)_8]_2(S_5)_2(S_4)\cdot4NH_3$. The displacement ellipsoids represent a probability of 50%. The hydrogen atoms are drawn with arbitrary radii. Interatomic distances are given in Å.

Table 7: Result of the continuous shape measure of the YbN_8 polyhedron in the structure of $[Yb(NH_3)_8]_2(S_5)_2(S_4) \cdot 4NH_3$.

Ideal Shape	CShM / % (YbN$_8$ polyhedron)
OP-8	33.051
HPY-8	24.327
HBPY-8	14.716
CU-8	7.878
SAPR-8	2.604
TDD-8	**0.139**
BTPR-8	2.336

The other building units in the structure are polysulfide chains (Figure 23) of two different lengths, (S_5) chains and (S_4) chains. Both chains are twofold negatively charged with the negative charges are located on the terminal sulfur atoms. The polysulfides can be described as spiral chains with S-S-S angles the chain of 110.8° and 111.2° for the (S_5)$^{2-}$ and 111.4° for the (S_4)$^{2-}$ chain. Interatomic distances between the sulfur atoms are in the expected region between 2.04 and 2.10 Å. Hence, the bond lengths are comparable to the ones in the structures presented above. Within the (S_4)$^{2-}$ chain the torsion angle is close to rectangular and amounts to 89.5 °.
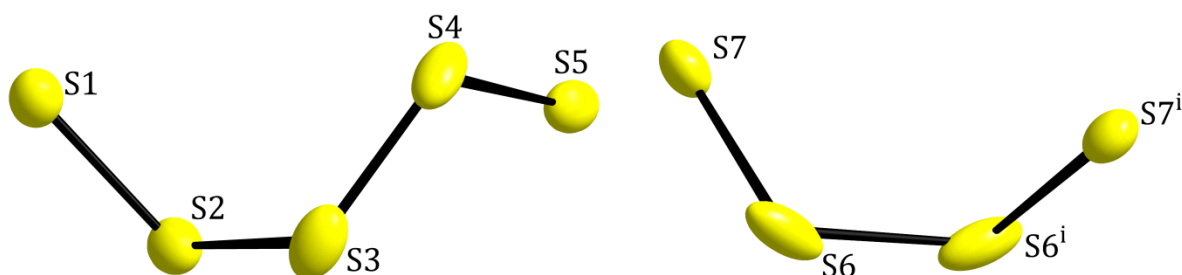
Figure 23: The two independent polysulfide chains in the structure of $[Yb(NH_3)_8]_2(S_5)_2(S_4) \cdot 4NH_3$. The displacement ellipsoids represent a probability of 50 %. The index *i* indicates the following symmetry operation: 1+*x*, -1+*y*, 1-*z*.
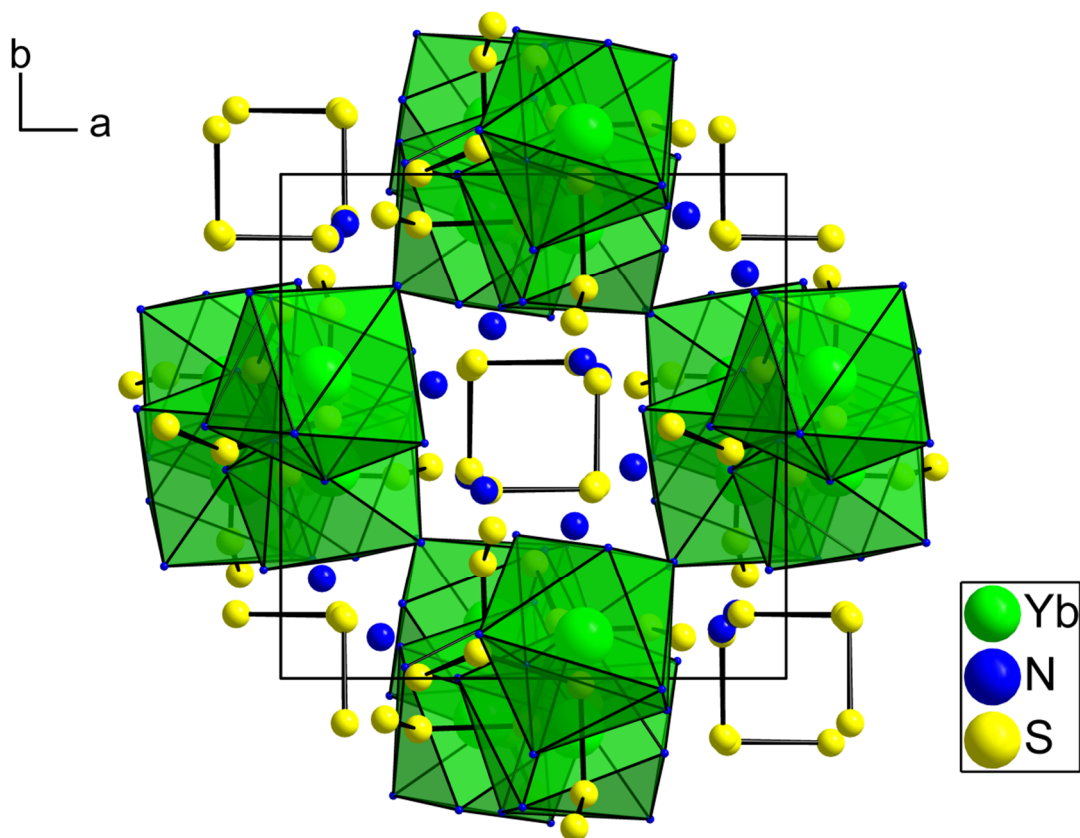
Figure 24: View of the unit cell of the structure or $[Yb(NH_3)_8]_2(S_5)_2(S_4) \cdot 4NH_3$ along the crystallographic c-axis. All atoms are drawn as spheres with arbitrary radii. The hydrogen atoms bound to the N atoms of the ammonia ligands are omitted for clarity.

The $(S_4)^{2-}$ chains run along the crystallographic c-axis. With their torsion angles of roughly 90°, they form rectangular channels running along the 2_1 screw axes at the cell edges and in the middle of the cell. Neither cationic complexes nor free ammonia molecules are placed in these channels. The $(S_5)^{2-}$ anions and the $[Yb(NH_3)_8]^{3+}$ cationic complexes form stacks along ½, 0, z and 0, ½, z. Within the stacks, anions and cationic complexes are alternating and they are linked via N-H···S hydrogen bonds. In Figure 25 the connection via hydrogen bonds within the stacks is shown. The shown N-H···S hydrogen bonds have H···S distances ranging between 2.54 Å and 2.91 Å. These bond lengths are significantly shorter than the sum of the *van-der-Waals* radii of sulfur and hydrogen ($r_{vdW}(H)+r_{vdW}(S) = 3.00$ Å [74]). The corresponding N-H···S angles range between 141.8° and 176.1°. Beside the connection via hydrogen bonds, Figure 25 allows for the explanation for the very long c-axis of 43.65 Å. The stacks of alternating $(S_5)^{2-}$ anions and the $[Yb(NH_3)_8]^{3+}$ cationic complexes run along a 4_1 screw axis. Therefore, 4 units of anions and 4 units of cationic complexes are necessary for a full repeating unit.
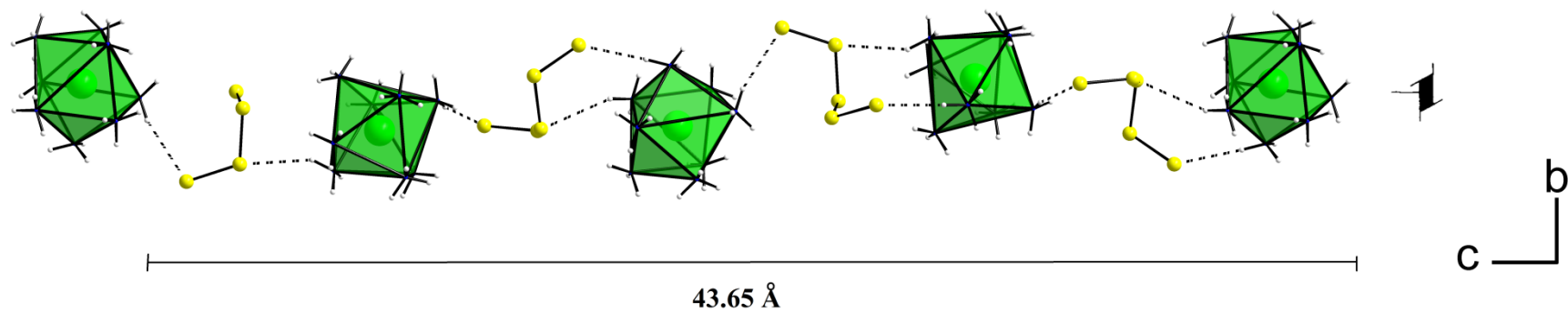
Figure 25: Chain formation via N-H···S hydrogen bonds within the structure of $[Yb(NH_3)_8]_2(S_5)_2(S_6)\cdot 4NH_3$. The chains of connected cations and anions run parallel to the crystallographic *c*-axis. All atoms are drawn with arbitrary radii.

3.1.4 [Yb(NH₃)₇(S₂O₃)]₂(S₆)·NH₃

During an attempt to reproduce the synthesis of $[Yb(NH_3)_8]_2(S_5)_2(S_4)\cdot 4NH_3$ the reaction ampoule contained accidentally traces of oxygen and moisture. The formed product was a different polysulfide, namely $[Yb(NH_3)_7(S_2O_3)]_2(S_6)\cdot NH_3$. It crystallizes in the acentric monoclinic space group Cc with the lattice parameters $a = 15.0761(8)$ Å, $b = 22.7055(12)$ Å, $c = 12.4593(6)$ Å and $\beta = 126.880(2)°$. The crystal structure consists of $(S_6)^{2-}$ polysulfide chains, ytterbium ammine complexes with one ammine ligand substituted by a thiosulfate ligand and a free ammonia molecule. In the complex $[Yb(NH_3)_7(S_2O_3)]^+$, thiosulfate coordinates the ytterbium ion as monodentate ligand via one of its oxygen atoms (Figure 26).
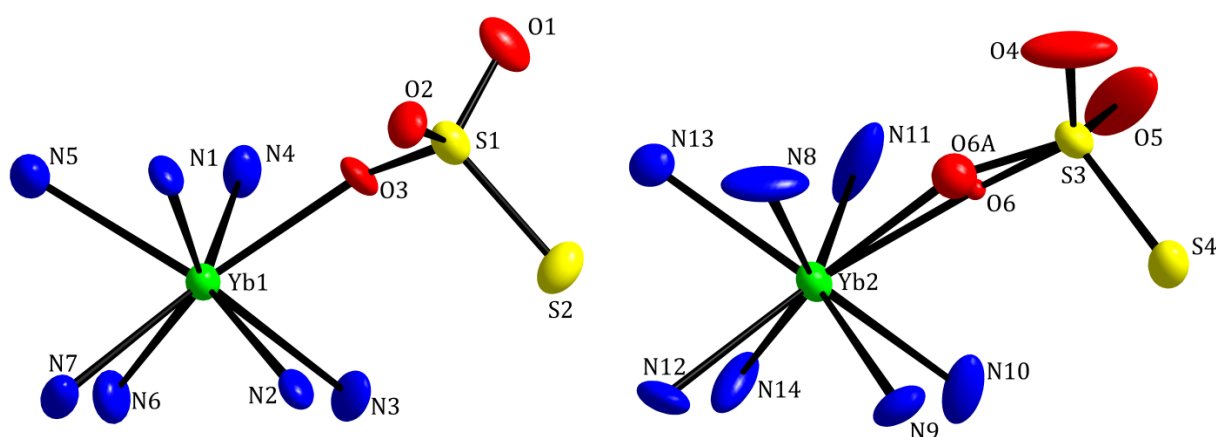
Figure 26: Coordination of the two independent Yb^{3+} ions in the structure of $[Yb(NH_3)_7(S_2O_3)]_2(S_6)\cdot NH_3$. The displacement ellipsoids represent a probability of 50 %. The atoms O6 and O6A are drawn with arbitrary radii. The hydrogen atoms bound to the N atoms of the ammonia ligands are omitted for clarity.

Each Ytterbium is located on a general site and is surrounded by seven ammine ligands and one thiosulfate ligand. The positions of the hydrogen atoms of the ammine ligands were not found in the difference *Fourier* map. They were placed on geometrically calculated positions and refined by using the riding model. The resulting coordination polyhedra can be best described as square antiprisms (D_{4d}). The deviation from the ideal shape was calculated by a continuous shape measure to 0.223 % for Yb1 and 0.337 % for Yb2, respectively (Table 8). The Yb-N

bond lengths, ranging between 2.43Å-2.49Å in Yb(1)N$_7$O and 2.40Å-2.47Å in Yb(2)N$_7$O, respectively, legitimate to assume Yb in the oxidation state +III. For Yb-N bond lengths with Yb in the oxidation state +II longer bond lengths are expected (2.61Å-2.77Å). The observed bond lengths within the thiosulfate ligand are similar to those found for non-coordinating thiosulfate ions (Figure 27). Since the thiosulfate is two-fold negatively charged and Yb is in the oxidation state +III, the whole $[Yb(NH_3)_7(S_2O_3)]^+$ complex gains one positive charge.

Table 8: Results of the continuous shape measures of both independent YbN$_7$O polyhedra in the structure of $[Yb(NH_3)_7(S_2O_3)]_2(S_6) \cdot NH_3$.

Ideal Shape	CShM / % (Yb(1)N$_7$O polyhedron)	CShM / % (Yb(2)N$_7$O polyhedron)
OP-8	29.304	30.210
HPY-8	23.081	22.338
HBPY-8	16.962	17.061
CU-8	10.201	10.112
SAPR-8	**0.223**	**0.337**
TDD-8	2.580	2.403
BTPR-8	2.396	2.126
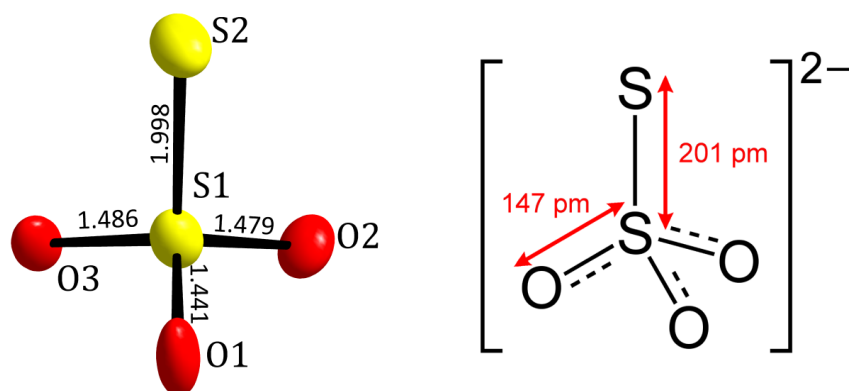
Figure 27: The thiosulfate ion in the structure of $[Yb(NH_3)_7(S_2O_3)]_2(S_6) \cdot NH_3$ with bond lengths given in Å (left) and the Lewis formula of a free thiosulfate ion with typical bond lengths (right)[74]. The displacement ellipsoids represent a probability of 50 %.

The $(S_6)^{2-}$ polysulfide chain is helically shaped (Figure 28) and two-fold negatively charged. S-S bond lengths are on an average of 2.07Å. Hence, they are in the expected range for S-S bond lengths in polysulfides and comparable to the observed bond lengths in the polysulfides presented in the previous chapters.

Within the unit cell all atoms are located on general sites. Therefore, the asymmetric unit contains the full sum formula. In Figure 29 the unit cell is shown from two different perspectives. Hydrogen bonds stabilize the structure. The N-H⋯S hydrogen bonds ranging between 2.56 Å - 3.01 Å, with N-H⋯S angles ranging between 125.6° - 176.1°. For N-H⋯O hydrogen bonds H⋯O distances between 2.05 Å – 2.63 Å with N-H⋯O angles ranging from 141.8° to 176.6° were observed. A table with all hydrogen bonds listed can be found in the appendix.
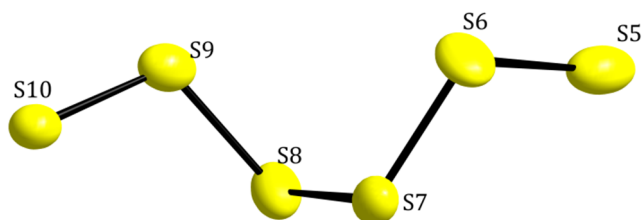
Figure 28: The $(S_6)^{2-}$ polysulfide chains in the structure of $[Yb(NH_3)_7(S_2O_3)]_2(S_6)\cdot NH_3$. The displacement ellipsoids represent a probability of 50%.
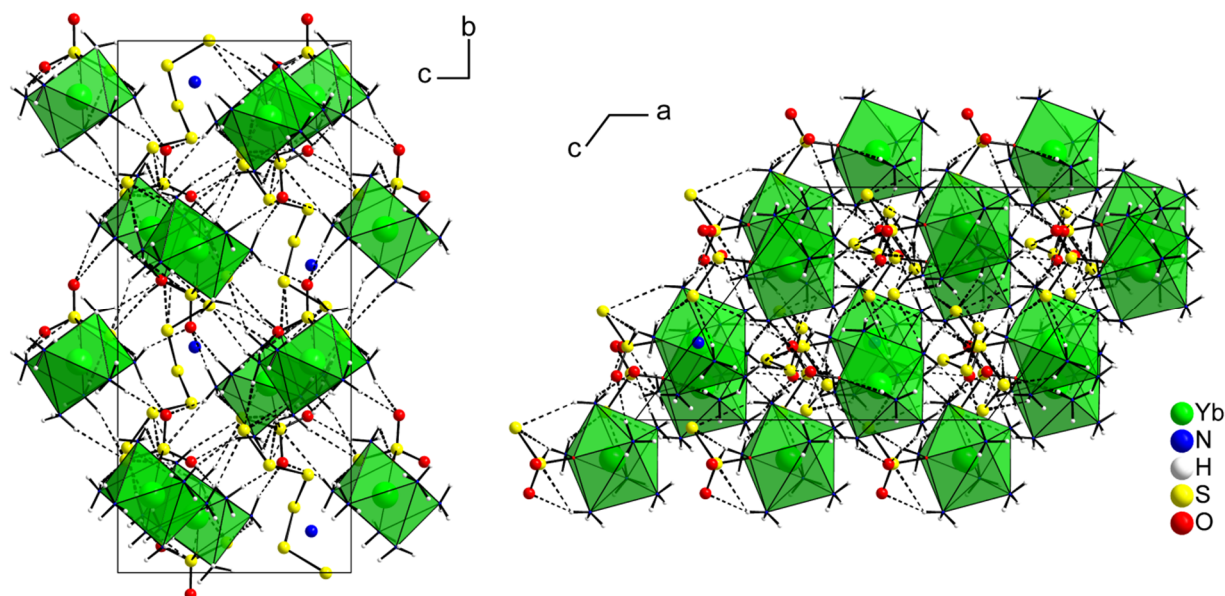
Figure 29: A view of the unit cell of $[Yb(NH_3)_7(S_2O_3)]_2(S_6)\cdot NH_3$ along the crystallographic *a*-axis (left) and along the crystallographic *b*-axis (right). All atoms are drawn with arbitrary radii. Hydrogen bonds are drawn with dashed lines.

**Table 9**: Ionic radii [74] of selected lanthanoid ions for the coordination numbers 8 and 9.

Ion	Coordination Number	Radius / Å
Sm^{3+}	8	1.219
	9	1.272
Eu^{3+}	8	1.206
	9	1.260
Er^{3+}	8	1.144
	9	1.202
Yb^{3+}	8	1.125
	9	1.182

In Table 9 the ionic radii of the lanthanoid ions used in course of this work are listed. The two smaller ions Er^{3+} and Yb^{3+} preferred in their homoleptic ammine complexes the coordination number 8 in comparison to Eu^{3+} and Sm^{3+} with coordination number 9. Elemental europium and ytterbium are soluble in liquid ammonia similar to the alkaline earth metals due to the formation of bivalent metal ions and solvated electrons [75] (Equation 2). Gradual removal of ammonia leds to the formation of a solid solutions containing hexaammoniates $[M(NH_3)_6]$ (with M = Eu or Yb) [76]. The results of this work presented so far show that the intermediary $[M(NH_3)_n]^{2+}$ complexes in the liquid phase probably contain more ammine ligands than expected from their solid solutions.

$$M_{(s)} \xrightarrow{\text{liq. } NH_3} M^{2+}_{(NH_3)} + 2\, e^{-}_{(NH_3)}, \text{ for M = Eu or Yb}$$
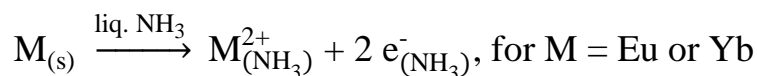
Equation 2: Dissolution of Eu or Yb in liquid ammonia.

In all experiments, a dark blue solution was formed on dissolution of the metal. The blue color originates from the solvated electrons and is also caused by the main species formed by the dissolution of sulfur in liquid ammonia, the $S_3^{\cdot-}$ radical [77]. The reaction sequence for the formation of $S_3^{\cdot-}$ radicals in liquid ammonia is schematically shown in Figure 30. Starting with a nucleophilic cleavage of the cyclic S_8, the intermediate $H_2NS_8^-$ will be degraded to S_7N^- and H_2S. The hydrogen sulfide reacts with ammonia and sulfur forming ammonium polysulfides.

In the last step the polysulfides form the $S_3^{\cdot-}$ radical by dissociation or disproportionation. This reaction scheme is based on different spectroscopic methods and describes one possible pathway.

$$H_2N^- + S_8 \longrightarrow H_2NS_8^- \longrightarrow S_7N^- + H_2S \xrightarrow{NH_3, S} (NH_4)_2S_x \longrightarrow S_3^{\cdot-}$$

$$\downarrow$$

$$S_4N^- + 3S$$
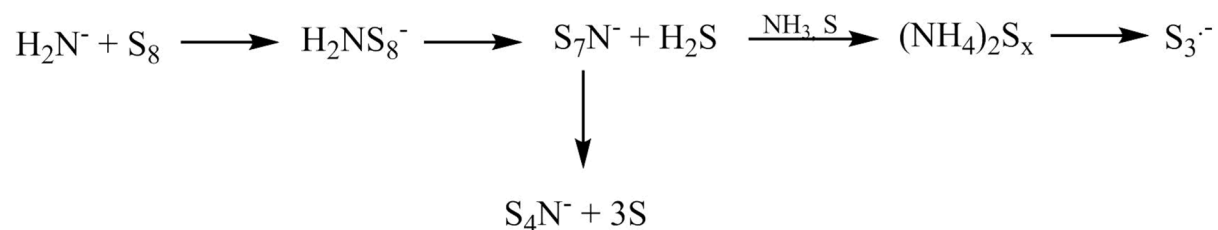
Figure 30: Forming mechanism scheme for the $S_3^{\cdot-}$ radical in liquid ammonia. The scheme is taken from the literature [78] and slightly modified.

The resulting reaction products presented in the chapters 3.1.1-4 show that the $S_3^{\cdot-}$ radicals are capable to oxidize Eu^{2+} and Yb^{2+} to the oxidation state +III while being reduced to a polysulfide with two negative charges. Whether the formation of $[Sm(NH_3)_9]_2(S_5)_3 \cdot 2NH_3$ and $[Er(NH_3)_8]_2(S_5)_2(S_6) \cdot 3NH_3$ follows the same pathway as described for $[Eu(NH_3)_9]_2(S_5)_3 \cdot 2NH_3$ and $[Yb(NH_3)_9]_2(S_5)_2(S_4) \cdot 4NH_3$ is not known. No literature exists dealing with the dissolution of Er and Sm in ammonia under supercritical conditions.

3.1.5 [Eu(NH$_3$)$_9$]$_2$(Se$_2$)$_2$(Se$_3$)

The compound [Eu(NH$_3$)$_9$]$_2$(Se$_2$)$_2$(Se$_3$) is of dark-red color and forms rod-shaped crystals. It crystallizes in the centric space group $P2_1/c$ with the lattice parameters are a = 15.2468(3) Å, b = 15.8655(3) Å, c = 13.7139(3) Å and β = 101.8530(10) °. The crystal structure contains homoleptic europium ammine complexes with the europium coordinated by nine ammine ligands. The positions of the hydrogen atoms of the ammine ligands were not found in the difference *Fourier* map. They were placed on geometrically calculated positions and refined by using the riding model. The EuN$_9$ coordination polyhedron can be described as capped square antiprism (C_{4v}) or as tricapped trigonal prism (D_{3h}). A calculation of the continuous shape measure with the program SHAPE gives a deviation from an ideal capped square antiprism of 0.107 % and a deviation of 1.101 % from an ideal tricapped trigonal prism (Table 10). So the capped square antiprism is the best choice to describe the coordination polyhedron. The Eu-N distances in the [Eu(NH$_3$)$_9$]$^{3+}$ complex range between 2.55 Å and 2.67 Å. This is comparable to the [Eu(NH$_3$)$_9$]$^{3+}$ complex in the polysulfide structure discussed in the chapter 3.1.1 above. In the crystal structure, two different polyselenides are present.
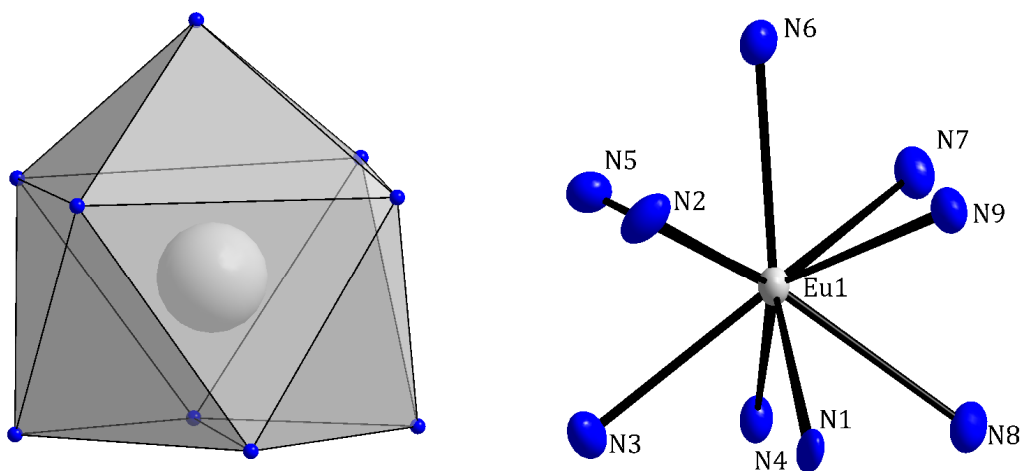
Figure 31: Coordination polyhedron of Eu^{3+} in the structure of [Eu(NH$_3$)$_9$]$_2$(Se$_2$)$_2$(Se$_3$). Displacement ellipsoids represent a probability of 50 %. Hydrogen atoms bound to the N atoms of the ammonia ligands are omitted for clarity.

Table 10: Result of the continuous shape measure calculation of the EuN$_9$ polyhedron in the structure of [Eu(NH$_3$)$_9$]$_2$(Se$_2$)$_2$(Se$_3$).

Ideal Shape	CShM / % (EuN$_9$ polyhedron)
EP-9	37.429
OPY-9	22.400
HBPY-9	19.396
JTC-9	16.372
CCU-9	9.523
CSAPR-9	**0.107**
TCTPR-9	1.101

One of the present polyselenide anions in this crystal structure has the simplest polychalcogenide motif, a dumbbell unit of (Se$_2$)$^{2-}$. The (Se$_2$)$^{2-}$ unit is isoelectronic to Br$_2$ with 14 valence electrons. Therefore, the (Se$_2$) dumbbell has two negative charges. The length of the Se-Se bond in the dumbbell amounts to 2.38 Å. This is the same Se-Se bond length as observed in Na$_2$Se$_2$ [79]. The second polyselenide motif present in this structure is a (Se$_3$)$^{2-}$ unit. The angle in this bent chain is 110.1 ° and therefore close to the expected angle of 109.5 ° according to the VSEPR model. The Se-Se bonds of 2.34 Å and 2.36 Å are normal Se-Se bonds (2 x r$_{Se}$ = 2.34 Å [74]). There are no interactions between the polyselenide chains in this crystal structure. The nearest Se···Se contact (4.47 Å) is much longer than twice the *van-der-Waals* radius of selenium (2r$_{vdw}$ = 3.80 Å).
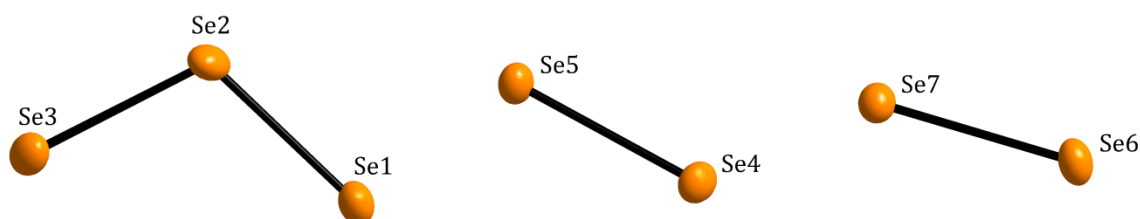
Figure 32: The three independent polyselenides in the structure of [Eu(NH$_3$)$_9$]$_2$(Se$_2$)$_2$(Se$_3$). The displacement ellipsoids represent a probability of 50%.

There are some short N-H···Se contacts with H···Se distances below 2.9 Å in the crystal structure indicating the presence of hydrogen bonding in the structure. The hydrogen bonds

stabilize the polyselenide ions and connect them to the cationic ammine complexes. In Figure 33 the unit cell is shown in projections along the crystallographic a-axis and the crystallographic c-axis. The hydrogen bonds are depicted as thin dotted lines. The $[Eu(NH_3)_9]^{3+}$ complexes are arranged in rods that are running parallel to the crystallographic a-axis. These rods are connected via hydrogen bonds to the polysulfide anions located in between the cationic rods.
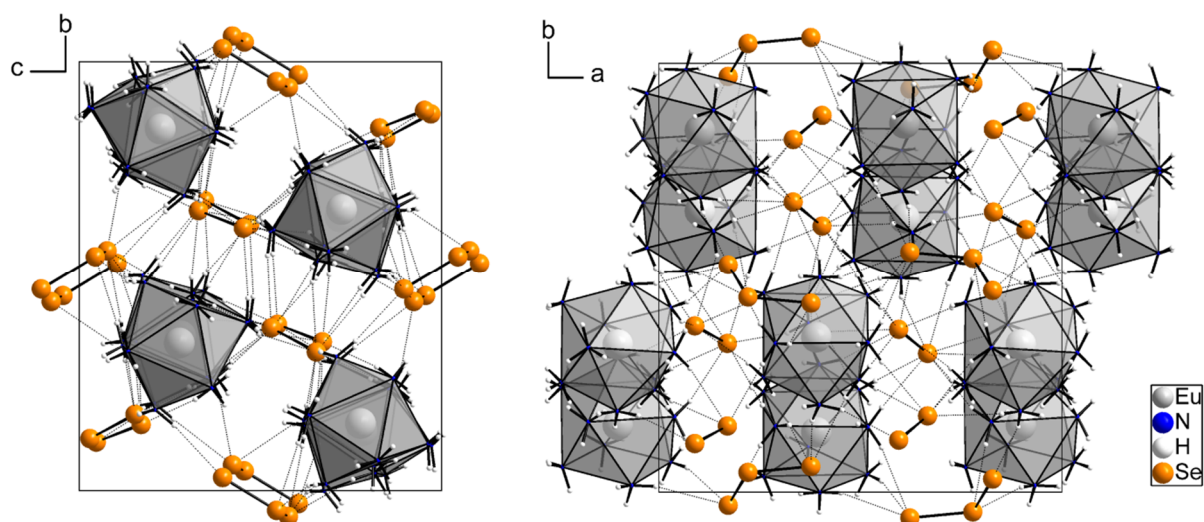
Figure 33: View of the unit cell of the structure of $[Eu(NH_3)_9]_2(Se_2)_2(Se_3)$ along the crystallographic a-axis (left) and along the crystallographic c-axis (right). All atoms are drawn as spheres with arbitrary radii.

Table 11: Interatomic distances within the $[Eu(NH_3)_9]^{3+}$ complexes and within the polyselenides in the structure of $[Eu(NH_3)_9]_2(Se_2)_2(Se_3)$.

Atoms	Bond length/ Å	Atoms	Bond length/ Å
Eu(1) - N(3)	2.575(9)	Eu(1) - N(7)	2.634(9)
Eu(1) - N(9)	2.586(9)	Eu(1) - N(5)	2.634(9)
Eu(1) - N(1)	2.587(9)	Se(1) - Se(2)	2.3604(17)
Eu(1) - N(4)	2.605(9)	Se(2) - Se(3)	2.3411(16)
Eu(1) - N(2)	2.605(10)	Se(4) - Se(5)	2.3786(15)
Eu(1) - N(8)	2.618(9)	Se(6) - Se(7)	2.3834(15)
Eu(1) - N(6)	2.628(9)		

3.1.6 [Sr(en)$_4$](Te$_3$)

Crystals with the composition [Sr(en)$_4$](Te$_3$) have a needle-shaped habitus and are of dark red appearance (Figure 34). The compound crystallizes in the monoclinic space group $P2_1/n$ with the lattice parameters $a = 9.0927(6)$ Å, $b = 13.5636(9)$ Å, $c = 17.7260(8)$ Å and $\beta = 95.569(4)$ °. The structure of consists of cationic strontium ethylenediamine complexes and anionic (Te$_3$)$^{2-}$ units in the ratio 1:1.

Figure 34: Image of a crystal with the composition [Sr(en)$_4$](Te$_3$) immersed in perfluorinated oil.

Strontium is surrounded by four ethylenediamine ligands forming a SrN$_8$ coordination polyhedron which is best described as twofold-capped trigonal prism (C_{2v}) (Figure 35). A continuous shape measure calculation gives a deviation of 1.545 % from the ideal shape (Table 12). The positions of the hydrogen atoms of the ethylenediamine ligands were not found in the difference *Fourier* map. They were placed on geometrically calculated positions and refined by using the riding model. The bond lengths between Sr^{2+} and the coordinating N atoms range between 2.69 Å and 2.77 Å. Hence, they are similar to Sr-N bond lengths found in other strontium amine complexes, as in the structure of [Sr(thd)(triethylenetetramine)] [80].
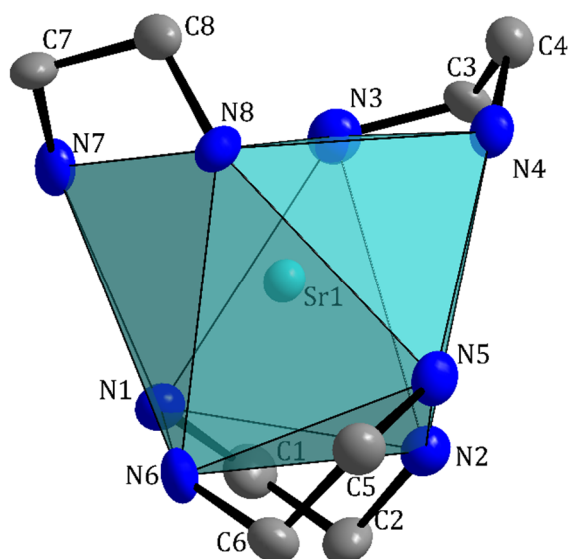
Figure 35: Coordination polyhedron of Sr^{2+} in the structure of $[Sr(en)_4](Te_3)$. The displacement ellipsoids represent a probability of 50 %. All hydrogen atoms are omitted for clarity.

Table 12: Result of the continuous shape measure of the SrN_8 polyhedron in the structure of $[Sr(en)_4](Te_3)$.

Ideal Shape	CShM / % (SrN₈ polyhedron)
OP-8	32.987
HPY-8	23.461
HBPY-8	15.133
CU-8	10.263
SAPR-8	2.718
TDD-8	2.212
BTPR-8	**1.545**

The anion in the presented structure is a polytelluride composed of three tellurium atoms (Figure 36). The (Te_3) unit is twofold negatively charged with each terminal tellurium atom formally carrying one negative charge. According to the VSEPR theory, Te2 is an AX_2E_2 type atom, where A represents the central atoms, X are bonding electron pairs and E are free electron pairs located on the central atom A. Therefore, the bent (Te_3) unit in the structure of $[Sr(en)_4]Te_3$ follows the expectation with a Te-Te-Te angle of 110.5 °. The interatomic distances Te1-Te2 and Te2-Te3 are well comparable with twice the covalent single bond radius

of tellurium ($2r_{Te} = 2.74$ Å). The smallest intermolecular distance between two $(Te_3)^{2-}$ units amounts to 5.80 Å and is therefore longer than twice the *van-der-Waals* radius of tellurium. Interactions between neighboring $(Te_3)^{2-}$ ions have not to be considered.
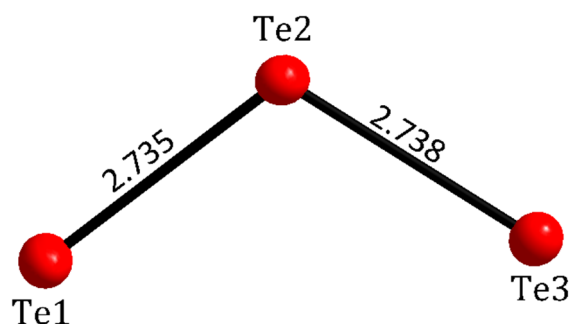
Figure 36: The Te_3^{2-} ion in the structure of $[Sr(en)_4](Te_3)$. Bond lengths are given in Å. The displacement ellipsoids represent a probability of 50 %.

In Figure 37 the unit cell of the crystal structure is depicted. The unit cell contains four formula units. All atoms are placed on a general site with the *Wyckhoff* position 4*e*. The structure can not be derived from a simple salt structure type.
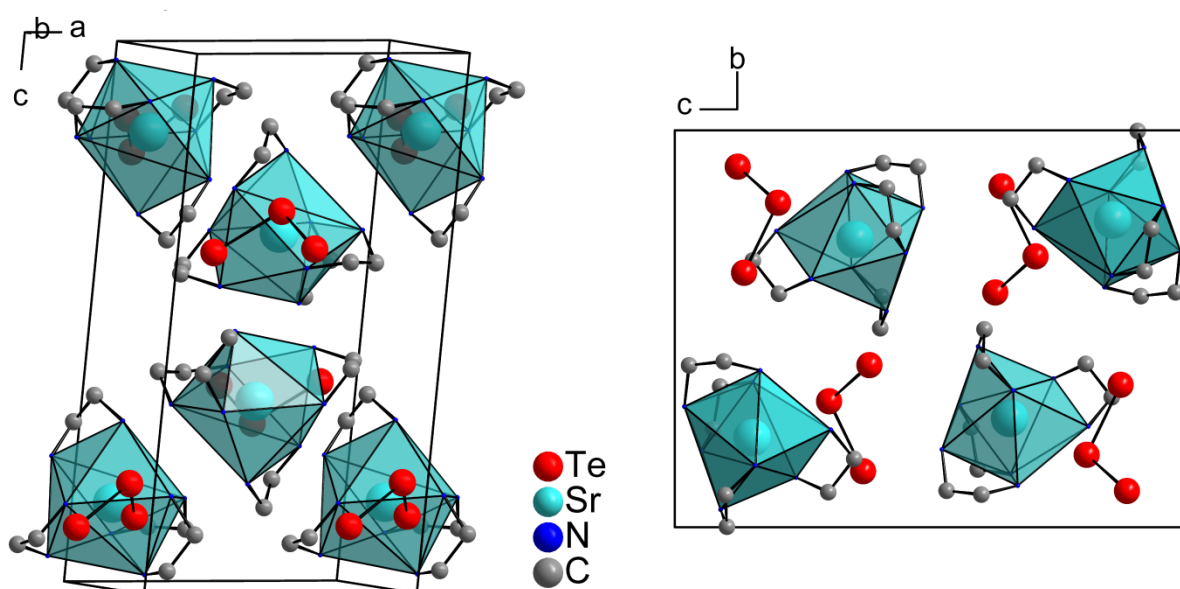
Figure 37: A view of the unit cell of the structure $[Sr(en)_4](Te_3)$ (left) and a view on the unit cell along the crystallographic *a*-axis. All atoms are drawn as spheres with arbitrary radii. Hydrogen atoms bound to the C and N atoms of the ethylenediamine ligands are omitted for clarity.

3.1.7 [Eu(NH₃)₉]₂(Te₄)₃, [Ba(NH₃)₈](Te₄) and [Ca(en)₄](Te₄)·0.5en

[Eu(NH$_3$)$_9$]$_2$(Te$_4$)$_3$ crystallizes in the triclinic space group $P\bar{1}$ with the lattice parameters $a = 10.6034(3)$ Å, $b = 13.3138(2)$ Å, $c = 16.5630(5)$ Å, $\alpha = 90.265(2)°$, $\beta = 104.4930(10)°$ and $\gamma = 90.493(2)°$. The lattice parameters show that the structure is close to the monoclinic crystal system. The platelet-shaped crystals are of a dark red appearance. [Ba(NH$_3$)$_8$](Te$_4$) crystallizes in the monoclinic space group $P\,2_1/c$ with the lattice parameters $a = 11.3006(4)$ Å, $b = 25.5827(10)$ Å, $c = 13.5640(5)$ Å and $\beta = 90.023(2)°$. Crystals of [Ba(NH$_3$)$_8$](Te$_4$) have a platy crystal habit and are of black metallic appearance. The investigated crystal of [Ba(NH$_3$)$_8$](Te$_4$) was a twin with one domain rotated by 180° around the crystallographic c-axis. The ratio of the twinned domains was refined to 73.4 : 26.6. Like the crystals of [Ba(NH$_3$)$_8$](Te$_4$), crystals of [Ca(en)$_4$](Te$_4$)·0.5en have a platy crystal habit and are of black metallic appearance. [Ca(en)$_4$](Te$_4$)·0.5en crystallizes in the orthorhombic space group $Pbca$ with the lattice parameters $a = 16.7867(4)$ Å, $b = 17.0564(7)$ Å and $c = 17.1660(7)$ Å. All three compounds are not stable against exposition to air and can not be handled at room temperature.

All three crystal structures have Te$_4$ polytelluride chains as the common structural motif. As cations in the structures, divalent or trivalent ions coordinated by solvent molecules of ammonia or ethylenediamine are present. Eu and Ba are coordinated by ammonia forming homoleptic ammine complexes. Eu is surrounded by nine ammonia molecules whereas Ba is surrounded by eight ammonia molecules. The coordination polyhedra of the two independent Eu complexes can best be described as capped square antiprisms (C_{4v}). A continuous shape measure shows a deviation from the ideal shape amounting to 0.250 % and 0.394 % respectively (Table 13). In Figure 38, the coordination of both independent Eu atoms and the coordination polyhedron of Eu1 is exemplarily shown. The coordination polyhedron of Eu2 is not shown since it is almost identical to the one of Eu1. The Eu-N bond lengths range from 2.56 Å to 2.66 Å. These bond lengths are typical for europium ammine complexes with europium in oxidation state +III. A continuous shape measure of the coordination polyhedra of both BaN$_8$ polyhedra (Figure 39) results in different ideal shapes as the respective best description. The Ba(1)N8 polyhedron is best described as twfold-capped trigonal prism (C_{2v}) with a deviation from the ideal shape amounting to 1.330 %. For the Ba(2)N$_8$ polyhedron a triangular dodecahedron (D_{2d}) is the best description with a deviation amounting to 1.361 %. The interatomic distances between Ba and N within the ammine complexes range from 2.82 Å to 2.99 Å. The displacement ellipsoid of N6 came out as very small and not spherically shaped. An explanation could be falsified data

because of absorption effects. Due to the twinning, the absorption correction could not be carried out in a satisfying way.

In [Ca(en)$_4$](Te$_4$)·0.5en, Ca is surrounded by 4 en ligands and has the coordination number 8. The resulting coordination polyhedron can be best described as triangular dodecahedron (D_{2d}) for all four possibilities resulting from the disorder. The deviations from the ideal shape, which were calculated via a continuous shape measures and range between 0.786 % and 1.186 %. The Ca-N bond lengths are between 2.46 Å and 2.66 Å are typical for bond lengths in calcium ethylene diamine complexes. Two of the en ligands are disordered. The occupation factors were refined to 61.4 : 38.6 (C2B/N2B:C2A/N2A) and 71.7 : 28.3 (C4A/N4A:C4B/N4B).

In all three crystal structures, the positions of the hydrogen atoms of the ammine ligands or the ethylene diamine ligands, respectively, were not found in the difference *Fourier* map. They were placed on geometrically calculated positions and refined by using the riding model.
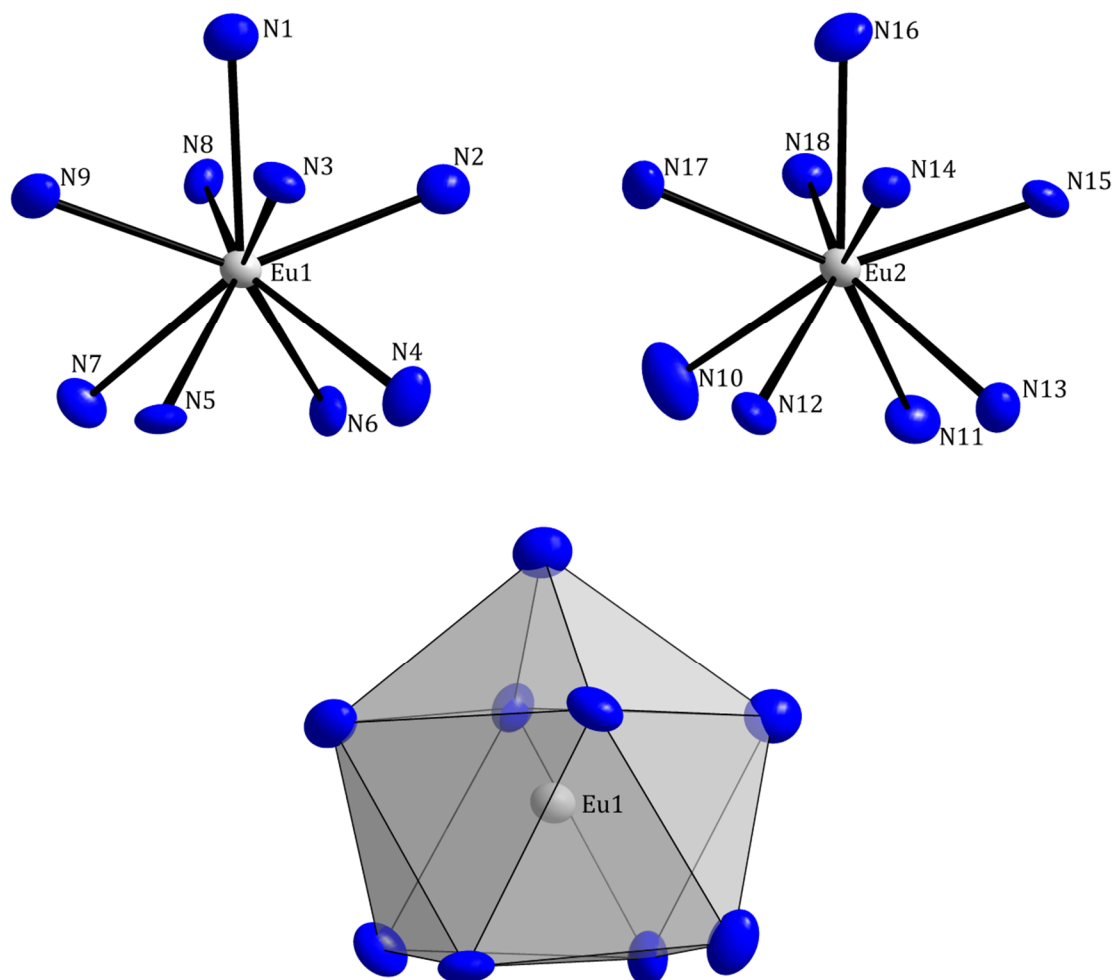
Figure 38: Coordination of Eu1 and Eu2 and the respective coordination polyhedron of Eu1 in the structure of [Eu(NH$_3$)$_9$]$_2$(Te$_4$)$_3$. The displacement ellipsoids represent a probability of 50 %. The hydrogen atoms bound to the N atoms of the ammonia ligands are omitted for clarity.
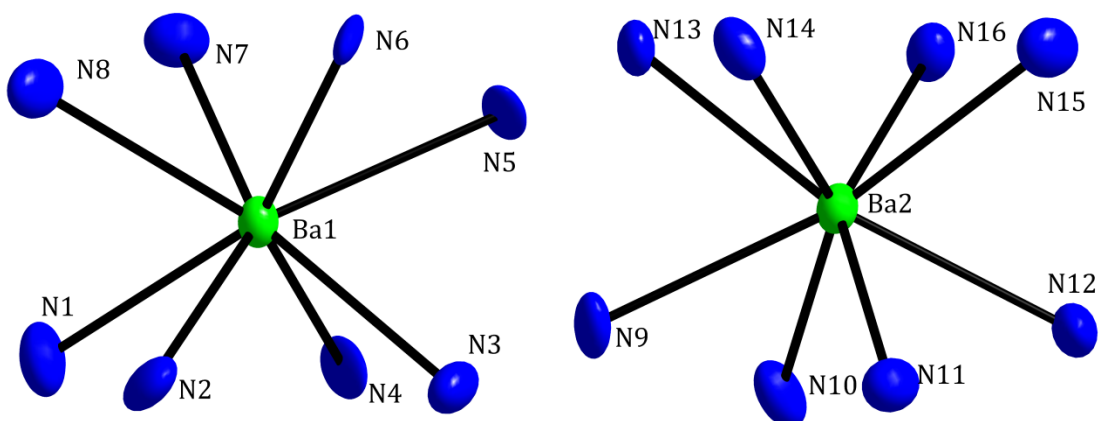
Figure 39: Coordination of Ba^{2+} in the structure of $[Ba(NH_3)_8](Te_4)$. The displacement ellipsoids represent a probability of 50 %. The hydrogen atoms bound to the N atoms of the ammonia ligands are omitted for clarity.
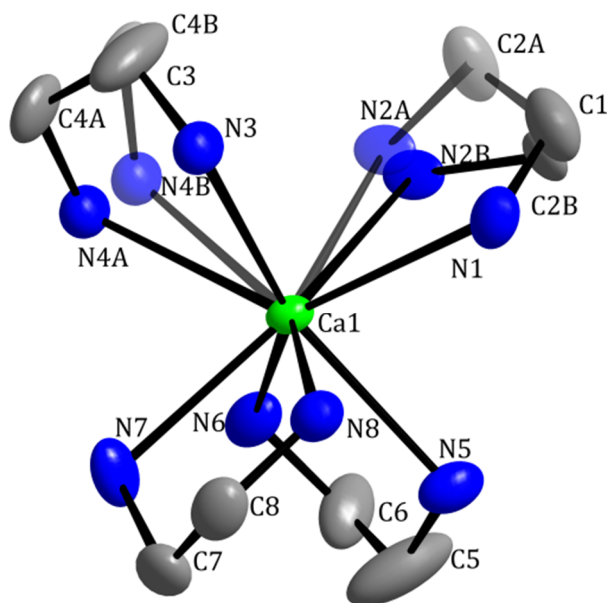
Figure 40: Coordination of Ca^{2+} in the structure of $[Ca(en)_4](Te_4) \cdot 0.5en$. The displacement ellipsoids represent a probability of 50%. Atoms N2A/C2A and N4B/C4B are drawn in transparent mode and represent a disordering of 38.6% and 28.3%, respectively. The hydrogen atoms bound to the C and N atoms of the ethylene diamine ligands are omitted for clarity.

Table 13: Results of the continuous shape measures of the EuN_9 polyhedra in the structure of $[Eu(NH_3)_9]_2(Te_4)_3$.

Ideal Shape	CShM / % (Eu(1)N₉ polyhedron)	CShM / % (Eu(2)N₉ polyhedron)
EP-9	37.205	36.933
OPY-9	22.313	22.611
HBPY-9	20.106	19.739
JTC-9	16.085	15.799
CCU-9	8.830	9.103
CSAPR-9	**0.250**	**0.394**
TCTPR-9	0.565	0.508

Table 14: Results of the continuous shape measures of the BaN_8 polyhedra in the structure of $[Ba(NH_3)_8](Te_4)$ and of the CaN_8 polyhedron in the structure of $[Ca(en)_4](Te_4)\cdot0.5en$.

Ideal Shape	CShM / % (Ba(1)N₈ polyhedron)	CShM / % (Ba(2)N₈ polyhedron)	CShM / % (Ca(1)N₈ polyhedron)
OP-8	31.665	32.857	33.055
HPY-8	23.007	22.363	23.943
HBPY-8	13.904	14.170	16.650
CU-8	9.583	9.408	11.551
SAPR-8	1.589	1.671	2.953
TDD-8	1.448	**1.361**	**0.786**
BTPR-8	**1.330**	1.559	2.495

The anionic part in these three crystal structures are $(Te_4)^{2-}$ units. All $(Te_4)^{2-}$ units can be described as oligomeric zigzag chains that are twofold negatively charged. Figure 41, Figure 42 and Figure 43 show the independent polytelluride chains of the structures. In the structure of $[Eu(NH_3)_9]_2(Te_4)_3$, all Te-Te bond lengths are between 2.73 Å and 2.76 Å. These distances compare well with twice the covalent radius of Te, $2\cdot r_{Te} = 2.74$ Å. The dihedral angles within the polytelluride chains in $[Eu(NH_3)_9]_2(Te_4)_3$ are all between 83.1 and 86.9°. Therefore, they indicate the gauche conformation of these anions. The closest intermolecular Te···Te distance amounts to 3.751 Å. Therefore, this and other intermolecular distances (3.762 Å – 3.824 Å) are shorter than twice the *van-der-Waals* radius of Te, $2\cdot r_{vdW}(Te) = 4.12$ Å. Taking these

interactions into account would lead to a three-dimensional polytelluride network. The resulting polytelluride did not show any similarities to other published polytellurides and would contain very small Te-Te-Te angles of 64.75 ° and 67.19 ° that are chemically not reasonable. However, the consideration as isolated $(Te_4)^{2-}$ units led to a crystallographic and chemical reasonable result.

In contrast to the isolated $(Te_4)^{2-}$ units in the structure of $[Eu(NH_3)_9]_2(Te_4)_3$, intermolecular interactions have to be considered in the structures of $[Ca(en)_4](Te_4) \cdot 0.5en$ and $[Ba(NH_3)_8](Te_4)$. The present intermolecular Te···Te distances amount to 3.55 Å and 3.56 Å in $[Ba(NH_3)_8](Te_4)$ and to only 3.28 Å in $[Ca(en)_4](Te_4) \cdot 0.5en$, respectively. These noncovalent interactions lead to chain formations in both structures (Figure 44 and Figure 45). The Te7-Te8-Te3 and Te3-Te4-Te7[i] angles in $[Ba(NH_3)_8](Te_4)$ as well as the Te2-Te1-Te4[i] angle in $[Ca(en)_4](Te_4) \cdot 0.5en$ are close to linearity, ranging from 168° to 170°. Hence, Te8 and Te4 in $[Ba(NH_3)_8](Te_4)$ and Te1 in $[Ca(en)_4](Te_4) \cdot 0.5en$ are partially hypervalent. Beside the bond length between Te1 and Te2 (2.84 Å) in the crystal structure of $[Ca(en)_4](Te_4) \cdot 0.5en$, all Te-Te bond lengths within the covalently bound $(Te_4)^{2-}$ units are between 2.72 Å and 2.76 Å. The slightly elongated bond length is caused by a bonding interaction between Te1 and Te4 of the adjacent polytelluride chain. The dihedral angles within the polytelluride chains in the structure of $[Ca(en)_4](Te_4) \cdot 0.5en$ and $[Ba(NH_3)_8](Te_4)$ range between 97.6 and 100°. Hence, they are in gauche conformation.

In 2013 *Kysliak* published the non isotypic crystal structure of $[Mn(NH_3)_6]Te_4$ [58] containing a $(Te_4)^{2-}$ unit that is very similar to those found in $[Ca(en)_4](Te_4) \cdot 0.5en$. The $(Te_4)^{2-}$ unit in $[Mn(NH_3)_6](Te_4)$ also has one slightly elongated bond length within the chain of 2.87 Å beside two typical Te-Te bond lengths of 2.76 Å and 2.75 Å. The torsion angle of 99.9 ° indicates gauche conformation and a noncovalent intermolecular interaction amounting to 3.25 Å leads to chain formation.

In the described crystal structures the size of the cationic complex correlates with the intermolecular Te···Te distances in inverse proportion. Therefore, in Figure 49 a spherical approximation to the size of the cationic complexes is shown. Although the structures described here support the thesis that the intermolecular Te···Te distances are adjustable with the size of the cationic complexes, the structure of $[Mn(NH_3)_6](Te_4)$ shows that there have to be additional reasons as well e.g. packing effects.
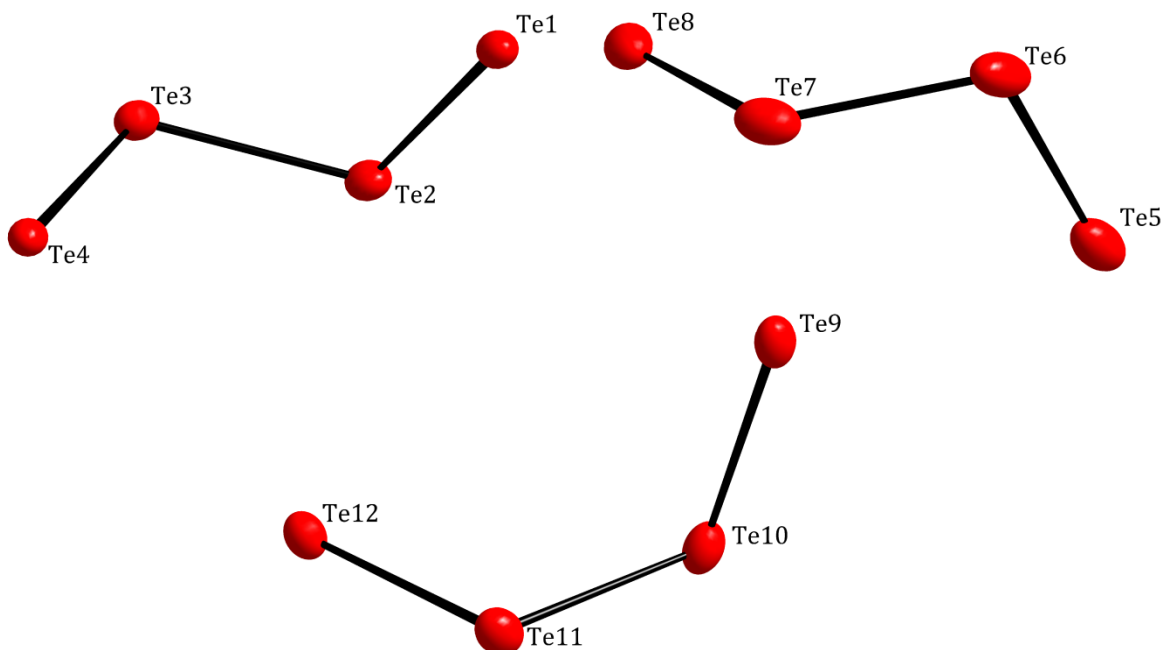
Figure 41: The three independent polytelluride chains in the structure of [Eu(NH$_3$)$_9$]$_2$(Te$_4$)$_3$. The displacement ellipsoids represent a probability of 50%.

Table 15: Bond lengths within the polytelluride chains in the structure of [Eu(NH$_3$)$_9$](Te$_4$)$_3$.

Atoms	Bond length/ Å	Atoms	Bond length/ Å	Atoms	Bond length/ Å
Te1-Te2	2.746(1)	Te5-Te6	2.731(2)	Te9-Te10	2.743(2)
Te2-Te3	2.757(1)	Te6-Te7	2.751(2)	Te10-Te11	2.754(1)
Te3-Te4	2.747(2)	Te7-Te8	2.732(2)	Te11-Te12	2.742(1)
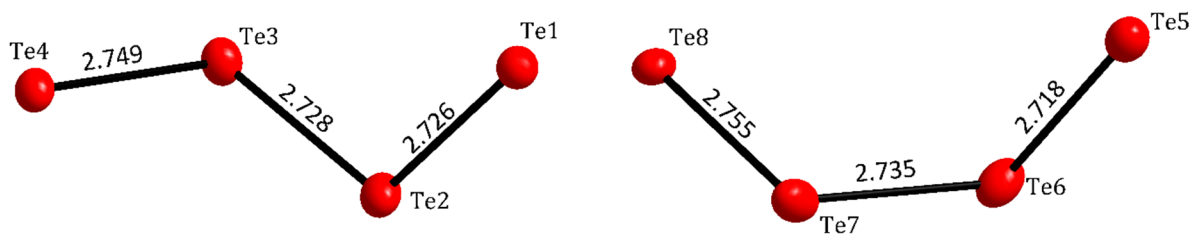
Figure 42: The two independent polytelluride chains in the structure of [Ba(NH$_3$)$_8$](Te$_4$). Bond lengths are given in Å. The displacement ellipsoids represent a probability of 50%.
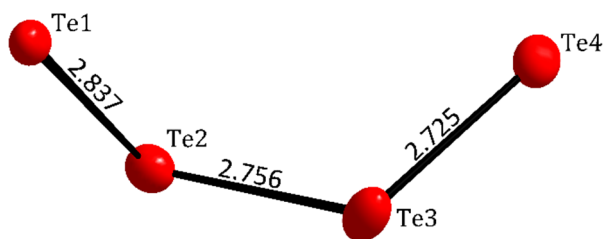
Figure 43: The polytelluride chain in the structure of [Ca(en)$_4$](Te$_4$)·0.5en. Bond lengths are given in Å. The displacement ellipsoids represent a probability of 50%.
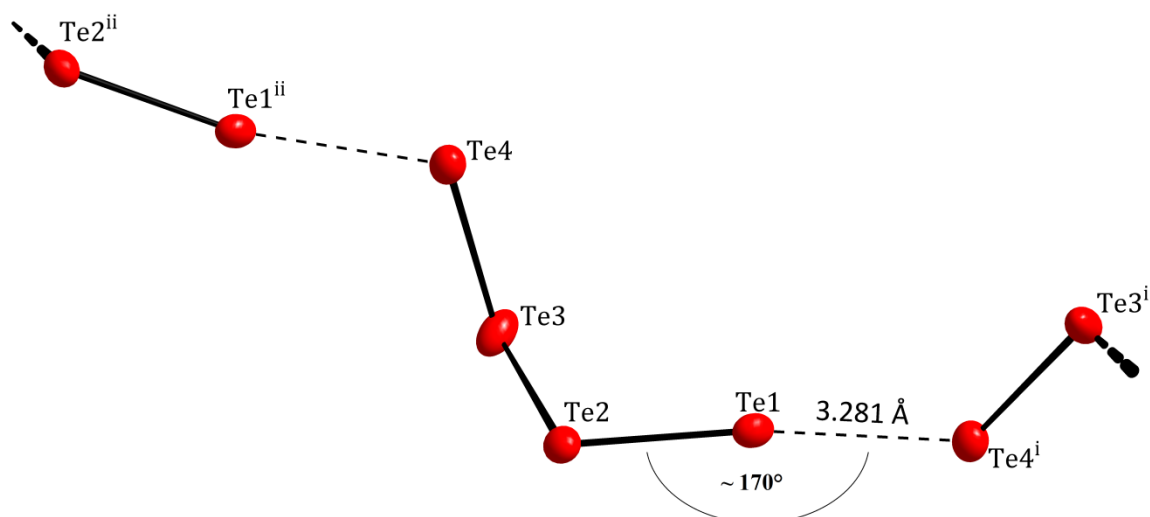
Figure 44: The chain formation between individual $(Te_4)^{2-}$ anions in the structure of $[Ca(en)_4](Te_4) \cdot 0.5en$. The displacement ellipsoids represent a probability of 50 %. The indices *i* indicate the following symmetry operations: (*i*) $^3/_2$-*x*, -$^1/_2$+*y*, *z* (*ii*) $^3/_2$-*x*, $^1/_2$+*y*, *z*.
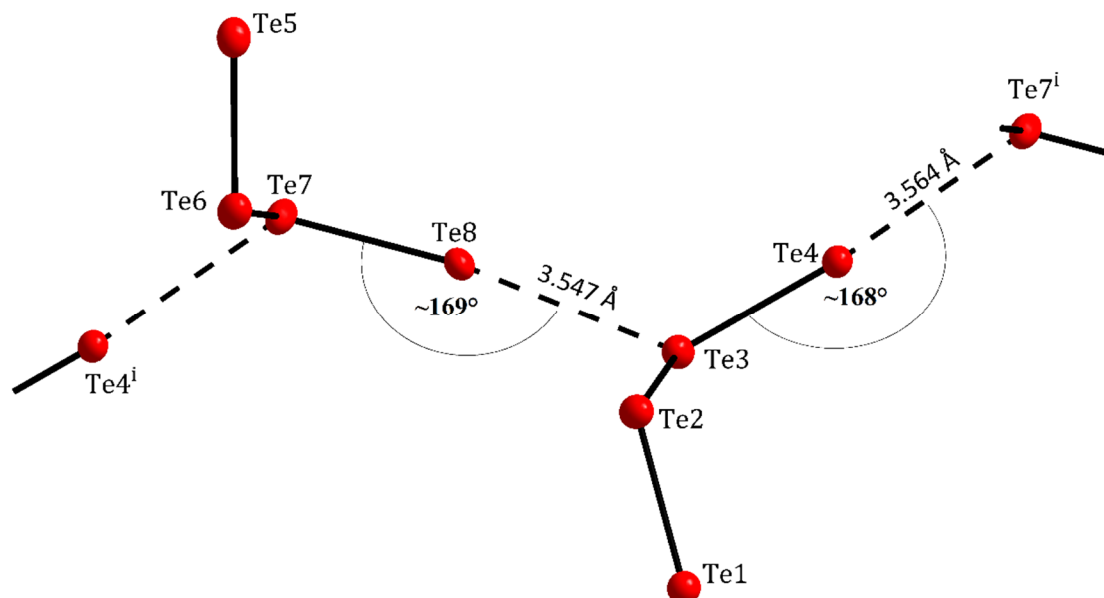
Figure 45: The chain formation of individual $(Te_4)^{2-}$ anions in the structure of $[Ba(NH_3)_8]Te_4$. The displacement ellipsoids represent a probability of 50 %. The index *i* indicates the following symmetry operation: -1+*x*, *y*, *z*.

Figure 46, Figure 47 and Figure 48 show extended unit cells of the three polytellurides bearing crystal structures. None of these crystal structures can be straightforward derived from a simple salt structure. The polytelluride units are arranged in a way that they can surround the cationic complexes in all three structures. For the structure of $[Ca(en)_4](Te_4) \cdot 0.5en$ can be seen that the infinite polytelluride chains run along the crystallographic *b*-axis. In the structure of $[Ba(NH_3)_8](Te_4)$ the chains run along the crystallographic *a*-axis.
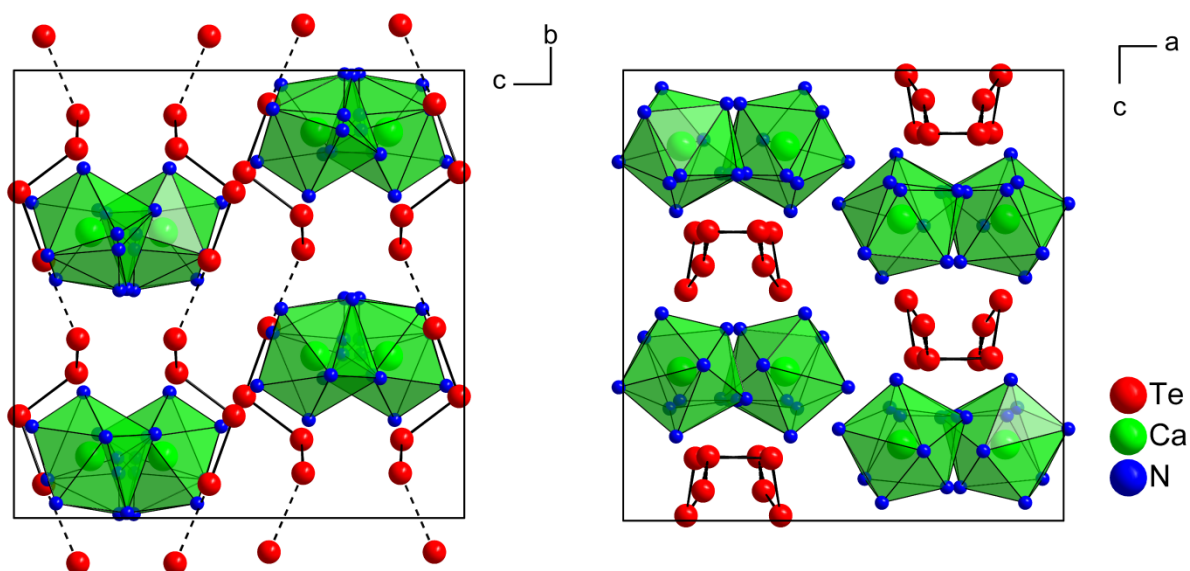
Figure 46: A view of the extended unit cell of [Ca(en)$_4$](Te$_4$)·0.5en along the crystallographic *a*-axis (left) and along the crystallographic *b*-axis (right). All atoms are drawn as spheres with arbitrary radii. The free en molecules, the bridging C atoms of the en ligands and all hydrogen atoms are omitted for clarity. Hypervalent Te-Te interactions are drawn with dashed lines.
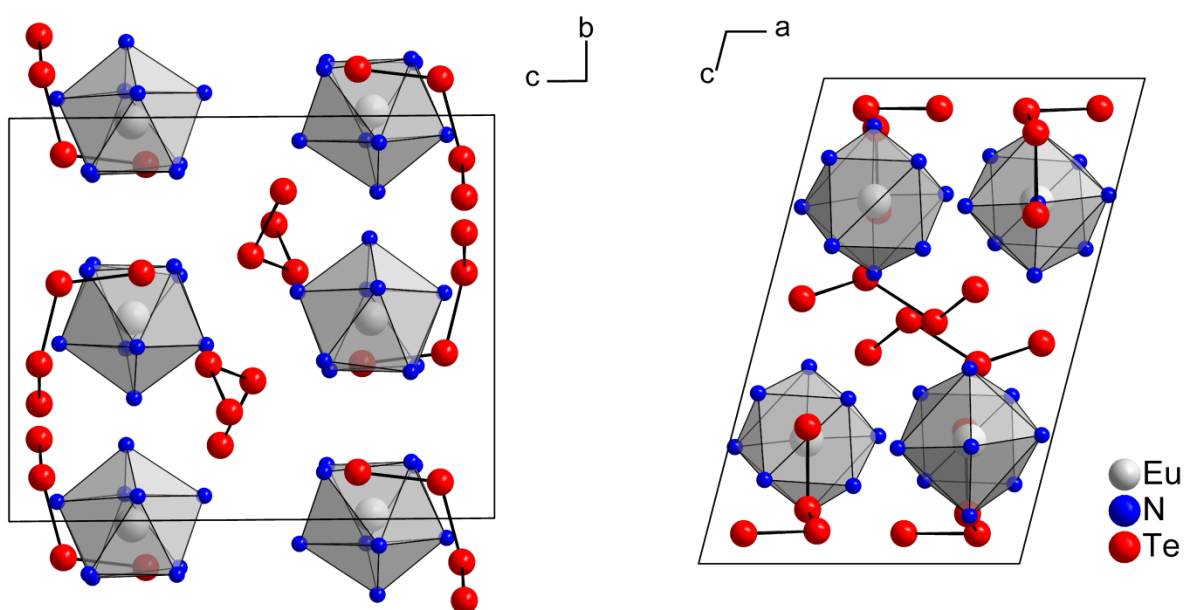
Figure 47: A view of the extended unit cell of [Eu(NH$_3$)$_9$]$_2$(Te$_4$)$_3$ along the crystallographic *a*-axis (left) and along the crystallographic *b*-axis (right). All atoms are drawn as spheres with arbitrary radii. The hydrogen atoms bound to the N atoms of the ammine ligands are omitted for clarity.
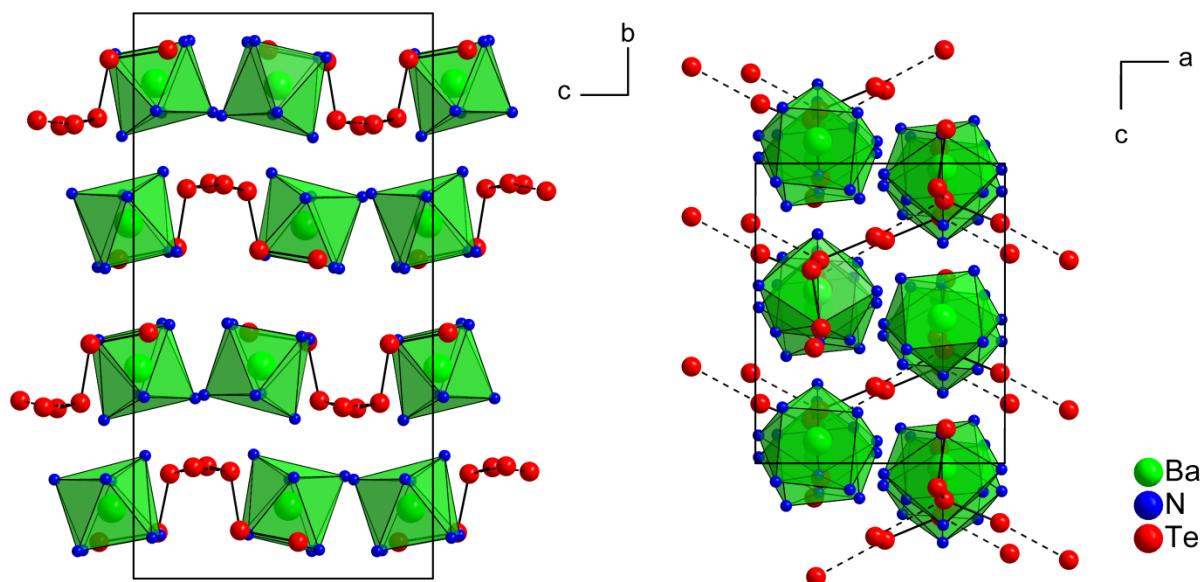
Figure 48: A view on the extended unit cell of [Ba(NH$_3$)$_8$](Te$_4$) along the crystallographic *a*-axis (left) and along the crystallographic *b*-axis (right). All atoms are drawn as spheres with arbitrary radii. The hydrogen atoms bound to the N atoms of the ammine ligands are omitted for clarity. Hypervalent Te-Te interactions are drawn with dashed lines.

| ~3.8 Å | ~3.3 Å | ~2.9 Å | ~2.8 Å |
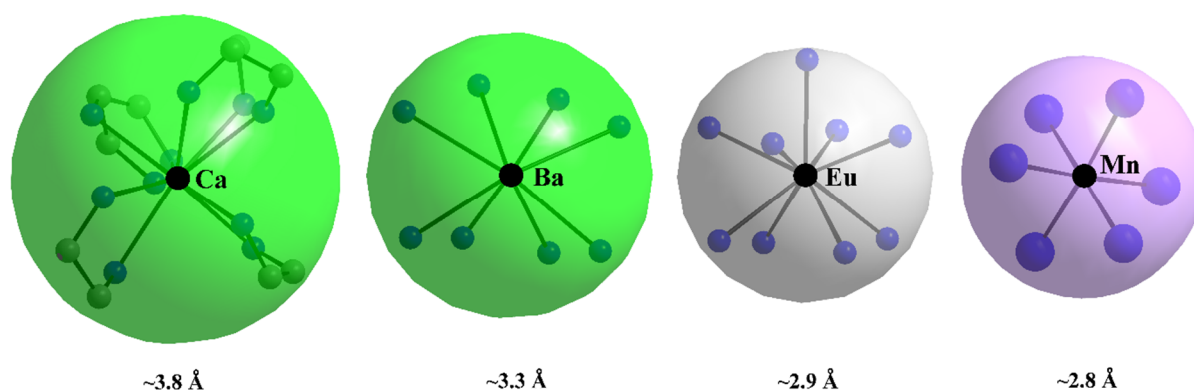
Figure 49: Sherical approximation of the different cationic complexes in the structures of [Ca(en)$_4$](Te$_4$)·0.5en, [Ba(NH$_3$)$_8$](Te$_4$), [Eu(NH$_3$)$_9$]$_2$(Te$_4$)$_3$ and [Mn(NH$_3$)$_6$)](Te$_4$). The approximated spherical radii are shown below the respective complex.

3.1.8 [Yb(NH₃)₈]₄(Te₂₀)(Te₃)₂·2NH₃

The compound with the composition $[Yb(NH_3)_8]_4(Te_{20})(Te_3)_2 \cdot 2NH_3$ crystallizes in the monoclinic space group $P2_1/c$ with the lattice parameters $a = 14.8371(4)$ Å, $b = 20.2111(6)$ Å, $c = 14.6159(4)$ Å and $\beta = 87.547(2)°$. The crystals have a platy crystal habit and are of black metallic appearance. Crystals of $[Yb(NH_3)_8]_4(Te_{20})(Te_3)_2 \cdot 2NH_3$ are not stable against exposition to air and they can not be handled at room temperature.

There are two independent ytterbium atoms in the asymmetric unit (Figure 50). Each is surrounded by eight ammine ligands forming polyhedra that can be best described as square antiprisms. A continuous shape measure shows a deviation from the ideal square antiprism (D_{4d}) that amounts to 0.482 % for the polyhedron of Yb1 and 0.492 % for the polyhedron of Yb2, respectively (Table 16). Both ytterbium atoms are in the oxidation state +III. The Yb^{3+}-N distances verify the oxidation state +III with their lengths ranging between 2.40-2.49 Å. Hence, they are much shorter than those found in ammine complexes with Yb in the oxidation state +II, $d(Yb^{2+}\text{-}N) = 2.61\text{-}2.75$ Å [72]. The positions of the hydrogen atoms of the ammine ligands were not found in the difference *Fourier* map. They were placed on geometrically calculated positions and refined by using the riding model.
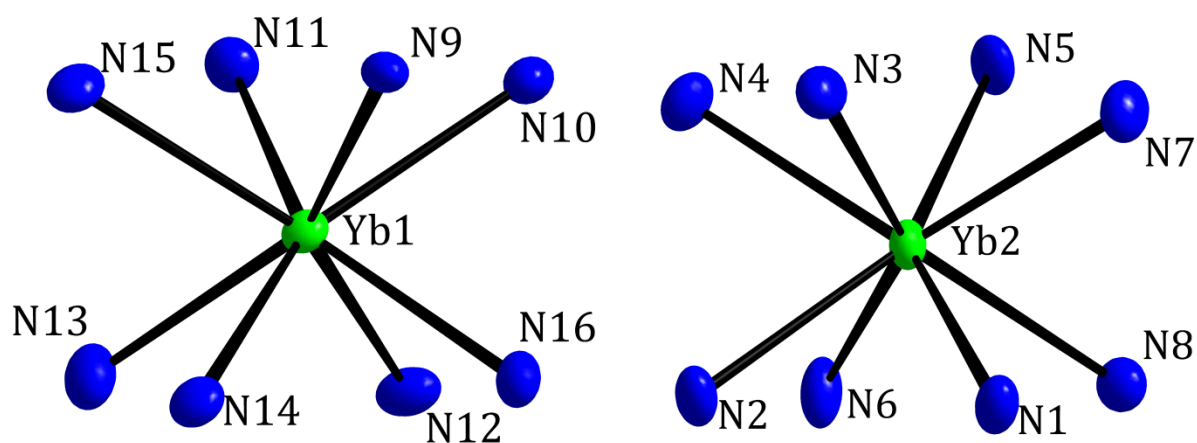
Figure 50: Coordination of Yb^{3+} in the structure of $[Yb(NH_3)_8]_4(Te_{20})(Te_3)_2 \cdot 2NH_3$. The displacement ellipsoids represent a probability of 50 %. The hydrogen atoms bound to the N atoms of the ammonia ligands are omitted for clarity.

Table 16: Results of the continuous shape measures of the YbN_8 polyhedra in the structure of $[Yb(NH_3)_8]_4(Te_{20})(Te_3)_2 \cdot 2NH_3$.

Ideal Shape	CShM / % (Yb(1)N₈ polyhedron)	CShM / % (Yb(2)N₈ polyhedron)
OP-8	30.482	30.483
HPY-8	23.091	23.697
HBPY-8	16.010	16.356
CU-8	8.905	9.540
SAPR-8	**0.482**	**0.492**
TDD-8	1.344	1.481
BTPR-8	2.021	1.592

Beside the ytterbium ammine complexes, the compound contains two different oligomeric polytellurides. One of them is a simple $(Te_3)^{2-}$ chain (Figure 52), which is bent with an angle of 106.3°. Within the $(Te_3)^{2-}$ chain, Te atoms are covalently bound with interatomic distances amounting to 2.75 Å and 2.73 Å.

The second oligomeric polytelluride in the crystal structure is a (Te_{20}) unit with an overall charge of -8. The molecular shaped polytelluride is built up of a centrosymmetric twelve-membered ring, which has two additional (Te_4) chains that are in opposite to each other (Figure 51). The average Te-Te bond length within the (Te_{20}) unit amounts to 2.86 Å, which is about 0.1 A longer than the normal Te-Te single bond length and indicating that not all bonds are classical Te-Te single bonds. Each of the terminal bound atoms Te10 and Te10^i carries one negative charge. All other charges are located on non covalently bound Te atoms. The atoms Te4 and Te4^i are almost linear coordinated by Te9^i and Te5 with an angle of 173.2°. According to the VSEPR model for an AX_2E_3 system, a linear coordination is expected. Therefore, it is formally hypervalently bound in a three center four electron ($4c$-$3e$) bond and carries two negative charges. Ideally, the bonds on the hypervalently bound Te4 are of same length. The found bond lengths between Te4 - Te5 and Te4 - Te9^i amount to 2.86 Å or 3.22 Å, respectively. Therefore, they are not symmetrically bound. Such unsymmetrical hypervalent bonds are present in the anion $[AgTe_7]^{2-}$, with hypervalent Te-Te bonds of 2.87 Å and 3.23 Å [81]. The common polyanion I_3^-, which is isoelectronic to $(Te_3)^{4-}$, has unsymmetrical hypervalent bonds as found in the structure of CsI_3, with I-I bond lengths that amount 2.84 Å and 3.04 Å [82].

The other formally hypervalently bound atoms are Te7 and the symmetry generated Te7^i. According to the VSEPR model, it is an AX_3E_2 system for which a T-shaped coordination is expected. The angles around Te7 of 95.1°, 87.3° and 172.5° show the T-shaped coordination to be well fulfilled. In the given environment, Te7 has one negative charge. Therefore, the whole molecule gains eight negative charges. All bonds not discussed here are presented in Table 17. If one half of the central ring is neglected (Te8, Te9, Te4^i, Te5^i and Te6^i), the shape of the remaining (Te15) chain shows large similarities to the $(Te_{15})^{4-}$ anion in the structure of $[Zn(NH_3)_6]_2(Te_{15})$ published by *Kysliak* in 2013 [58]. The main difference is the arrangement around the respective linear (Te3) unit. In $[Zn(NH_3)_6]_2(Te_{15})$ a perfect cis configuration is present whereas in $[Yb(NH_3)_8]_4(Te_{20})(Te_3)_2 \cdot 2NH_3$ a configuration between cis and trans is present, indicated by a dihedral angle of 108.1°.
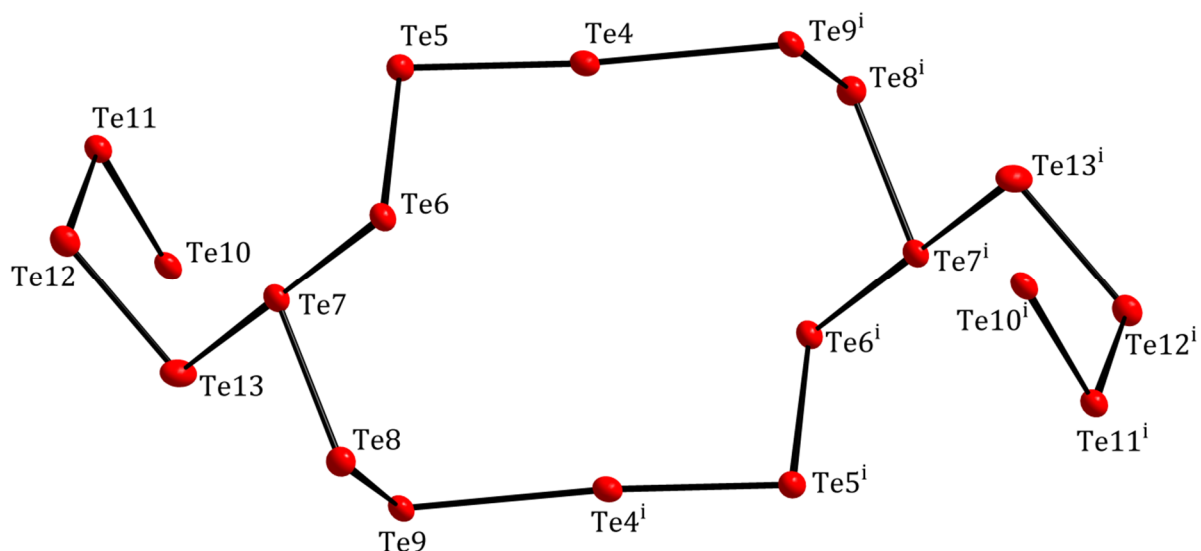
Figure 51: The $(Te_{20})^{8-}$ unit in the structure of $[Yb(NH_3)_8]_4(Te_{20})(Te_3)_2 \cdot 2NH_3$. The displacement ellipsoids represent a probability of 50 %. The index *i* indicates the following symmetry operation: 1-*x*, -*y*, 2-*z*.

Table 17: Bond lengths within the $(Te_{20})^{8-}$ polytelluride in the structure of $[Yb(NH_3)_8]_4(Te_{20})(Te_3)_2 \cdot 2NH_3$.

Atoms	Bond length/ Å	Atoms	Bond length/ Å	Atoms	Bond length/ Å
Te1-Te2	2.753(1)	Te5-Te6	2.827(1)	Te8-Te9	2.801(1)
Te2-Te3	2.732(1)	Te6-Te7	2.897(1)	Te10-Te11	2.795(1)
Te4-Te5	2.863(1)	Te7-Te8	2.751(1)	Te11-Te12	2.825(1)
Te4-Te9^i	3.223(1)	Te7-Te13	3.085(1)	Te12-Te13	2.718(1)
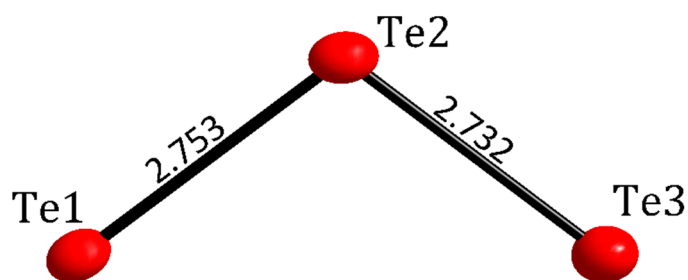
Figure 52: The $(Te_3)^{2-}$ unit in the structure of $[Yb(NH_3)_8]_4(Te_{20})(Te_3)_2 \cdot 2NH_3$. Bond lengths are given in Å. The displacement ellipsoids represent a probability of 50 %.

Within the unit cell, the $(Te_{20})^{8-}$ molecules are placed with their centers of gravity in the middle of four cell edges and one $(Te_{20})^{8-}$ molecule is placed in the middle of the unit cell. The rings of the molecules form channels that run parallel to the crystallographic c-axis (Figure 53). These channels are not filled by cations. Only the free ammonia molecules are placed in those channels. The $(Te_3)^{2-}$ polytellurides and the cationic ammine complexes fill the voids between the (Te_{20}) molecules.
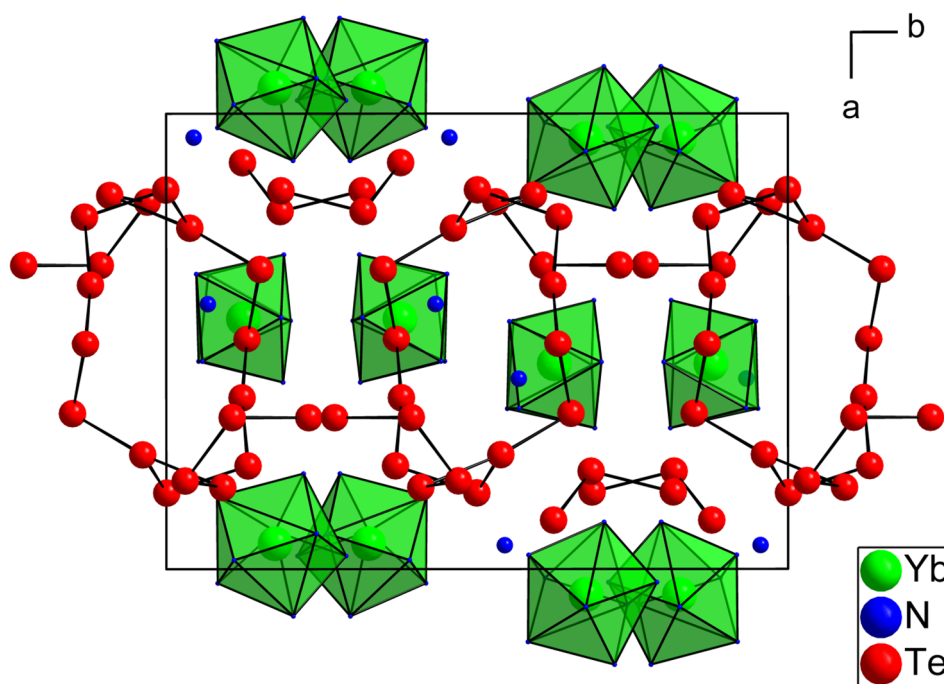
Figure 53: View on the unit cell of $[Yb(NH_3)_8]_4(Te_{20})(Te_3)_2 \cdot 2NH_3$ along the crystallographic c-axis. All atoms are drawn as spheres with arbitrary radii. Hydrogen atoms are omitted for clarity.

3.1.9 [Eu(en)₄]Te₆

The compound with the composition $[Eu(en)_4]Te_6$ crystallizes in the monoclinic space group $C2/c$ with the lattice parameters $a = 11.4252(3)$ Å, $b = 28.7635(9)$ Å, $c = 9.5547(3)$ Å and $\beta = 127.350(1)°$. The crystals of $[Eu(en)_4]Te_6$ have a platy crystal habit and are of black appearance. Figure 54 shows two reciprocal lattice images of one analyzed crystal. The image of the $h0l$ plane shows the crystal to consist of multiple domains. Furthermore, the image of the $hk3$ plane shows a stacking disorder or a modulation present in the crystal structure. These problems were present in all analyzed crystals and lead to problems in the structure refinement, such as non satisfactory quality factors and high residual electron density. However, the crystal structure could be solved. The Eu to Te ratio of 1:6 was confirmed by EDX analysis (Table 18).
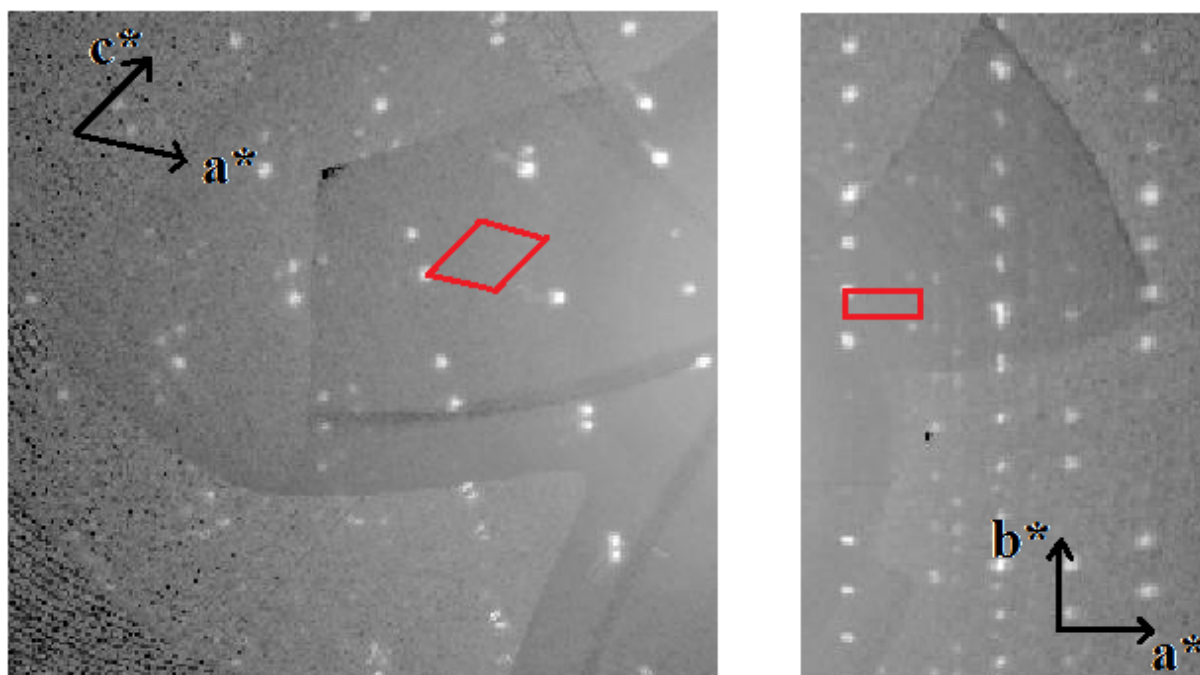
Figure 54: Two detailed parts of reconstructed precession images of the $h0l$ plane (left) and of the $hk3$ plane (right) of the analyzed crystal with the composition $[Eu(en)_4]Te_6$. The unit cell is drawn in red.

Table 18: Results of the EDX analysis of a crystal of $[Eu(en)_4]Te_6$.

Measurement	Eu / Atomic %	Te / Atomic %
1	85.1	14.9
2	86.5	13.5
Average	85.8	14.2
Normalized	1.00	6.04

The cation in the crystal structure is an europium ethylenediamine complex. Europium is surrounded by four en ligands and is in the formal oxidation state +II. The positions of the hydrogen atoms of the ethylenediamine ligands were not found in the difference *Fourier* map. They were placed on geometrically calculated positions and refined by using the riding model. The coordination polyhedron can be best described as a square antiprism (D_{4d}). A continuous shape measure gives a deviation from an ideal square antiprism of 0.804%. The other ideal coordination polyhedra show larger deviations (Table 19). Eu is placed on the *Wyckhoff* position 4*e* with the site symmetry 2. The Eu-N bond lengths are quite uniform in the range between 2.52 and 2.59 Å.
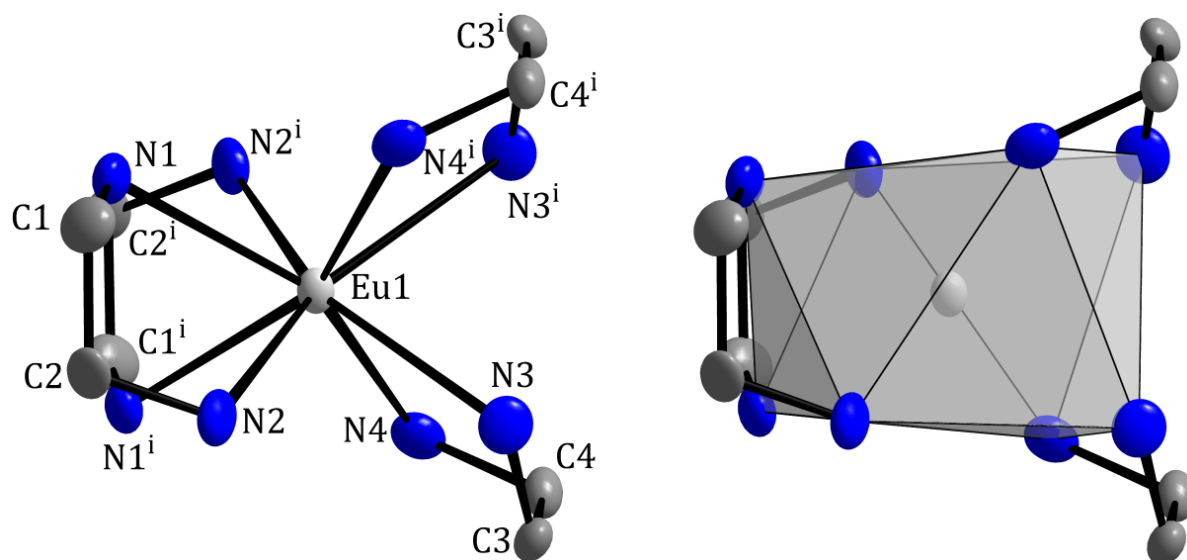
Figure 55: Coordination and coordination polyhedron of Eu^{2+} in the structure of $[Eu(en)_4]Te_6$. The displacement ellipsoids represent a probability of 50%. All hydrogen atoms bound to the N and C atoms of the en ligands are omitted for clarity. The index *i* indicates the following symmetry operation: 1-*x*, *y*, ½-*z*.

Table 19: Result of the continuous shape measure of the EuN_8 polyhedron in the structure of $[Eu(en)_4]Te_6$.

Ideal Shape	CShM / % (EuN₈ polyhedron)
OP-8	28.517
HPY-8	22.779
HBPY-8	15.621
CU-8	8.012
SAPR-8	**0.804**
TDD-8	1.735
BTPR-8	2.512

The other building block in the crystal structure of $[Eu(en)_4]Te_6$ is a two-dimensional polymeric polytelluride that forming layers in the a-c plane of the crystals (Figure 56). These layers consist of fused 14-membered rings and are stacked perpendicular to the crystallographic *b*-axis. Within the layers, Te atoms of normal valence and of hypervalency are present. In Figure 57, a detailed part of a layer with all different tellurium atoms is shown. According to the VSEPR model, the hypervalent atoms Te1 and Te4 are AX_2E_3 systems. Therefore, linear bonding is expected. The angles Te2-Te1-Te2[i] (179.2°) and Te3-Te4-Te3[i] (163.0°) are close to 180° and show the expected linear bonding. The bond lengths amount to 3.05 and 3.24 Å, respectively, and are in a typical range for this kind of hypervalently bound tellurium atoms. Each linear bonded tellurium carries two negative charges. The interatomic distance between Te2 and Te3 amounts to 2.70 Å. This bond length indicates a covalent bonding between Te2 and Te3. Te2 does not carry any charges. According to the VSEPR model, Te3 is an AX_3E system carrying one positive charge. For AX_3E systems, atoms in a trigonal pyramidal coordination with angles at the central atom around 100° are expected.. The angles at Te3 of 101.2°, 96.5° and 151.9°, however, show a strong deviation from trigonal pyramidal coordination.
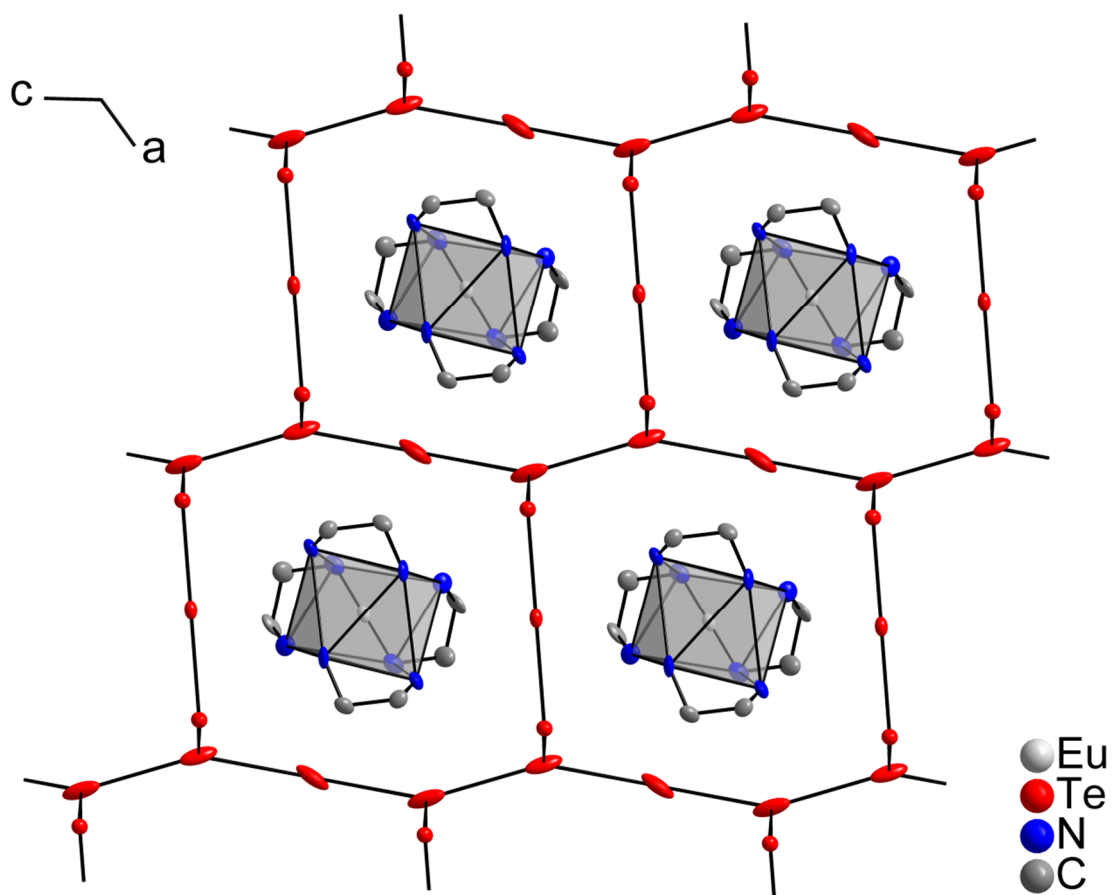
Figure 56: Section of one layer in the structure of [Eu(en)$_4$]Te$_6$ in a view along the crystallographic *b*-axis. The displacement ellipsoids represent a probability of 50%. The hydrogen atoms bound to the N and C atoms of the en ligands are omitted for clarity.
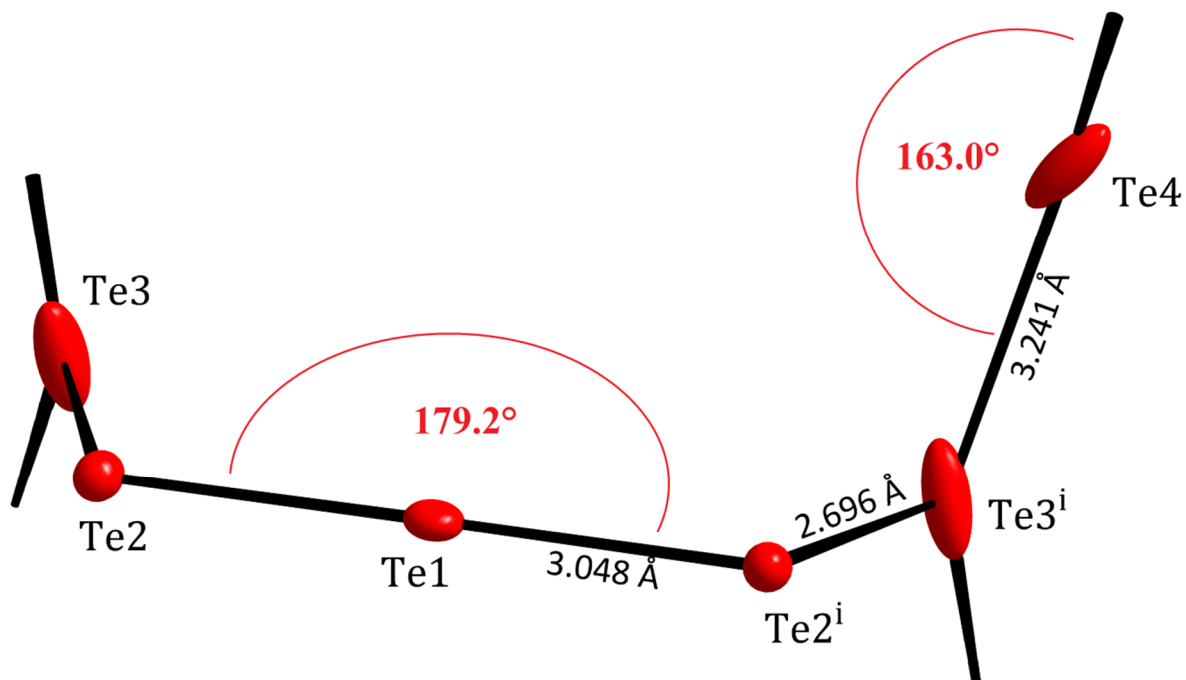
Figure 57: A detailed view of a section of the anionic layer in the structure of [Eu(en)$_4$]Te$_6$. The displacement ellipsoids represent a probability of 50%. The index *i* indicates the symmetry operation: 1-*x*, *y*, $^3/_2$-*z*.
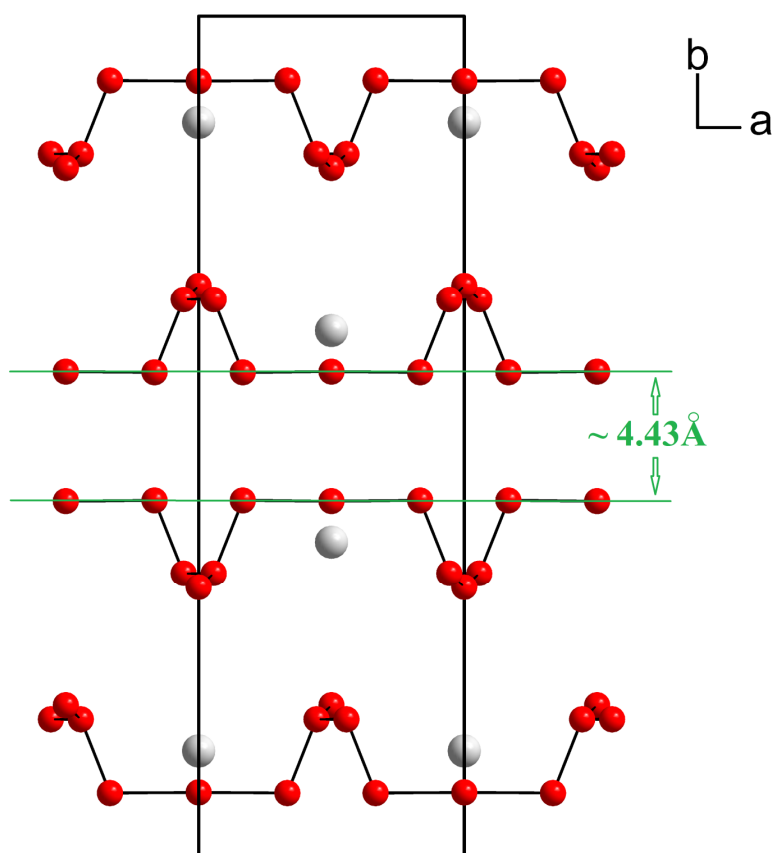
Figure 58: View of the unit cell of [Eu(en)$_4$]Te$_6$ along the crystallographic *c*-axis. All atoms are drawn as spheres with arbitrary radii. The coordinating en ligands are omitted for clarity.

Each 14-membered ring of the anionic layer is twofold negatively charged. In the viewing direction along the crystallographic *b*-axis, every ring contains an europium ethylenediamine complex in its center for charge balancing within one layer (Figure 56). The rings of different layers are shifted against each other. Therefore, no channels running along the crystallographic *b*-axis are formed.

In Figure 58 the closest distance between the different layers is shown. The distance of 4.43 Å is significantly longer than twice the *van-der-Waals* radius of tellurium. Therefore, the energy barrier for shifting or rotating single layers against each other can expected to be low, which might be the cause for the notorious disorder in all examined crystals. The only interactions between the layers are weak hydrogen bonds between the hydrogen atoms of the coordinating en ligands and the tellurium atoms.
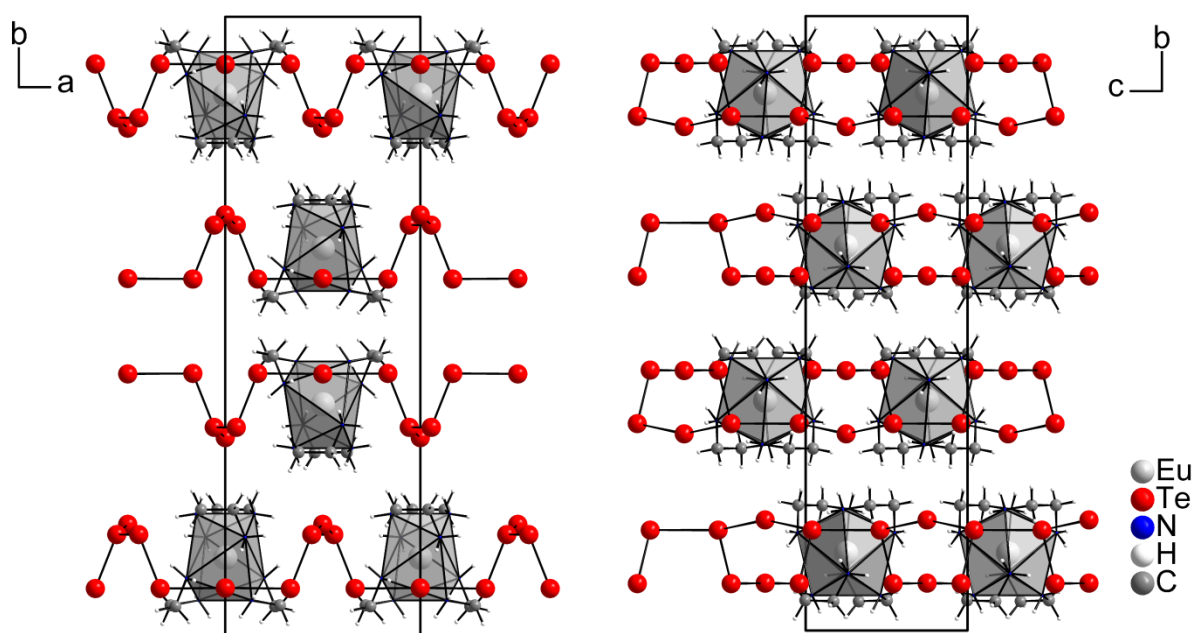
Figure 59: Extended unit cell of [Eu(en)$_4$]Te$_6$ along the crystallographic *c*-axis (left) and along the crystallographic *a*-axis (right). All atoms are drawn as spheres with arbitrary radii.

3.2 Compounds containing Chalcogenidoarsenates

Chalcogenidoarsenates gained high interest for the last decades because of their rich structural variety, demonstrated by several review articles [83] [84] [85] published in this field of research. Most of the known chalcogenidoarsenates are synthesized in fluxes [86] or via solvothermal syntheses in polar fluids such as ethylene diamine [87], ammonia [88], acetonitrile [89] or water [88].

The main building unit of the investigated chalcogenidoarsenates is the Ψ-tetrahedral AsQ_3-unit. Therefore, the basic structural motif is a $(AsQ_3)^{3-}$ anion e.g. in the structure of Na_3AsS_3 [90] or Tl_3AsSe_3 [91]. No literature reports on discrete $(AsTe_3)^{3-}$ anions could be found. These AsQ_3 units are prone to condensation by forming dipyramidal $(As_2Q_5)^{4-}$ ions (with $Q = S$ [92] or Se [92]) or to cyclic anions. The $(As_3Q_6)^{3-}$ anion (with $Q = S$ [93] or Se [94]) and the $(As_4Se_8)^{4-}$ [95] anion are known as representatives for cyclic anions without homonuclear bond formation. For $Q = S$ or Se, cyclic anions with homonuclear Q-Q bond formation are known. There are six-membered rings with either one exo-cyclic chalcogenide atom e.g. $(QAsQ_5)^{-}$ [96] [97] or $(QAsQ_7)^{-}$ [98] [99] (with $Q = S$ or Se) or two exo-cyclic chalcogenide atoms e.g. $(As_2Q_6)^{2-}$ (with $Q = S$ [100] or Se [101]). The six-membered rings are all in chair conformation with the exo-cyclic chalcogenide atoms placed in equatorial positions. For tellurium, only cyclic anions with homonuclear As-As bond formation are known. The first published telluridoarsenate of the formula type $(As_4Q_6)^{4-}$ was $[Ba(en)_4]_2(As_4Te_6)$ by *Eisenmann* and *Zangler* in 1987 [102], built up of a six-membered As_4Te_2-ring and four exo-cyclic tellurium atoms. There is no cyclic selenidoarsenate of the formula type $(As_4Q_6)^{4-}$ known, which shows the same structural motif as the above mentioned $(As_4Te_6)^{4-}$ ion. The only known (As_4Q_6) anion, with $Q = S$ or Se, is present in $[K(2.2.2-crypt)]_2(As_4Se_6)$ [103] or $(pipH)_2[As_4S_6]$ [104] with an As-As bond forming two five-membered rings with an exocyclic selenium atom on each ring. The fact that there are many molecular telluridoarsenates with one or more As-As bonds in their structures but only a few selenidoarsenates or thioarsenates with As-As bonds is due to the weakness of the Te-As bond in comparison to a S/Se-As bond. The 4s orbitals of As and the more diffuse 5p orbitals of Te show a poor overlap and the difference in electronegativity between As and Te is negligible.

Beside the molecular chalcogenidoarsenates, polymeric chalcogenidoarsenates are also reported in the literature. The most simple polymeric motif is a $^{1}_{\infty}[AsQ_2^{-}]$ chain, formed by the condensation of (AsQ_3) units. This structural motif was first found in the structure of $NaAsS_2$ by *Pallazi* and *Jaulmes* in 1977 [105] and in the structure of $NaAsSe_2$ [106] by *Eisenmann* and

Schäfer in 1979. In 1988 *Sheldrick* and *Häusler* published the structures of the compounds KAsSe$_2$, RbAsSe$_2$ and CsAsSe$_2$ [107], all containing the structural motif of polymeric $^1_\infty$[AsSe$_2^-$] selenidoarsenate chains. The difference between those chains is the lengths of their repeating units (Figure 60). In NaAsSe$_2$ and CsAsSe$_2$ *zweier* chains and in KAsSe$_2$ and RbAsSe$_2$ *vierer* chains are present. For $^1_\infty$[AsS$_2^-$] a second example was published in the dissertation of Häusler in 1987 [108], RbAsS$_2$. During hydrothermal reaction of alkali carbonates with As$_2$Se$_3$ the formation of $^1_\infty$[AsSe$_3^-$] chains with homonuclear Se-Se bond formation was observed [109]. Some chalcogenidoarsenates chains are built up of 5- or 6-membered rings, which are linked to infinite chains e.g. in Cs$_2$As$_4$Se$_6$ [110] or in [Mn(tren)](As$_4$S$_7$) [111]. The only telluridoarsenate chain published is the $^1_\infty$[As$_2$Te$_5^{2-}$] anion in the structure of [Et$_4$N]$_2$(As$_2$Te$_5$) [112]. Higher-dimensional chalcogenidoarsenates are not known except the $^2_\infty$[As$_8$S$_{13}^{2-}$] anion in the structure of Cs$_2$As$_8$S$_{13}$ [113].
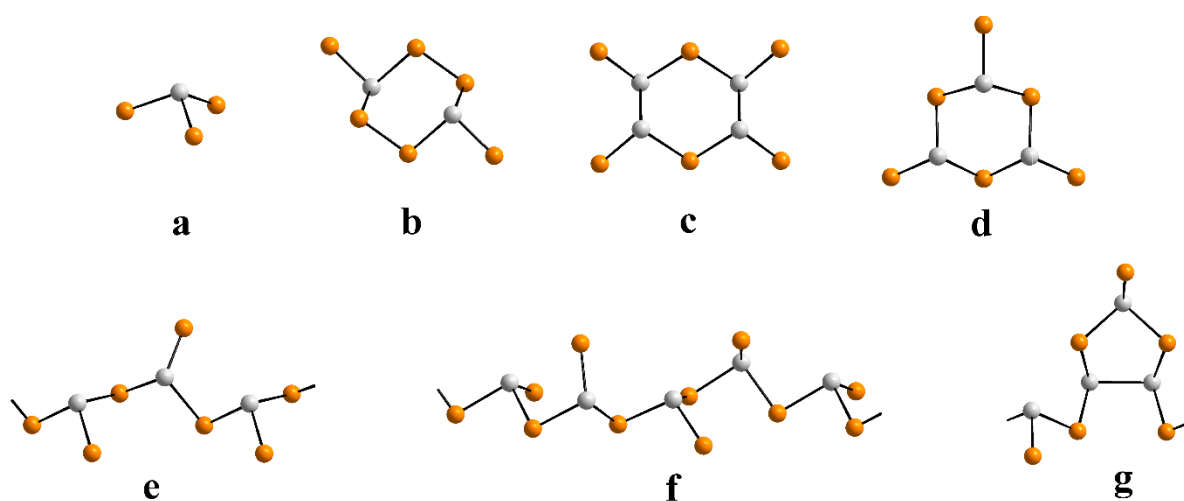
Figure 60: Selected chalcogenidoarsenate ions. All atoms are drawn with arbitrary radii. a) (AsQ$_3$)$^{3-}$, b) (As$_2$Q$_6$)$^{2-}$, c) (As$_4$Q$_6$)$^{4-}$, d) (As$_3$Q$_6$)$^{3-}$, e) $^1_\infty$[AsQ$_2^-$] *zweier* chain, f) $^1_\infty$[AsQ$_2^-$] *vierer* chain, g) $^1_\infty$[As$_4$Q$_6^{2-}$].

3.2.1 [M(en)$_4$]$_2$(As$_4$Q$_6$) with M = Ca, Sr and Q = Te or M = Eu and Q = Se

The compounds [Ca(en)$_4$]$_2$(As$_4$Te$_6$) **1**, [Sr(en)$_4$]$_2$(As$_4$Te$_6$) **2** and [Eu(en)$_4$]$_2$(As$_4$Se$_6$) **3** are all isotypic. All three compounds crystallize in the orthorhombic space group *Pbca*. The lattice parameters a = 17.1043(5) Å, b = 16.4652(6) Å and c = 17.3352(5) Å for **1**, a = 17.2116(2) Å, b = 16.3773(3) Å and c = 17.6420(3) Å for **2** and a = 16.7021(2) Å, b = 15.7063(2) Å and c = 17.2826(2) Å for **3**, show pseudo-cubic cells for all three structures. The crystals of the tellurium containing compounds are of dark red appearance whereas the crystals of [Eu(en)$_4$]$_2$(As$_4$Se$_6$) have an orange color.

The compounds **1**, **2** and **3** are composed of (As$_4$Q$_6$)$^{4-}$ molecules and divalent cations that are each surrounded by four ethylene diamine ligands. The anionic molecules form As$_4$Te$_2$ six-membered rings in chair conformation. The rings are formed by two As-As groups that are bridged via chalcogen atoms. Each As atom is bound to an exocyclic chalcogen atom. The exocyclic atoms are located in equatorial positions with respect to the plane of the As$_4$Q$_2$ ring. All exocyclic atoms carry a negative charge giving the entire molecule four negative charges. A general Lewis formula for the (As$_4$Q$_6$)$^{4-}$ ion is shown in Figure 61. It is the first time that an anion of this type containing selenium has been synthesized and characterized. In the (As$_4$Se$_6$)$^{4-}$ anion, As is in the formal oxidation state +II. The oxidation state of Se is –II for both, the endocyclic and exocyclic selenium atoms. If attribution of the oxidation states is strictly performed following the respective electronegativities, As takes the uncommon oxidation state –II, the endocyclic Te atoms the oxidation state +II and the exocyclic Te the oxidation state 0, based on the higher electronegativity of As compared to Te. The *Allred-Rochow* scale shows a electronegativity difference of 0.19 and the *Pauling* scale a difference of 0.08 [114]. Due to this negligible difference in electronegativity and due to the fact that (As$_4$Te$_6$)$^{4-}$ shows the same crystallographic properties as (As$_4$Se$_6$)$^{4-}$, it is not reasonable to put oxidation states on the atoms of this telluridoarsenate anion.
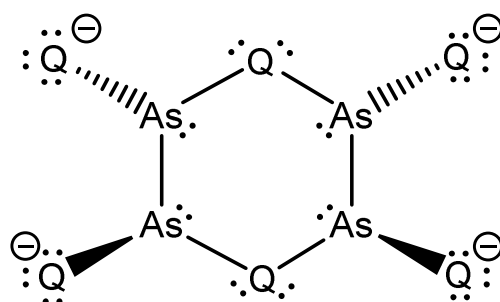
Figure 61: Lewis formula of the (As$_4$Q$_6$)$^{4-}$ anion.
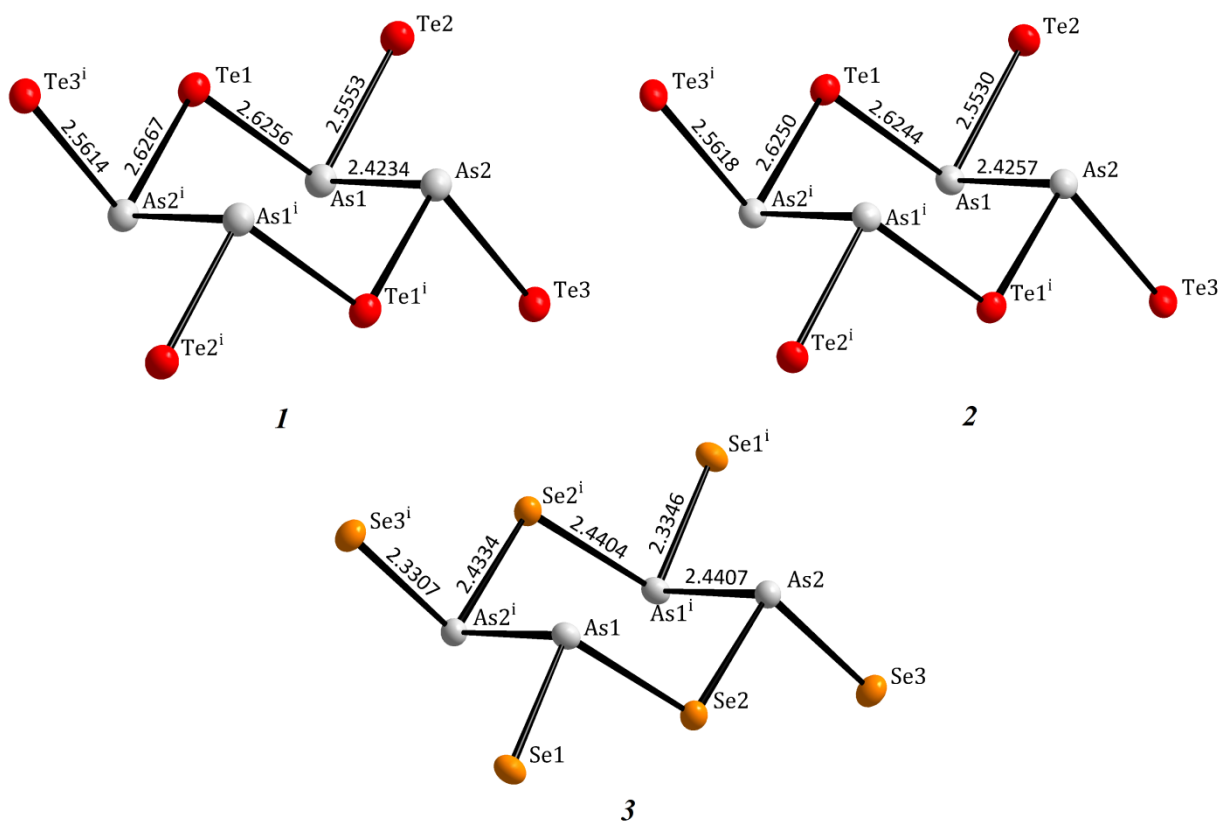
Figure 62: The $(As_4Q_6)^{4-}$ anions of the compounds *1*, *2* and *3*. The displacement ellipsoids represent a probability of 50 %. The bond lengths are given in Å. The index *i* indicates the following symmetry operation: 1-*x*, 1-*y*, 1-*z*.

All ring atoms have a Ψ-tetrahedral or a Ψ²-tetrahedral coordination. As atoms can be described as AX_3E-type atoms and the endocyclic Se/Te atoms as AX_2E_2-type atoms. For the Ψ- and Ψ²-tetrahedral structures an ideal angle of 109.5° is expected, based on electrostatic repulsion according to the VSEPR model. For the many molecules and especially molecules with heavier atoms further influences have to be taken into account. The actual bond angles of the As atoms in structures *1* and *2* of 89.8 – 100.2° differ significantly from the ideal tetrahedral angle. With bond angles of 102.9° in *1* and 103.2° in *2* on the Te atoms, these angles are smaller than the ideal tetrahedral angle. The As-As bonds of 2.42 Å or 2.43 Å, respectively, are comparable to the covalent bond lengths in the element structure of grey arsenic. The As-Te bonds within the ring correspond to the sum of the covalence radii. The terminal bond lengths are slightly shortened. In *3* the bond angles on the As atoms range from 93.3° to 98.9° and the bond angle

between As1-Se2-As2 amounts to 104.7°. The ratio of the bond lengths between the endocyclic and terminal As-Se bonds with respect to the smaller radius of Se compared Te are the same as found in *1* or *2*. In the crystal, the anions occupy the *Wyckhoff* positions *4a* and *4b* with site symmetry $\bar{1}$. In the idealized form, a $(As_4Se_6)^{4-}$ anion has the point symmetry 2/*m*. Therefore, the symmetry of the anions in the crystal is lower than the highest symmetried point group these molecules can achieve.

For additional analysis of the compositions, energy dispersive X-ray spectroscopy was used. Therefore, the crystals that were used for X-ray diffraction were placed on a sample carrier for EDX analysis. This was done at room temperature and under not oxygen-free conditions. In Table 20 the compositions are shown in atomic percentages. For *3* the EDX analysis shows a smaller Se content than for the expected ratio of 1Eu:2As:3Se. The low content of selenium in the crystals may origin from partial decomposition during exposure of the crystals to air and the evolution of H_2Se. This gas was generated on handling the crystals in open air and could be detected by its specific smell. However, the EDX analysis shows that selenium was present in the measured crystal. This is important for the structure solution since Se and As are not distinguishable by X-ray diffraction. For *1* the amount of Ca is lower than expected. The emission lines for Ca and Te are on similar levels in the EDX spectrum (Figure 63), which makes an accurate determination difficult. However, the spectrum shows that Ca is present in the analyzed crystal since only with Ca and Te the spectrum could be fitted well. The fit is depicted as blue line in the spectrum. The results for the amount of As in *1* and *2* are small compared to the values found for tellurium because the crystals lost arsine after exposition to air and handling the crystals at room temperature.

Table 20: Results of the EDX analysis for the crystals of *1*, *2* and *3*.

Compound	M / Atomic %	As / Atomic %	Q / Atomic %
1	7.94	29.46	62.70
Normalized	*1.00*	*3.71*	*7.90*
2	23.81	19.05	57.14
Normalized	*1.00*	*0.80*	*2.40*
3	18.80	41.30	39.90
Normalized	*1.00*	*2.20*	*2.12*
Expected	*1.00*	*2.00*	*3.00*
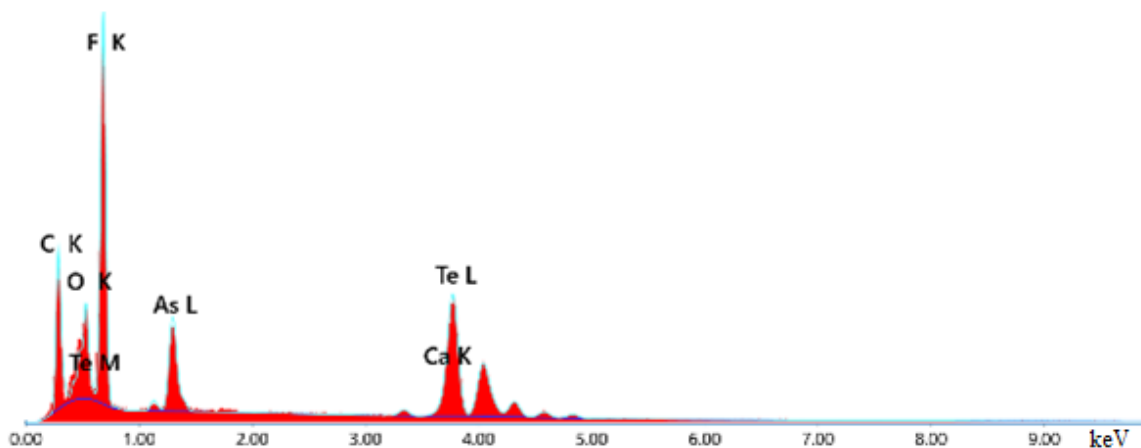
Figure 63: EDX spectrum of the analyzed crystal of *1*.

The counterions Ca^{2+}, Sr^{2+} and Eu^{2+} are each coordinated by four ethylene diamine ligands (Figure 64). Positions of the hydrogen atoms of the ethylene diamine ligands were not found in the difference *Fourier* map. They were placed on geometrically calculated positions and refined by a riding model. The coordination of the cations in the structures *1*, *2* and *3* can be best described as trigonal dodecahedra (D_{2d}). The deviation from the ideal polyhedron was calculated by a continuous shape evaluation with the help of the program SHAPE. The deviation from an ideal triangular dodecahedron (D_{2d}) amounts to 0.854 % in *1*, 1.280 % in *2* and 1.526 % in *3*. A table with continuous shape measurements for other polyhedra with coordination number 8 can be found in Table 21.
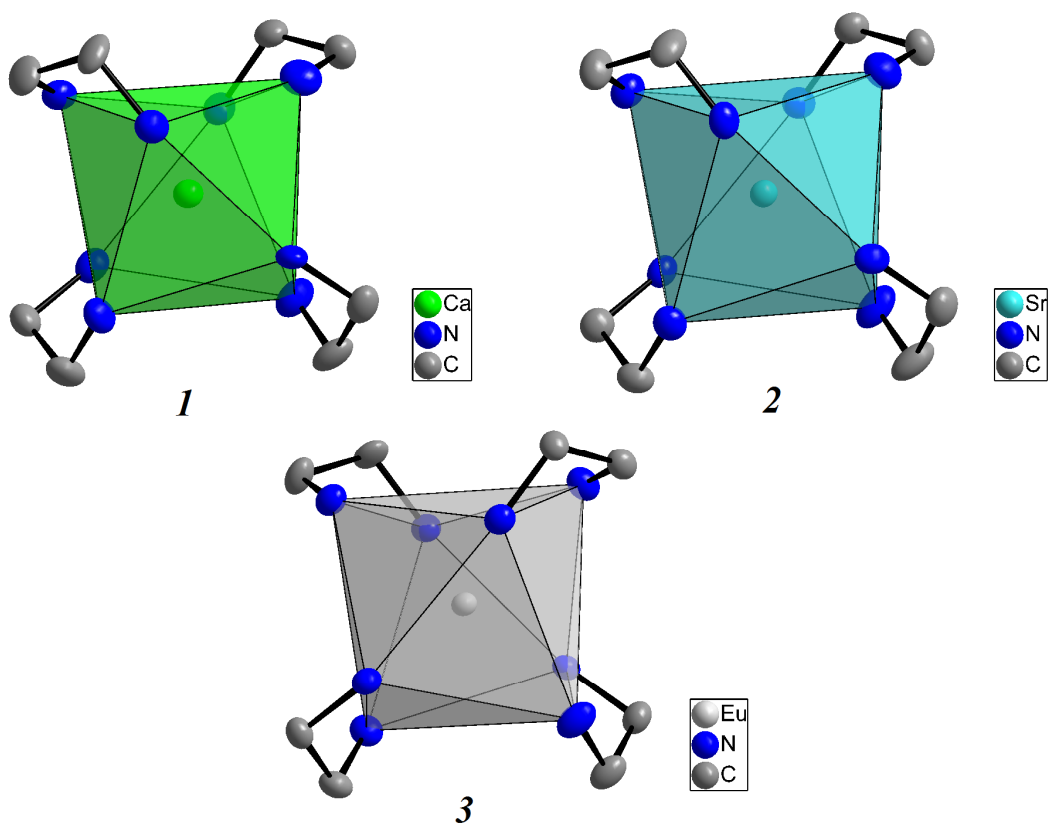
Figure 64: The coordination of Ca^{2+} (**1**), Sr^{2+}(**2**) and Eu^{2+}(**3**) by the ethylene diamine molecules in the structures of $[Ca(en)_4]_2(As_4Te_6)$ **1**, $[Sr(en)_4]_2(As_4Te_6)$ **2** and $[Eu(en)_4]_2(As_4Se_6)$ **3**. The displacement ellipsoids represent a probability of 50 %. The hydrogen atoms bound to the C and N atoms of the ethylenediamine ligands are omitted for clarity.

The interatomic distances between the central atom and the ligands are according to their ionic radii. The M^{2+}-N distances range between 2.57 – 2.63 Å for **1**, 2.70 – 2.76 Å for **2** and between 2.69 – 2.75 Å for **3**.
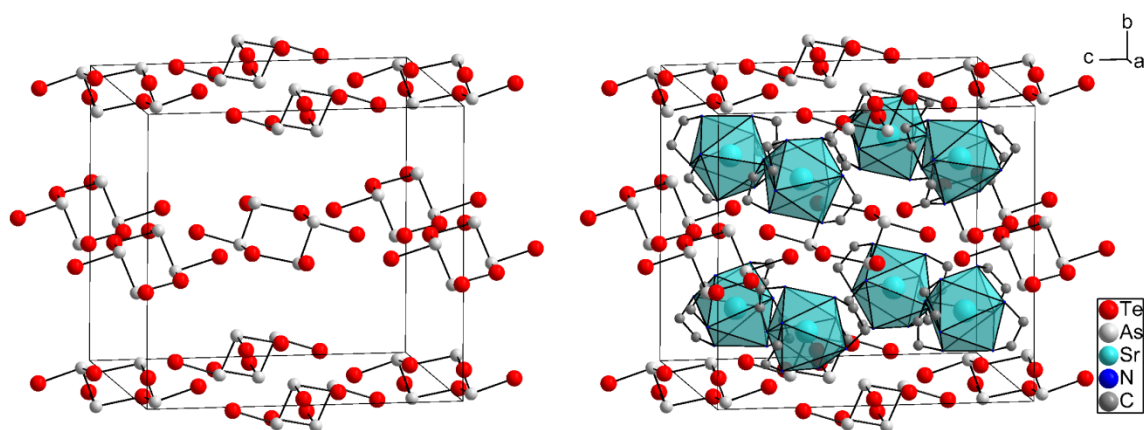
Figure 65: A perspective view of the unit cell of $[Sr(en)_4]_2(As_4Te_6)$ as a representative for the structure type $[M(en)_4]_2(As_4Q_6)$. The unit cell without the $[Sr(en)_4]^{2+}$ complexes is shown on the left and with the complexes on the right. The hydrogen atoms bound to the ethylenediamine ligands are omitted for improved clarity.

In Figure 65 the unit cell of *2* is exemplarily shown as representation of the structures of *1*, *2* and *3*. The chalcogenido arsenate ions are placed with their centers of gravity on the positions (½,0,0), (0,½,0), (0,0,½) and (½,½,½). The structure can be derived from the crystal structure of Li_2O, the anti-fluorspar-type (Figure 66). The chalcogenido arsenate ions build a slightly distorted cubic closest packing according to the oxide ions in Li_2O with the cationic complexes occupying all tetrahedral voids.
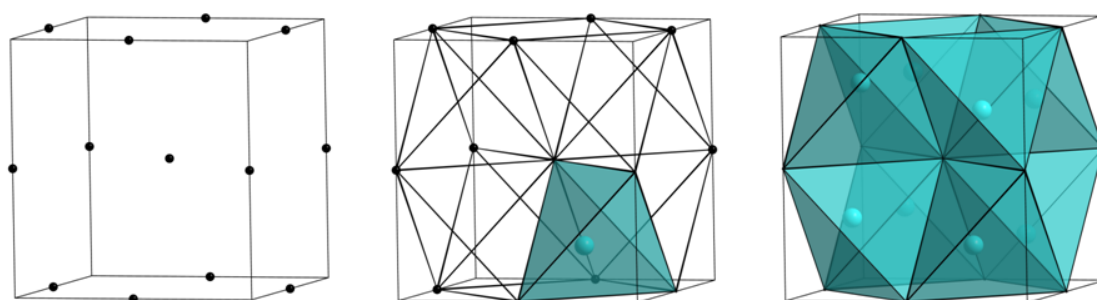
Figure 66: Perspective view of the unit cell of *2* as representation for the structure type $[M(en)_4]_2(As_4Q_6)$ with centers of gravity of the anions shown as black spheres (left), unit cell with all tetrahedral voids and one exemplarily filled void (middle) and unit cell with all tetrahedral voids filled (right)**.**

Table 21:Results of the continuous shape measures of the CaN_8 polyhedron in the structure of $[Ca(en)_4]_2(As_4Te_6)$, of the SrN_8 polyhedron in the structure of $[Sr(en)_4]_2(As_4Te_6)$ and of the EuN_8 polyhedron in the structure of $[Eu(en)_4]_2(As_4Se_6)$.

Ideal Shape	CShM / % (CaN_8 polyhedron)	CShM / % (SrN_8 polyhedron)	CShM / % (EuN_8 polyhedron)
OP-8	33.851	34.762	34.278
HPY-8	23.852	22.919	23.427
HBPY-8	16.252	16.064	14.987
CU-8	11.565	12.141	12.211
SAPR-8	3.124	3.581	3.694
TDD-8	**0.854**	**1.280**	**1.526**
BTPR-8	2.413	2.647	2.656

3.2.2 [Ca(en)$_4$](As$_2$Se$_6$)

The salt-like compound [Ca(en)$_4$](As$_2$Se$_6$) crystallizes in the monoclinic space group $C2/c$. The crystals of [Ca(en)$_4$](As$_2$Se$_6$) are orange and transparent and contain the chalcogen rich *Zintl* ion (As$_2$Se$_6$)$^{2-}$, which was already found in structures with bulky counterions such as [M(dien)$_3$]$^{2+}$ (M = Co or Ni) [115], (Et$_4$N)$^+$ [99] or (Ph$_4$P)$^+$ [116]. The compound presented here is the first one with an alkaline earth metal containing complex as counterion and it is not isostructural to one of the structures named before.

The results of the energy dispersive X-ray spectrum are shown in Table 22. Therefore, the crystals used for X-ray diffraction were placed on a sample carrier for EDX analysis. This was done at room temperature and under not oxygen-free conditions. The EDX analysis shows a smaller As and Se content than expected for the ratio of Ca:2As:6Se. Se as well as As are expected to leave the crystal by evolution of hydrogen selenide or arsine, respectively, on exposure to air.

The (As$_2$Se$_6$)$^{2-}$ ion is located at an inversion center in the center of gravity inside the As$_2$Se$_4$ ring resulting in the site symmetry $\bar{1}$. Therefore, the site symmetry is lower than the highest symmetry the (As$_2$Se$_6$)$^{2-}$ ion could achieve ($2/m$). The ion made up of two pyramidal AsSe$_3$ units joined via two Se-Se bonds. The anion consists of an As$_2$Se$_4$-ring in chair conformation with two homonuclear Se-Se bonds and an exocyclic Se atom bound to each As atom (Figure 67). The exocyclic Se atoms are located in equatorial positions with respect to the plane of the As$_2$Se$_4$ ring. The two negative charges are located formally on the exocyclic selenium atoms. Both As atoms are in their typical oxidation state +III. The oxidation states for the Se atoms are –I for the Se within the ring and –II for the exocyclic Se.

Table 22: Result of the EDX analysis for the crystal of the compound with the composition [Ca(en)$_4$](As$_2$Se$_6$).

	Ca	As	Se
Atomic %	17.74	24.19	58.06
Normalized	1.00	1.36	3.27
Expected	1.00	2.00	6.00
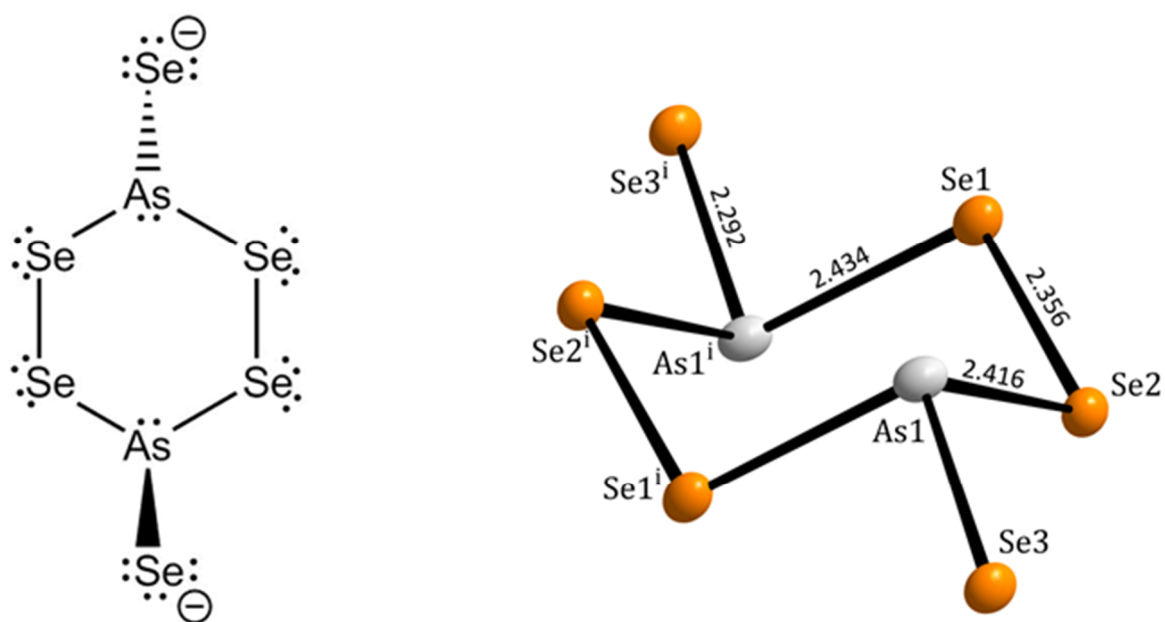
Figure 67: Lewis formula of the $(As_2Se_6)^{2-}$ ion (left) and the $(As_2Se_6)^{2-}$ ion as present in the structure of $[Ca(en)_4](As_2Se_6)$ (right). Bond lengths are given in Å. The displacement ellipsoids represent a probability of 50 %. The index *i* indicates the following symmetry operation: -*x*+1/2, -*y*+3/2, -*z*+1.

The terminal As1-Se3 bond length of 2.292 Å is shorter than those of the bridging ones As1-Se1 (2.434 Å) and As1-Se2 (2.416 Å). The bond length Se1-Se2 of 2.356 Å is in agreement of twice the covalent radius of selenium (2.34 Å).

The bulky counterion in this presented structure is the cationic ethylenediamine complex $[Ca(en)_4]^{2+}$. The position of the hydrogen atoms of the ethylenediamine ligands were not found in the difference *Fourier* map. They were placed on geometrically calculated positions and refined by a riding model. Calcium has the coordination number 8 and is surrounded by four ethylenediamine ligands (Figure 68). For the best description of the CaN_8 polyhedron, a continuous shape evaluation was performed. A square antiprism (D_{4d}) with a deviation of 0.818 % of the ideal shape is the best polyhedron to describe the $[Ca(en)_4]^{2+}$ complex. For other possible shapes of coordination number 8, for example a triangular dodecahedron (D_{2d}) or a twofold capped triangular prism (C_{2v}), the continuous shape evaluation yielded higher deviations from their ideal shapes of 1.481 % and 2.366 %, respectively. The Ca-N bond lengths range from 2.57 to 2.62 Å and are nearly the same as those found in $[Ca(en)_4]_2(As_4Te_6)$.
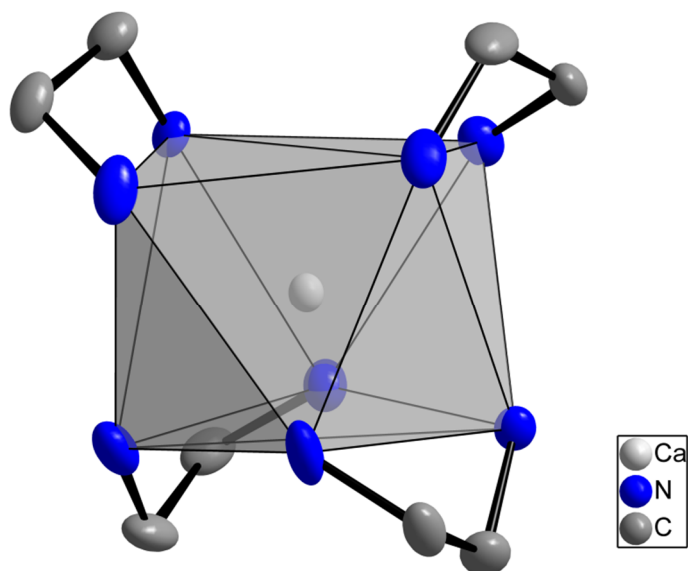
Figure 68: The coordination of Ca^{2+} by the ethylenediamine molecules in the structure of [Ca(en)$_4$](As$_2$Se$_6$). The displacement ellipsoids represent a probability of 50 %. The hydrogen atoms bound to the C and N atoms of the ethylenediamine ligands are omitted for clarity.

Table 23: Result of a continuous shape measure of the CaN$_8$ polyhedron in the structure of [Ca(en)$_4$](As$_2$Se$_6$).

Ideal Shape	CShM / % (CaN$_8$ polyhedron)
OP-8	31.041
HPY-8	22.630
HBPY-8	16.602
CU-8	8.995
SAPR-8	**0.818**
TDD-8	1.481
BTPR-8	2.366

In Figure 69 (left) the unit cell along the crystallographic *b*-axis is shown. The compound shows a structure where an alternating pattern of cations and anions running perpendicular to the crystallographic *c*-axis is present. Connections between the (As$_2$Se$_6$)$^{2-}$ molecules and the Ca-complexes are present in form of N-H$\cdots$Se contacts (Figure 69, right). For the shown N-H$\cdots$Se

contacts only contacts with N-H···Se bond lengths smaller than 2.9 Å and N-H-Se angles larger than 135 ° were used. These contacts may be assumed to play a reasonable role in connecting $(As_2Se_6)^{2-}$ molecules and the Ca-complexes inside the layers. Every anion is connected to six complexes via hydrogen contacts.
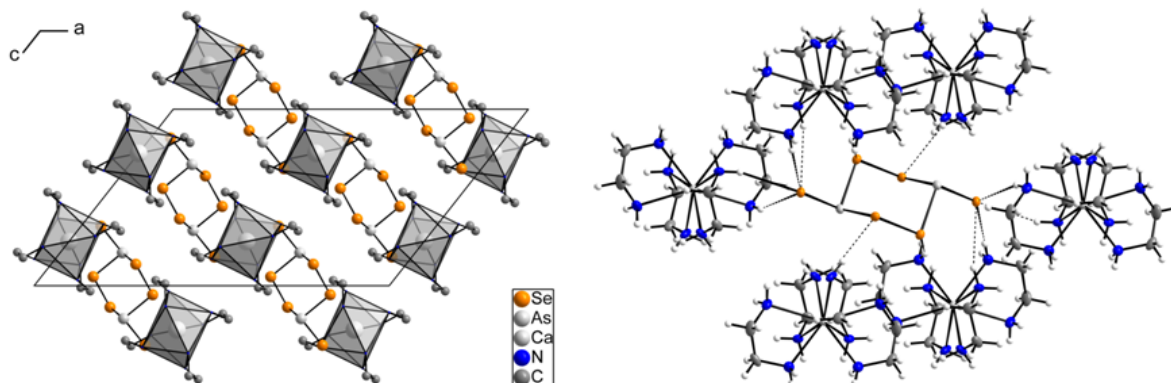
Figure 69: On the left a view on the extended unit cell along the crystallographic *b*-axis is shown. All atoms are shown with arbitrary radii. On the right the coordination of an $(As_2Se_6)^{2-}$ ion by $[Ca(en)_4]^{2+}$ complexes via hydrogen bonds is shown. The displacement ellipsoids represent a probability of 50 %. The hydrogen atoms are drawn with arbitrary radii.

As it was shown in the chapter before, also this *Zintl* compound can be derived from the structure type of a simple salt, in this case from the CsCl structure type. The Ca^{2+} ions build up a lattice of slightly distorted cubes. Every cubic void is filled with an $(As_2Se_6)^{2-}$ ion to reach the ratio of 1:1. In Figure 70, the cubic network formed by the Ca atoms is shown with black lines and the original unit cell is shown with red lines. One exemplary filled cubic void is shown in orange with an $(As_2Se_6)^{2-}$ ion inside.
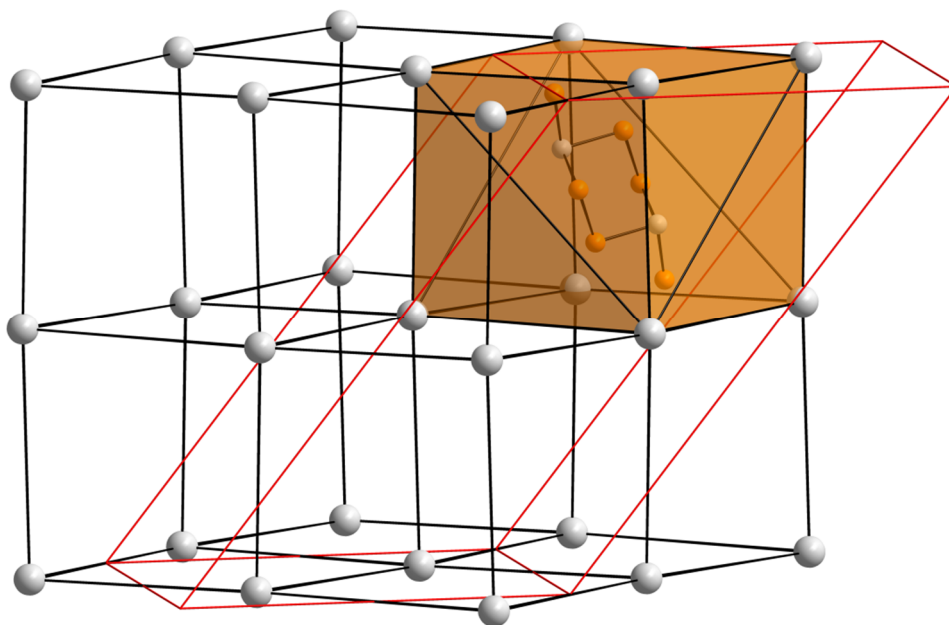
Figure 70: The distorted cubic network of Ca atoms with an exemplarily filled void (orange) in the structure of [Ca(en)$_4$](As$_2$Se$_6$). All atoms are drawn with arbitrary radii. The actual crystallographic unit cell is drawn with red lines.

3.2.3 [Ca(en)₄]₂(As₂Se₇O)
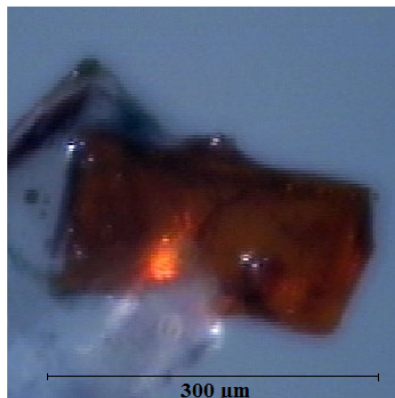
Figure 71: Microscopic image of the red crystal with the composition [Ca(en)₄]₂(As₂Se₇O) on the goniometer head of the diffractometer.

[Ca(en)$_4$]$_2$(As$_2$Se$_7$O) crystallizes in the acentric orthorhombic space group *Iba*2 with the lattice parameters a = 16.6561(3) Å, b = 31.2220(5) Å and c = 16.5018(3) Å. The absolute structure factor of roughly 0.52(3) shows that the crystal was an inversion twin and both enantiomers were present in the investigated crystal. Crystals of [Ca(en)$_4$]$_2$(As$_2$Se$_7$O) are of red appearance and are not stable on exposition to air and humidity. Nevertheless, they are stable at room temperature for some hours under inert gas conditions.

The structure is built up of cationic complexes and partially oxidized *Zintl* ions. The cations are three independent calcium ethylene diamine complexes. Each Ca atom is surrounded by four ethylene diamine ligands forming cationic [Ca(en)$_4$]$^{2+}$ complexes (Figure 72). The positions of the hydrogen atoms of the ethylene diamine ligands were not found in the difference *Fourier* map. They were placed on geometrically calculated positions and refined by using the riding model. Ca1 and Ca3 are placed on special positions on twofold axes, with the *Wyckhoff* positions 4*a* and 4*b*, respectively, giving the [Ca(en)$_4$]$^{2+}$ complexes C$_2$ symmetry. Ca2 occupies a general position inside the unit cell. Hence, the asymmetric unit contains one complete calcium ethylene diamine complex and two half complexes. For the description of the coordination polyhedra of Ca1, Ca2 and Ca3 a continuous shape measurement was performed. The evaluation shows a triangular dodecahedron (D_{2d}) to be the best description for all three coordination polyhedra. The deviation from the ideal shape of a triangular dodecahedron (D_{2d}) was calculated to 1.679 % for Ca1, 0.961 % for Ca2 and 1.211 % for Ca3. Other calculated deviations from ideal shapes can be found in Table 25. Ca-N bond lengths ranging from 2.55 Å

to 2.65 Å in $[Ca(1)(en)_4]^{2+}$ and $[Ca(2)(en)_4]^{2+}$ and from 2.50 to 2.84 Å in $[Ca(3)(en)_4]^{2+}$. With exception of the Ca3-N15 distance, the bond lengths are similar to that found in the structures of $[Ca(en)_4]As_2Se_6$ and $[Ca(en)_4]_2As_4Te_6$. The elongated Ca3-N15 bond length is a result of the diffuse position of N15 shown by its elongated displacement ellipsoid (Figure 72). The origin of the cigar-shaped ellipsoid of the N atom is not clear. An actual strong vibration amplitude is physically dubious since N15 is coordinated to Ca3. Attempts to refine the position of N15 with two closely neighbored split positions were not successful.
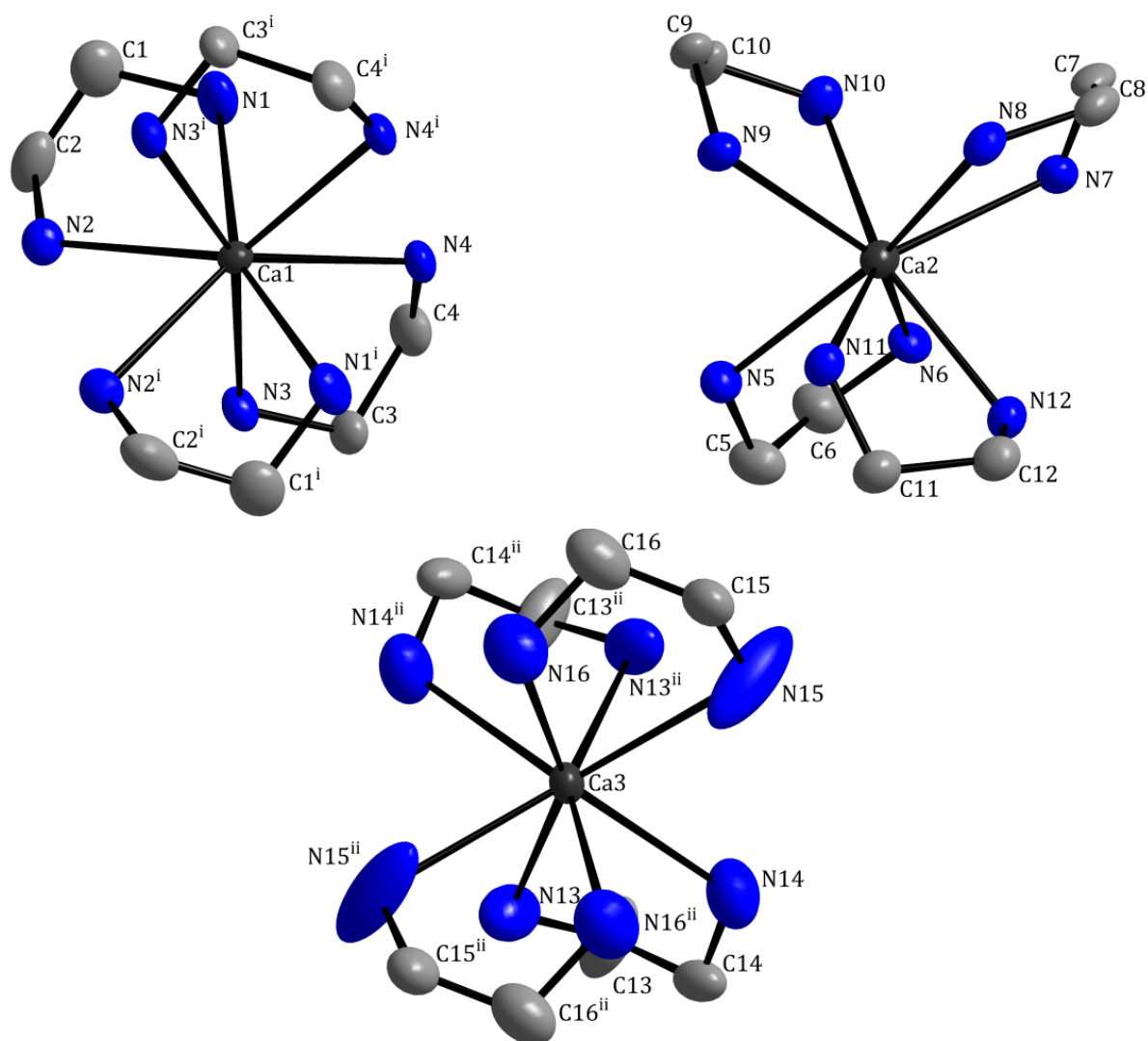
Figure 72: Coordination polyhedra of the three independent Ca^{2+} ions in the structure of $[Ca(en)_4]_2(As_2Se_7O)$. The displacement ellipsoids represent a probability of 50 %. The hydrogen atoms of the ethylenediamine ligands are omitted for clarity. The indices i indicate the following symmetry operations: (*i*) 1-*x*, 1-*y*, *z*; (*ii*) 2-*x*, 1-*y*, *z*.

The partially oxidized *Zintl* ion $(As_2Se_7O)^{4-}$ is found as the anion in the presented structure. This *Zintl* ion is built of two AsE_3 pyramids linked by a (Se_2) unit. One terminal position within an AsE_3 pyramid is occupied by an oxygen atom. Overall, the anion is fourfold negatively charged. Formally, each terminal atom bound to As carries one negative charge and both arsenic atoms carry one positive charge. Arsenic is in the oxidation state +V, the terminal atoms are in the oxidation state -II and the bridging Se atoms are in the oxidation state -I. The Se-Se bond length of 2.33 Å is slightly shortened with respect to typical $(Se_2)^{2-}$ dumbbells (2.38 Å – 2.47 Å). The inter-atomic distances between As and the terminal Se or O atoms are similar to the sum of their covalent bond radii. Hence, the bonds in the anionic substructure are significantly covalent.
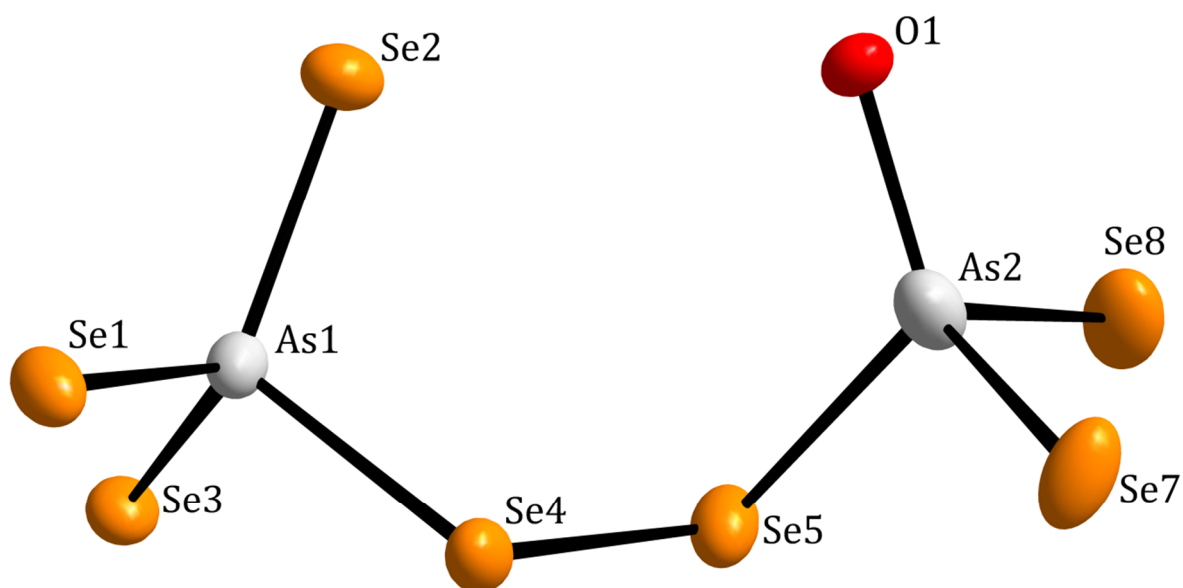
Figure 73: $(As_2Se_7O)^{4-}$ anion in the structure of $[Ca(en)_4]_2(As_2Se_7O)$. The displacement ellipsoids represent a probability of 50 %.

Table 24: Bond lengths and angles within the $(As_2Se_7O)^{4-}$ ion in the structure of $[Ca(en)_4]_2(As_2Se_7O)$.

Atoms	Bond length / Å	Atoms	Angle / °
As1 – Se2	2.264(2)	Se2–As1–Se3	113.73(8)
As1 – Se3	2.282(2)	Se2–As1–Se1	114.28(7)
As1 – Se1	2.286(2)	Se3–As1–Se1	113.24(8)
As1 – Se4	2.405(2)	Se2–As1–Se4	110.65(8)
As2 – O1	1.879(2)	Se3–As1–Se4	107.34(7)
As2 – Se7	2.311(2)	Se1–As1–Se4	95.96(8)
As2 – Se8	2.344(2)	O1–As2–Se7	120.2(3)
As2 – Se5	2.439(2)	O1–As2–Se8	108.8(3)
Se4 – Se5	2.327(2)	Se7–As2–Se8	106.27(9)
		Se8–As2–Se5	88.84(8)
		Se5–Se4–As1	105.69(7)
		Se4–Se5–As2	103.57(7)

Within the crystal structure, the $[Ca(en)_4]^{2+}$ complexes build up a lattice of distorted cubes. Since every second cubic void is filled with one $(As_2Se_7O)^{4-}$ anion with its elongated shape, the cubic voids are distorted. Thus the crystal structure of $[Ca(en)_4]_2(As_2Se_7O)$ can be derived from the antifluorite structure type of Li_2O. In Figure 74, the Li_2O type related structure of $[Ca(en)_4]_2(As_2Se_7O)$ is shown. The actual crystallographic unit cell edges are shown in red.
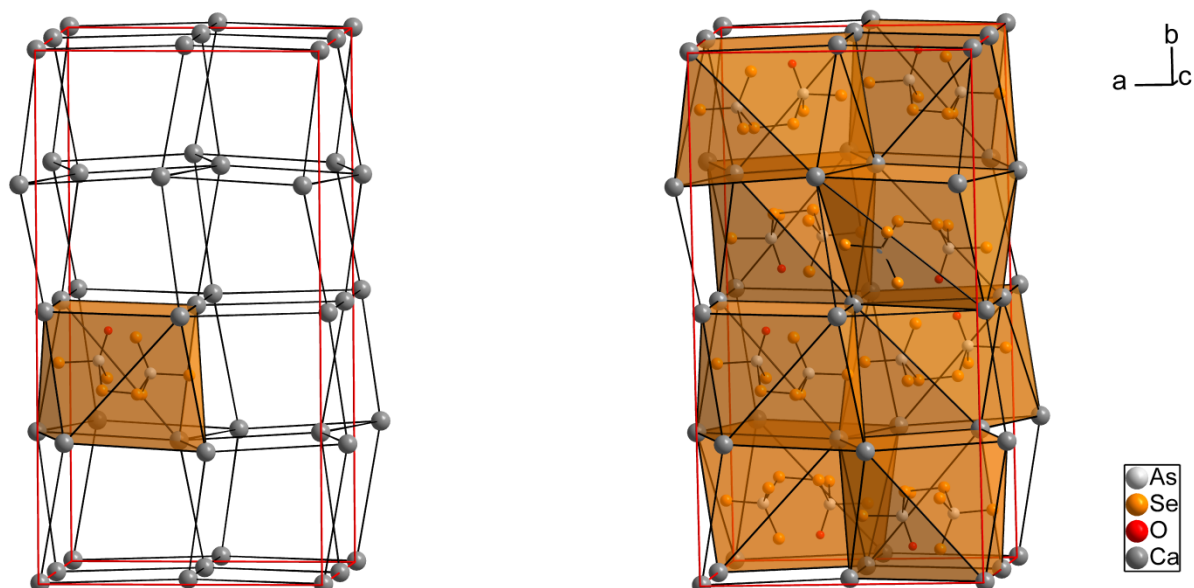
Figure 74: View of the unit cell of [Ca(en)$_4$]$_2$(As$_2$Se$_7$O) along the crystallographic *c*-axis. The actual crystallographic unit cell edges are drawn in red. One exemplarily filled cubic void is shown (left). Every second cubic void is filled (right). All atomic radii are drawn with arbitrary radii. The ethylenediamine ligands coordinated to the Ca atoms are omitted for improved clarity.

Table 25: Results of the continuous shape measures of the CaN$_8$ polyhedra in the structure of [Ca(en)$_4$]$_2$(As$_2$Se$_7$O).

Ideal Shape	CShM / % (Ca(1)N$_8$ polyhedron)	CShM / % (Ca(2)N$_8$ polyhedron)	CShM / % (Ca(3)N$_8$ polyhedron)
OP-8	33.405	33.572	33.503
HPY-8	24.186	23.207	23.107
HBPY-8	13.114	15.353	15.939
CU-8	9.514	11.882	10.987
SAPR-8	2.504	2.601	1.843
TDD-8	**1.679**	**0.961**	**1.211**
BTPR-8	2.579	2.496	2.415

3.2.4 [M(en)$_3$(H$_2$O)$_2$]As$_2$Se$_4$, M = Ca or Sr

The compounds [Ca(en)$_3$(H$_2$O)$_2$]As$_2$Se$_4$ and [Sr(en)$_3$(H$_2$O)$_2$]As$_2$Se$_4$ crystallize isotypically in the acentric hexagonal space group $P6_1$22 with the lattice parameters $a = b = 9.8708(3)$ Å and $c = 40.2274(12)$ Å for [Ca(en)$_3$(H$_2$O)$_2$]As$_2$Se$_4$ and $a = b = 9.9512(3)$ Å and $c = 40.1420(11)$ Å for [Sr(en)$_3$(H$_2$O)$_2$]As$_2$Se$_4$, respectively. Each of the five examined crystals of both structures shows only the space group $P6_1$22 with absolute structure parameters that amount to 0. Hence, crystals of the enantiomorphous space group $P6_5$22 were not found so far. The crystals are yellow-orange hexagonal, transparent rods. A good crystal quality made it possible to resolve the reflections along the c-direction. An image of the $h0l$ plane of one investigated crystal is shown in Figure 75. In addition to the sufficiently separated reflexions, this simulated precession image shows the only extinction present in the reciprocal space, the serial extinction $00l : l = 6n$.
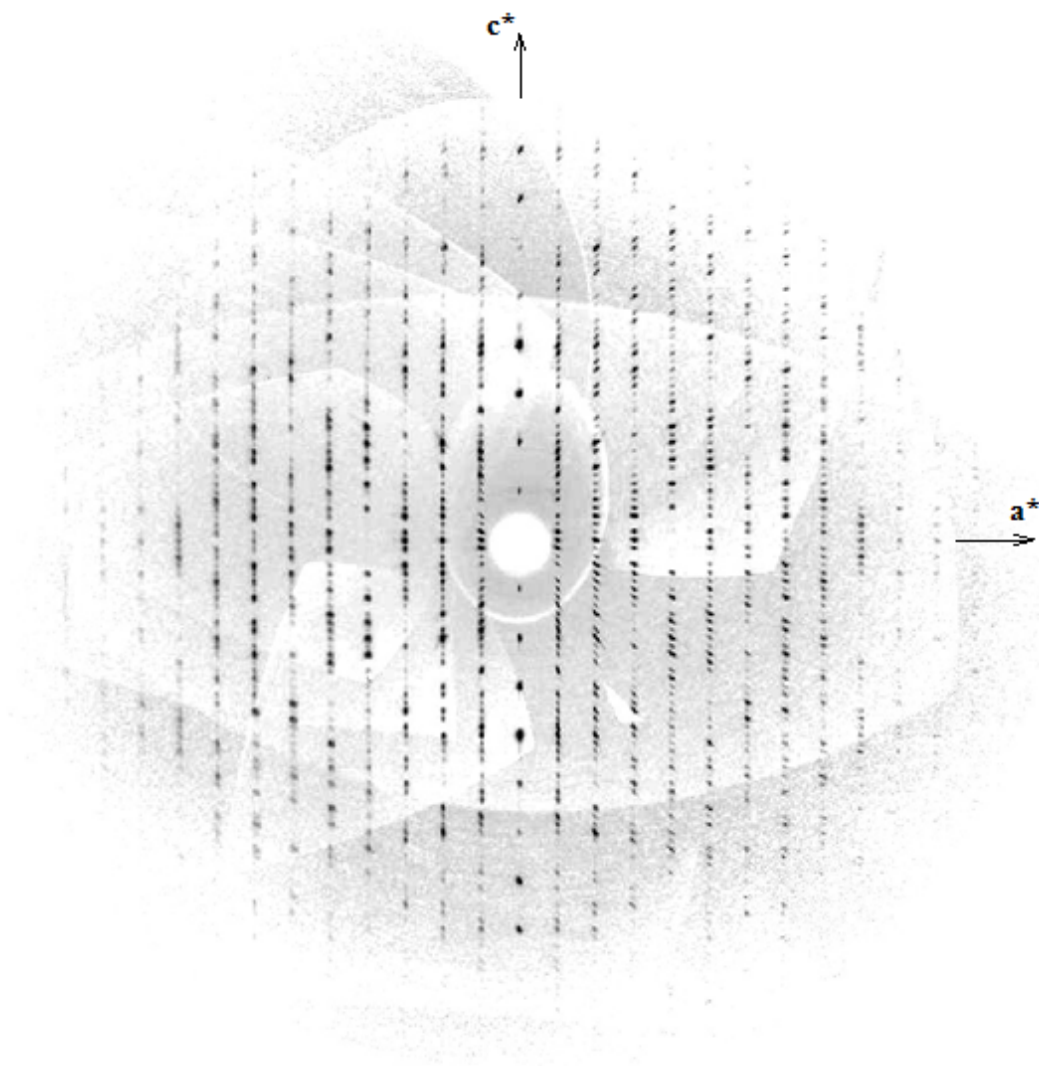
Figure 75: Reconstructed precession image of the $h0l$ plane of a crystal of [Ca(en)$_3$(H$_2$O)$_2$]As$_2$Se$_4$.

The anions of the structure are infinite $[AsSe_2^-]_n$ selenidoarsenate(III) chains (Figure 76). These chains are built up on Ψ^1-tetrahedral $AsSe_3$ units connected via common corners. Each $AsSe_3$ unit contains two bridging Se atoms and one terminal bound Se atom that is negatively charged. This structural motif was first found in the structure of $NaAsSe_2$ [106] by *Eisenmann* and *Schäfer* in 1979. In 1988 *Sheldrick* and *Häusler* published the structures of the compounds $KAsSe_2$, $RbAsSe_2$ and $CsAsSe_2$ [107], all containing the structural motif of polymeric $[AsSe_2]_n^-$ selenidoarsenate(III) chains. The difference between those chains is their repeating units (Figure 78). In $NaAsSe_2$ and $CsAsSe_2$ *zweier* chains and in $KAsSe_2$ and $RbAsSe_2$ *vierer* chains are present. The chains found in the structures presented in this work represent *zwölfer* chains. This is a new conformation in the field of polymeric selenidoarsenate(III) anions.

$$\frac{1}{\infty}\{[AsSe^e_{2/2}Se^t_{1/1}]^-\}$$
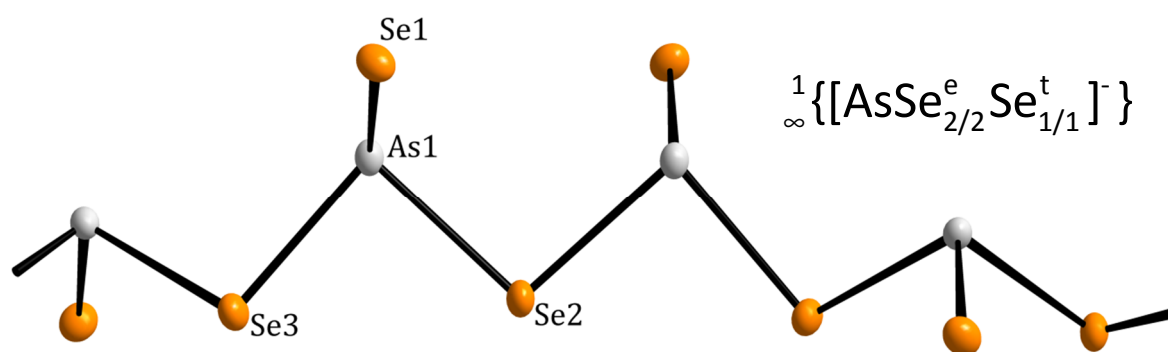
Figure 76: A section of the polymeric selenidoarsenate(III) chain in the structure of $[Ca(en)_3(H_2O)_2]As_2Se_4$ and the respective *Niggli* formula. The displacement ellipsoids represent a probability of 50 %.

Within one Ψ^1-tetrahedral $AsSe_3$ unit, the angles range between 104°-107°. As is in its typical oxidation state +III and both types of Se atoms are in the oxidation state –II. Interatomic distances between As1 and the bridging Se atoms Se2 and Se3 amount to 2.436 Å and 2.431 Å, respectively. These bond lengths are comparable to the endocyclic As-Se bond lengths in discrete cyclic anions like $As_3Se_6^{3-}$ or $As_2Se_6^{2-}$. The bond between As1 and Se1 of 2.310 Å is significantly shorter than those to the bridging Se atoms. This short bond length implies distinct multiple-bond character between As1 and Se1. There are some intramolecular interactions present within the chain. The distance between Se2 and Se3 amounts to 3.369 Å which is significantly shorter than twice the *van-der-Waals* radius of Se ($2r_{vdW}(Se)= 3.80$ Å) and much shorter than the intramolecular Se···Se distance in Na_3AsSe_3 amounting to 3.72 Å [117]. This is

the shortest intramolecular Se-Se distance present in the simple polymeric selenidoarsenate(III) chains so far. The intramolecular Se⋯Se distance correlates with the repeating unit of the respective chain. In the zweier chains of $NaAsSe_2$ and $CsAsSe_2$ the Se⋯Se distance amount to 3.68 Å and 3.66 Å, respectively. In the vierer chains of $KAsSe_2$ and $RbAsSe_2$ intramolecular Se⋯Se distances of 3.44 Å and 3.49 Å, respectively, are present. Since the present very short distances Se2-Se3 and As1-Se1, it is reasonable to assume interactions between them leading to an infinite Se-chain and an As-Se-dumbbell. In Figure 77, the Lewis formulas of both possible descriptions are shown. Interactions between neighboring chains in the crystal structure are not present.
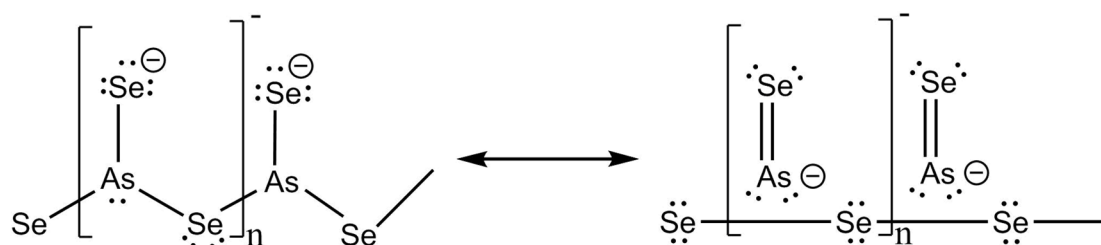
Figure 77: Resonance between two contributing forms in the polymetaselenoarsenite anion.
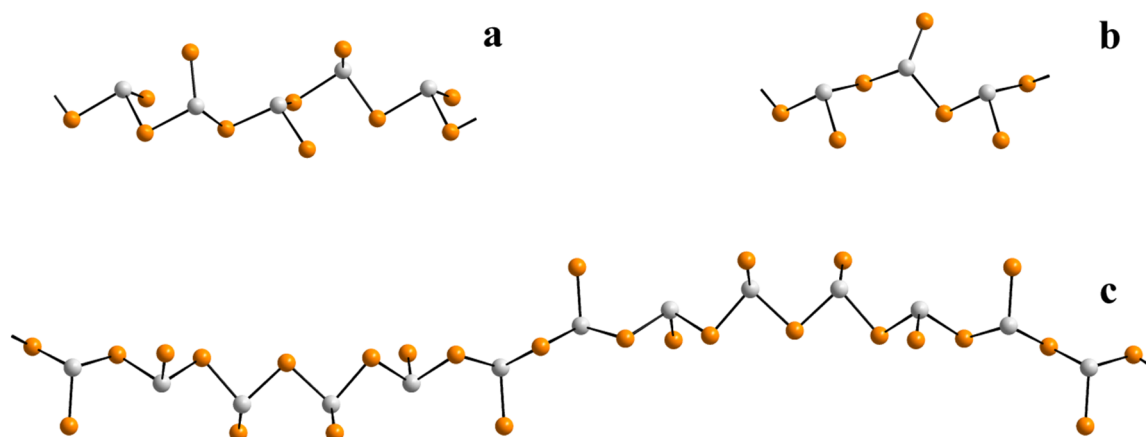
Figure 78: The different conformations of $AsSe_2$-chains: (**a**) *vierer* chains in the structure of $KAsSe_2$ (**b**) *zweier* chains in the structure of $CsAsSe_2$ (**c**) *zwölfer* chains in the structure of $[M(en)_3(H_2O)_2]As_2Se_4$, M = Ca or Sr.

The counterions in the crystal structures are cationic complexes with alkaline earth metal cations as central atoms, namely Ca^{2+} or Sr^{2+}. Each metal ion is surrounded by three en ligands

and two aqua ligands, forming complexes with the coordination number 8 (Figure 79). The coordination polyhedron of $[Ca(en)_3(H_2O)_2]^{2+}$ as well as the coordination polyhedron of $[Sr(en)_3(H_2O)_2]^{2+}$ can be best described as trigonal dodecahedra (D_{2d}). A continuous shape measure gives a deviation from the ideal trigonal dodecahedron (D_{2d}) of 1.082 % for the CaN_8 polyhedron and 1.037 % for the SrN_8 polyhedron. Two of the three en ligands contain a disordering of the CH_2 groups of the ethylene bridge between the N atoms. The disorder was refined to occupation factors of the positions of the C atoms of 40.5 : 59.5. Because of the good single crystal quality, the positions of the hydrogen atoms on the aqua ligands were found in the difference *Fourier* map. The hydrogen atoms of the en ligands were placed on geometrically calculated positions and refined by a riding model. The interatomic distances between the central atom and the coordinating N atoms range between 2.70-2.72 Å for Sr^{2+}-N and between 2.58-2.61 Å for Ca^{2+}-N. These bond lengths are roughly the same found in the ethylenediamine complexes reported in the chapters before.
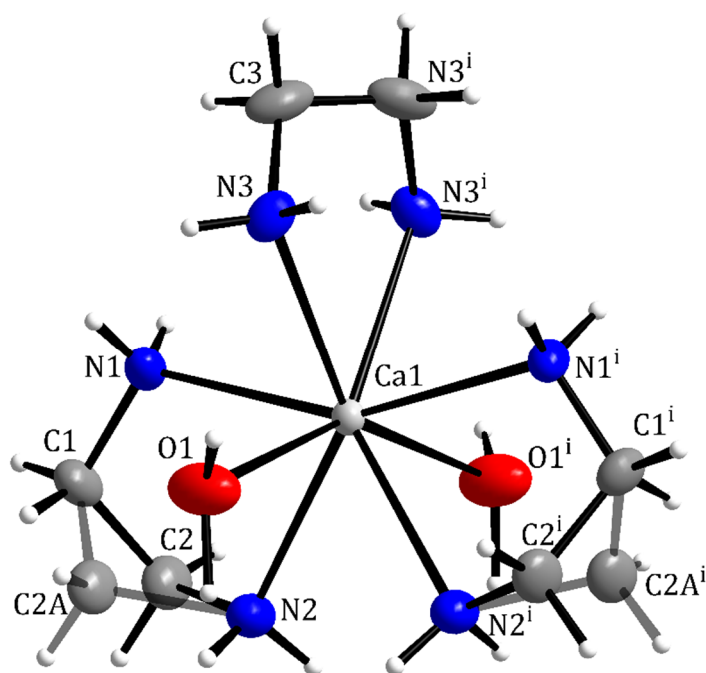
Figure 79: Coordination of Ca^{2+} in the structure of $[Ca(en)_3(H_2O)_2]As_2Se_4$. The displacement ellipsoids represent a probability of 50 %. All hydrogen atoms are drawn with arbitrary radii. The transparency represents a disordering of 40.5 %. The index *i* indicates the symmetry operation: x, $1+x-y$, $7/6-z$.

Table 26: Results of the continuous shape measures of the CaN_8 polyhedron in the structure of $[Ca(en)_4]As_2Se_4$ and of the SrN_8 polyhedron in the structure of $[Sr(en)_4]As_2Se_4$.

Ideal Shape	CShM / % (CaN_8 polyhedron)	CShM / % (SrN_8 polyhedron)
OP-8	30.965	31.466
HPY-8	24.457	23.839
HBPY-8	14.454	15.086
CU-8	10.954	12.013
SAPR-8	1.894	2.589
TDD-8	**1.082**	**1.037**
BTPR-8	2.104	2.438

In Figure 80 the position of the polymeric anion within the unit cell is shown. The chain runs along the crystallographic c-axis and coils around the edge of the unit cell. This figure also shows the reason for the length of the c-axis. Because of the 6_1 screw axis along the c-axis and a twofold rotation axis orthogonal to the c-axis, twelve $AsSe_2$ units are needed to complete the translational unit. On the right side of Figure 80 can be seen that the negatively charged and terminal bound Se atoms are pointing away from the c-axis. This orientation allows structure directing hydrogen bonds between cations and the polymeric anion in the crystal structure.
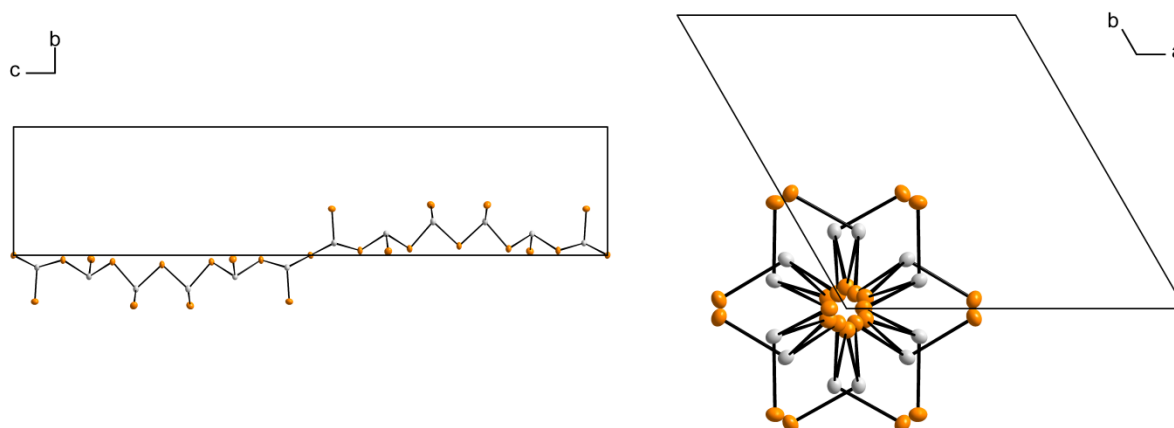
Figure 80: A view of the unit cell of $[M(en)_3(H_2O)_2]As_2Se_4$, M = Ca or Sr, along the crystallographic a-axis(left) and along the crystallographic c-axis (right). Only one polymeric $[AsSe_2]_n^-$ unit is shown exemplarily. The displacement ellipsoids represent a probability of 50 %.

The three most important hydrogen bonds are depicted in Figure 81. Two of the three hydrogen bonds have the atom N2 as donor. For N2 as donor the donor-hydrogen-acceptor angle amounts to 169° or 144°, respectively and the hydrogen bond lengths amounts to 3.09 Å or 2.92 Å, respectively. The most significant hydrogen bond is the one with O1 as donor, since the position of this hydrogen atom could be found in the difference *Fourier* map. The angle O1-H-Se differs not much from linearity and amounts to 171°. Furthermore, the hydrogen bond length is relatively short, $d_{O1-H\cdots Se} = 2.58$ Å.

A filled unit cell of the structure is depicted in Figure 82. The anionic chains run parallel to the c-axis along all four cell edges. The cationic complexes fill the voids between the chains connecting them via hydrogen bonds.
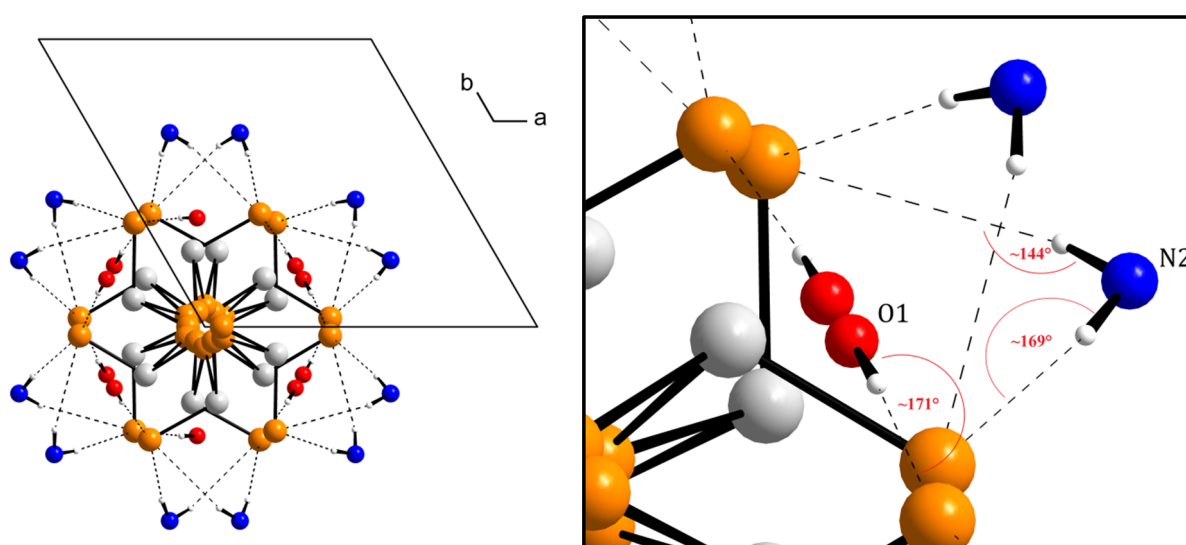
Figure 81: View on the structure directing hydrogen bonds along the crystallographic *c*-axis (left) and a zoom (right).
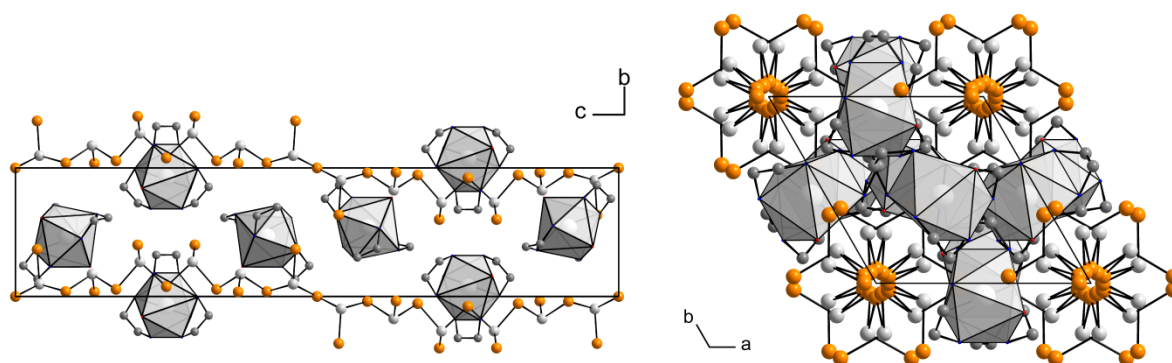
Figure 82: View of the extended unit cell of $[M(en)_3(H_2O)_2]As_2Se_4$, M = Ca or Sr, along the crystallographic *a*-axis (left) and the crystallographic *c*-axis (right). Hydrogen atoms are omitted for clarity.

EDX analyses of the examined crystals gave M:As:Se ratios of 1.00:1.72:2.00 for [Ca(en)$_3$(H$_2$O)$_2$]As$_2$Se$_4$ (

Table 27) and 1.00:1.30:1.65 for [Sr(en)$_3$(H$_2$O)$_2$]As$_2$Se$_4$ (Table 28), respectively. The expected ratio is 1.00:2:00:4.00. The low content of selenium and arsenic in the crystals may origin from partial decomposition during exposure to air and the evolution of H$_2$Se and arsine. These gases were generated on handling the crystals and warming them up to room temperature. They were detected by their specific odors. The most important information given by these EDX analyses is that all elements according to the respective formula are actually present in the crystals.

Table 27: Result of the EDX analysis for the crystal of the compound with the composition [Ca(en)$_3$(H$_2$O)$_2$]As$_2$Se$_4$.

	Ca	As	Se
Atomic %	21.2	36.5	42.3
Normalized	1.00	1.72	2.00
Expected	1	2	4

Table 28: Result of the EDX analysis for the crystal of the compound with the composition [Sr(en)$_3$(H$_2$O)$_2$]As$_2$Se$_4$.

	Sr	As	Se
Atomic %	25.3	32.9	41.8
Normalized	1.00	1.30	1.65
Expected	1	2	4

3.3 Compounds containing coinage metal chalcogenides

Coinage metal chalcogenides are of interest because of their properties. In most cases, they are small band gap semiconductors and they often have interesting thermoelectric properties. Thermoelectric compounds show semiconducting behavior with a small band gap and a large *Seebeck* coefficient [118]. Beside the properties, compounds containing coinage metals and chalcogenides show a rich structural variety. Interconnecting chain-like polychalcogenides with coinage metals can lead either to molecular structures or to one or more dimensional structural motifs. The known coinage metal chalcogenides mostly synthesized at high temperatures in classical solid-state reactions [119], in fluxes of molten alkaline metals [120] or via electrochemical synthesis [121]. These syntheses were performed starting from the elements or from some precursor compounds such as A_2Q, with A = Na-Cs [122].

The biggest problem during the implementation of coinage metals in compounds via chemical synthesis is their low reactivity. To increase the reactivity ammonothermal synthesis was used in the course of this thesis work. It is known that gold can be dissolved in liquid ammonia in presence of a alkaline metal as auride ions [123]. Since alkaline earth metals and the lanthanoids europium and ytterbium forming blue colored electride solution during their dissolution in liquid ammonia it could be possible to bring gold into solution.

Ammonothermal synthesis led to the observation of the first homoleptic lanthanide ammine complexes $[Yb(NH_3)_8]^{3+}$ and $[La(NH_3)_9]^{3+}$ [73]. As counterions thiometallates of the type $[M(S_4)_2]^{3-}$(M = Cu or Ag) were formed. Chalcogenidocuprates or chalcogenidoargentates commonly form low-dimensional motifs as found in α- or β-KCuS$_4$ [124] and in $[(Ph_4P)AgSe_4]_n$ [125].

In 1985 *Haushalter* observed the molecular ring-shaped $[Au_4Te_4]^{4-}$ anion in $[Ph_4P]_2[K_2Au_4Te_4(en)_4]$ [126] by extraction from a KAuTe alloy. A few years later in 1993 *Warren* and *Haushalter* described another possibility to synthesize telluridoaurates. By electrochemically dissolution of an AuTe$_2$ cathode in a tetrabutylammonium iodide solution, the molecular telluridometallate $[Au_3Te_4]^{3-}$ in the structure of (TBA)$_3$[Au$_3$Te$_4$] [121] was formed. Discrete anionic complexes are also present with sulfur and selenium, e.g. in $(PPh_4)_2[Au_2(Se_2)_2(Se_3)]$ [127], Li$_3$AuS$_2$ [120] or in Na$_5$AuSe$_{12}$ [128].

Simple AuQ$_2$ (Q = S, Se or Te) zig-zag chains with linear coordinated gold(I) are present in the structures of MAuTe (M = Rb or Cs) [122], MAuSe and MAuS (M = K, Rb or Cs) [129]. At 40 kbar a high pressure modification of RbAuTe exists, where the chains are pushed together forming hexagonal layers with coordination number 3 for gold and tellurium [130]. More

complex one-dimensional chalcogenidoaurates as the $(AuSe_5)^-$ or the coiled "chicken-wire"-like $(AuS)^-$ anions were found in the structures of $CsAuSe_5$ [131] or $NaAuS$ [132], respectively. Higher-dimensional chalcogenidoaurates are only known for selenium and tellurium. Layered chalcogenidoaurates were observed in the structures of $NaAuSe_2$ [133] and $CrAuTe_4$ [134]. In both structures, gold is in the oxidation state +III and square planar coordinated by the respective chalcogen atoms.

3.3.1 [Ln(NH$_3$)$_8$][Cu(S$_4$)$_2$]·NH$_3$ with Ln = Eu or Er

The compounds [Eu(NH$_3$)$_8$][Cu(S$_4$)$_2$]·NH$_3$ and [Er(NH$_3$)$_8$][Cu(S$_4$)$_2$]·NH$_3$ crystallize isotypic in the tetragonal space group $I\bar{4}$ with the lattice parameters a = 10.0716(1) Å, c = 9.8677(2) Å for Ln = Eu and a = 10.0096(3) Å, c = 9.8212(3) Å for Ln = Er, respectively. Crystals with with Ln = Eu are of orange and crystals with with Ln = Er are of yellow color. The crystals are transparent and block-shaped. An EDX analysis (Table 29) of a crystal of [Er(NH$_3$)$_8$][Cu(S$_4$)$_2$]·NH$_3$ verifies the ratio Er:Cu:S of 1:1:8. For the structure solution and refinement, the examined crystal of [Eu(NH$_3$)$_8$][Cu(S$_4$)$_2$]·NH$_3$ was treated as a merohedral twin. Figure 83 shows images of the *hk*0 planes of the investigated crystals of [Eu(NH$_3$)$_8$][Cu(S$_4$)$_2$]·NH$_3$ (right) and [Er(NH$_3$)$_8$][Cu(S$_4$)$_2$]·NH$_3$ (left). The intensities of the reflections show for Ln = Er 4/*m Laue* symmetry, while the crystal with Ln = Eu seems to have 4/*mmm Laue* symmetry. In Figure 83, some reflections are exemplarily marked for better comparability. Equation 3 shows the used twin law for the structure solution and refinement. The twin law defines a 180° rotation about the [110] direction. Another proof for the existing twinning gave the quality factors R_{int}. The quality factor R_{int} on averaging symmetry equivalent reflections in the *Laue* class 4/*mmm* amounted to 9.3 % for [Eu(NH$_3$)$_8$][Cu(S$_4$)$_2$]·NH$_3$ but to 31.1 % for [Er(NH$_3$)$_8$][Cu(S$_4$)$_2$]·NH$_3$. The crystal structures, however, belong to the low symmetric tetragonal *Laue* class 4/*m*.

Table 29: Result of an EDX analysis of a crystal of [Er(NH$_3$)$_8$][Cu(S$_4$)$_2$]·NH$_3$.

	Er	**Cu**	**S**
Atomic %	9.90	10.30	79.80
Normalized	1.00	1.04	8.06
Expected	1	1	8
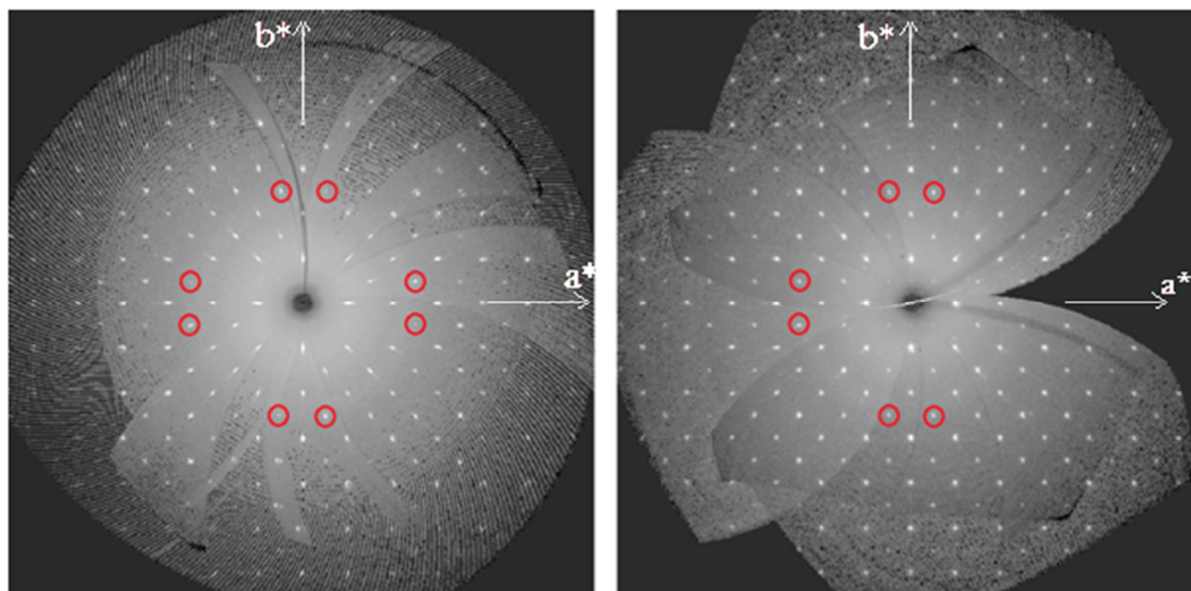
Figure 83: Reconstructed precession images of the $hk0$ planes with exemplarily marked reflections (red) of the analyzed crystals of $[Er(NH_3)_8][Cu(S_4)_2] \cdot NH_3$ (left) and of $[Eu(NH_3)_8][Cu(S_4)_2] \cdot NH_3$ (right).

$$\begin{pmatrix} h^2 \\ k^2 \\ l^2 \end{pmatrix} = \begin{pmatrix} 0 & 1 & 0 \\ 1 & 0 & 0 \\ 0 & 0 & -1 \end{pmatrix} \begin{pmatrix} h^1 \\ k^1 \\ l^1 \end{pmatrix}$$

Equation 3: Twin law used for structure refinement of $[Eu(NH_3)_8][Cu(S_4)_2] \cdot NH_3$.

The crystal structure contains three different building blocks, a cationic homoleptic ammine complex, a sulfido metallate and a free ammonia molecule. In the homoleptic ammine complexes, the trivalent lanthanides Eu^{3+} and Er^{3+} are surrounded by eight ammine ligands (Figure 84). The position of the hydrogen atoms were not found in the difference *Fourier* map. They were placed on geometrically calculated positions and refined by a riding model. The formed coordination polyhedra can be best described as triangular dodecahedra (D_{2d}). A continuous shape measure gives small deviations from the ideal shape amounting to 0.261 % and 0.218 %, respectively. The Eu-N bond lengths of 2.54 and 2.55 Å are comparable to other homoleptic ammine complexes of Eu^{3+}. Eu-N bond lengths in homoleptic ammine complexes with divalent Eu^{2+} are in general significantly longer (2.72 – 2.82 Å [72]). Interatomic distances within the homoleptic erbium ammine complex, 2.48 and 2.49 Å, are roughly the same as they can be found in the structure of $[Er(NH_3)_8]_2(S_6)_2(S_7) \cdot 3NH_3$ (see chapter 3.1.2).

The free ammonia molecules are symmetrically disordered. They are located on the Wyckhoff position 4e with the site symmetry 2 (C_2). The site of the N atom of the free ammonia molecule was only refined with an isotropic displacement factor. The position of the hydrogen atoms of the free ammonia were not found in the difference *Fourier* map.
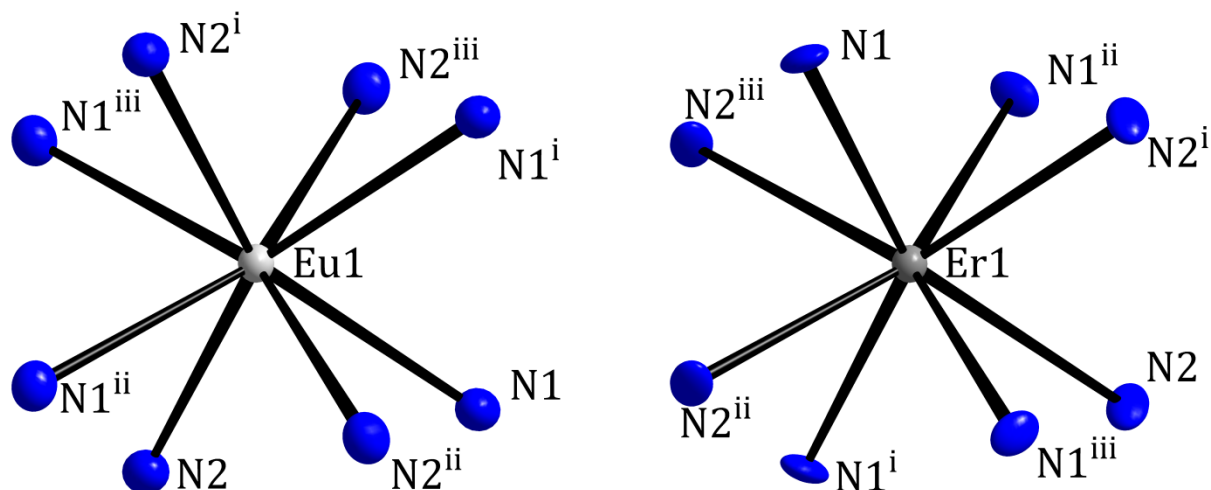
Figure 84: Coordination of the lanthanide ions in the structure of [Ln(NH$_3$)$_8$][Cu(S$_4$)$_2$]·NH$_3$. The displacement ellipsoids represent a probability of 50%. All hydrogen atoms bound to the N atoms of the ammine ligands are omitted for clarity. The indices *i* indicate the following symmetry operations: (*i*) 1-*x*, 1-*y*, *z*; (*ii*) 1-*y*, *x*, 1-*z*; (*iii*) *y*, 1-*x*, 1-*z*.

Table 30: Results of the continuous shape measures of the EuN$_8$ polyhedron in the structure of [Eu(NH$_3$)$_8$][Cu(S$_4$)$_2$]·NH$_3$ and of the ErN$_8$ polyhedron in the structure of [Er(NH$_3$)$_8$][Cu(S$_4$)$_2$]·NH$_3$.

Ideal Shape	CShM / % (EuN$_8$ polyhedron)	CShM / % (ErN$_8$ polyhedron)
OP-8	33.911	33.836
HPY-8	25.283	25.281
HBPY-8	13.474	13.737
CU-8	5.545	5.832
SAPR-8	3.153	3.093
TDD-8	**0.261**	**0.218**
BTPR-8	3.434	3.332

The anion $[Cu(S_4)_2]^{3-}$ was first reported by *Kohlis et al.* in 1996 in the structure of $[Yb(NH_3)_8][Cu(S_4)_2]\cdot NH_3$ [73], which is isotypic to the crystal structure presented here. Copper is in the formal oxidation state +I and is coordinated by two chelating $(S_4)^{2-}$ units forming two CuS_4 five-membered rings with a distorted tetrahedral environment on central atom. The angles within the coordination of Cu1 amount to 99.9° and 114.5°. The Cu1-S1 bond length of 2.320 Å is similar to that of $[Yb(NH_3)_8][Cu(S_4)_2]\cdot NH_3$ (2.316 Å). Within the chelating $(S_4)^{2-}$ units the interatomic distances amount to 2.064 Å and 2.085 Å. These bonds are consistent with bond lengths in known polysulfides and the S_8 rings of elemental sulfur. The S-S-S angle amounts to 103.9°. Cu1 is located on a special position with the site symmetry $\bar{4}$, S1 and S2 are placed on general positions. Hence, the anionic molecule has $\bar{4}$ (S_4) symmetry and therefore its point group and the crystal class are coincident.
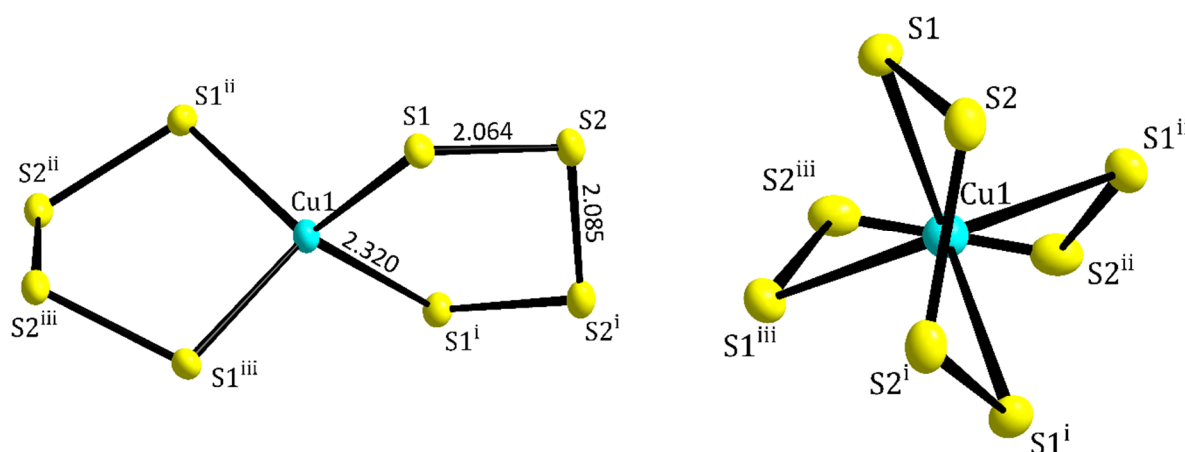
Figure 85: $[Cu(S_4)_2]^{3-}$ anion in the structure of $[Er(NH_3)_8][Cu(S_4)_2]\cdot NH_3$. Bond lengths are given in Å. The displacement ellipsoids represent a probability of 50%. The indices *i* indicate the following symmetry operations: (*i*) 2-*x*, 1-*y*, *z*; (*ii*) ½+*y*, ⅔-*x*, ½-*z*; (*iii*) ³/₂-*y*, -½+*x*, ½-*z*.

The lanthanide complexes are placed on all corners and in the center of the pseudo cubic unit cell forming a pseudo body-centered cubic cell. Therefore, they adopt the tungsten structure type. There are compressed octahedral voids present on each cell edge, in which the $[Cu(S_4)_2]^{3-}$ anions are placed with their centers of gravity on unit cell faces in the position $(1,^1/_2,^1/_4)$. Hence, each anion is surrounded by eight lanthanide complexes. The resulting coordination polyhedron

can be described as two compressed interpenetrating octahedra (Figure 86). The free ammonia molecules occupy voids on four cell edges and two cell faces. In each case the position of the free ammonia molecules is slightly shifted from the center of the respective cell edge or cell face along the crystallographic c-axis.
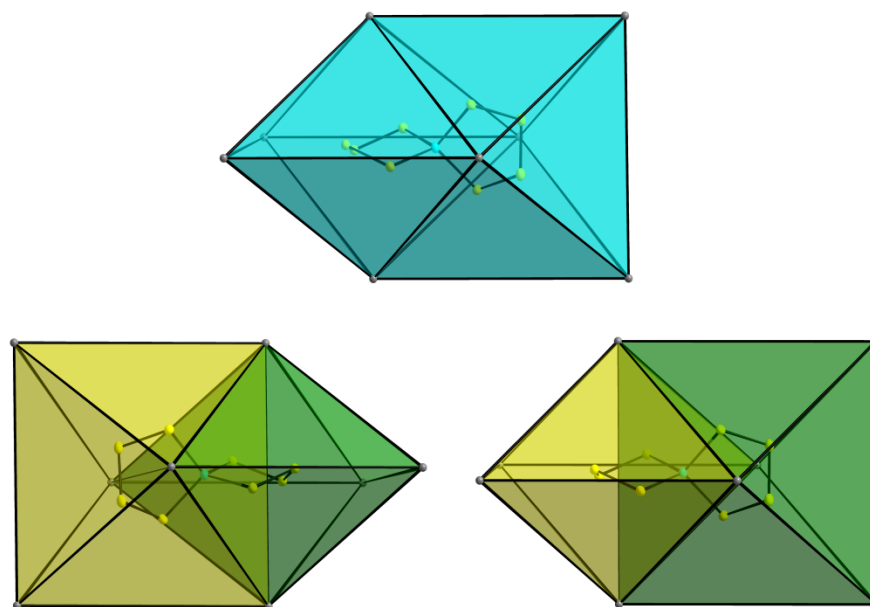
Figure 86: Coordination of the $[Cu(S_4)_2]^{3-}$ anions in the structure of $[Ln(NH_3)_8][Cu(S_4)_2]\cdot NH_3$. The whole coordination polyhedron is shown in blue; the different compressed octahedra are shown in green and yellow. The displacement ellipsoids represent a probability of 50%. The ammonia molecules of the ammine complexes are omitted for clarity.
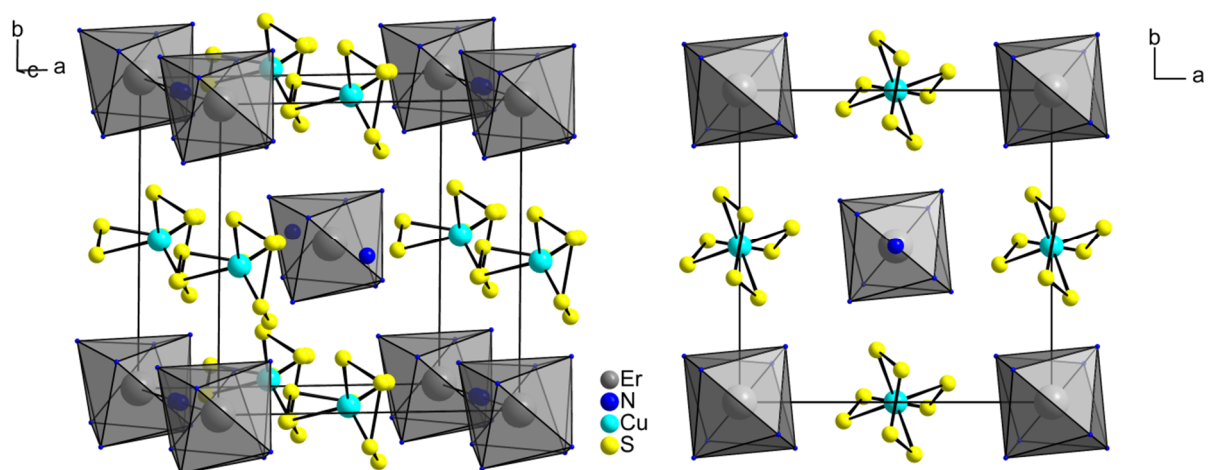
Figure 87: A perspective view on the unit cell (right) and a view along the crystallographic c-axis of the structure $[Er(NH_3)_8][Cu(S_4)_2]\cdot NH_3$. All atoms are drawn with arbitrary radii. Hydrogen atoms are omitted for clarity.

3.3.2 [Eu(NH$_3$)$_9$][Ag(Se$_4$)$_2$]·2NH$_3$

The structure of the crystals with the composition [Eu(NH$_3$)$_9$][Ag(Se$_4$)$_2$]·2NH$_3$ is not isotypic to the crystal structure of [Ln(NH$_3$)$_8$][Cu(S$_4$)$_2$]·NH$_3$ presented in the previous chapter. [Eu(NH$_3$)$_9$][Ag(Se$_4$)$_2$]·2NH$_3$ crystallizes in the acentric tetragonal space group $P\bar{4}n2$ with the lattice parameters a = 15.2120(7) Å and c = 11.2754(6) Å. The quality factor R$_{int}$ on averaging symmetry equivalent reflections amounted to 20.0% and shows the limited quality of the dataset. The high R$_{int}$ value originates from some crystalline adhesions caused by the crystal preparation on the goniometer head. An EDX analysis of the crystal showed a composition Eu:Ag:Se of 1:1:6.6 (Table 32), which differs slightly from the expected composition of 1:1:8. The low content of selenium in the crystal may origin from partial decomposition during exposure of the crystal to air and the evolution of H$_2$Se. This gas was generated on handling the crystals und detected by its specific odour.

A homoleptic europium ammine complex is present as cation in this compound. In contrast to the europium ammine complex in the structure of [Eu(NH$_3$)$_8$][Cu(S$_4$)$_2$]·NH$_3$, this complex bears nine ammine ligands. Europium is in the formal oxidation state +III. The coordination polyhedron of Eu can be best described as capped square antiprism (D_{4d}) (Figure 88). A continuous shape measure gives a very small deviation from the ideal polyhedron of 0.233 % (Table 31). N3 is located on the *Wyckhoff* position 4f with the site symmetry 2. Therefore, the hydrogen atoms bound to N3 are disordered and have site occupancy factors of 0.5. The Eu-N bond lengths within the ammine complex range from 2.50 Å to 2.65 Å. Hence, they are in average (2.58 Å) slightly longer than that found in europium ammine complexes with the coordination number 8 (2.55 Å). The positions of the hydrogen atoms of the ammine ligands were not found in the difference *Fourier* map. They were placed on geometrically calculated positions and refined using the riding model.
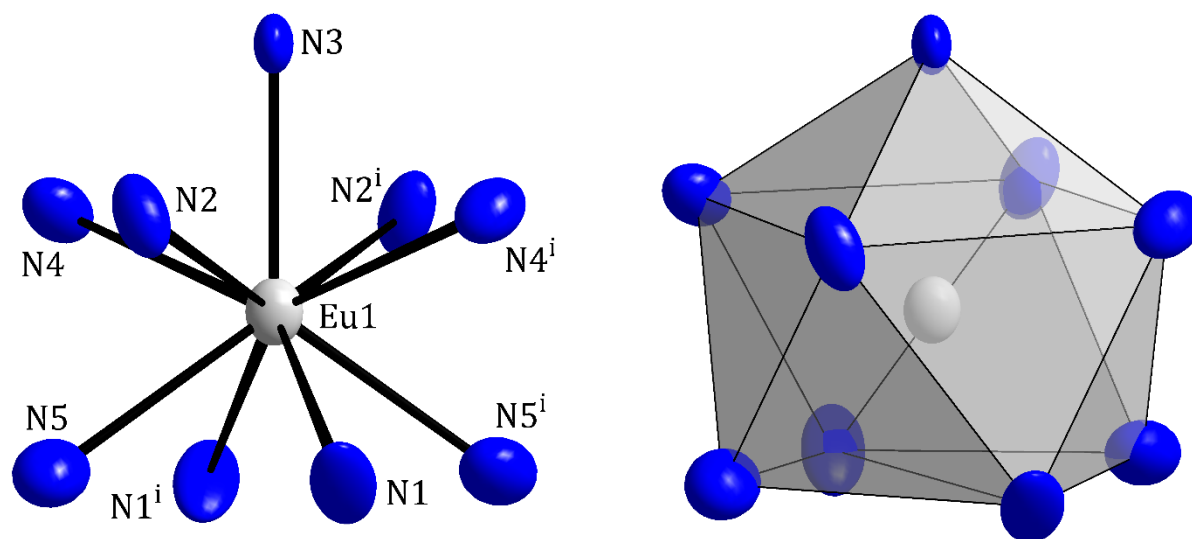
Figure 88: Left: Coordination of Eu^{3+} in the structure of $[Eu(NH_3)_9][Ag(Se_4)_2] \cdot 2NH_3$. The displacement ellipsoids represent a probability of 50%. The index i indicates the following symmetry operation: $-\frac{1}{2}+y$, $\frac{1}{2}+x$, $\frac{2}{3}-z$. Right: Coordination polyhedron of Eu^{3+} in the structure of $[Eu(NH_3)_9][Ag(Se_4)_2] \cdot 2NH_3$. Hydrogen atoms are omitted for clarity.

Table 31: Result of a continuous shape measure of the EuN_9 polyhedron in the structure of $[Eu(NH_3)_9][Ag(Se_4)_2] \cdot 2NH_3$.

Ideal Shape	CShM / % (EuN₉ polyhedron)
EP-9	37.645
OPY-9	21.255
HBPY-9	19.772
JTC-9	16.709
CCU-9	8.042
CSAPR-9	**0.233**
TCTPR-9	0.892

The anion of the compound, a selenido argentate anion, was not reported before. However, an isostructural anion with the lighter homologue sulfur is known [73]. The $[Ag(Se_4)_2]^{3-}$ anion is built up by two chelating $(Se_4)^{2-}$ units that form two five-membered chelate rings with the

central silver ion. Silver is in the formal oxidation state +I. Hence, the anion is threefold negatively charged. The two chelating (Se$_4$) units form a strongly distorted tetrahedral coordination of the silver ion with Se-Ag-Se angles ranging from 98.6 ° to 129.4 °. Angles within the chelating (Se$_4$) units amount to 102.34 ° and 102.39 °. The bond lengths Se1-Se2 and Se3-Se4 of 2.345 Å and 2.341 Å are similar to twice the covalent radius of Se ($2 \cdot r_{Se}$=2.34 Å). The slightly elongated bond length between Se2 and Se3 is comparable to bond lengths found in other polyselenides, such as in (Se$_4$)$^{2-}$ in Na$_2$Se$_4$ (d_{Se-Se}=2.35 Å and 2.36 Å)[135]. Ag-Se bond lengths of 2.68 Å and 2.66 Å are typical for such bonds and can be found in other cluster anions like [Ag(Se$_4$)]$_4$$^{4-}$[136]. Ag1 is located in a special position with the site symmetry 2. Therefore, the symmetry of the point group of the molecular anion (C_2) is lower than the symmetry of the crystal class (D_{2d}).
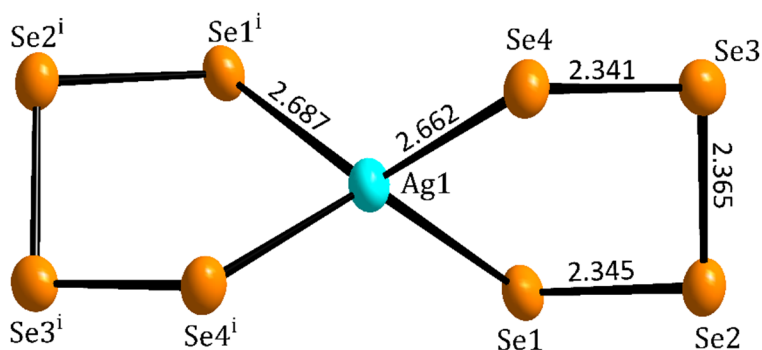
Figure 89: The [Ag(Se$_4$)$_2$]$^{3-}$ ion in the structure of [Eu(NH$_3$)$_9$][Ag(Se$_4$)$_2$]·2NH$_3$. Bond lengths are given in Å. The displacement ellipsoids represent a probability of 50 %. The index *i* indicates the following symmetry operation: -½+*y*, ½+*x*, ½-*z*.

Table 32: Result of the EDX analysis of a crystal of [Eu(NH$_3$)$_9$][Ag(Se$_4$)$_2$]·2NH$_3$.

	Eu	**Ag**	**Se**
Atomic %	11.6	11.7	76.7
Normalized	1.00	1.01	6.61
Expected	1.00	1.00	8.00
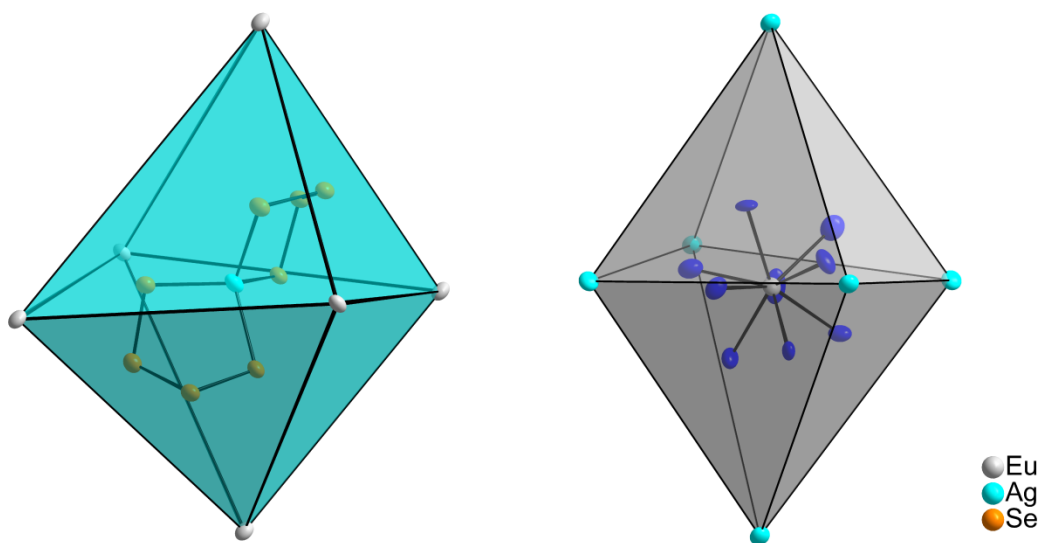
Figure 90: Coordination of the $[Ag(Se_4)_2]^{3-}$ anion by Eu^{3+} (left) and the coordination of $[Eu(NH_3)_9]^{3+}$ by $[Ag(Se_4)_2]^{3-}$ (right) in the structure of $[Eu(NH_3)_9][Ag(Se_4)_2] \cdot 2NH_3$. The displacement ellipsoids represent a probability of 50%. The hydrogen atoms bound to the N atoms of the ammine ligands were omitted for clarity.

In Figure 90, the coordination environments of the ions $[Ag(Se_4)_2]^{3-}$ and $[Eu(NH_3)_9]^{3+}$ in the crystal structure is shown. Each $[Ag(Se_4)_2]^{3-}$ anion is surrounded by six $[Eu(NH_3)_9]^{3+}$ cationic complexes and vice versa. The formed coordination polyhedra can be described as distorted octahedra. The structure of $[Eu(NH_3)_9][Ag(Se_4)_2] \cdot 2NH_3$ can be derived from the rock salt structure type. The anions form a pseudo cubic closest packing as chloride ions in the rock salt structure. All octahedral voids in the pseudo cubic closest packing of $[Ag(Se_4)_2]^{3-}$ ions are occupied by $[Eu(NH_3)_9]^{3+}$ ions. In Figure 91, the pseudo cubic closest packing is shown with the anions and cations reduced to their center of gravity. In the case of the $[Ag(Se_4)_2]^{3-}$ ion, the center of gravity was approximately placed in the position of the silver atoms and for the $[Eu(NH_3)_9]^{3+}$ ions, the position of the europium ions was approximately used as center of gravity. The free ammonia fill in half of the tetrahedral voids in the crystal structure (Figure 92). Each filled tetrahedral void contains two free ammonia molecules. Therefore, the overall ratio between the anions, cations and free ammonia molecules is 1:1:2.

In Figure 93 the actual tetragonal unit cell is shown. The short crystallographic c-axis in this pseudo cubic structure can be explained by the shape of the anions, which lie perpendicular to the crystallographic c-axis with their flat sites.
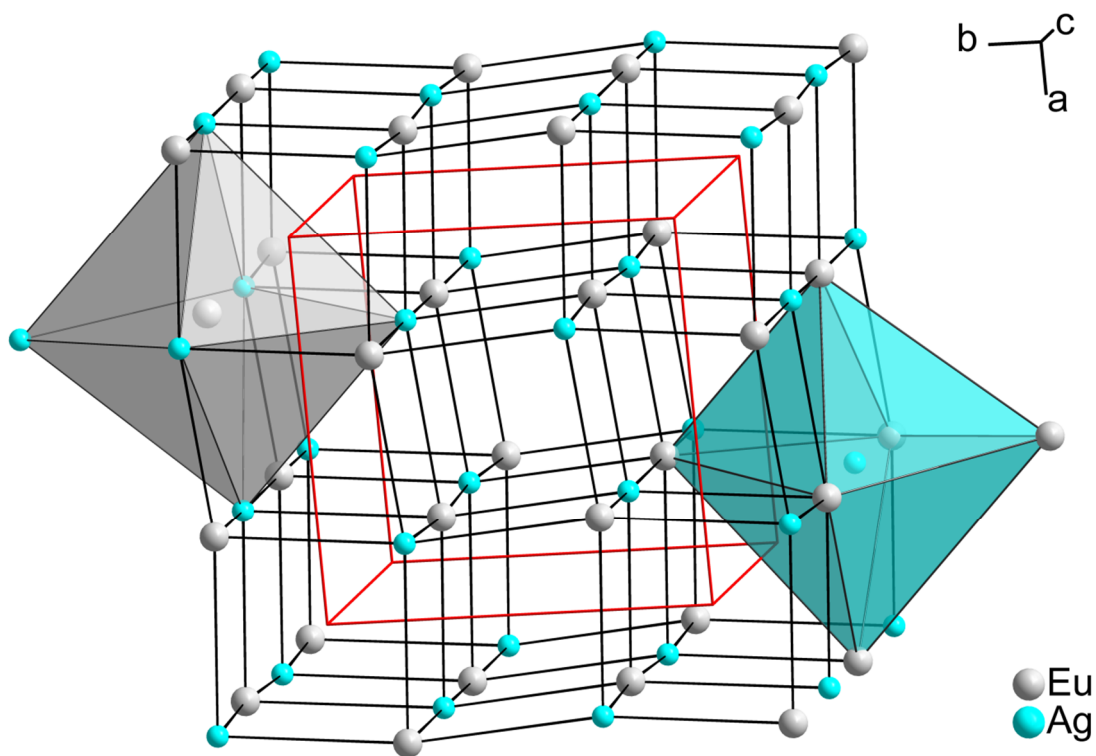
Figure 91: The pseudo rock salt structure like lattice in the structure of $[Eu(NH_3)_9][Ag(Se_4)_2]\cdot 2NH_3$. All atoms are drawn with arbitrary radii. The anions and cations were reduced to their center of gravity. The free ammonia molecules are omitted for clarity. The actual crystallographic unit cell edges are drawn in red.
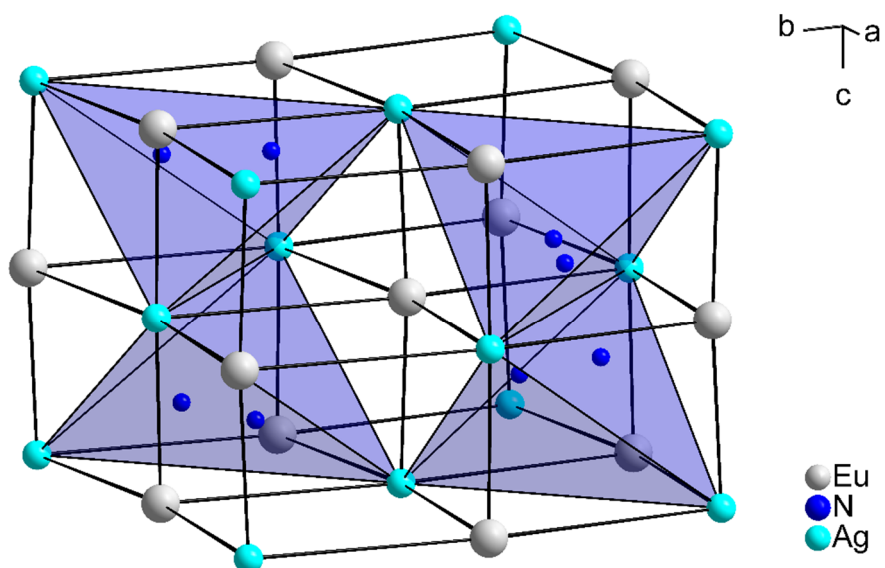
Figure 92: The pseudo rock salt structure like lattice in the structure of $[Eu(NH_3)_9][Ag(Se_4)_2]\cdot 2NH_3$. All atoms are drawn with arbitrary radii. The anions and cations were reduced to their center of gravity.
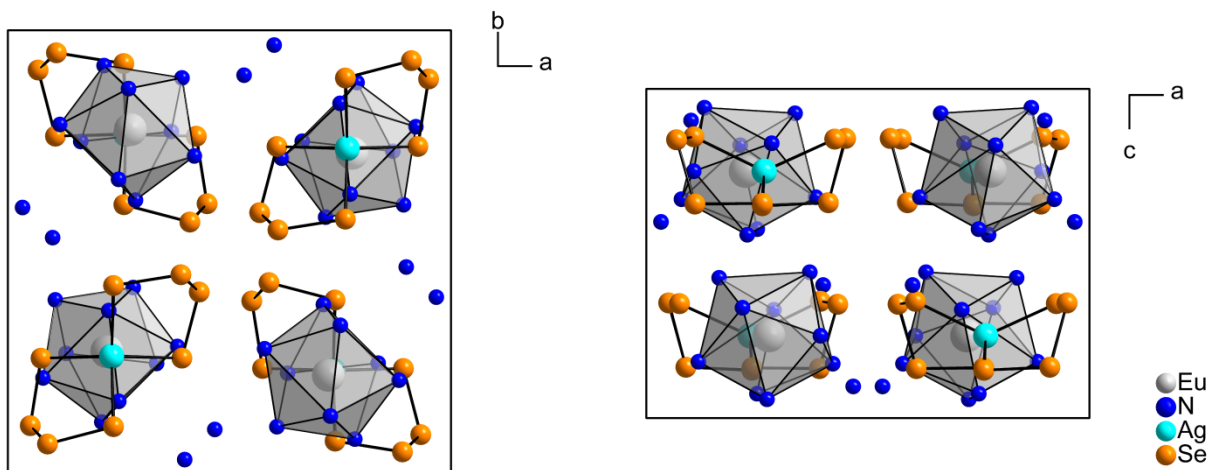
Figure 93: A view of the actual crystallographic unit cell of [Eu(NH$_3$)$_9$][Ag(Se$_4$)$_2$]·2NH$_3$ along the crystallographic *c*-axis (left) and along the crystallographic *b*-axis.. All atoms are drawn with arbitrary radii. All hydrogen atoms are omitted for clarity.

3.3.3 [Yb(NH$_3$)$_8$](AuSe$_5$S$_7$)·NH$_3$

[Yb(NH$_3$)$_8$]$_2$(Au$_2$Se$_{10}$S$_{14}$)·2NH$_3$ is a compound with a polymeric, mixed-chalcogen gold(III)chalcogenido complex in its crystal structure. The compound crystallizes in the centrosymmetric triclinic space group $P\bar{1}$ with the lattice parameters a = 9.1610(3), b = 9.5272(2), c = 15.4891(5), α = 87.445(2)°, β = 84.318(1)° and γ = 67.723(2)°. Crystals of [Yb(NH$_3$)$_8$](AuSe$_5$S$_7$)·NH$_3$ are of black metallic appearance (Figure 94) and they have a columnar crystal habit. The crystals are not stable at room temperature due to the loss of ammonia.
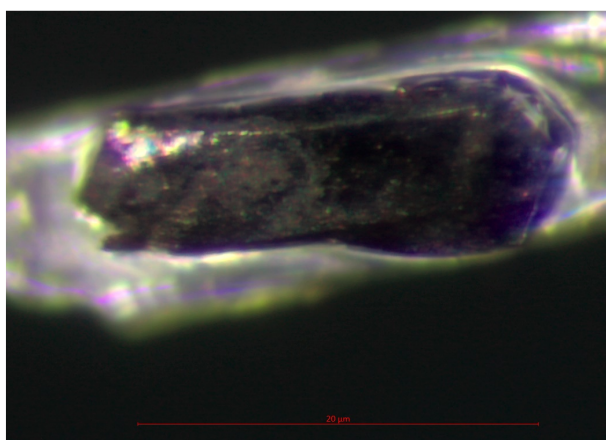
Figure 94: Image of the analyzed crystal with the composition [Yb(NH$_3$)$_8$](AuSe$_5$S$_7$)·NH$_3$. The image was directly taken with a video microscope after the crystal was placed outside the cooling system of the single crystal x-ray diffractometer.

Besides the named chalcogenidoaurate(III), the crystal structure contains free ammonia molecules and ytterbium ethylene diamine complexes serving as counterions. The positions of the hydrogen atoms of the free ammonia molecule and the ammine ligands were not found in the difference *Fourier* map. All hydrogen atoms bound to the N atoms of the ammine ligands were placed on geometrically calculated positions and refined by using a riding model. For the free ammonia molecule only the N atoms without hydrogen atoms was refined. In the complex, Yb is in the oxidation state +III. It is surrounded by eight ammine ligands forming a distorted square antiprism (D_{4d}). A continuous shape measure with the program SHAPE gives a deviation from the ideal square antiprism (D_{4d}) that amounts to 0.504%. Deviations to all other ideal polyhedra are entirely larger (Table 33). The bond lengths between Yb^{3+} and the N atoms of the ammine ligands range between 2.40 Å and 2.48 Å. Therefore, they are in a typical range of

Yb-N bond lengths and they verify the oxidation state +III of Yb. For Yb in the oxidation state +II, the Yb-N bond lengths were significantly longer, ranging between 2.61 Å and 2.75 Å.
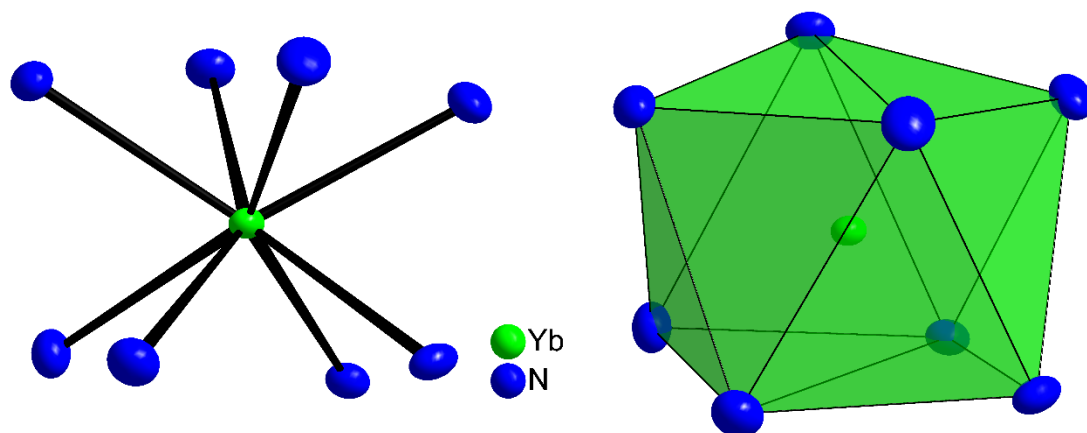
Figure 95: Coordination polyhedron of Yb^{3+} in two different representations in the structure of $[Yb(NH_3)_8](AuSe_5S_7) \cdot NH_3$. The displacement ellipsoids represent a probability of 50%. All hydrogen atoms bound to the N atoms of the ammine ligands are omitted for clarity.

Table 33: Result of a continuous shape measure calculation of the YbN_8 polyhedron in the structure of $[Yb(NH_3)_8](AuSe_5S_7) \cdot NH_3$.

Ideal Shape	CShM / % (YbN_8 polyhedron)
OP-8	30.133
HPY-8	23.783
HBPY-8	16.761
CU-8	10.437
SAPR-8	**0.504**
TDD-8	1.513
BTPR-8	1.475

The anion consists of square planar coordinated gold atoms, which are connected to a one dimensional, infinite chain by diselenide bridges. Perpendicular to the chain, five-atomic chalcogenide chains are terminally bound to the gold atoms. These chains are of mixed S/Se composition, mainly (SeS_4) and (Se_2S_3). There are anions known with Au^{+III} connected via selenides e.g. in $NaAuSe_2$ [133]. In contrast to the anion presented here, the anion in $NaAuSe_2$ is two-dimensional infinite.

Each gold atom in the polyanionic chain is coordinated by four Se atoms in almost perfectly square planar fashion. Therefore, Au is in the oxidation state +III. The Se-Au-Se angles with symmetry equivalent Se atoms all amount to 180°, since the gold atoms are located on special positions with symmetry $\bar{1}$. All other Se-Au-Se angles range between 88.5° and 91.5°. The average interatomic distance between Au and Se amounts to 2.455 Å. Therefore, it is comparable to that found in other selenoaurates(III) e.g. in K_3AuSe_{13} (2.475 Å) [137]. All bond lengths can be found in Table 35. The bond length between the Se atoms within the gold connecting (Se_2)-dumbbell amounts to 2.28 Å. Hence, it is slightly shorter than expected for a (Se_2) covalent single bond. The S-S bond lengths amount on average to 2.09 Å, which is in the range of typical S-S bond lengths. The interatomic distances between Se4-S1 and Se5-S5 amount to 2.17 Å and 2.13 Å, respectively.

The short distances between Se5-S5 and Se4-S1 in connection with the big displacement ellipsoids of Se4 and Se5 indicate a probably mixed site comprising of Se and S on the positions of Se5 and Se4. Furthermore, the small displacement ellipsoids of the atoms S1 and S2 indicate a possible S/Se mixed site on these positions. However, in the course of the structure solution, mixed sites on the four named positions could not be refined. Either the refinement gave chemically not reasonable structure solutions or atoms were refined with non positive defined displacement factors.

An EDX analysis of the crystal also gave a slightly higher sulfur content than the presented structure solution contains (Table 34). The EDX spectrum (Figure 96) shows that the Au *M* and the S *K* lines as well as the Yb *M* and the Se *L* lines are overlapping. Therefore, the results of the EDX analysis were not exact. However, except of the possible mixed site the structure solution is plausible and the charges are balanced for the found structure solution. For charge balancing a breakdown of the anion into ionic parts is useful. Therefore, the sum formula can be divided into $[Yb(NH_3)_8]^{3+} [Au^{3+}(Se_2)^{2-}(SeS_4)^{2-}(Se_2S_3)^{2-}]^{3-}$.

Table 34: Result of an EDX analysis of a crystal of $[Yb(NH_3)_8](AuSe_5S_7)\cdot NH_3$.

	S	Se	Yb	Au
Atomic %	60.3	26.9	6.5	6.3
Normalized	9.30	4.10	1.00	0.97
Expected	7.00	5.00	1.00	1.00
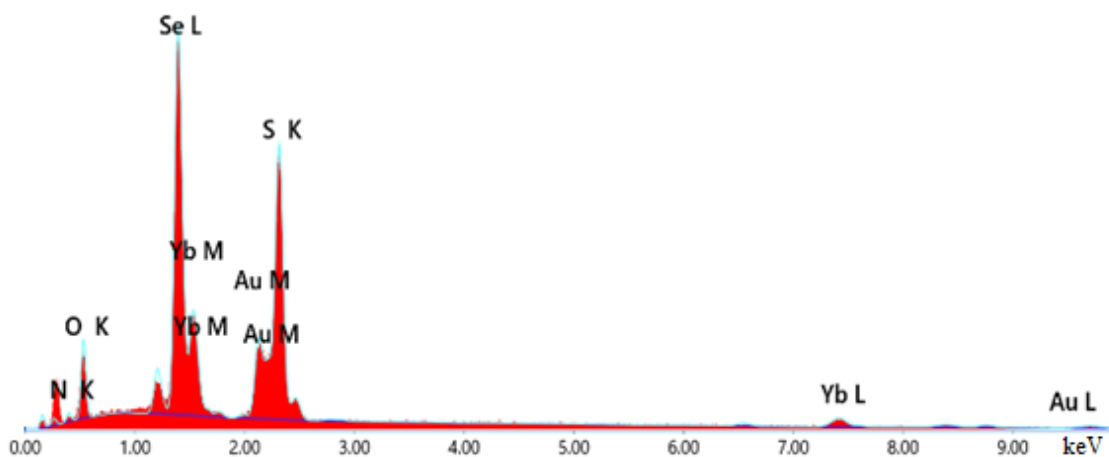
Figure 96: EDX spectrum of a crystal of $[Yb(NH_3)_8](AuSe_5S_7)\cdot NH_3$.
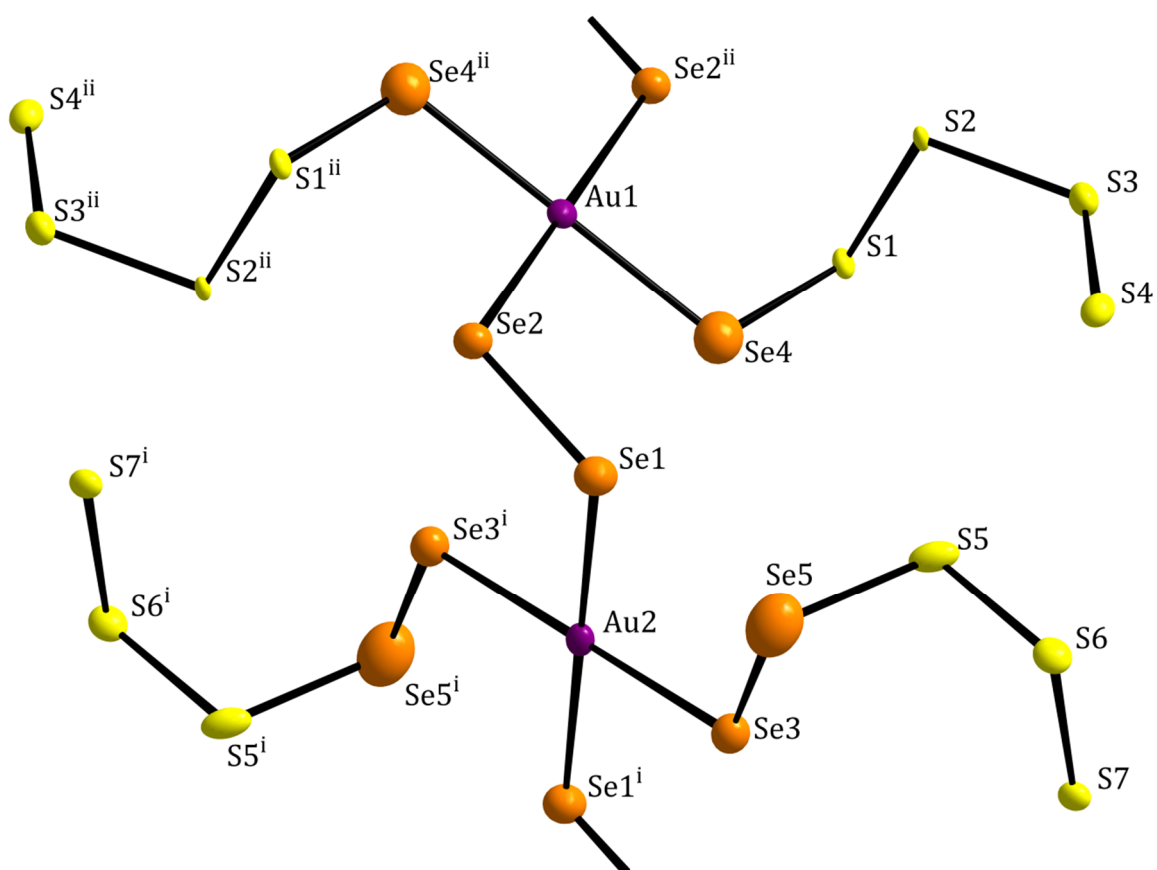
Figure 97: A detailed view of a section the polymeric anion in the structure of $[Yb(NH_3)_8](AuSe_5S_7)\cdot NH_3$. The displacement ellipsoids represent a probability of 50%. The indices *i* indicate the following symmetry operations: (*i*) 1-*x*, 1-*y*, 1-*z*; (*ii*) 2-*x*, -*y*, 1-*z*.

Table 35: Bond lengths of the anion in the structure $[Yb(NH_3)_8](AuSe_5S_7)\cdot NH_3$.

Atoms	Bond length/ Å	Atoms	Bond length/ Å	Atoms	Bond length/ Å
Au1-Se4	2.411(2)	Se1-Se2	2.286(2)	S3-S4	2.053(5)
Au1-Se2	2.484(2)	Se3-Se5	2.279(3)	Se5-S5	2.133(5)
Au2-Se1	2.457(2)	Se4-S1	2.165(4)	S5-S6	2.068(5)
Au2-Se3	2.470(2)	S1-S2	2.177(4)	S6-S7	2.070(5)
		S2-S3	2.104(4)		
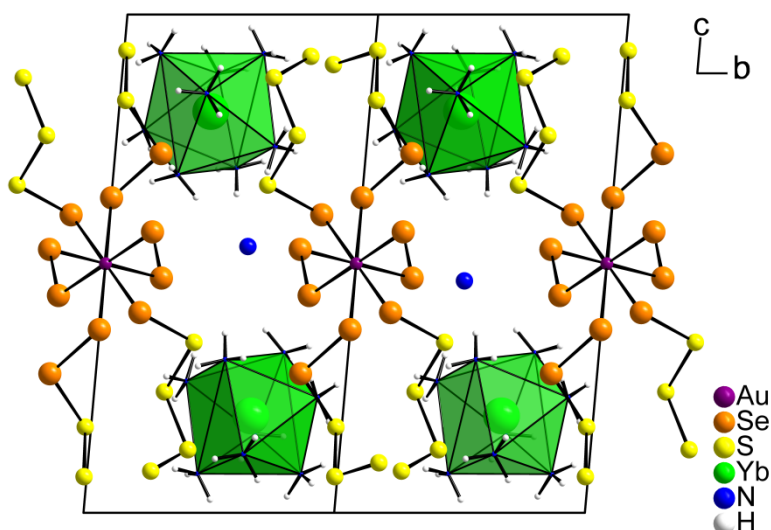
Figure 98: Extended unit cell of $[Yb(NH_3)_8](AuSe_5S_7)\cdot NH_3$ in a view along the <1-10> direction. All atoms are drawn with arbitrary radii.

The infinite anionic chains run diagonal through the unit cell along in the <1-10> direction (Figure 98). The $[Yb(NH_3)_8]^{3+}$ complexes are located in between the chains. The mixed polychalcogenide residues of the anionic chains are placed in a way that they surround the cationic complexes. Free ammonia molecules fill in the remaining voids of the crystal structure. The unit cell is shown from two different sites in Figure 99 for a deeper insight of the crystal structure.
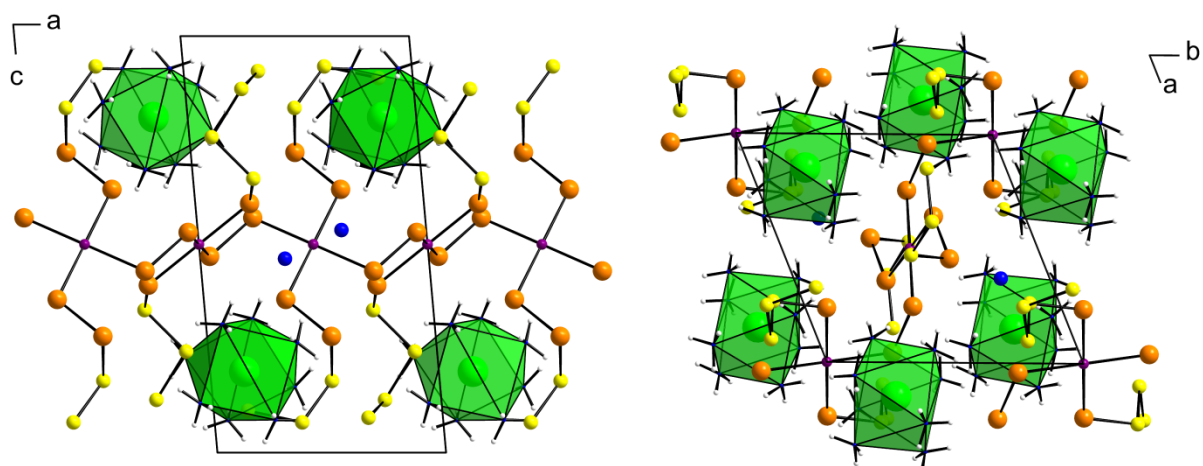
Figure 99: View on the extended unit cell of [Yb(NH$_3$)$_8$](AuSe$_5$S$_7$)·NH$_3$ along the crystallographic *b*-axis (left) and along the crystallographic *c*-axis (right). All atoms are drawn with arbitrary radii.

3.3.4 [Yb(NH₃)₈](AuS₄Se₆)

The compound with the composition $[Yb(NH_3)_8](AuS_4Se_6)$ crystallizes in the monoclinic acentric space group *C*2 with the lattice parameter a = 15.9560(7) Å, b = 9.7517(3) Å, c = 15.7527(7) Å and β = 115.597(2)°. The absolute structure parameter amounts to 0.49(3). Therefore, both domains of an inversion twin are present in equal amounts. Crystals of $[Yb(NH_3)_8](AuS_4Se_6)$ are of dark-red to black color and have rhombic columnar crystal habits (Figure 100). Like the compound described in the chapter before, this compound also contains a homoleptic ytterbium ammine complex and a polymeric mixed-chalcogen gold(III)chalcogenido complex in its crystal structure. The crystals are not stable at room temperature due to the loss of ammonia.
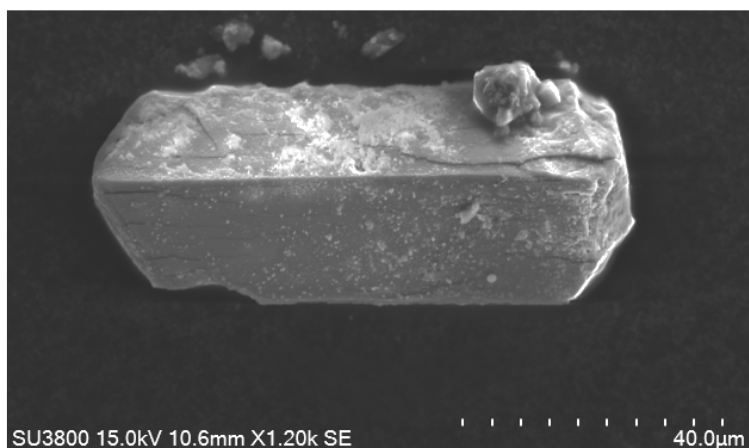
Figure 100: Image of the analyzed crystal with the structure of $[Yb(NH_3)_8](AuS_4Se_6)$. The image was taken with a scanning electron microscope (SU3800, Hitachi).

Both independent ytterbium atoms are in the formal oxidation state +III. Each ytterbium is surrounded by eight ammine ligands forming homoleptic ammine complexes (Figure 101). The resulting polyhedra $Yb(1)N_8$ and $Yb(2)N_8$ can be best described as square antiprisms (D_{4d}). The deviation from the ideal square antiprism (D_{4d}) was calculated by a continuous shape measure and amounts to 0.251% for $Yb(1)N_8$ and to 0.385% for $Yb(2)N_8$, respectively. The deviations from all other ideal shapes are higher (Table 36). The positions of the hydrogen atoms of the ammine ligands were not found in the difference *Fourier* map. They were placed on geometrically calculated positions and refined by using a riding model. Both ytterbium atoms lie on special positions, Yb1 on the *Wyckhoff* position 2*b* and Yb2 on the *Wyckhoff* position 2*a*.

Therefore, a two-fold rotation axis runs trough each ytterbium atom and only half of the ammine ligands were symmetrically independent. The Yb-N bond lengths range between 2.45 Å and 2.55 Å for Yb1 and between 2.44 and 2.53 Å for Yb2. These bond lengths are in a typical range for ytterbium ammine complexes with ytterbium in the oxidation state +III and are comparable to the Yb^{III}-N bond lengths presented in the previous chapters. Yb-N bond lengths, where ytterbium is in the formal oxidation state +II, would be significantly longer (2.61 Å and 2.75 Å [72]).
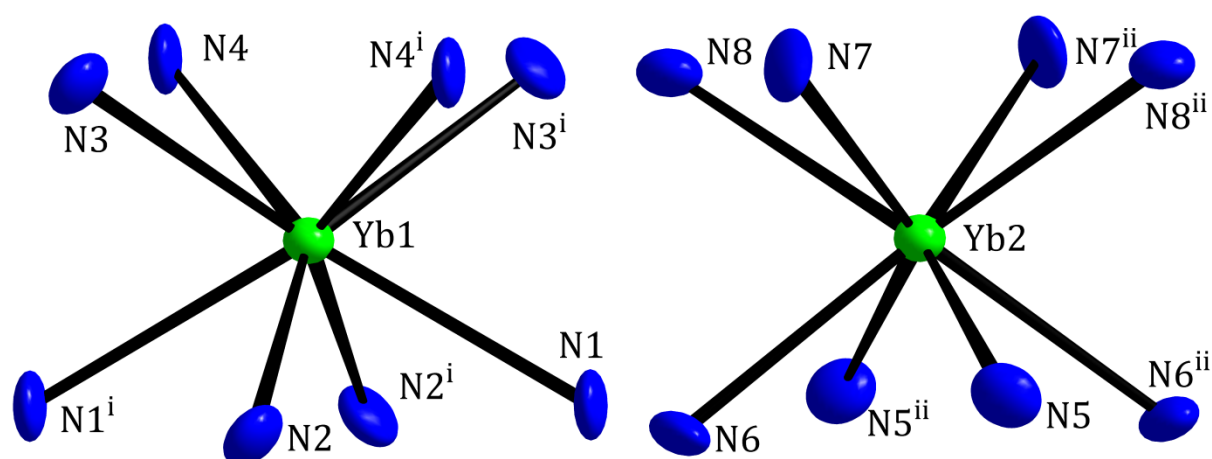
Figure 101: The coordination of the two independent Yb^{3+} ions by ammonia molecules in the structure of [Yb(NH$_3$)$_8$](AuS$_4$Se$_6$). The displacement ellipsoids represent a probability of 50%. All hydrogen atoms bound to the N atoms of the ammine ligands are omitted for clarity. The indices i indicate the following symmetry operations: (i) -x, y, 1-z; (ii) 2-x, y, 2-z.

Table 36: Results of continuous shape measures of both independent YbN$_8$ polyhedra in the structure of [Yb(NH$_3$)$_8$](AuS$_4$Se$_6$).

Ideal Shape	CShM / % (Yb(1)N$_8$ polyhedron)	CShM / % (Yb(2)N$_8$ polyhedron)
OP-8	28.834	29.285
HPY-8	23.877	23.752
HBPY-8	17.050	16.375
CU-8	10.520	10.221
SAPR-8	**0.251**	**0.385**
TDD-8	1.909	1.708
BTPR-8	1.698	1.500

The anion in this compound is a polymeric mixed-chalcogen gold(III)chalcogenido complex, in form of infinite chains (Figure 102). Each gold atom, Au1 and Au2, is coordinated by four selenium atoms in a slightly distorted square planar fashion. The gold atoms are connected via $(Se_4)^{2-}$ units to an infinite chain. Perpendicular to the chain, three-atomic chalcogenide chains are terminally bound to the gold atoms. These terminally bound chains are of mixed S/Se composition, namely $(SeS_2)^{2-}$ units. For each Au the formal oxidation state +III is assumed because of the square planar coordination. For charge balancing a breakdown of the anion into ionic parts is useful. Therefore, the sum formula can be divided into $[Yb(NH_3)_8]^{3+}[Au^{3+}(Se_4)^{2-}((SeS_2)^{2-})_2]^{3-}$. The Se-Au-Se angles between two symmetry equivalent Se atoms and Au range between 173.8 and 177.3°. All other Se-Au-Se angles range between 89.5 and 90.3°. Therefore, each gold atom is coordinated in an almost perfectly square planar fashion. The average Au-Se bond length amounts to 2.464 Å and is therefore in between the Au-Se bond lengths found in $[Yb(NH_3)_8](AuSe_5S_7)\cdot NH_3$ (2.455 Å) and in K_3AuSe_{13} (2.475 Å). Interatomic distances within the connecting $(Se_4)^{2-}$ unit are between 2.31 Å and 2.33 Å with Se-Se-Se angles amounting to 105.6 and 101.3°. The Se-S bond lengths amount to 2.20 Å for Se5-S1 and to 2.22 Å for Se6-S4. The S-S bond lengths of 2.13 Å and 2.18 Å are longer than expected for a S-S single bond. These elongated bonds, the small displacement ellipsoids of the sulfur atoms, the big displacement ellipsoids of Se5 and Se6 and the non-spherical shaped ellipsoids of the Au atoms indicate some problems with the structure refinement. There is a possible S/Se mixed site on every position within the terminally bound chalcogenide chains. In Figure 103, a probable disordering of the anion is shown. The residual electron densities are labeled with *Q* and their positions were found in the difference Fourier map. The mixed sites in connection with the disordering led to no satisfactory structure refinement. Either the refinement gave chemically not reasonable structure parameters or atoms were refined with non positive defined displacements. For these reasons, the structure was refined without implementation of disordering and mixed sites. The described problems arose in all examined crystals with this composition. However, the structure could be solved reasonable. In Table 37 the result of an energy dispersive X-ray spectroscopy analysis is shown. The EDX analysis results in a composition, which is similar to the expected on the basis of the structure refinement. The slightly smaller content of selenium and sulfur may origin from partial decomposition during the exposure of the crystals to air and the evolution of H_2S and H_2Se. The gases were generated on handling the crystals in open air and could be detected by their specific odour.
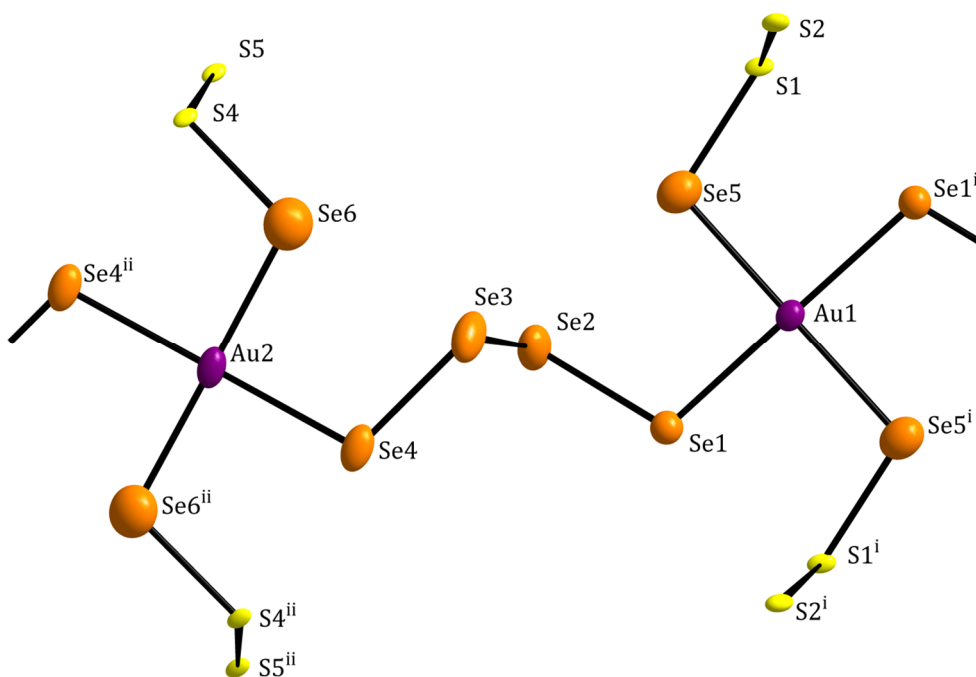
Figure 102: Part of the polymeric anion in the structure of $[Yb(NH_3)_8](AuS_4Se_6)$. The displacement ellipsoids represent a probability of 50%. The indices i indicate the following symmetry operations: (i) $1-x, y, 2-z$; (ii) $-x, y, 1-z$.
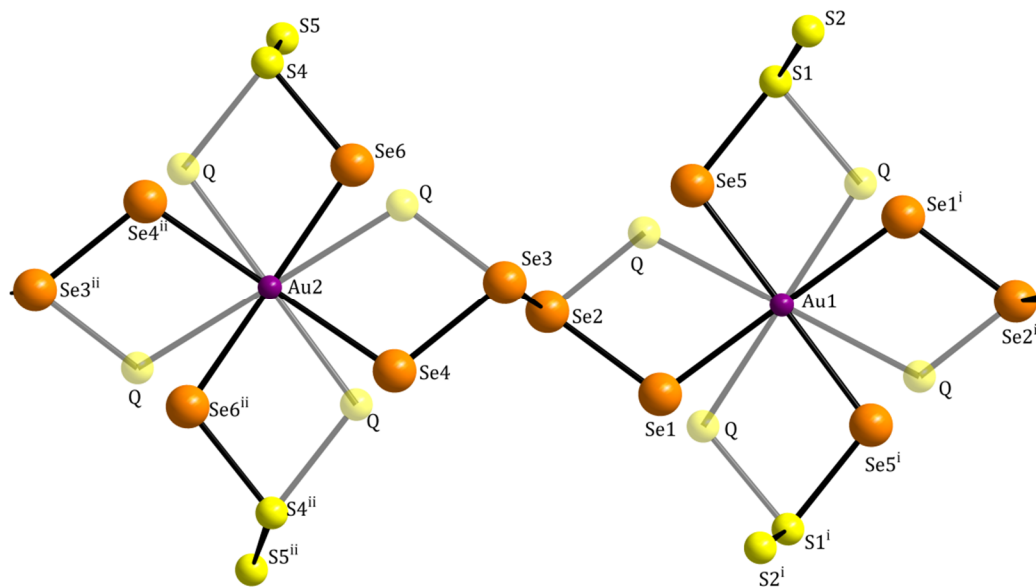
Figure 103: Positions labeled with Q show residual electron density, found in the difference *Fourier* map. All atoms are drawn with arbitrary radii. The indices i indicate the following symmetry operations: (i) $1-x, y, 2-z$; (ii) $-x, y, 1-z$.

Table 37: Results of the EDX analysis of a crystal of $[Yb(NH_3)_8](AuS_4Se_6)$.

	Yb / Atomic %	Au / Atomic %	Se / Atomic %	S / Atomic %
Spot (1)	9.17	10.05	51.35	29.43
Spot (2)	10.01	10.59	51.28	28.11
Spot (3)	10.55	11.90	49.00	28.54
Spot (4)	9.71	8.89	52.76	28.64
Spot (5)	9.76	11.95	48.27	30.02
Spot (6)	10.91	10.96	47.27	30.86
Ø	10.02	10.72	49.99	29.27
Normalized	1.00	1.07	4.99	2.92
Expected	1.00	1.00	6.00	4.00

Figure 104 shows the $^1_\infty[Au(Se_4)(SeS_2)_2]^{3-}$ chains running along the <101> direction within the crystal structure. There is only one inter chain interaction present in the crystal structure between the terminal sulfur atom S5 and the bridging selenium atom Se5. The inter atomic distance amounts to 3.44 Å, which is smaller than the sum of the respective *van-der-Waals* radii (3.70 Å). The Au and the Yb atoms are stacked about each other parallel to the crystallographic *b*-axis. The terminal and bridging chalcogenide chains are arranged in a way, that they can surround the $[Yb(NH_3)_8]^{3+}$ complexes.
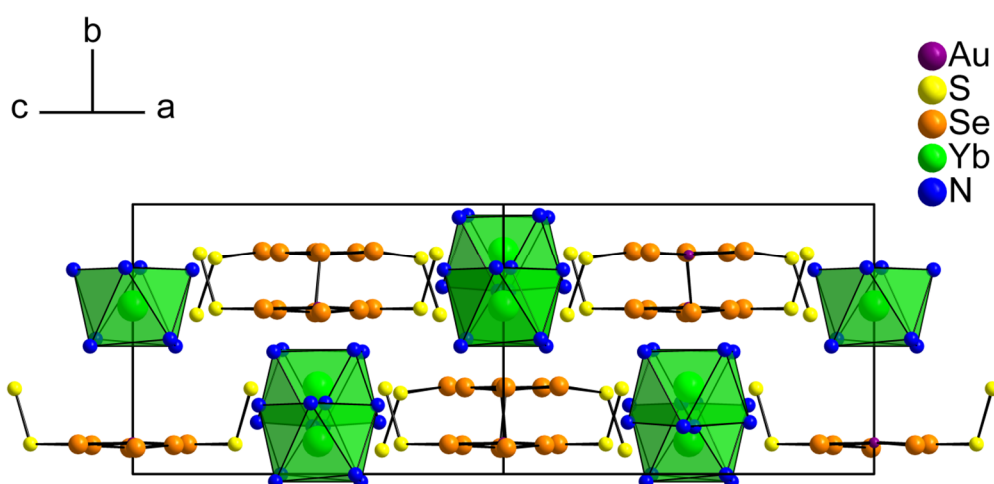
Figure 104: View of the extended unit cell of $[Yb(NH_3)_8](AuS_4Se_6)$ along the <101> direction. All atoms are drawn with arbitrary radii. Hydrogen atoms bound to the N atoms of the ammine ligands are omitted for clarity.
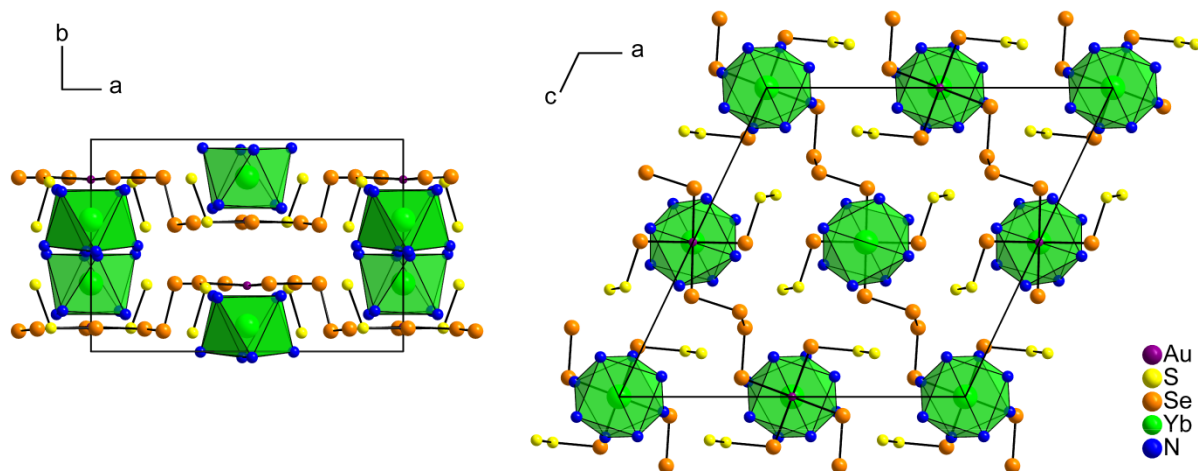
Figure 105: A view of the extended unit cell of [Yb(NH$_3$)$_8$](AuS$_4$Se$_6$) along the crystallographic c-axis (left) and along the crystallographic b-axis (right). All atoms are drawn with arbitrary radii. The hydrogen atoms bound to the N atoms of the ammine ligands are omitted for clarity.

3.3.5 [Ca(en)₄](AuTe₅)₂

The compound with the composition $[Ca(en)_4](AuTe_5)_2$ crystallizes in the triclinic space group $P\bar{1}$ with the lattice parameters $a = 9.4108(7)$ Å, $b = 9.4927(7)$ Å, $c = 19.7263(13)$ Å, $\alpha = 87.035(5)°$, $\beta = 77.389(4)°$ and $\gamma = 77.790(3)°$. Crystals of $[Ca(en)_4](AuTe_5)_2$ have a platy crystal habit and are of black metallic appearance. The crystals are stable at room temperature for some hours under oil. It was tried to wash the crystals with ethanol. After drying the washed crystals a powder diffraction analysis was done. Beside the two phases $AuTe_2$ and Te in the powder diffractogram, no $[Ca(en)_4](AuTe_5)_2$ was observed. The powder diffractograms is shown in the appendix. The analyzed crystals of this compound all show a highly disordered layer of the polyanion. Figure 106 shows a simulated precession image of the diffraction pattern of an analyzed crystal of $[Ca(en)_4](AuTe_5)_2$. It can be seen that the reflections along the c^* direction are not well separated, but rather form streaks along c^* which is indicative of the disordering.

The composition of $[Ca(en)_4](AuTe_5)_2$ was confirmed by an EDX analysis (Figure 109). The quantification results are presented in Table 39. All atomic percentages fit very well, except the one for tellurium. The content of Te is overestimated in this case. A reason for this may be the overlapping Ca K and Te L EDX lines.
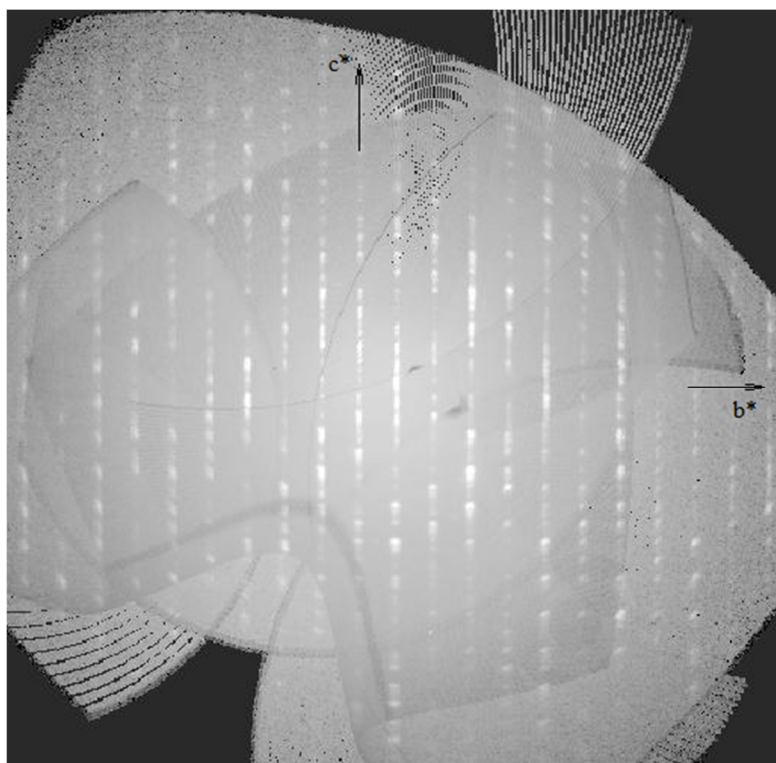
Figure 106: Reconstructed precession image of the $3kl$ layer of an analyzed crystal with the composition $[Ca(en)_4](AuTe_5)_2$.

A calcium ethylenediamine complex is the cation in this compound (Figure 107). The entire complex is twofold positively charged. Ca is surrounded by four en ligands. The resulting coordination polyhedron of Ca with the coordination number eight can be best described as triangular dodecahedron (D_{2d}). A continuous shape measure gives a deviation from the ideal triangular dodecahedron (D_{2d}) of 0.601%. The deviation from other ideal polyhedra of the coordination number eight is higher (Table 38). The sites of the C and N atoms of the ethylene diamine ligands could not be refined anisotropically. Beside the disordering in the crystal, bad data due to high absorption effects could be an explanation. A satisfactory absorption correction for the thin and platy crystal was not possible, because it was treated and measured under oil. Positions of the hydrogen atoms of the en ligands were not found in the difference *Fourier* map. They were placed on geometrically calculated positions and refined by a riding model. The Ca-N bond lengths range between 2.55 and 2.64 Å. Therefore, they are in the expected range for Ca-N bond lengths in such amine complexes and they are similar to those found in the structure of [Ca(en)$_4$]$_2$(As$_4$Te$_6$) presented in chapter 3.2.1 of this work.
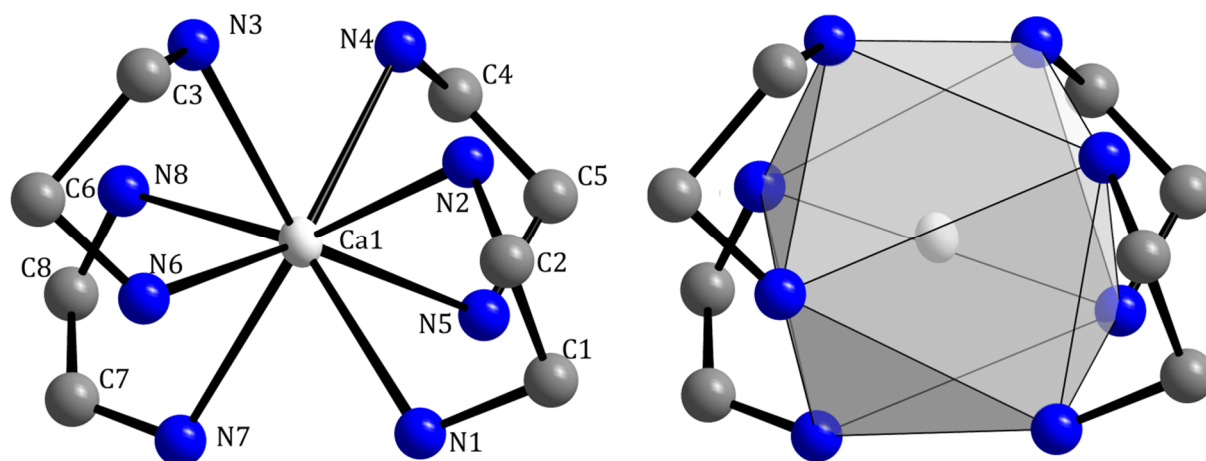
Figure 107: Coordination of Ca^{2+} in the structure of [Ca(en)$_4$](AuTe$_5$)$_2$ in two different representations. The displacement ellipsoid of the Ca atoms represents a probability of 50%. The N and C atoms are drawn with arbitrary radii. All hydrogen atoms are omitted for clarity.

Table 38: Result of a continuous shape measure of the CaN$_8$ polyhedron in the structure of [Ca(en)$_4$](AuTe$_5$)$_2$.

Ideal Shape	CShM / % (CaN$_8$ polyhedron)
OP-8	32.954
HPY-8	24.478
HBPY-8	16.955
CU-8	9.995
SAPR-8	3.259
TDD-8	**0.601**
BTPR-8	2.560

The anion in this compound is a polymeric telluro aurate(III). The anion forms corrugated layers perpendicular to the crystallographic *c*-axis. Within a layer, gold is coordinated by four tellurium atoms in a square planar fashion, typical for gold in the oxidation state +III. A different layered anion where gold is square planar coordinated by tellurium atoms can be found in the structure of AuTe$_2$I from *Rabenau et al.*[138]. In the structure of AuTe$_2$I only (Te$_2$) dumbbells interconnecting the gold atoms are present. In the structure of [Ca(en)$_4$](AuTe$_5$)$_2$, also (Te$_3$) units are present (Figure 108). (AuTe$_5$)$^-$ can be separated into ions, namely (Te$_3$)$^{2-}$ units, (Te$_2$)$^{2-}$ units and Au^{3+} ions. The Te-Te bonds within the polytelluride units range between 2.75 and 2.76 Å. Therefore, all tellurium atoms are covalently bound. There are no hypervalently bound tellurium atoms present in this structure. The Te2-Te1-Te5^v angle of 101.5° confirms that Te1 is bound by two covalent 2*c*-2*e* bonds. The Au-Te bond lengths range between 2.64 and 2.69 Å, in line to those found in AuTe$_2$I (2.67 Å) or in the (Au$_6$Te$_{18}$X$_n$)$^{(6-n)+}$ (2.69 Å) cation, which was described by *C. Landvogt* in his PhD thesis[139]. The Au-Te bond lengths show substantial covalent bond character within the Au-Te interactions. There are no Au-Au interactions present in the structure. The shortest found Au···Au distance amounts to 5.34 Å and it is therefore much longer than twice the *van-der-Waals* radius of Au (2r$_{vdW}$(Au)= 3.40 Å [74]). All angles between symmetry equivalent Te atoms and Au are 180° because the gold atoms are placed on special positions with the site symmetry $\bar{1}$. All other Te-Au-Te angles within the square planar coordination of Au range between 88.4 and 91.6°. Therefore, the gold atoms are almost perfectly square planar coordinated. Two (Te$_3$) units and two (Te$_2$) units interconnect four Au atoms to 14-membered rings are formed within the layers. Two

independent layers of the polymeric anion are present in the crystal structure. One non disordered, layer A, (Figure 110) and one highly disordered layer, layer B. Figure 111 shows the highly disordered layer B with all found residual electron densities shown as tellurium atoms. It was possible to refine all found residual electron densities to three different layers taking part of the disordering shown in Figure 112. The disordering between the blue part and the green/pink part was refined to 75:25. The green/violet part has a second, symmetry dependent disordering because of the inversion centers. Therefore, all site occupancy factors for atoms of these parts were set to 0.5.
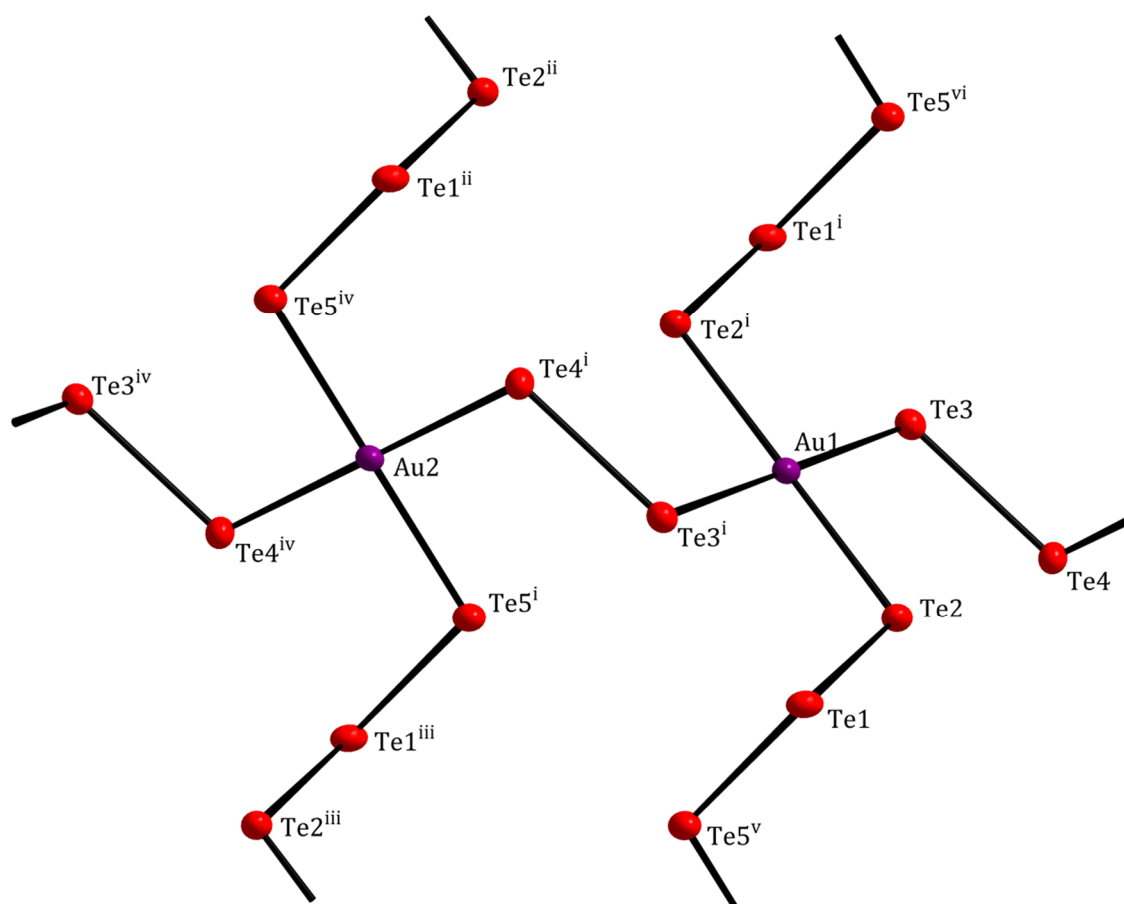
Figure 108: A detailed view of a polyanionic layer A in the structure of $[Ca(en)_4](AuTe_5)_2$. The displacement ellipsoids represent a probability of 50%. The indices *i* indicate the following symmetry operations: (*i*) 1-*x*, 2-*y*, 1-*z*; (*ii*) *x*, 1+*y*, *z*; (*iii*) –*x*, 2-*y*, 1-*z*; (*iv*) -1+*x*, 1+*y*, *z*; (*v*) -1+*x*, *y*, *z*; (*vi*) 2-*x*, 2-*y*, 1-*z*.
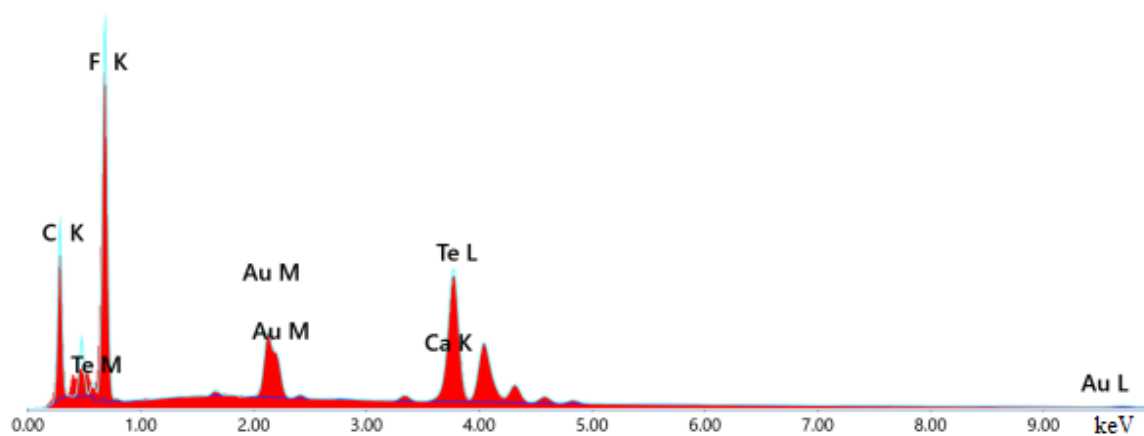
Figure 109: EDX spectrum of the analyzed crystal of $[Ca(en)_4](AuTe_5)_2$.

Table 39: Result of the EDX analysis of a crystal of $[Ca(en)_4](AuTe_5)_2$.

	Au	**Ca**	**Te**
Atomic %	13.29	6.29	80.42
Normalized	2.00	0.94	12.10
Expected	2.00	1.00	10.00
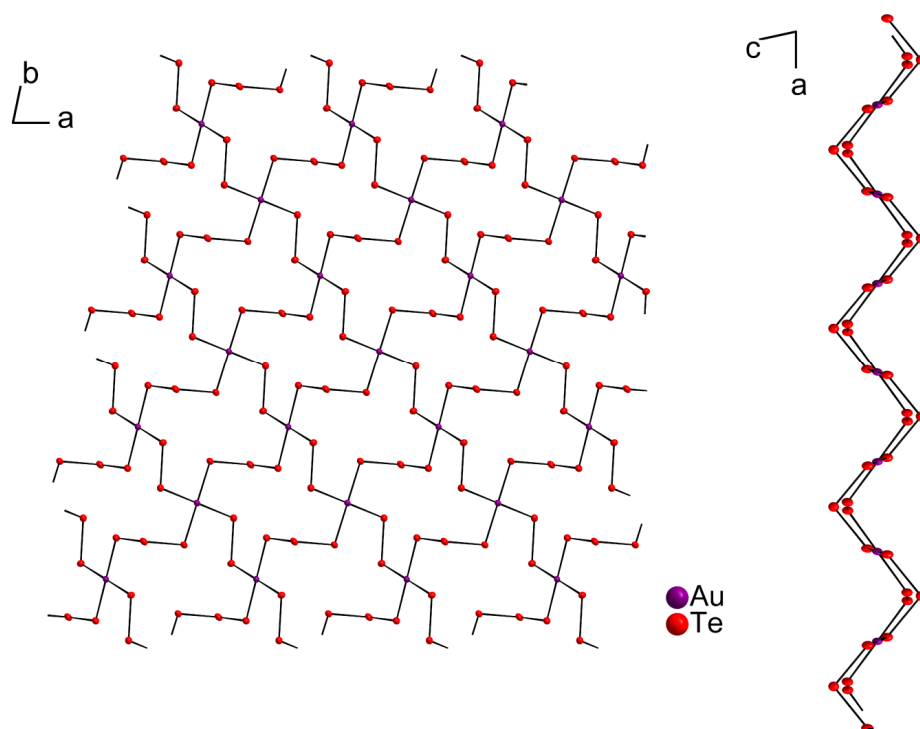
Figure 110: A view of the non disordered polyanionic layer A in the structure of $[Ca(en)_4](AuTe_5)_2$ along the crystallographic *c*-axis (left) and along the crystallographic *b*-axis (right). The displacement ellipsoids represent a probability of 50%.
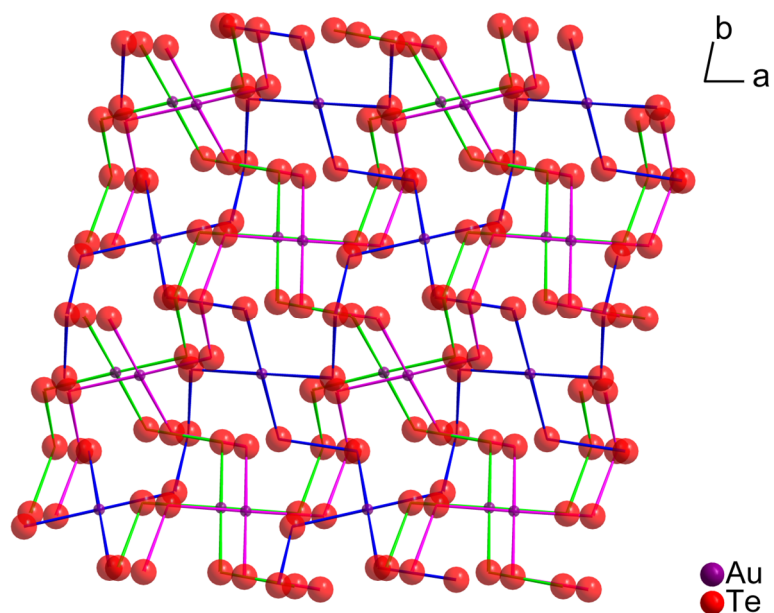
Figure 111: A view of the different domains of the disordered layer B along the crystallographic *c*-axis in the structure of $[Ca(en)_4](AuTe_5)_2$. All atoms are drawn with arbitrary radii.
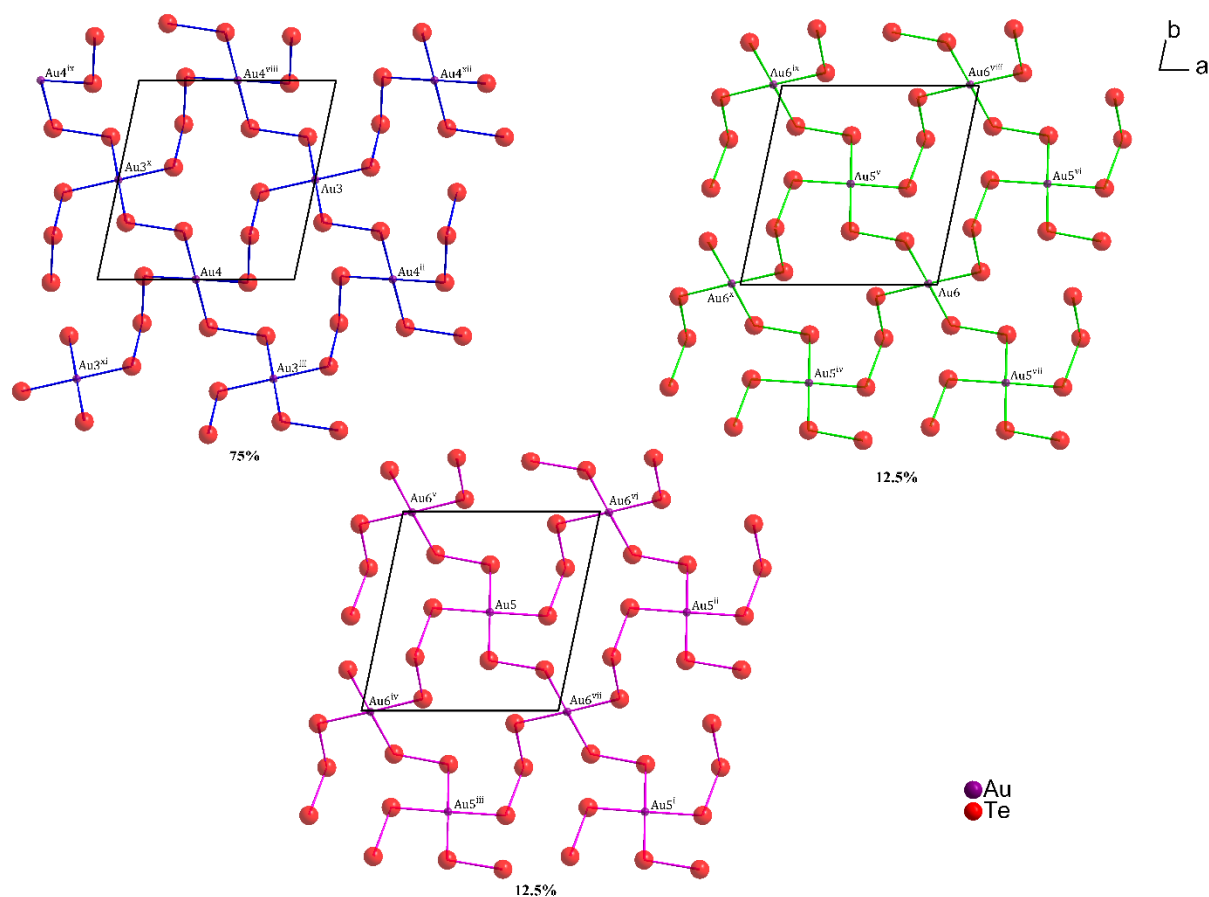
Figure 112: A view of the three disordered part of the second independent anionic layer B in the structure of $[Ca(en)_4](AuTe_5)_2$ along the crystallographic *c*-axis. All atoms are drawn with arbitrary radii. The percentages under each disordered part give their refined occupancies. The indices *i* indicate the following symmetry operations: (*i*) $1+x, -1+y, z$; (*ii*) $1+x, y, z$; (*iii*) $x, -1+y, z$; (*iv*) $1-x, -y, -z$; (*v*) $1-x, 1-y, -z$; (*vi*) $2-x, 1-y, -z$; (*vii*) $2-x, -y, -z$; (*viii*) $x, 1+y, z$; (*ix*) $-x+1, 1+x, -z$; (*x*) $-1+x, y, z$; (*xi*) $-1+x, -1+y, z$; (*xii*) $1+x, 1+y, z$.

In Figure 113 and Figure 114 extended unit cells of $[Ca(en)_4](AuTe_5)_2$ are shown. It can be seen that the anionic layers are stacked along the crystallographic *c*-axis with a stacking order *ABABAB*…, where the layers *A* and *B* are twisted against each other by 90° around the crystallographic *c*-axis. In between the anionic layers the cationic complexes are placed. There are no interactions between the independent layers. The smallest inter layer Te-Te distance amounts to 5.53 Å.
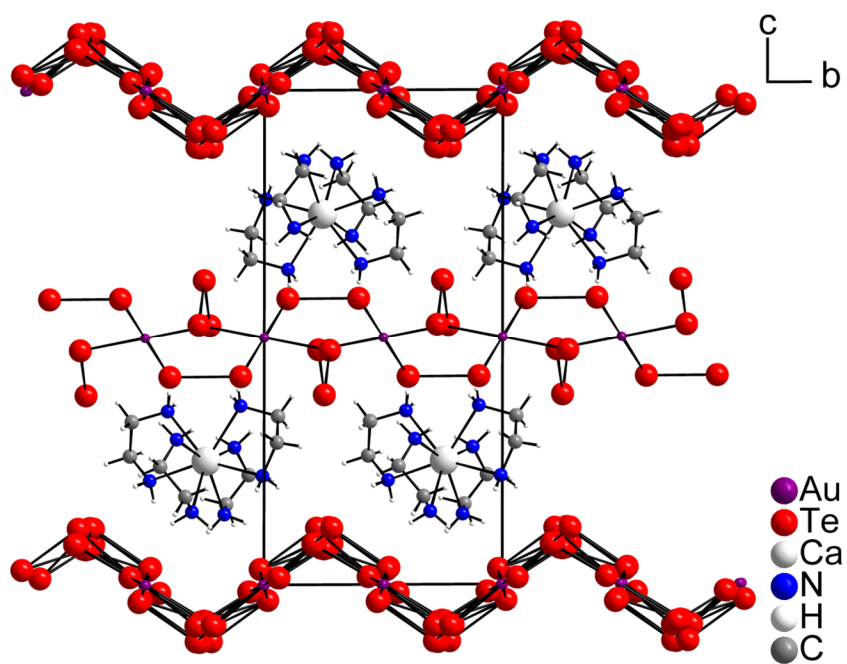
Figure 113: A view of the extended unit cell of $[Ca(en)_4](AuTe_5)_2$ along the crystallographic *a*-axis. All atoms are drawn with arbitrary radii.
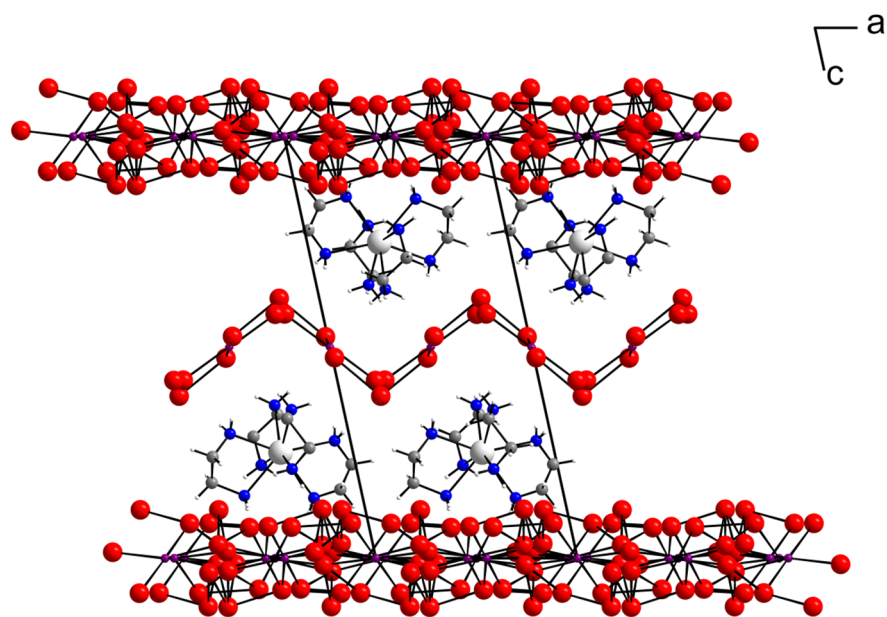
Figure 114: A view of the extended unit cell of $[Ca(en)_4](AuTe_5)_2$ along the crystallographic *b*-axis. All atoms are drawn with arbitrary radii.

3.3.6 [Yb(NH₃)₈](AuSe₄)₃

Crystals with the composition $[Yb(NH_3)_8](AuSe_4)_3$ are of black appearance with a golden metallic luster. The crystal habitus is isometric. The compound crystallizes in the trigonal space group $R\bar{3}$ with the lattice parameters $a = 15.9319(4)$ Å and $c = 8.7617(2)$ Å. The crystal structure of $[Yb(NH_3)_8](AuSe_4)_3$ contains beside a homoleptic ytterbium ammine complex the first selenidoaurate(III) forming a three-dimensional network. Only an oxoaurate(III) by *Jansen et al.* with a three dimensional network of a gold(III)chalcogenide has been mentioned [140].
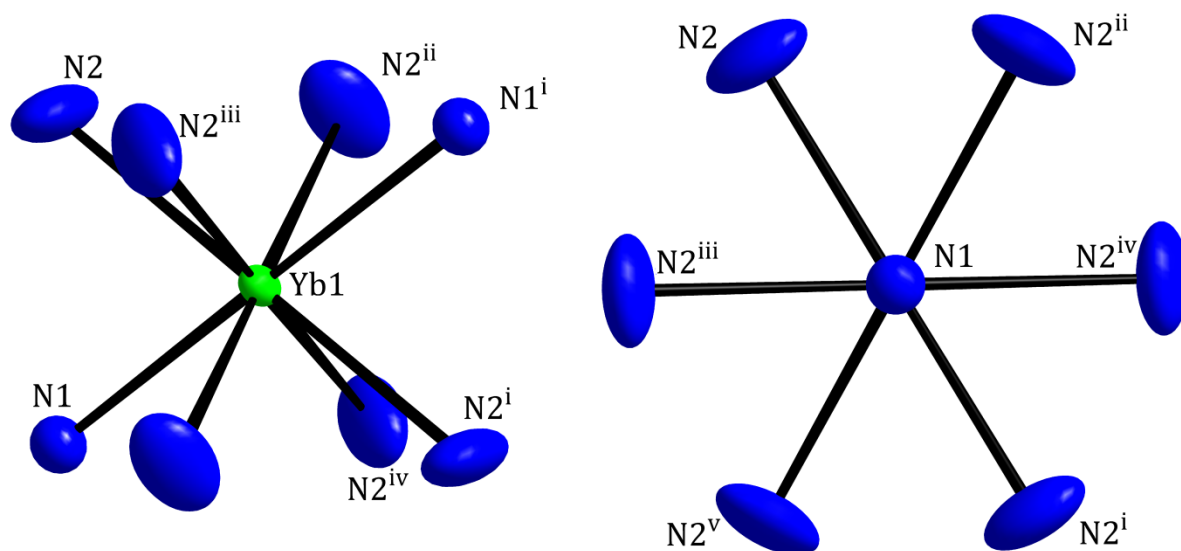
Figure 115: A view of the coordination of Yb^{3+} by ammine ligands (left) and a view along the N1-Yb1-N1ⁱ axis parallel to the crystallographic *c*-axis (right) in the structure of $[Yb(NH_3)_8](AuSe_4)_3$. The displacement ellipsoids represent a probability of 50%. All hydrogen atoms bound to the N atoms of the ammine ligands are omitted for clarity. The indices *i* indicate the following symmetry operations: (*i*) $^4/_3$-x, $^2/_3$-y, $^5/_3$-z; (*ii*) $^1/_3$+y, $^2/_3$-x, $^5/_3$-z; (*iii*) $^1/_3$+x-y, -$^1/_3$+x, $^5/_3$-z; (*iv*) 1+x+y, 1-x, z; (*v*) 1-y, x-y, z.

Table 40: Result of a continuous shape measure of the YbN$_8$ polyhedron in the structure of [Yb(NH$_3$)$_8$](AuSe$_4$)$_3$.

Ideal Shape	CShM / % (YbN$_8$ polyhedron)
OP-8	36.984
HPY-8	29.045
HBPY-8	6.486
CU-8	**0.133**
SAPR-8	11.108
TDD-8	8.075
BTPR-8	12.677

The crystal structure contains two different building blocks, [Yb(NH$_3$)$_8$]$^{3+}$ complexes and a three-dimensional network of connected [AuSe$_4$]$^-$ units. The ytterbium ion is coordinated by eight ammine ligands. The positions of the hydrogen atoms of the ammine ligands were not found in the difference *Fourier* map. They were placed on geometrically calculated positions and refined by using the riding model. Its coordination polyhedron can be described as a cube (O_h). A continuous shape measure gives a deviation amounting to 0.133 % from an ideal cube (O_h) (Table 40). Ytterbium is in the oxidation state +III, for which typically square antiprisms or twofold-capped trigonal prisms as coordination polyhedra are found. Ytterbium is located on the special position *3a* with the site symmetry $\bar{3}$. Therefore, a three-fold inversion axis, parallel to the *c*-axis, runs through the space diagonal of the YbN$_8$ cube. The coordination polyhedron is shown in Figure 115. In Figure 115 on the right side, the coordination of ytterbium with the view along the crystallographic *c*-axis is shown. It can be seen that the displacement ellipsoids of N1 and N1^i, which are located on the threefold axis with the *Wyckhoff* position 6*c*, are almost spherical. The displacement ellipsoids of the six symmetry generated N2 atoms are in contrast elongated perpendicular to the threefold axis. Apparently, the entire [Yb(NH$_3$)$_8$]$^{3+}$ complex ion performs a libration vibration in the form of a rotary oscillation around the threefold axis. The interatomic distances Yb-N1 and Yb-N2 are identical, amounting to 2.447 Å for Yb-N2 and to 2.450 Å for Yb-N1, respectively. These bond lengths are typical for ytterbium ammine complexes with ytterbium in the oxidation state +III. The N-Yb-N angles differ minimally from the ideal angles in a cubic environment, amounting from 68.2° to 72.94°

(ideal: 70.5°), from 107.1° to 111.8° (ideal: 109.5°) and to 180° (ideal: 180°). These small deviations reflect the symmetry decrease from O_h to D_{3d} and finally to C_{3i} ($^4/_m \bar{3}\,^2/_m$ to $\bar{3}\,^2/_m$ to $\bar{3}$). The loss of the mirror planes and the fourfold and twofold axes allows for the angular distortions. A table with all individual N-Yb-N angles is shown in the appendix.
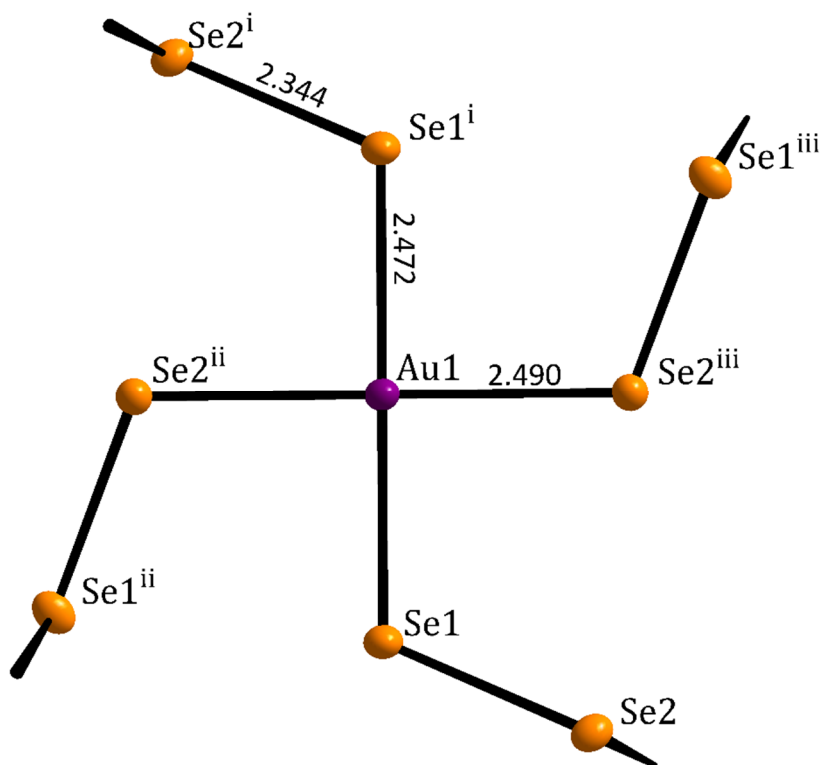
Figure 116: A section of the $(AuSe_4)_n^{n-}$ polyanion in the structure of $[Yb(NH_3)_8](AuSe_4)_3$. Bond lengths are given in Å. The displacement ellipsoids represent a probability of 50%. The indices i indicate the following symmetry operations: (*i*) $^5/_3$-x, $^4/_3$-y, $^1/_3$-z; (*ii*) $^1/_3$+x-y, $^{-1}/_3$+x, $^2/_3$-z; (*iii*) $^4/_3$-x+y, $^5/_3$-x, $^{-1}/_3$+z.

The second building block in the crystal structure of $[Yb(NH_3)_8](AuSe_4)_3$ is a three-dimensional network of $(AuSe_4)^-$ units. The central building block of the polyanion is shown in Figure 116. Au is in the oxidation state +III. Its coordination by selenium is almost perfectly square planar. Both angles, Se1-Au-Se1^i and Se2^{ii}-Au1-Se2^{iii}, amount to 180°. The other Se-Au-Se angles within the square planar coordination are 89.87° and 90.13°. The Au-Se bond lengths of 2.47 Å and 2.49 Å are comparable to those found in the literature for Au-Se bond lengths in a square planar coordination, e.g. in the structures of Na_5AuSe_{12} [128] or $NaAuSe_2$ [133]. The homonuclear Se1-Se2 bond lengths amount to 2.34 Å. Therefore, these bond lengths are similar to twice the covalent bond radius of selenium and slightly shorter in comparison to the Se-Se bond lengths found in $(Se_2)^{2-}$ dumbbells (2.38 Å [141]). There are some interactions within four pairs of symmetry equivalent Se atoms e.g. Se1 and Se1^{ii}. These inter atomic distances within those pairs ranging between 3.37 Å and 3.45 Å. Therefore, they are shorter than twice the *van-der-*

Waals radius of Se ($2r_{vdw}(Se) = 3.80$ Å). The three-dimensional network which is formed by the polyanion is shown in Figure 117. Channels running parallel to the crystallographic *c*-axis are formed. In these channels the ytterbium ammine complexes are placed as shown in Figure 119. The displacement ellipsoids of the nitrogen atoms N2 of the ammine ligands show that the complexes can perform a rotational libration movement in these channels parallel to the crystallographic *c*-axis. Every $[Yb(NH_3)_8]^{3+}$ complex is surrounded by six $(AuSe_4)^-$ units forming a distorted octahedron as coordination polyhedron (Figure 120). Every $(AuSe_4)^-$ unit belongs to two different ytterbium ammine complexes. Therefore, the ratio between $[Yb(NH_3)_8]^{3+}$ complexes and $(AuSe_4)^-$ units is 1:3.
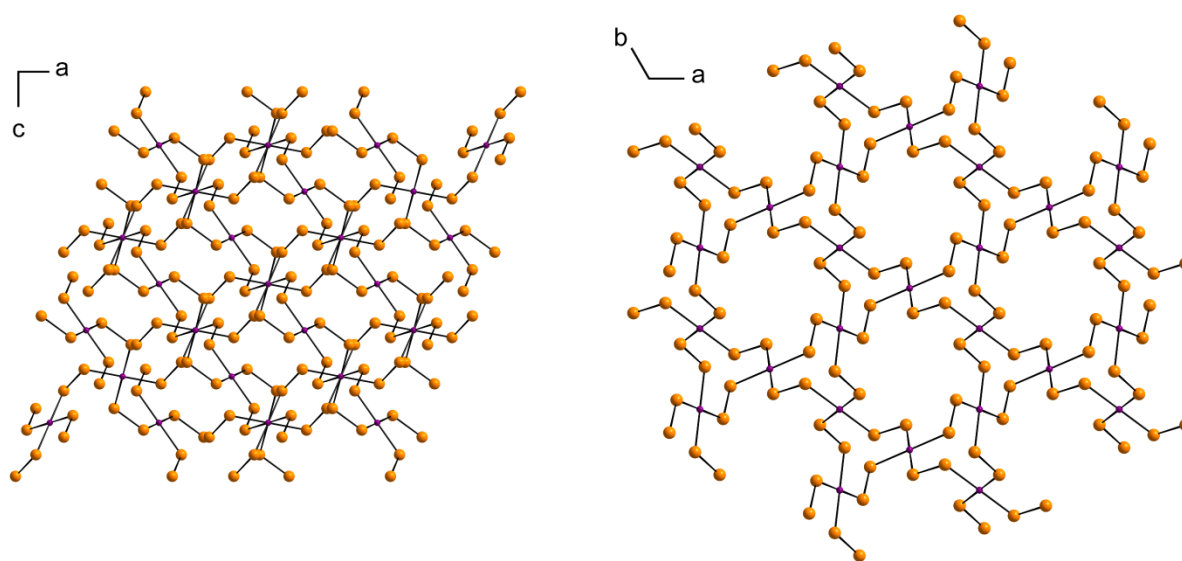
Figure 117: Two different views on the three-dimensional network of the polyanion in the structure of $[Yb(NH_3)_8](AuSe_4)_3$ along the crystallographic *b*-axis (left) and along the crystallographic *c*-axis (right). All atoms are drawn with arbitrary radii.

An EDX analysis of the crystal showed that the elements that were used for the structure refinement are all present the crystal. Instead of the expected Au : Yb : Se ratio of 1.00 : 0.33 : 4.00 the analysis gave a ratio of 1.00 : 0.48 : 4.78 (Table 41). The EDX spectrum (Figure 118) shows that the Se *L* and Yb *M* lines are completely overlapping. Therefore, the individual content of these two elements cannot be determined exactly. The Yb *L* line was not taken for the quantitative analysis because the excitation energy should be 2-3 times the energy of the observed lines in the spectrum. This criterion is not valid for the Yb *L* lines because the used excitation energy was 15kV.
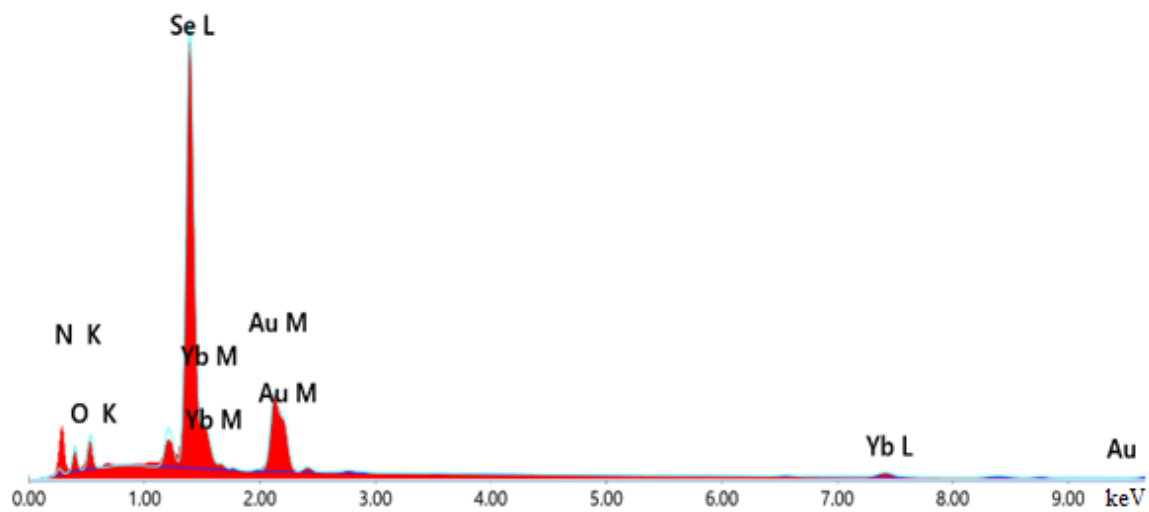
Figure 118: EDX spectrum of the analyzed crystal of $[Yb(NH_3)_8](AuSe_4)_3$.

Table 41: Result of the EDX analysis of a crystal of $[Yb(NH_3)_8](AuSe_4)_3$.

	Au	Yb	Se
Atomic %	16.0	7.6	76.4
Normalized	1.00	0.48	4.78
Expected	1.00	0.33	4.00
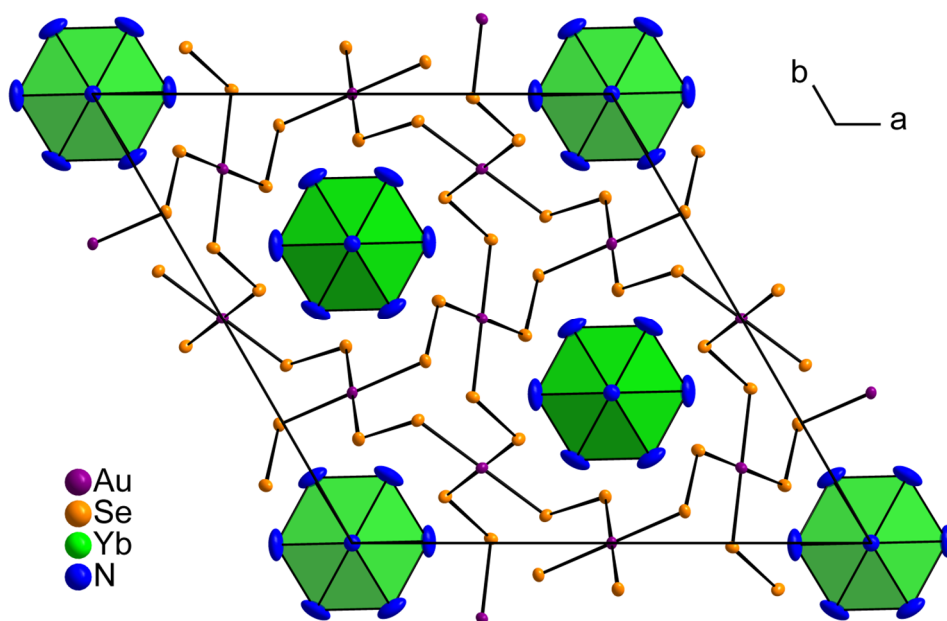
Figure 119: Extended unit cell of $[Yb(NH_3)_8](AuSe_4)_3$ in a view along the crystallographic *c*-axis. The displacement ellipsoids represent a probability of 50 %. The hydrogen atoms bound to the N atoms of the ammine ligands are omitted for clarity

.
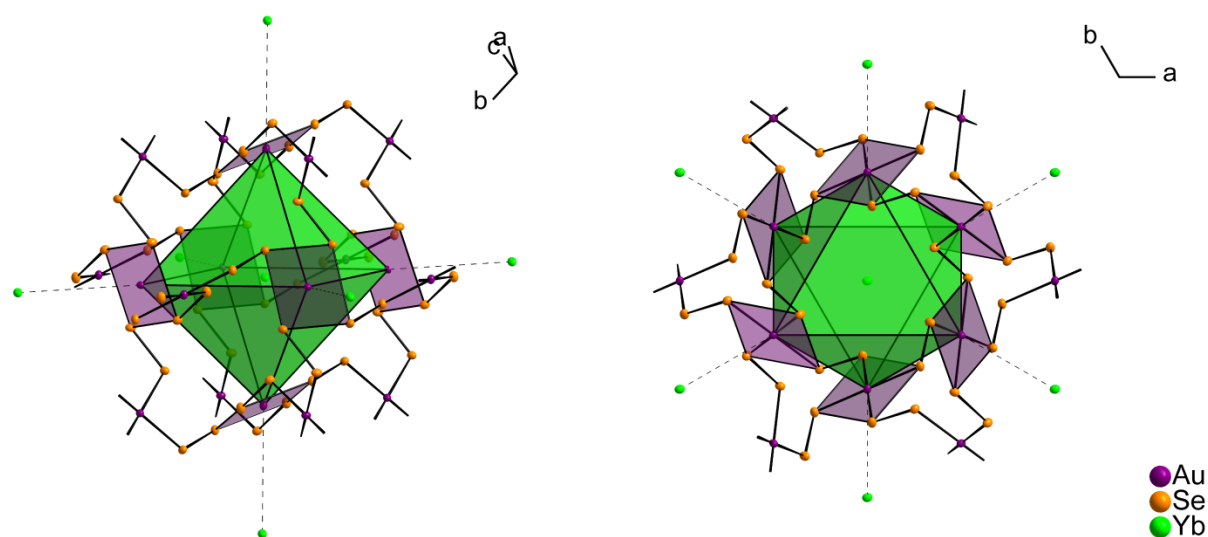
Figure 120: Coordination of Yb^{3+} by $(AuSe_4)$ units from two different perspectives in the structure of $[Yb(NH_3)_8](AuSe_4)_3$. The displacement ellipsoids represent a probability of 50%. The ammine ligands of the Yb^{3+} ions are omitted for clarity.

3.3.6a Classification of the cubic YbN$_8$ coordination polyhedron

The almost perfect cubic YbN$_8$ coordination polyhedron in the crystal structure of [Yb(NH$_3$)$_8$](AuSe$_4$)$_3$ is a rarely occurring coordination polyhedron. To the best of our knowledge only one other example for an almost cubic coordination polyhedron formed by monodentate ligands is present, [U(NCS)$_8$]$^{4-}$ [142]. The complex ion [U(NCS)$_8$]$^{4-}$ is present in the crystal structure [Et$_4$N]$_4$[U(NCS)$_8$] with the weakly coordinating cations Et$_4$N$^+$ as counterions. There are other examples for a cubic environment, for example the coordination of Pa in Na$_3$PaF$_8$ [143], but they are all ionic solids and therefore not comparable to the cubic coordination present in the complex ions ion [U(NCS)$_8$]$^{4-}$ and [Yb(NH$_3$)$_8$]$^{3+}$. For the coordination number 8, square antiprisms (D_{4d}) or triangular dodecahedra (D_{2d}) are the frequently found coordination polyhedra. Both are energetically preferred in comparison to cubic coordination polyhedra since there is less repulsion between the ligands. There are no cubic complexes with d-block elements known. In 1956 *Coulson* and *Lester* first described the participation of f orbitals in hybridization during the formation of complexes [144]. Later on the requirement of an f orbital in cubic hybridization is described [145]. For cubic hybridization, the square planar hybridization dsp^2 is supplemented with a set of fpd^2 orbitals [146]. The set of fpd^2 orbitals result from multiplying the polynomials of the square planar hybrid orbitals with z. Therefore, f$_{xyz}$d^{3}sp^3 hybrid metal orbitals result in a cubic coordination.

Table 42: Results of continuous shape measures of the YbN$_8$ polyhedron in the structure of [Yb(NH$_3$)$_8$](AuSe$_4$)$_3$, the UN$_8$ polyhedron in the structure of [Et$_4$N]$_4$[U(NCS)$_8$].

Ideal Shape	CShM / % (YbN$_8$ polyhedron)	CShM / % (UN$_8$ polyhedron)
OP-8	36.984	38.128
HPY-8	29.045	30.524
HBPY-8	6.486	8.397
CU-8	**0.133**	**0.002**
SAPR-8	11.108	10.972
TDD-8	8.075	7.930
BTPR-8	12.677	12.845
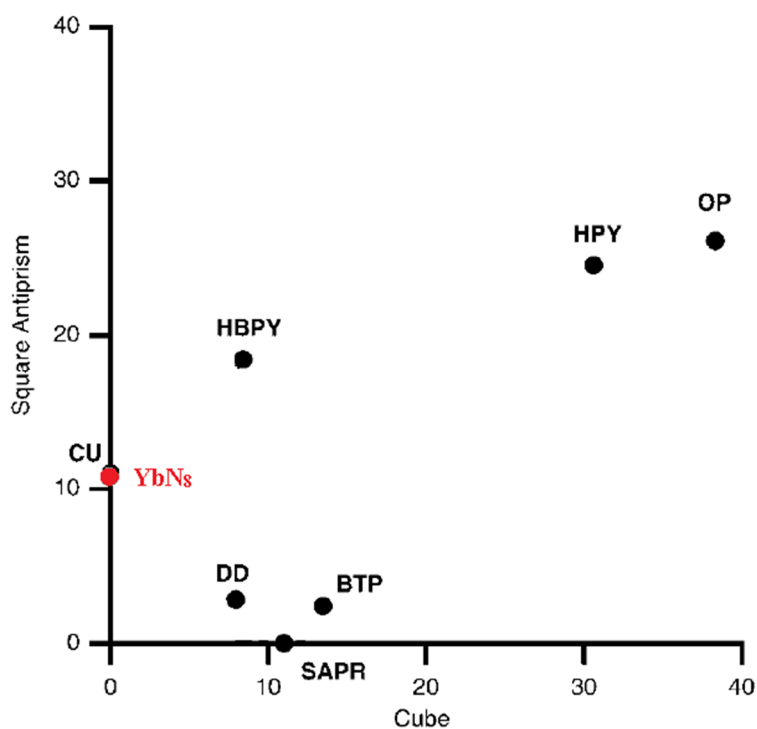
Figure 121: Shape map in the cube–square antiprism space. The points indicate the positions of the respective ideal polyhedra in this map. The deviations are given in percent. The picture was taken from reference [38] and slightly modified. The coordination polyhedron of Yb in the structure of $[Yb(NH_3)_8](AuSe_4)_3$ is inserted as a red dot.

In Table 42 the results of continuous shape measures of the above named almost cubic coordination polyhedra are shown. The YbN_8 polyhedron shows a higher but still very small deviation from an ideal cubic coordination (0.133%) compared to the UN_8 polyhedron with a deviation amounting to 0.002 %. However, the deviations to all other ideal shapes is significantly higher. For a better classification of the deviations some deviations of ideal polyhedra are shown in a shape map depicted in Figure 121. The higher deviation from the ideal cubic shape present in YbN_8 polyhedron compared to the UN_8 polyhedron could be due to the fact that Yb in the oxidation state +III is a f^{13} ion. A fd^3sp^3 hybridization of Yb^{3+} leads to a capacity for 15 electrons, but a capacity of 16 is required for the eight ammine ligands. One additional d orbital has to be taken into account for the hybridization, which leads to a distortion of the ideal cubic shape. Uranium in $[Et_4N]_4[U(NCS)_8]$ is in the oxidation state +IV and therefore a f^2 ion. Compared to the f^{13} configuration of Yb^{3+}, U^{4+} have the full required capacity of 16 electrons in a fd^3sp^3 hybridization.

4. Summary and Outlook

Within the scope of this work, 27 compounds were firstly synthesized and structurally characterized via single crystal X-ray diffraction. A list with all compounds is shown in the following table.

Compounds containing oligomeric Q_n^{2-} units or polymeric chalcogenides	Compounds containing chalcogenidoarsenates	Compounds containing chalcogenido-cuprates(I); -argentates(I) or -aurates(III)
$[Eu(NH_3)_9]_2(S_5)_3 \cdot 2NH_3$	$[Ca(en)_4]_2(As_4Te_6)$	$[Eu(NH_3)_8][Cu(S_4)_2] \cdot NH_3$
$[Sm(NH_3)_9]_2(S_5)_3 \cdot 2NH_3$	$[Sr(en)_4]_2(As_4Te_6)$	$[Er(NH_3)_8][Cu(S_4)_2] \cdot NH_3$
$[Er(NH_3)_8]_2(S_5)_2(S_6) \cdot 3NH_3$	$[Eu(en)_4]_2(As_4Se_6)$	$[Eu(NH_3)_9][Ag(Se_4)_2] \cdot 2NH_3$
$[Yb(NH_3)_8]_2(S_5)_2(S_6) \cdot 3NH_3$	$[Ca(en)_4](As_2Se_6)$	$[Yb(NH_3)_8](AuSe_5S_7) \cdot NH_3$
$[Yb(NH_3)_8]_2(S_5)_2(S_4) \cdot 4NH_3$	$[Ca(en)_4]_2(As_2Se_7O)$	$[Yb(NH_3)_8](AuS_4Se_6)$
$[Yb(NH_3)_7(S_2O_3)]_2(S_6) \cdot NH_3$	$[Ca(en)_3(H_2O)_2]As_2Se_4$	$[Ca(en)_4](AuTe_5)_2$
$[Eu(NH_3)_9]_2(Se_2)_2(Se_3)$	$[Sr(en)_3(H_2O)_2]As_2Se_4$	$[Yb(NH_3)_8](AuSe_4)_3$
$[Sr(en)_4](Te_3)$		
$[Eu(NH_3)_9]_2(Te_4)_3$		
$[Ba(NH_3)_8](Te_4)$		
$[Ca(en)_4](Te_4) \cdot 0.5en$		
$[Yb(NH_3)_8]_4(Te_{20})(Te_3)_2 \cdot 2NH_3$		
$[Eu(en)_4]Te_6$		

Despite the great interest in solvothermal syntheses and especially in ammonothermal syntheses for decades, the outcome of this work showed that there is still a lot to discover in the subjects *Zintl* phases and polychalcogenides. Synthesis approaches in ammonia and ethylene diamine turned out to be suitable even for the work with elemental coinage metals as educts and the single crystal manipulations at very low temperatures made it possible to characterize actually very temperature and air sensitive compounds. In contrast to these advantages, it seemed to be impossible to synthesize phase pure products by the used synthetic methods. The notorious multiphase products in combination with the very high temperature and air sensitivity of the target compounds, hampered any further analysis of physical properties like magnetism or electrical conductivity.

The coordination number of the bi- and trivalent cations varies between eight and nine. For ethylene diamine complexes only coordination number eight was observed with triangular dodecahedral polyhedra as dominating shape in 75% of the analyzed complex cations. With exception of europium, in ethylene diamine none of the used lanthanides reacted under formation of suitable single crystals. Coordination number eight is mainly observed for the ammine complexes. For the smaller lanthanides Yb and Er exclusively coordination number eight was observed. For ammine complexes of the larger lanthanides Eu and Sm, coordination numbers eight and nine were observed. The most frequent polyhedral shape of the ammine complexes is the square antiprism or the capped square antiprism, respectively.

The very small differences in the compositions and the polysulfide chain lengths of the compounds $[Ln(NH_3)_9]_2(S_5)_3 \cdot 2NH_3$ (Ln = Eu or Sm), $[Er(NH_3)_8]_2(S_5)_2(S_6) \cdot 3NH_3$ and $[Yb(NH_3)_8]_2(S_5)_2(S_4) \cdot 4NH_3$ allow for the presumption that the composition highly depends on filling degree of the ampoules with ammonia. The ionic radii are all very close to each other and the weighed ratios were the same in all syntheses; only the filling degree was not exactly manageable. Usage of different reaction approaches for the synthesis of $[Eu(NH_3)_9]_2(S_5)_3 \cdot 2NH_3$ gave no differences for the resulting products, independent if the synthesis was performed under ambient conditions or under supercritical conditions, if all educts were soluble in ammonia.

Syntheses of chalcogenidoarsenate(III) anions in ethylene diamine led to the first observation of a cyclic $(As_4Se_6)^{4-}$ anion. Beside the $(As_4Se_6)^{4-}$ anion, $(As_4Te_6)^{4-}$ anions could be synthesized in two isotypic structures. All crystal structures presented in this thesis containing molecular chalcogenidoarsenate(III) anions could be derived from simple salt structures. Structures of the compounds $[M(en)_4]_2(As_4Q_6)$ (M = Ca, Sr and Q = Te or M = Eu and Q = Se) and $[Ca(en)_4](As_2Se_6)$ adopt the anti-fluorite structure type Li_2O and $[Ca(en)_4](As_2Se_7O)$ the CsCl structure type. The polymeric chalcogenidoarsenate(III) anions present in $[M(en)_3(H_2O)_2]As_2Se_4$ (M = Ca or Sr) are representatives of *zwölfer* chains, a new chain conformation in the field of polymeric chalcogenidoarsenate(III) anions. Beside the new conformation, the chains show interesting interactions leading to a plausible description of an almost linear selenium chain with As-Se dumbbells attached next to it. Theoretical calculations should be made to quantify these interactions and the double bond character of the As-Se dumbbell.

With the syntheses of $[Ln(NH_3)_8][Cu(S_4)_2] \cdot NH_3$, with Ln = Eu or Er, two representatives were structurally analyzed being isotypic to the known structure of $[Ln(NH_3)_8][Cu(S_4)_2] \cdot NH_3$. Their crystal structures can be derived from the tungsten structure type. Introduction of the heavier homologues silver and selenium, led to the formation of $[Eu(NH_3)_9][Ag(Se_4)_2] \cdot NH_3$,

crystallizing in a different structure type. This type of isolated metallates with Ag or Cu as central atoms are very uncommon, they typically form polynuclear clusters or low dimensional infinite motifs. All attempts to synthesize compounds containing tellurometallates of the described type only led to the formation of polytelluride containing compounds.

Two one-dimensional infinite chalcogenidoaurates(III), namely $[Yb(NH_3)_8](AuSe_5S_7)\cdot NH_3$ and $[Yb(NH_3)_8](AuS_4Se_6)$, were successfully synthesized. Within the chains, the gold atoms are connected via polyselenides. The chains differ in the length of the connecting polyselenide and they show differently bound terminal polychalcogenides. Crystals of both compounds made problems in their structure refinements due to the mixed sulfur/selenium sites present in the terminally bound polychalcogenides. EDX analyses of the compounds gave only a rough hint for the S/Se ratio due to partial decomposition of the crystals during exposure to air and the following probable loss of H_2S and H_2Se, respectively. $[Yb(NH_3)_8](AuS_4Se_6)$ additionally show a disordering within the coordination of the gold atoms. The problems of S/Se mixed sites and especially the disordering were are intrinsic problems and were present in all analyzed crystals. It was not possible to obtain one of these chalcogenidoaurates(III) only with sulfur or selenium, respectively. Nevertheless, suitable and chemically reasonable structure solutions could be made for both compounds.

With calcium, tellurium and gold in ethylene diamine, $[Ca(en)_4](AuTe_5)_2$ which contains a two-dimensional telluridoaurate(III) anion could be synthesized. The layered structure contains two independent telluridoaurate(III) layers of which one is highly disordered. It is exceptional that only one of the independent layers show a disordering, whereas the other does not. Within the layers, the gold atoms are connected via bridging di- and tritellurides. The same synthetical approach with the heavier homologues of calcium, strontium and barium did not lead to formation of suitable single crystals.

Beside the one- and two-dimensional chalcogenidoaurate(III) anions, a three-dimensional selenidoaurate(III) was successfully synthesized. The compound $[Yb(NH_3)_8](AuSe_4)_3$ shows a three-dimensional network of gold atoms that were interconnected via selenium dumbbells. The ytterbium ammine complex shows a very particular coordination polyhedron, an almost perfect cube. Such a cubic coordination for a complex has only been described for $[U(SCN)_8]^{4-}$ in literature. According to literature, $f_{xyz}d^3sp^3$ hybrid metal orbitals are necessary for cubic coordination. Generally, a square antiprism would be favored as coordination polyhedron for coordination number eight, so cation-anion interactions or packing effects might be present to stabilize the cubic environment. One assumption is the stabilizing effect of the six $(AuSe_4)^-$ units coordinating to $[Yb(NH_3)_8]^{3+}$ perpendicular to the cubic faces. It is necessary to do further

research on the origin of the cubic coordination polyhedron e.g. theoretical calculations on the stabilization effects of the $(AuSe_4)^-$ units.

The syntheses of the four chalcogenidoaurate(III) anion containing compounds show the capability of solvothermal syntheses in liquid ammonia and ethylene diamine, to enhance the reactivity of gold. The same syntheses as solid state reactions would lead to the formation of binary alkaline earth or lanthanide chalcogenide compounds and elemental gold. It was not possible to synthesize thioaurates(III). A reason could be the very fast formation of binary polysulfides.

The structural variety of polychalcogenides and their connection possibilities with arsenic or coinage metals is presented in this work. It was shown that ammonothermal synthesis or the solvothermal synthesis in ethylene diamine are suitable synthetic methods to obtain polychalcogenides and *Zintl* phases. With the structural investigation of 27 crystal structures, this work provides the basis for further research on the bonding behavior of chalcogens within polychalcogenides or their interactions with arsenic or coinage metals.

Appendix

A.1 Single crystal data

A.1.1 [Eu(NH$_3$)$_9$]$_2$(S$_5$)$_3$ · 2NH$_3$

Table A.1: Crystal data and structure refinement for [Eu(NH$_3$)$_9$]$_2$(S$_5$)$_3$ · 2NH$_3$.

Empirical formula	Eu$_2$ H$_{60}$ N$_{20}$ S$_{15}$
Formula weight / *g/mol*	1159.56
Temperature / *K*	123(2)
Crystal system; Space group	Monoclinic; *P*2$_1$/*n*
Lattice constants / *Å*	*a* = 10.9036(4)
	b = 15.0138(4); *β* = 94.5860(10)°
	c = 13.5679(4)
Volume / *Å^3*	2214.01(12)
Z; F(000); calc. density / *g/cm^3*	4, 1172, 1.739
Wavelength / *Å*	0.71073
Crystal size / *mm*	0.058 × 0.055 × 0.045
Theta range for data collection / °	3.012 to 27.494
Limiting indices	-14 ≤ *h* ≤ 14, -18 ≤ *k* ≤ 19, -17 ≤ *l* ≤ 17
Reflections collected / unique	26350 / 5048
Completeness to *ϑ* = 25.242	99.3 %
R$_{int}$	6.80 %
Absorption coefficient / *mm^{-1}*	3.546
Refinement method	Full-matrix least-squares on F^2
Data / restrains / parameters	5048 / 0 / 191
R indices (all data) R_1 ; wR_2	0.0450; 0.1139
R indices [*I* > 4σ(*I*)] R_1 ; wR_2	0.0599; 0.1222 (for 4088 reflections)
Godness-of-fit for F^2	1.048
Largest diff. peak and hole / *e$^-$/A^3*	3.889 and -1.607

Table A.2: Fractional coordinates ($\cdot\ 10^4$) and equivalent isotropic displacement parameter U_{eq} ($\text{Å}^2 \cdot 10^3$) for the independent atoms in the structure of $[Eu(NH_3)_9]_2(S_5)_3 \cdot 2NH_3$.

	Wyck.	*x*	*y*	*z*	U_{eq}
Eu(1)	4*e*	5127(1)	8364(1)	7601(1)	21(1)
N(8)	4*e*	4013(5)	7664(3)	6033(3)	28(1)
N(4)	4*e*	4438(5)	8954(3)	9305(4)	30(1)
N(1)	4*e*	6032(6)	6787(4)	7192(4)	40(1)
N(6)	4*e*	4726(5)	9632(3)	6323(4)	34(1)
N(3)	4*e*	6816(5)	7938(4)	8966(4)	34(1)
N(5)	4*e*	6285(5)	9833(3)	8143(4)	30(1)
N(7)	4*e*	7091(5)	8490(3)	6625(4)	31(1)
N(9)	4*e*	2861(5)	8891(4)	7509(4)	39(1)
N(2)	4*e*	3906(6)	7110(4)	8378(4)	46(2)
S(2)	4*e*	6562(2)	4949(2)	10287(2)	56(1)
S(1)	4*e*	5040(4)	4243(3)	9596(3)	52(1)
S(3)	4*e*	7525(2)	5687(1)	9288(1)	41(1)
S(8)	4*e*	6591(2)	8884(1)	1469(1)	32(1)
S(7)	4*e*	5565(2)	7772(1)	1681(1)	40(1)
S(5)	4*e*	5832(2)	8085(1)	4113(1)	40(1)
S(4)	4*e*	6402(2)	6848(1)	4602(1)	38(1)
S(6)	4*e*	4592(2)	7988(1)	2905(1)	43(1)
N(10)	4*e*	8565(7)	9594(5)	9686(6)	60(2)
N(11)	4*e*	5016(9)	4890(8)	7388(9)	113(4)

Table A.3: Anisotropic displacement parameters $U_{ij}\ /\ \text{Å}^2 \cdot 10^3$ for the independent atoms in the structure of $[Eu(NH_3)_9]_2(S_5)_3 \cdot 2NH_3$.

	U_{11}	U_{22}	U_{33}	U_{23}	U_{13}	U_{12}
Eu(1)	28(1)	18(1)	18(1)	1(1)	3(1)	-2(1)
N(8)	36(3)	28(3)	21(2)	0(2)	6(2)	-3(2)
N(4)	35(3)	27(3)	26(2)	-4(2)	0(2)	0(2)
N(1)	62(4)	29(3)	28(3)	-2(2)	-4(3)	12(3)
N(6)	34(3)	27(3)	38(3)	11(2)	-7(2)	-7(2)

N(3)	47(3)	30(3)	24(2)	0(2)	0(2)	11(2)
N(5)	34(3)	28(3)	28(2)	0(2)	2(2)	-3(2)
N(7)	36(3)	29(3)	30(3)	-1(2)	6(2)	2(2)
N(9)	37(3)	55(4)	26(3)	-4(2)	4(2)	4(3)
N(2)	63(4)	38(4)	37(3)	-3(3)	18(3)	-17(3)
S(2)	43(1)	80(2)	44(1)	3(1)	0(1)	6(1)
S(1)	40(2)	41(2)	75(3)	-27(2)	5(2)	-3(2)
S(3)	49(1)	33(1)	38(1)	-6(1)	-10(1)	11(1)
S(8)	38(1)	32(1)	29(1)	2(1)	8(1)	7(1)
S(7)	59(1)	27(1)	32(1)	0(1)	-8(1)	-1(1)
S(5)	56(1)	34(1)	30(1)	3(1)	12(1)	7(1)
S(4)	45(1)	40(1)	30(1)	3(1)	12(1)	13(1)
S(6)	32(1)	43(1)	53(1)	18(1)	5(1)	2(1)
N(10)	55(4)	56(4)	69(5)	16(4)	-3(4)	-15(3)
N(11)	95(8)	102(9)	146(1)	-34(7)	47(7)	-48(6)

Table A.4: Selected bond lengths for of $[Eu(NH_3)_9]_2(S_5)_3 \cdot 2NH_3$. Symmetry transformations used to generate equivalent atoms: #1: $-x+1$, $-y+1$, $-z+2$.

Atoms 1, 2	Distance / Å	Atoms 1, 2	Distance / Å
Eu(1)-N(2)	2.579(5)	S(2)-S(3)	2.097(3)
Eu(1)-N(3)	2.586(5)	S(2)-S(1)	2.123(4)
Eu(1)-N(8)	2.587(5)	S(2)-S(1)#1	2.143(4)
Eu(1)-N(9)	2.588(6)	S(1)-S(2)#1	2.143(4)
Eu(1)-N(6)	2.589(5)	S(1)-S(1)#1	2.527(7)
Eu(1)-N(7)	2.613(5)	S(8)-S(7)	2.042(2)
Eu(1)-N(5)	2.618(5)	S(7)-S(6)	2.067(3)
Eu(1)-N(4)	2.641(5)	S(5)-S(6)	2.044(3)
Eu(1)-N(1)	2.641(5)	S(5)-S(4)	2.052(2)

Table A.5: Selected bond angles for of $[Eu(NH_3)_9]_2(S_5)_3 \cdot 2NH_3$. Symmetry transformations used to generate equivalent atoms: #1: $-x+1, -y+1, -z+2$.

Atoms 1, 2, 3	Angle / °	Atoms 1, 2, 3	Angle / °
S(3)-S(2)-S(1)	113.14(16)	S(2)#1-S(1)-S(1)#1	53.30(16)
S(3)-S(2)-S(1)#1	101.69(17)	S(8)-S(7)-S(6)	107.87(10)
S(1)-S(2)-S(1)#1	72.66(17)	S(6)-S(5)-S(4)	110.99(11)
S(2)-S(1)-S(2)#1	107.34(17)	S(5)-S(6)-S(7)	107.86(11)
S(2)-S(1)-S(1)#1	54.03(15)		

A.1.2 $[Sm(NH_3)_9]_2(S_5)_3 \cdot 2NH_3$

Table A.6: Crystal data and structure refinement for $[Sm(NH_3)_9]_2(S_5)_3 \cdot 2NH_3$.

Empirical formula	$Sm_2 H_{60} N_{20} S_{15}$
Formula weight / *g/mol*	1156.34
Temperature / *K*	123(2)
Crystal system; Space group	Monoclinic; $P2_1/n$
Lattice constants / *Å*	$a = 10.8879(3)$
	$b = 15.0272(4); \beta = 94.5120(10)°$
	$c = 13.5817(4)$
Volume / *Å³*	2215.28(11)
Z; F(000); calc. density / *g/cm³*	4; 1168; 1.734
Wavelength	0.71073
Crystal size / *mm*	$0.061 \times 0.045 \times 0.053$
Theta range for data collection / °	3.009 to 27.502
Limiting indices	$-14 \leq h \leq 14, -18 \leq k \leq 19, -17 \leq l \leq 17$
Reflections collected / unique	22521 / 4958
Completeness to $\vartheta = 25.242$	98.3 %
R_{int}	9.13 %
Absorption coefficient / *mm⁻¹*	3.363
Refinement method	Full-matrix least-squares on F^2
Data / restrains / parameters	4958 / 0 / 191
R indices (all data) R_1 ; wR_2	0.0459; 0.1062
R indices [$I > 4\sigma(I)$] R_1 ; wR_2	0.0743; 0.1172 (for 3633 reflections)
Godness-of-fit for F^2	1.051
Largest diff. peak and hole / e^-/A^3	2.694 and -1.291

Table A.7: Fractional coordinates ($\cdot$ 10^4) and equivalent isotropic displacement parameter U_{eq} ($\text{Å}^2 \cdot 10^3$) for the independent atoms in the structure of $[Sm(NH_3)_9]_2(S_5)_3 \cdot 2NH_3$.

	Wyck.	x	y	z	U_{eq}
Sm(1)	4e	4879(1)	1637(1)	2399(1)	19(1)
N(9)	4e	6004(4)	2341(3)	3971(4)	26(1)
N(2)	4e	3710(5)	173(3)	1855(4)	28(1)
N(5)	4e	5573(5)	1046(3)	690(4)	29(1)
N(6)	4e	3970(5)	3212(3)	2820(4)	36(1)
N(4)	4e	3188(5)	2067(3)	1029(4)	30(1)
N(3)	4e	5280(5)	361(3)	3685(4)	31(1)
N(7)	4e	6112(6)	2909(4)	1622(4)	41(2)
N(1)	4e	2900(5)	1509(3)	3380(4)	30(1)
N(8)	4e	7162(4)	1106(4)	2497(4)	35(1)
S(5)	4e	3426(2)	1115(1)	8528(1)	30(1)
S(1)	4e	3620(2)	3153(1)	5402(1)	36(1)
S(2)	4e	4190(2)	1913(1)	5886(1)	38(1)
S(4)	4e	4455(2)	2225(1)	8316(1)	38(1)
S(3)	4e	5428(2)	2009(1)	7093(2)	39(1)
S(6)	4e	2491(2)	4321(1)	706(1)	36(1)
S(7)	4e	3446(2)	5052(2)	-293(2)	49(1)
S(8)	4e	4947(3)	5749(3)	415(3)	45(1)
N(10)	4e	1441(6)	401(5)	308(6)	60(2)
N(11)	4e	4976(9)	5124(8)	2621(8)	120(4)

Table A.8: Anisotropic displacement parameters U_{ij} / $\text{Å}^2 \cdot 10^3$ for the independent atoms in the structure of $[Sm(NH_3)_9]_2(S_5)_3 \cdot 2NH_3$.

	U_{11}	U_{22}	U_{33}	U_{23}	U_{13}	U_{12}
Sm(1)	23(1)	18(1)	17(1)	1(1)	-1(1)	-1(1)
N(9)	29(3)	24(3)	23(3)	-2(2)	-1(2)	-1(2)
N(2)	28(3)	31(3)	26(3)	5(2)	-1(2)	3(2)
N(5)	29(3)	30(3)	26(3)	0(2)	0(2)	2(2)
N(6)	52(4)	28(3)	26(3)	-2(2)	-10(3)	5(3)

N(4)	40(3)	27(3)	23(3)	0(2)	-3(2)	8(2)
N(3)	27(3)	30(3)	36(3)	7(2)	-6(2)	-6(2)
N(7)	58(4)	36(3)	31(3)	-3(3)	16(3)	-13(3)
N(1)	30(3)	26(3)	33(3)	-2(2)	5(2)	2(2)
N(8)	25(3)	57(4)	24(3)	-2(3)	0(2)	1(3)
S(5)	32(1)	30(1)	29(1)	3(1)	5(1)	6(1)
S(1)	40(1)	40(1)	29(1)	2(1)	10(1)	12(1)
S(2)	51(1)	34(1)	29(1)	3(1)	9(1)	6(1)
S(4)	50(1)	28(1)	32(1)	-1(1)	-10(1)	0(1)
S(3)	27(1)	40(1)	51(1)	16(1)	4(1)	2(1)
S(6)	40(1)	31(1)	34(1)	-3(1)	-9(1)	6(1)
S(7)	35(1)	67(1)	43(1)	4(1)	-4(1)	2(1)
S(8)	31(2)	39(2)	66(3)	-22(2)	5(2)	-5(2)
N(10)	50(4)	59(5)	68(5)	14(4)	-11(4)	-11(4)
N(11)	94(8)	109(9)	162(1)	-19(7)	33(8)	-55(6)

Table A.9: Selected bond lengths for of $[Sm(NH_3)_9]_2(S_5)_3 \cdot 2NH_3$. Symmetry transformations used to generate equivalent atoms: #1: $-x+1$, $-y+1$, $-z$.

Atoms 1, 2	Distance / Å	Atoms 1, 2	Distance / Å
Sm(1)-N(4)	2.595(5)	S(5)-S(4)	2.044(2)
Sm(1)-N(9)	2.600(5)	S(1)-S(2)	2.056(2)
Sm(1)-N(8)	2.605(5)	S(2)-S(3)	2.044(3)
Sm(1)-N(7)	2.606(5)	S(4)-S(3)	2.064(3)
Sm(1)-N(3)	2.607(5)	S(6)-S(7)	2.085(3)
Sm(1)-N(2)	2.619(5)	S(7)-S(8)	2.109(4)
Sm(1)-N(1)	2.628(5)	S(7)-S(8)#1	2.141(4)
Sm(1)-N(6)	2.645(5)	S(8)-S(7)#1	2.141(4)
Sm(1)-N(5)	2.651(5)	S(8)-S(8)#1	2.523(7)

Table A.10: Selected bond lengths for of [Sm(NH$_3$)$_9$]$_2$(S$_5$)$_3\cdot$2NH$_3$. Symmetry transformations used to generate equivalent atoms: #1: -x+1, -y+1, -z.

Atoms 1, 2, 3	Angle / °	Atoms 1, 2, 3	Angle / °
S(3)-S(2)-S(1)	110.82(12)	S(8)-S(7)-S(8)#1	72.85(17)
S(5)-S(4)-S(3)	107.86(10)	S(7)-S(8)-S(7)#1	107.15(16)
S(2)-S(3)-S(4)	108.00(10)	S(7)-S(8)-S(8)#1	54.16(14)
S(6)-S(7)-S(8)	111.92(16)	S(7)#1-S(8)-S(8)#1	52.99(14)
S(6)-S(7)-S(8)#1	101.92(15)		

A.1.3 $[Er(NH_3)_8]_2(S_5)_2(S_6) \cdot 3NH_3$

Table A.11: Crystal data and structure refinement for $[Er(NH_3)_8]_2(S_5)_2(S_6) \cdot 3NH_3$.

Empirical formula	$Er_2\,H_{48}\,N_{19}\,S_{16}$
Formula weight / *g/mol*	1162.05
Temperature / *K*	123(2)
Crystal system; Space group	Monoclinic; $P\,2_1/c$
Lattice constants / *Å*	$a = 15.0988(2)$
	$b = 20.7571(4); \beta = 110.0460(10)$
	$c = 13.9957(3)$
Volume / *Å³*	4120.62(13)
Z; F(000); calc. density / *g/cm³*	4 ; 2292 ; 1.873
Wavelength / *Å*	0.71073
Crystal size / *mm*	$0.082 \times 0.110 \times 0.092$
Theta range for data collection / °	2.926 to 27.529
Limiting indices	$-19 \leq h \leq 19, -27 \leq k \leq 27, -18 \leq l \leq 18$
Reflections collected / unique	30239 / 8992
Completeness to $\vartheta = 25.242$	96.4 %
R_{int}	14.75 %
Absorption coefficient / *mm⁻¹*	4.884
Refinement method	Full-matrix least-squares on F^2
Data / restrains / parameters	8992 / 0 / 336
R indices (all data) R_1 ; wR_2	0.0675; 0.1310
R indices [$I > 4\sigma(I)$] R_1 ; wR_2	0.0512; 0.1216 (for 7169 reflections)
Godness-of-fit for F^2	1.020
Largest diff. peak and hole / e^-/A^3	1.324 and -2.326

Table A.12: Fractional coordinates ($\cdot$ 10^4) and equivalent isotropic displacement parameter U_{eq} ($\text{Å}^2 \cdot 10^3$) for the independent atoms in the structure of $[Er(NH_3)_8]_2(S_5)_2(S_6) \cdot 3NH_3$.

	Wyck.	*x*	*y*	*z*	U_{eq}
S(1)	4*e*	-124(1)	5773(1)	3426(1)	27(1)
S(2)	4*e*	885(1)	5640(1)	2777(1)	28(1)
S(3)	4*e*	265(1)	5478(1)	1246(1)	25(1)
S(4)	4*e*	14(1)	6349(1)	494(1)	25(1)
S(5)	4*e*	1276(1)	6677(1)	421(1)	21(1)
S(6)	4*e*	3266(1)	9672(1)	3189(1)	24(1)
S(7)	4*e*	3627(1)	8851(1)	2615(1)	24(1)
S(8)	4*e*	3954(1)	9041(1)	1334(1)	26(1)
S(9)	4*e*	2733(1)	9064(1)	68(1)	21(1)
S(10)	4*e*	2324(1)	8114(1)	-194(1)	22(1)
S(11)	4*e*	3338(1)	7623(1)	-560(1)	25(1)
S(12)	4*e*	6836(1)	9476(1)	1098(1)	20(1)
S(13)	4*e*	6484(1)	8541(1)	1273(1)	23(1)
S(14)	4*e*	6162(1)	8418(1)	2575(1)	23(1)
S(15)	4*e*	7393(1)	8158(1)	3720(1)	23(1)
S(16)	4*e*	7799(1)	7280(1)	3337(1)	24(1)
Er(1)	4*e*	31(1)	6493(1)	6781(1)	14(1)
N(1)	4*e*	1058(4)	5863(3)	8251(4)	20(1)
N(2)	4*e*	965(4)	5688(3)	6189(4)	20(1)
N(3)	4*e*	-1098(4)	5740(3)	5578(4)	23(1)
N(4)	4*e*	-993(4)	6102(3)	7719(4)	21(1)
N(5)	4*e*	102(4)	7365(3)	8027(4)	21(1)
N(6)	4*e*	-1421(4)	7198(3)	6076(5)	28(1)
N(7)	4*e*	2(4)	6934(3)	5145(4)	19(1)
N(8)	4*e*	1551(4)	7063(3)	7164(4)	20(1)
Er(2)	4*e*	4602(1)	6276(1)	2521(1)	14(1)
N(9)	4*e*	4503(4)	5125(3)	2151(4)	23(1)
N(10)	4*e*	4698(4)	5833(3)	4205(4)	24(1)
N(11)	4*e*	3000(4)	6022(3)	2530(4)	23(1)
N(12)	4*e*	3648(5)	7266(3)	2057(4)	27(1)

N(13)	4e	5421(4)	7125(3)	3806(4)	24(1)
N(14)	4e	5446(4)	6858(3)	1550(4)	21(1)
N(15)	4e	6286(4)	5905(3)	3245(4)	23(1)
N(16)	4e	3692(4)	6128(3)	675(4)	21(1)
N(17)	4e	2381(5)	4876(4)	677(5)	34(2)
N(18)	4e	5629(5)	5908(4)	-38(5)	36(2)
N(19)	4e	7813(6)	6087(5)	1296(7)	54(2)

Table A.13: Anisotropic displacement parameters U_{ij} / Å^2 · 10^3 for the independent atoms in the structure of [Er(NH$_3$)$_8$]$_2$(S$_5$)$_2$(S$_6$) · 3NH$_3$.

	U_{11}	U_{22}	U_{33}	U_{23}	U_{13}	U_{12}
S(1)	33(1)	28(1)	24(1)	-5(1)	14(1)	-4(1)
S(2)	24(1)	38(1)	23(1)	7(1)	8(1)	-2(1)
S(3)	33(1)	21(1)	26(1)	-2(1)	15(1)	-5(1)
S(4)	20(1)	30(1)	24(1)	5(1)	7(1)	2(1)
S(5)	20(1)	20(1)	21(1)	2(1)	6(1)	1(1)
S(6)	26(1)	27(1)	25(1)	-2(1)	14(1)	-3(1)
S(7)	26(1)	22(1)	23(1)	-1(1)	7(1)	-3(1)
S(8)	20(1)	35(1)	24(1)	-9(1)	10(1)	-7(1)
S(9)	20(1)	23(1)	22(1)	0(1)	10(1)	1(1)
S(10)	19(1)	23(1)	23(1)	0(1)	7(1)	-5(1)
S(11)	32(1)	23(1)	20(1)	1(1)	11(1)	4(1)
S(12)	17(1)	20(1)	24(1)	1(1)	7(1)	1(1)
S(13)	26(1)	18(1)	21(1)	0(1)	4(1)	2(1)
S(14)	20(1)	18(1)	33(1)	4(1)	12(1)	2(1)
S(15)	26(1)	24(1)	19(1)	0(1)	7(1)	-4(1)
S(16)	18(1)	25(1)	26(1)	2(1)	5(1)	2(1)
Er(1)	13(1)	16(1)	14(1)	0(1)	6(1)	0(1)
N(1)	16(3)	22(3)	20(3)	-5(2)	5(2)	0(2)
N(2)	16(3)	21(3)	26(3)	-3(2)	9(2)	-1(2)
N(3)	26(3)	24(3)	21(3)	-5(2)	9(2)	-3(2)
N(4)	18(3)	25(3)	20(3)	3(2)	8(2)	-3(2)

N(5)	20(3)	21(3)	23(3)	-3(2)	9(2)	0(2)
N(6)	24(3)	39(4)	25(3)	10(3)	12(3)	10(3)
N(7)	17(3)	21(3)	21(3)	2(2)	9(2)	-1(2)
N(8)	18(3)	23(3)	21(3)	-3(2)	8(2)	-4(2)
Er(2)	14(1)	14(1)	15(1)	1(1)	6(1)	1(1)
N(9)	25(3)	22(3)	21(3)	-1(2)	6(2)	3(2)
N(10)	18(3)	25(3)	28(3)	5(2)	9(2)	0(2)
N(11)	18(3)	31(3)	20(3)	3(2)	6(2)	4(2)
N(12)	36(3)	28(3)	18(3)	4(2)	8(3)	11(3)
N(13)	26(3)	25(3)	20(3)	-2(2)	6(2)	-4(3)
N(14)	25(3)	21(3)	20(3)	-1(2)	10(2)	-2(2)
N(15)	25(3)	21(3)	26(3)	-1(2)	12(2)	1(2)
N(16)	20(3)	24(3)	20(3)	2(2)	9(2)	3(2)
N(17)	33(1)	28(1)	24(1)	-5(1)	14(1)	-4(1)
N(18)	24(1)	38(1)	23(1)	7(1)	8(1)	-2(1)
N(19)	33(1)	21(1)	26(1)	-2(1)	15(1)	-5(1)

Table A.14: Selected bond lengths for [Er(NH$_3$)$_8$]$_2$(S$_5$)$_2$(S$_6$)·3NH$_3$.

Atoms 1, 2	Distance / Å	Atoms 1, 2	Distance / Å
S(1)-S(2)	2.042(3)	Er(1)-N(8)	2.472(5)
S(2)-S(3)	2.051(3)	Er(1)-N(1)	2.482(6)
S(3)-S(4)	2.061(3)	Er(1)-N(4)	2.482(5)
S(4)-S(5)	2.059(2)	Er(1)-N(5)	2.490(6)
S(6)-S(7)	2.035(3)	Er(1)-N(3)	2.493(6)
S(7)-S(8)	2.055(3)	Er(1)-N(2)	2.504(5)
S(8)-S(9)	2.074(2)	Er(1)-N(6)	2.538(6)
S(9)-S(10)	2.062(2)	Er(2)-N(9)	2.439(6)
S(10)-S(11)	2.044(2)	Er(2)-N(12)	2.466(6)
S(12)-S(13)	2.049(2)	Er(2)-N(14)	2.474(5)
S(13)-S(14)	2.056(3)	Er(2)-N(11)	2.479(6)
S(14)-S(15)	2.067(3)	Er(2)-N(10)	2.487(6)
S(15)-S(16)	2.051(3)	Er(2)-N(16)	2.495(6)
Er(1)-N(7)	2.453(5)	Er(2)-N(15)	2.515(6)
Er(2)-N(13)	2.518(6)		

Table A.15: Selected bond angles for [Er(NH$_3$)$_8$]$_2$(S$_5$)$_2$(S$_6$)·3NH$_3$.

Atoms 1, 2, 3	Angle / °	Atoms 1, 2, 3	Angle / °
S(1)-S(2)-S(3)	110.09(11)	S(10)-S(9)-S(8)	108.47(10)
S(2)-S(3)-S(4)	109.14(11)	S(11)-S(10)-S(9)	111.95(11)
S(5)-S(4)-S(3)	107.71(11)	S(12)-S(13)-S(14)	107.25(10)
S(6)-S(7)-S(8)	111.13(11)	S(13)-S(14)-S(15)	107.42(10)
S(7)-S(8)-S(9)	109.91(10)		

A.1.4 [Yb(NH$_3$)$_8$]$_2$(S$_5$)$_2$(S$_6$) · 3NH$_3$

Table A.16: Crystal data and structure refinement for [Yb(NH$_3$)$_8$]$_2$(S$_5$)$_2$(S$_6$) · 3NH$_3$.

Empirical formula	H$_{57}$ N$_{19}$ S$_{16}$ Yb$_2$
Formula weight / *g/mol*	1182.68
Temperature / *K*	123(2)
Crystal system; Space group	Monoclinic; *P* 2$_1$/*c*
Lattice constants / *Å*	*a* = 15.0942(4)
	b = 20.7195(9); *β* = 109.900(2)°
	c = 14.0036(4)
Volume / *Å^3*	4118.0(2)
Z; F(000); calc. density / *g/cm^3*	4; 2344; 1.908
Wavelength / *Å*	0.71073
Crystal size / *mm*	0.180 × 0.160 × 0.110
Theta range for data collection / °	2.928 to 27.471
Limiting indices	-19 ≤ *h* ≤ 17, -25 ≤ *k* ≤ 21, -18 ≤ *l* ≤ 16
Reflections collected / unique	13532 / 7161
Completeness to ϑ = 25.242	78.3 %
R$_{int}$	5.87 %
Absorption coefficient / *mm^{-1}*	5.354
Refinement method	Full-matrix least-squares on F^2
Data / restrains / parameters	7161 / 0 / 351
R indices (all data) R_1 ; wR_2	0.0838 ; 0.0974
R indices [$I > 4\sigma(I)$] R_1 ; wR_2	0.0453 ; 0.0861 (for 4844 reflections)
Godness-of-fit for F^2	0.953
Largest diff. peak and hole / *e$^-$/A^3*	1.188 and -1.752

Table A.17: Fractional coordinates ($\cdot 10^4$) and equivalent isotropic displacement parameter U_{eq} ($\text{Å}^2 \cdot 10^3$) for the independent atoms in the structure of $[Yb(NH_3)_8]_2(S_5)_2(S_6) \cdot 3NH_3$.

	Wyck.	*x*	*y*	*z*	U_{eq}
Yb(1)	4*e*	4596(1)	3727(1)	7516(1)	14(1)
N(1)	4*e*	4678(4)	4161(4)	9181(4)	18(2)
N(2)	4*e*	6259(4)	4098(4)	8221(5)	27(2)
N(3)	4*e*	5403(4)	2877(4)	8765(5)	22(2)
N(4)	4*e*	5425(4)	3157(4)	6548(5)	22(2)
N(5)	4*e*	3650(4)	2765(4)	7055(5)	27(2)
N(6)	4*e*	3705(4)	3877(4)	5697(5)	19(2)
N(7)	4*e*	3011(4)	3980(4)	7521(5)	21(2)
N(8)	4*e*	4498(4)	4883(4)	7173(5)	23(2)
Yb(2)	4*e*	33(1)	3503(1)	1773(1)	14(1)
N(9)	4*e*	107(4)	2642(4)	3021(5)	24(2)
N(10)	4*e*	1031(4)	4117(4)	3233(5)	24(2)
N(11)	4*e*	1536(4)	2931(4)	2137(5)	25(2)
N(12)	4*e*	964(4)	4306(4)	1190(5)	23(2)
N(13)	4*e*	2(4)	3067(4)	151(4)	18(2)
N(14)	4*e*	-1077(4)	4245(4)	574(5)	18(2)
N(15)	4*e*	-1406(5)	2815(4)	1087(5)	29(2)
N(16)	4*e*	-977(4)	3911(4)	2699(5)	21(2)
S(1)	4*e*	3331(1)	2390(1)	4433(2)	20(1)
S(2)	4*e*	2309(1)	1888(1)	4799(1)	16(1)
S(3)	4*e*	2732(1)	929(1)	5059(2)	19(1)
S(4)	4*e*	3959(1)	954(1)	6329(2)	22(1)
S(5)	4*e*	3625(1)	1151(1)	7615(2)	23(1)
S(6)	4*e*	3263(1)	329(1)	8192(2)	23(1)
S(7)	4*e*	1278(1)	3330(1)	5412(2)	19(1)
S(8)	4*e*	0(1)	3658(1)	5476(2)	18(1)
S(9)	4*e*	263(2)	4533(1)	6239(2)	23(1)
S(10)	4*e*	884(1)	4355(1)	7777(2)	24(1)
S(11)	4*e*	-135(2)	4225(1)	8420(2)	25(1)
S(12)	4*e*	6835(1)	4482(1)	11076(1)	14(1)
S(13)	4*e*	6485(1)	3531(1)	11257(2)	21(1)

S(14)	4e	6154(1)	3419(1)	12562(2)	23(1)
S(15)	4e	7395(1)	3161(1)	13723(2)	21(1)
S(16)	4e	7811(1)	2266(1)	13327(1)	15(1)
N(17)	4e	2366(5)	5130(5)	5674(6)	32(2)
N(18)	4e	5624(5)	4102(5)	4967(5)	43(3)
N(19)	4e	7816(5)	3913(5)	6288(6)	47(3)

Table A. 18: Anisotropic displacement parameters U_{ij} / $\text{Å}^2 \cdot 10^3$ for the independent atoms in the structure of $[\text{Yb}(\text{NH}_3)_8]_2(\text{S}_5)_2(\text{S}_6) \cdot 3\text{NH}_3$.

	U_{11}	U_{22}	U_{33}	U_{23}	U_{13}	U_{12}
Yb(1)	14(1)	13(1)	14(1)	-1(1)	5(1)	-1(1)
N(1)	15(4)	26(6)	9(3)	3(3)	-2(3)	1(3)
N(2)	21(4)	37(7)	25(4)	0(4)	10(3)	-3(4)
N(3)	20(4)	27(6)	19(4)	-1(3)	5(3)	-1(3)
N(4)	27(4)	21(6)	19(4)	2(3)	10(3)	-1(3)
N(5)	23(4)	44(7)	15(4)	5(4)	7(3)	-13(4)
N(6)	29(4)	15(5)	15(4)	0(3)	11(3)	1(3)
N(7)	20(4)	22(6)	20(4)	-1(3)	5(3)	-8(3)
N(8)	21(4)	20(6)	26(4)	-4(3)	4(3)	-8(3)
Yb(2)	13(1)	15(1)	13(1)	0(1)	4(1)	0(1)
N(9)	21(4)	28(6)	27(4)	7(4)	11(3)	4(3)
N(10)	17(4)	34(6)	20(4)	-1(4)	5(3)	-2(3)
N(11)	21(4)	32(6)	17(4)	-4(4)	1(3)	1(3)
N(12)	16(4)	36(6)	19(4)	6(4)	8(3)	-3(3)
N(13)	24(4)	13(5)	13(3)	1(3)	3(3)	3(3)
N(14)	17(4)	17(5)	20(4)	-1(3)	6(3)	5(3)
N(15)	34(4)	35(7)	19(4)	-4(4)	11(3)	-9(4)
N(16)	13(4)	32(6)	14(4)	-4(3)	-1(3)	4(3)
S(1)	26(1)	20(2)	14(1)	-3(1)	6(1)	-2(1)
S(2)	13(1)	18(2)	16(1)	-1(1)	3(1)	5(1)
S(3)	19(1)	19(2)	19(1)	0(1)	8(1)	-1(1)
S(4)	17(1)	29(2)	21(1)	10(1)	7(1)	7(1)
S(5)	24(1)	21(2)	22(1)	1(1)	3(1)	4(1)
S(6)	22(1)	24(2)	24(1)	0(1)	11(1)	3(1)

S(7)	17(1)	18(2)	19(1)	0(1)	3(1)	0(1)
S(8)	14(1)	20(2)	19(1)	-6(1)	5(1)	-2(1)
S(9)	33(1)	16(2)	24(1)	3(1)	14(1)	5(1)
S(10)	14(1)	41(2)	17(1)	-6(1)	3(1)	0(1)
S(11)	32(1)	24(2)	20(1)	5(1)	12(1)	3(1)
S(12)	10(1)	15(1)	16(1)	2(1)	2(1)	2(1)
S(13)	23(1)	16(2)	20(1)	-2(1)	2(1)	2(1)
S(14)	22(1)	17(2)	30(1)	4(1)	11(1)	1(1)
S(15)	23(1)	20(2)	16(1)	1(1)	3(1)	-3(1)
S(16)	9(1)	17(1)	14(1)	2(1)	-1(1)	0(1)
N(17)	20(4)	33(7)	40(5)	5(4)	5(3)	-1(4)
N(18)	27(4)	72(9)	26(4)	21(5)	5(3)	-9(4)
N(19)	39(5)	55(8)	44(5)	3(5)	10(4)	18(5)

Table A.19: Selected bond lengths for [Yb(NH$_3$)$_8$]$_2$(S$_5$)$_2$(S$_6$)·3NH$_3$.

Atoms 1, 2	Distance / Å	Atoms 1, 2	Distance / Å
Yb(1)-N(5)	2.408(8)	Yb(2)-N(15)	2.499(7)
Yb(1)-N(8)	2.437(8)	S(1)-S(2)	2.064(3)
Yb(1)-N(4)	2.438(7)	S(2)-S(3)	2.080(3)
Yb(1)-N(7)	2.453(6)	S(3)-S(4)	2.087(3)
Yb(1)-N(6)	2.462(6)	S(4)-S(5)	2.069(3)
Yb(1)-N(1)	2.463(6)	S(5)-S(6)	2.038(4)
Yb(1)-N(2)	2.486(6)	S(7)-S(8)	2.077(3)
Yb(1)-N(3)	2.489(7)	S(8)-S(9)	2.072(3)
Yb(2)-N(13)	2.430(6)	S(9)-S(10)	2.068(3)
Yb(2)-N(10)	2.444(7)	S(10)-S(11)	2.048(3)
Yb(2)-N(11)	2.453(7)	S(12)-S(13)	2.078(3)
Yb(2)-N(16)	2.463(6)	S(13)-S(14)	2.066(3)
Yb(2)-N(14)	2.466(6)	S(14)-S(15)	2.090(3)
Yb(2)-N(9)	2.472(7)	S(15)-S(16)	2.092(3)
Yb(2)-N(12)	2.489(7)		

Table A.20: Selected bond angles for [Yb(NH$_3$)$_8$]$_2$(S$_5$)$_2$(S$_6$)·3NH$_3$.

Atoms 1, 2, 3	Angle / °	Atoms 1, 2, 3	Angle / °
S(1)-S(2)-S(3)	108.28(12)	S(10)-S(9)-S(8)	108.66(15)
S(2)-S(3)-S(4)	104.87(14)	S(11)-S(10)-S(9)	109.84(12)
S(5)-S(4)-S(3)	109.75(12)	S(14)-S(13)-S(12)	111.22(15)
S(6)-S(5)-S(4)	110.96(15)	S(13)-S(14)-S(15)	107.13(12)
S(9)-S(8)-S(7)	106.90(12)	S(14)-S(15)-S(16)	106.90(12)

A.1.5 [Yb(NH₃)₈]₂(S₅)₂(S₄) · 4NH₃

Table A.21: Crystal data and structure refinement for [Yb(NH₃)₈]₂(S₅)₂(S₄) · 4NH₃.

Empirical formula	$H_{24} N_{10} S_7 Yb$
Formula weight / *g/mol*	561.75
Temperature / *K*	123(2)
Crystal system; Space group	Tetragonal; $P\,4_12_12$
Lattice constants / *Å*	$a = 9.6150(2)$
	$c = 43.6485(10)$
Volume / *Å³*	4035.23(19)
Z; F(000); calc. density / *g/cm³*	8 ; 2208 ; 1.849
Wavelength / *Å*	0.71073
Crystal size / *mm*	
Theta range for data collection / °	2.996 to 27.501
Limiting indices	$-11 \leq h \leq 11, -12 \leq k \leq 12, -56 \leq l \leq 43$
Reflections collected / unique	20785 / 4614
Completeness to $\vartheta = 25.242$	99.0 %
R_{int}	8.88 %
Absorption coefficient / *mm⁻¹*	5.360
Refinement method	Full-matrix least-squares on F^2
Data / restrains / parameters	4614 / 0 / 172
R indices (all data) R_1 ; wR_2	0.0527 ; 0.0822
R indices [$I > 4\sigma(I)$] R_1 ; wR_2	0.0379 ; 0.0777 (for 3909 reflections)
Godness-of-fit for F^2	1.032
Largest diff. peak and hole / e^-/A^3	1.399 and -0.898

Table A.22: Fractional coordinates ($\cdot\ 10^4$) and equivalent isotropic displacement parameter U_{eq} ($\text{Å}^2 \cdot 10^3$) for the independent atoms in the structure of $[Yb(NH_3)_8]_2(S_5)_2(S_4) \cdot 4NH_3$.

	Wyck.	x	y	z	U_{eq}
Yb(1)	8*b*	-814(1)	4006(1)	4453(1)	16(1)
N(1)	8*b*	-2307(7)	2227(7)	4672(2)	26(2)
N(2)	8*b*	218(7)	2458(8)	4073(2)	29(2)
N(3)	8*b*	623(7)	2365(7)	4740(2)	22(2)
N(4)	8*b*	1495(7)	5007(7)	4392(2)	31(2)
N(5)	8*b*	-270(8)	5153(8)	4940(2)	30(2)
N(6)	8*b*	-869(8)	6080(7)	4116(2)	29(2)
N(7)	8*b*	-2844(8)	5340(8)	4617(2)	43(3)
N(8)	8*b*	-2595(9)	3524(8)	4064(2)	38(2)
S(1)	8*b*	7276(3)	-16(3)	3877(1)	33(1)
S(2)	8*b*	6104(3)	-502(3)	4251(1)	32(1)
S(3)	8*b*	4070(3)	136(3)	4196(1)	40(1)
S(4)	8*b*	3999(3)	2280(3)	4221(1)	41(1)
S(5)	8*b*	4190(2)	2938(2)	4668(1)	30(1)
S(6)	8*b*	8836(3)	-1247(3)	4760(1)	45(1)
S(7)	8*b*	10882(3)	-1267(2)	4603(1)	33(1)
N(9)	8*b*	-4026(10)	6273(8)	3790(2)	48(3)
N(10)	8*b*	-5814(8)	6977(8)	4676(2)	36(2)

Table A.23: Anisotropic displacement parameters U_{ij} / $\text{Å}^2 \cdot 10^3$ for the independent atoms in the structure of $[Yb(NH_3)_8]_2(S_5)_2(S_4) \cdot 4NH_3$.

	U_{11}	U_{22}	U_{33}	U_{23}	U_{13}	U_{12}
Yb(1)	15(1)	17(1)	16(1)	-1(1)	-2(1)	0(1)
N(1)	24(4)	18(4)	37(5)	-1(4)	-2(4)	-2(3)
N(2)	22(4)	33(4)	31(5)	-9(4)	-2(4)	3(4)
N(3)	20(4)	18(4)	27(5)	1(3)	0(3)	-1(3)
N(4)	22(4)	30(4)	41(5)	8(4)	-4(4)	-3(3)
N(5)	36(5)	36(5)	17(4)	-4(4)	2(4)	7(4)
N(6)	33(4)	23(4)	30(4)	0(3)	-9(4)	-4(4)

N(7)	28(5)	34(5)	66(7)	-21(5)	-3(5)	5(4)
N(8)	36(5)	32(5)	47(7)	-11(4)	-20(4)	4(4)
S(1)	31(1)	35(1)	32(2)	-4(1)	-1(1)	0(1)
S(2)	39(1)	34(1)	24(1)	-1(1)	-3(1)	3(1)
S(3)	27(1)	64(2)	29(2)	-11(1)	-2(1)	-6(1)
S(4)	35(2)	63(2)	24(2)	14(1)	5(1)	16(2)
S(5)	19(1)	34(1)	36(2)	6(1)	-2(1)	2(1)
S(6)	29(1)	28(1)	79(2)	-19(1)	-20(1)	7(1)
S(7)	37(1)	31(1)	31(2)	-6(1)	-8(1)	1(1)
N(9)	62(6)	30(4)	54(7)	1(4)	-36(5)	9(4)
N(10)	22(4)	42(5)	46(6)	-8(4)	-10(4)	1(4)

Table A.24: Selected bond lengths for [Yb $(NH_3)_8$]$_2$(S_5)$_2$(S_4)·4NH$_3$. Symmetry transformations used to generate equivalent atoms: #1 *y*+1, *x*-1, -*z*+1.

Atoms 1, 2	Distance / Å	Atoms 1, 2	Distance / Å
Yb(1)-N(1)	2.430(7)	Yb(1)-N(6)	2.474(7)
Yb(1)-N(4)	2.435(7)	S(1)-S(2)	2.037(4)
Yb(1)-N(2)	2.437(7)	S(2)-S(3)	2.063(4)
Yb(1)-N(3)	2.444(7)	S(3)-S(4)	2.067(4)
Yb(1)-N(7)	2.445(8)	S(4)-S(5)	2.059(4)
Yb(1)-N(5)	2.452(8)	S(6)-S(7)	2.086(4)
Yb(1)-N(8)	2.453(8)	S(6)-S(6)#1	2.098(7)

Table A.25: Selected bond angles for [Yb $(NH_3)_8$]$_2$(S_5)$_2$(S_4) · 4NH$_3$. Symmetry transformations used to generate equivalent atoms: #1 *y*+1, *x*-1, -*z*+1.

Atoms 1, 2, 3	Angle / °	Atoms 1, 2, 3	Angle / °
S(1)-S(2)-S(3)	111.30(16)	S(5)-S(4)-S(3)	110.77(16)
S(2)-S(3)-S(4)	108.74(17)	S(7)-S(6)-S(6)#1	111.39(16)

A.1.6 [Yb(NH$_3$)$_7$(S$_2$O$_3$)]$_2$(S$_6$)·NH$_3$

Table A. 26: Crystal data and structure refinement for [Yb(NH$_3$)$_7$(S$_2$O$_3$)]$_2$(S$_6$)·NH$_3$.

Empirical formula	H$_{42}$ N$_{15}$ O$_6$ S$_{10}$ Yb$_2$
Formula weight / *g/mol*	1015.16
Temperature / *K*	123(2)
Crystal system; Space group	Monoclinic; *Cc*
Lattice constants / *Å*	*a* = 15.0761(8)
	b = 22.7055(12); *β* = 126.880(2)°
	c = 12.4593(6)
Volume / *Å^3*	3411.5(3)
Z; F(000); calc. density / *g/cm^3*	4; 1980;1.977
Wavelength / *Å*	0.71073
Crystal size / *mm*	0.070 × 0.086 × 0.040
Theta range for data collection / °	1.912 to 27.485
Limiting indices	-19 ≤ *h* ≤ 19, -29 ≤ *k* ≤ 28, -16 ≤ *l* ≤ 16
Reflections collected / unique	19567 / 7446
Completeness to *ϑ* = 25.242	99.4 %
R$_{int}$	10.75 %
Absorption coefficient / *mm^{-1}*	6.101
Refinement method	Full-matrix least-squares on F^2
Data / restrains / parameters	7446 / 2 / 308
R indices (all data) R_1 ; *wR$_2$*	0.0888; 0.1269
R indices [$I > 4σ(I)$] R_1 ; *wR$_2$*	0.0544; 0.1133 (for 5438 reflections)
Godness-of-fit for F^2	0.974
Largest diff. peak and hole / *e$^-$/A^3*	2.187 and -1.515
Absolute structure parameter	-0.050(14)

Table A. 27: Fractional coordinates ($\cdot\ 10^4$) and equivalent isotropic displacement parameter U_{eq} ($\text{Å}^2 \cdot 10^3$) for the independent atoms in the structure of $[Yb(NH_3)_7(S_2O_3)]_2(S_6) \cdot NH_3$.

	Wyck.	x	y	z	U_{eq}
Yb(1)	4a	5176(1)	1055(1)	6664(1)	22(1)
N(1)	4a	5671(15)	1068(8)	8930(17)	26(3)
N(2)	4a	3762(15)	1689(8)	6464(19)	26(3)
N(3)	4a	3519(15)	1062(8)	4288(18)	29(4)
N(4)	4a	5394(15)	113(8)	5920(20)	32(5)
N(5)	4a	7195(16)	832(9)	8160(20)	35(5)
N(6)	4a	5810(16)	1392(9)	5350(20)	38(5)
N(7)	4a	5998(16)	2051(9)	7490(20)	44(6)
Yb(2)	4a	6175(1)	3549(1)	3539(1)	23(1)
N(8)	4a	6960(20)	2543(9)	4140(20)	57(8)
N(9)	4a	6674(18)	3473(9)	5779(19)	34(5)
N(10)	4a	5071(17)	4238(11)	3800(20)	43(6)
N(11)	4a	4590(20)	3704(15)	1200(20)	75(10
N(12)	4a	8190(16)	3716(9)	5120(20)	37(5)
N(13)	4a	6770(16)	3296(8)	2165(19)	27(4)
N(14)	4a	6490(20)	4522(9)	3070(30)	49(6)
S(1)	4a	3225(5)	222(2)	6862(6)	26(1)
S(2)	4a	1774(5)	559(3)	5337(6)	36(2)
O(1)	4a	3110(14)	-407(7)	6882(17)	36(4)
O(2)	4a	3544(13)	495(7)	8128(15)	29(4)
O(3)	4a	4053(12)	361(6)	6617(15)	24(3)
S(3)	4a	3907(4)	2689(2)	3038(6)	24(1)
S(4)	4a	3989(5)	2893(3)	4664(6)	34(1)
O(4)	4a	3947(18)	2054(8)	2942(18)	65(7)
O(5)	4a	2898(17)	2928(12)	1862(19)	73(8)
O(6)	4a	4893(18)	2913(12)	3210(20)	80(9)
S(5)	4a	2775(6)	4993(4)	1082(8)	57(2)
S(6)	4a	3338(7)	5466(3)	2877(7)	52(2)
S(7)	4a	2461(5)	6224(3)	2442(7)	39(2)
S(8)	4a	3133(6)	6829(3)	1851(7)	46(2)
S(9)	4a	4699(6)	7011(3)	3500(7)	42(2)

S(10)	4a	4647(5)	7665(3)	4591(7)	39(2)
N(15)	4a	5150(30)	5776(13)	1700(40)	86(9)

Table A. 28: Anisotropic displacement parameters U_{ij} / Å^2 · 10^3 for the independent atoms in the structure of [Yb(NH$_3$)$_7$(S$_2$O$_3$)]$_2$(S$_6$)·NH$_3$.

	U_{11}	U_{22}	U_{33}	U_{23}	U_{13}	U_{12}
Yb(1)	19(1)	21(1)	24(1)	1(1)	12(1)	-1(1)
N(1)	25(7)	29(7)	24(7)	2(6)	16(6)	-8(6)
N(2)	25(7)	29(7)	24(7)	2(6)	16(6)	-8(6)
N(3)	25(10)	30(10)	20(9)	-14(9)	6(8)	-4(9)
N(4)	22(10)	35(11)	40(12)	-7(9)	18(9)	-1(9)
N(5)	27(11)	28(10)	41(12)	2(10)	15(10)	-3(9)
N(6)	25(10)	45(13)	47(13)	1(11)	23(10)	-6(10)
N(7)	21(10)	27(11)	57(14)	7(10)	9(10)	1(9)
Yb(2)	19(1)	26(1)	23(1)	0(1)	12(1)	-2(1)
N(8)	100(20)	19(11)	33(13)	-5(10)	27(14)	-5(12)
N(9)	41(12)	37(12)	26(11)	-5(9)	21(10)	10(10)
N(10)	32(11)	77(17)	25(11)	24(11)	20(10)	25(12)
N(11)	46(15)	150(30)	35(13)	8(16)	29(12)	38(17)
N(12)	27(10)	31(10)	37(12)	-17(10)	10(10)	-12(9)
N(13)	27(10)	23(10)	27(11)	3(8)	14(9)	6(8)
N(14)	82(18)	24(11)	86(18)	0(11)	75(17)	5(11)
S(1)	29(3)	22(3)	31(3)	-5(2)	20(3)	-5(2)
S(2)	27(3)	47(4)	24(3)	-3(3)	11(3)	5(3)
O(1)	52(11)	31(9)	49(11)	-10(8)	44(10)	-12(8)
O(2)	25(8)	39(9)	17(8)	-3(7)	9(7)	-5(7)
O(3)	29(8)	15(7)	37(9)	-1(7)	25(8)	-6(6)
S(3)	20(3)	24(3)	26(3)	-2(2)	12(2)	-3(2)
S(4)	25(3)	49(4)	26(3)	-2(3)	15(3)	0(3)
O(4)	88(17)	27(9)	31(10)	-6(9)	9(11)	11(11)
O(5)	43(12)	120(20)	25(10)	2(11)	2(9)	49(13)

O(6)	73(15)	130(20)	69(14)	-68(15)	61(13)	-92(16)
S(5)	44(4)	60(5)	59(5)	26(4)	28(4)	11(4)
S(6)	64(5)	41(4)	38(4)	19(3)	23(4)	15(4)
S(7)	38(4)	39(3)	35(4)	-5(3)	20(3)	-1(3)
S(8)	59(4)	36(4)	32(4)	7(3)	20(3)	2(3)
S(9)	42(4)	43(4)	48(4)	14(3)	30(3)	6(3)
S(10)	35(3)	40(4)	40(4)	7(3)	21(3)	4(3)
N(15)	78(19)	90(20)	100(20)	-20(20)	65(18)	10(20)

Table A.29: Selected bond lengths for $[Yb(NH_3)_7(S_2O_3)]_2(S_6) \cdot NH_3$.

Atoms 1, 2	Distance / Å	Atoms 1, 2	Distance / Å
Yb(1)-O(3)	2.289(13)	Yb(2)-N(8)	2.47(2)
Yb(1)-N(4)	2.430(18)	S(1)-O(1)	1.440(17)
Yb(1)-N(1)	2.449(17)	S(1)-O(2)	1.480(16)
Yb(1)-N(6)	2.46(2)	S(1)-O(3)	1.486(15)
Yb(1)-N(2)	2.457(19)	S(1)-S(2)	1.999(8)
Yb(1)-N(3)	2.476(17)	S(3)-O(5)	1.443(19)
Yb(1)-N(7)	2.48(2)	S(3)-O(4)	1.450(18)
Yb(1)-N(5)	2.487(19)	S(3)-O(6)	1.457(17)
Yb(2)-O(6)	2.247(17)	S(3)-S(4)	2.008(8)
Yb(2)-N(14)	2.40(2)	S(5)-S(6)	2.144(12)
Yb(2)-N(9)	2.422(19)	S(6)-S(7)	2.036(10)
Yb(2)-N(13)	2.430(19)	S(7)-S(8)	2.086(10)
Yb(2)-N(10)	2.44(2)	S(8)-S(9)	2.036(10)
Yb(2)-N(11)	2.45(2)	S(9)-S(10)	2.047(10)
Yb(2)-N(12)	2.464(19)		

Table A.30: Selected bond angles for $[Yb(NH_3)_7(S_2O_3)]_2(S_6) \cdot NH_3$.

Atoms 1, 2, 3	Angle / °	Atoms 1, 2, 3	Angle / °
O(1)-S(1)-O(2)	111.3(10)	O(4)-S(3)-O(6)	105.7(15)

O(1)-S(1)-O(3)	109.8(9)	O(5)-S(3)-S(4)	109.1(9)
O(2)-S(1)-O(3)	110.7(9)	O(4)-S(3)-S(4)	109.4(10)
O(1)-S(1)-S(2)	108.8(8)	O(6)-S(3)-S(4)	109.1(8)
O(2)-S(1)-S(2)	108.9(7)	S(3)-O(6)-Yb(2)	160.2(18)
O(3)-S(1)-S(2)	107.3(7)	S(7)-S(6)-S(5)	111.0(4)
S(1)-O(3)-Yb(1)	147.2(9)	S(6)-S(7)-S(8)	105.9(4)
O(5)-S(3)-O(4)	111.1(13)	S(9)-S(8)-S(7)	107.0(4)
O(5)-S(3)-O(6)	112.3(16)	S(8)-S(9)-S(10)	109.5(4)

Table A.31: Selected hydrogen bond lengths and angles for $[Yb(NH_3)_7(S_2O_3)]_2(S_6) \cdot NH_3$. Symmetry transformations used to generate equivalent atoms: #1 x, $-y+1$, $z+^1/_2$ #2 $x+^1/_2$, $y-^1/_2$, $z+1$ #3 x, $-y$, $z-^1/_2$ #4 $x+^1/_2$, $-y+^1/_2$, $z+^1/_2$ #5 $x+^1/_2$, $y+^1/_2$, z #6 x, $-y+1$, $z-^1/_2$ #7 $x+^1/_2$, $y-^1/_2$, z #8 $x+^1/_2$, $-y+^1/_2$, $z-^1/_2$.

D-H···A	d(D-H) / Å	d(H···A) / Å	d(D···A) / Å	∢ (DHA) / °
N(1)-H(1A)...S(1)	0.91	2.87	3.539(18)	131.1
N(1)-H(1A)...O(2)	0.91	2.16	3.02(2)	158.5
N(1)-H(1B)...S(10)#1	0.91	2.81	3.59(2)	143.6
N(1)-H(1C)...S(5)#2	0.91	2.74	3.60(2)	158.3
N(2)-H(2A)...S(1)	0.91	2.93	3.533(19)	125.5
N(2)-H(2A)...S(2)	0.91	2.66	3.533(19)	160.6
N(2)-H(2B)...S(4)	0.91	2.85	3.679(19)	152.8
N(2)-H(2C)...S(9)#1	0.91	2.84	3.58(2)	140.5
N(2)-H(2C)...S(10)#1	0.91	2.68	3.59(2)	172.3
N(3)-H(3A)...O(1)#3	0.91	2.23	3.06(2)	151.7
N(3)-H(3B)...O(4)	0.91	2.33	3.10(3)	142.7
N(3)-H(3C)...S(2)	0.91	2.91	3.75(2)	154.3
N(4)-H(4B)...S(5)#4	0.91	2.58	3.48(2)	170.6
N(4)-H(4C)...O(2)#3	0.91	2.32	3.19(2)	158.8
N(5)-H(5A)...S(5)#2	0.91	2.82	3.72(2)	170.9
N(5)-H(5B)...S(4)#4	0.91	2.72	3.62(2)	172.2
N(5)-H(5C)...S(5)#4	0.91	2.79	3.70(2)	172.8
N(5)-H(5C)...S(6)#4	0.91	2.85	3.54(2)	133.1
N(6)-H(6B)...O(5)#4	0.91	2.05	2.95(3)	169.5

N(6)-H(6C)...O(4)	0.91	2.10	3.01(3)	176.6
N(7)-H(7A)...S(4)	0.91	2.64	3.52(2)	164.0
N(7)-H(7B)...S(4)#4	0.91	2.77	3.61(2)	154.7
N(7)-H(7B)...O(5)#4	0.91	2.63	3.39(3)	141.8
N(7)-H(7C)...S(9)#1	0.91	2.90	3.60(2)	134.2
N(8)-H(8A)...S(3)#4	0.91	3.01	3.92(2)	176.1
N(8)-H(8A)...O(5)#4	0.91	2.16	2.98(3)	149.9
N(9)-H(9A)...S(4)	0.91	2.78	3.65(2)	160.2
N(9)-H(9B)...O(1)#5	0.91	2.28	3.08(3)	145.4
N(9)-H(9C)...S(3)#4	0.91	2.95	3.85(2)	170.5
N(9)-H(9C)...O(4)#4	0.91	2.21	3.06(3)	155.2
N(10)-H(10A)...S(5)	0.91	2.65	3.51(2)	158.4
N(10)-H(10A)...S(6)	0.91	2.95	3.51(2)	121.0
N(10)-H(10B)...S(2)#5	0.91	2.84	3.65(3)	150.3
N(11)-H(11A)...S(10)#6	0.91	2.86	3.73(3)	160.2
N(12)-H(12A)...S(10)#7	0.91	3.03	3.56(2)	119.6
N(12)-H(12B)...O(1)#5	0.91	2.14	3.02(3)	161.7
N(12)-H(12C)...O(2)#8	0.91	2.50	3.36(3)	157.1
N(13)-H(13A)...S(10)#7	0.91	2.88	3.777(19)	170.3
N(13)-H(13B)...S(2)#8	0.91	2.56	3.46(2)	170.5
N(13)-H(13C)...S(10)#6	0.91	2.71	3.60(2)	165.2
N(14)-H(14A)...N(15)	0.91	2.67	3.31(4)	128.1
N(14)-H(14B)...S(1)#8	0.91	2.90	3.77(2)	159.8
N(14)-H(14B)...O(2)#8	0.91	2.17	3.06(3)	167.5
N(14)-H(14C)...S(2)#5	0.91	2.61	3.50(2)	164.2

A.1.7 [Eu(NH$_3$)$_9$]$_2$(Se$_2$)$_2$(Se$_3$)

Table A.32: Crystal data and structure refinement for [Eu(NH$_3$)$_9$]$_2$(Se$_2$)$_2$(Se$_3$).

Empirical formula	H$_{54}$ N$_{18}$ Eu$_2$ Se$_7$
Formula weight / *g/mol*	1163.25
Temperature / *K*	123(2)
Crystal system; Space group	Monoclinic; *P* 2$_1$/*c*
Lattice constants / *Å*	*a* = 15.2468(3)
	b = 15.8655(3); *β* = 101.8530(10)°
	c = 13.7139(3)
Volume / *Å^3*	3246.63(11)
Z; F(000); calc. density / *g/cm^3*	4; 2176; 2.380
Wavelength / *Å*	0.71073
Crystal size / *mm*	0.160 × 0.034 × 0.034
Theta range for data collection / °	2.983 to 27.504
Limiting indices	-19 ≤ *h* ≤ 19, -20 ≤ *k* ≤ 20, -17 ≤ *l* ≤ 17
Reflections collected / unique	66375 / 7454
Completeness to ϑ = 25.242	99.9 %
R$_{int}$	016.14 %
Absorption coefficient / *mm^{-1}*	11.699
Refinement method	Full-matrix least-squares on F^2
Data / restrains / parameters	7454 / 0 / 263
R indices (all data) R_1 ; wR_2	0.0747; 0.1486
R indices [*I* > 4σ(*I*)] R_1 ; wR_2	0.0533; 0.1400 (for 5726 reflections)
Godness-of-fit for F^2	1.139
Largest diff. peak and hole / *e$^-$/A^3*	3.252 and -2.882

Table A.33: Fractional coordinates ($\cdot\ 10^4$) and equivalent isotropic displacement parameter U_{eq} ($\text{Å}^2 \cdot 10^3$) for the independent atoms in the structure of [Eu(NH$_3$)$_9$]$_2$(Se$_2$)$_2$(Se$_3$).

	Wyck.	*x*	*y*	*z*	U_{eq}
Eu(1)	4*e*	1018(1)	6564(1)	2761(1)	17(1)
N(1)	4*e*	671(6)	5155(6)	1809(8)	24(2)
N(2)	4*e*	1749(7)	6635(6)	1205(8)	30(2)
N(3)	4*e*	2393(6)	5583(6)	3110(8)	28(2)
N(4)	4*e*	1357(6)	6095(6)	4621(7)	21(2)
N(5)	4*e*	2414(6)	7446(6)	3661(7)	25(2)
N(6)	4*e*	1029(6)	8116(6)	2097(7)	22(2)
N(7)	4*e*	109(6)	7612(6)	3666(7)	26(2)
N(8)	4*e*	-295(6)	5704(6)	3246(7)	25(2)
N(9)	4*e*	-383(6)	6755(6)	1354(7)	24(2)
Eu(2)	4*e*	6094(1)	6396(1)	2802(1)	16(1)
N(10)	4*e*	6006(6)	4993(5)	1756(7)	19(2)
N(11)	4*e*	4830(6)	5416(6)	3137(7)	23(2)
N(12)	4*e*	4817(6)	6517(6)	1220(7)	22(2)
N(13)	4*e*	5044(6)	7374(6)	3532(7)	21(2)
N(14)	4*e*	6023(6)	7969(6)	2088(7)	21(2)
N(15)	4*e*	7400(6)	7325(6)	3764(7)	25(2)
N(16)	4*e*	6293(6)	6056(6)	4711(7)	22(2)
N(17)	4*e*	7104(6)	6537(6)	1542(7)	20(2)
N(18)	4*e*	7396(5)	5367(6)	3432(7)	21(2)
Se(1)	4*e*	1720(1)	5305(1)	-1043(1)	23(1)
Se(2)	4*e*	2211(1)	4541(1)	446(1)	25(1)
Se(3)	4*e*	3772(1)	4401(1)	772(1)	25(1)
Se(4)	4*e*	3333(1)	8227(1)	1542(1)	23(1)
Se(5)	4*e*	4049(1)	8788(1)	298(1)	21(1)
Se(6)	4*e*	-1700(1)	6539(1)	6711(1)	24(1)
Se(7)	4*e*	-892(1)	6131(1)	5472(1)	22(1)

Table A.34: Anisotropic displacement parameters U_{ij} / Å$^2 \cdot 10^3$ for the independent atoms in the structure of [Eu(NH$_3$)$_9$]$_2$(Se$_2$)$_2$(Se$_3$).

	U_{11}	U_{22}	U_{33}	U_{23}	U_{13}	U_{12}
Eu(1)	13(1)	20(1)	18(1)	0(1)	4(1)	0(1)
N(1)	12(4)	22(5)	40(6)	-2(4)	14(4)	-1(3)
N(2)	33(5)	26(5)	36(6)	-8(4)	16(5)	-13(4)
N(3)	18(5)	24(5)	37(6)	-4(4)	-1(4)	2(4)
N(4)	14(4)	28(5)	22(5)	-1(4)	3(4)	-2(4)
N(5)	26(5)	21(5)	27(5)	-1(4)	6(4)	-2(4)
N(6)	18(4)	24(5)	25(5)	-3(4)	4(4)	-4(4)
N(7)	20(5)	36(6)	23(5)	1(4)	5(4)	3(4)
N(8)	18(4)	34(6)	24(5)	0(4)	5(4)	-3(4)
N(9)	18(4)	28(5)	27(5)	2(4)	8(4)	3(4)
Eu(2)	12(1)	19(1)	17(1)	-1(1)	5(1)	0(1)
N(10)	16(4)	16(4)	26(5)	0(4)	7(4)	2(3)
N(11)	19(4)	22(5)	27(5)	-1(4)	4(4)	4(4)
N(12)	13(4)	26(5)	24(5)	2(4)	-2(4)	2(3)
N(13)	14(4)	26(5)	20(5)	-3(4)	1(3)	-5(4)
N(14)	19(4)	19(5)	24(5)	-3(4)	3(4)	-2(3)
N(15)	21(5)	27(5)	27(5)	3(4)	2(4)	-6(4)
N(16)	15(4)	21(5)	28(5)	2(4)	4(4)	-1(3)
N(17)	16(4)	22(5)	22(5)	-3(4)	4(4)	2(3)
N(18)	13(4)	21(5)	30(5)	-5(4)	8(4)	-5(3)
Se(1)	18(1)	23(1)	28(1)	-1(1)	3(1)	2(1)
Se(2)	25(1)	25(1)	28(1)	2(1)	14(1)	4(1)
Se(3)	23(1)	26(1)	25(1)	2(1)	0(1)	-3(1)
Se(4)	18(1)	25(1)	27(1)	2(1)	8(1)	1(1)
Se(5)	18(1)	26(1)	22(1)	0(1)	7(1)	-1(1)
Se(6)	19(1)	23(1)	32(1)	-1(1)	10(1)	1(1)
Se(7)	19(1)	25(1)	22(1)	-3(1)	5(1)	-2(1)

Table A.35: Selected bond lengths for [Eu(NH$_3$)$_9$]$_2$(Se$_2$)$_2$(Se$_3$).

Atoms 1, 2	Distance / Å	Atoms 1, 2	Distance / Å
Eu(1)-N(3)	2.575(9)	Eu(2)-N(18)	2.579(9)
Eu(1)-N(9)	2.586(9)	Eu(2)-N(11)	2.589(9)
Eu(1)-N(1)	2.587(9)	Eu(2)-N(15)	2.607(9)
Eu(1)-N(4)	2.605(9)	Eu(2)-N(12)	2.608(9)
Eu(1)-N(2)	2.605(10	Eu(2)-N(16)	2.630(9)
Eu(1)-N(8)	2.618(9)	Eu(2)-N(10)	2.636(9)
Eu(1)-N(6)	2.628(9)	Eu(2)-N(14)	2.674(9)
Eu(1)-N(7)	2.634(9)	Se(1)-Se(2)	2.3604(17)
Eu(1)-N(5)	2.634(9)	Se(2)-Se(3)	2.3411(16)
Eu(2)-N(17)	2.549(9)	Se(4)-Se(5)	2.3786(15)
Eu(2)-N(13)	2.575(9)	Se(6)-Se(7)	2.3834(15)

Table A.36: Selected bond angles for [Eu(NH$_3$)$_9$]$_2$(Se$_2$)$_2$(Se$_3$).

Atoms 1, 2, 3	Angle / °	Atoms 1, 2, 3	Angle / °
Se(3)-Se(2)-Se(1)	110.07(6)		

A.1.8 [Sr(en)₄](Te₃)

Table A.37: Crystal data and structure refinement for [Sr(en)₄](Te₃).

Empirical formula	$C_8 H_{32} N_8 Sr Te_3$
Formula weight / *g/mol*	710.83
Temperature / *K*	123(3)
Crystal system; Space group	Monoclinic; $P\,2_1/n$
Lattice constants / *Å*	$a = 9.0927(6)$
	$b = 13.5636(9); \beta = 95.569(4)°$
	$c = 17.7260(8)$
Volume / *Å³*	2175.8(2)
Z; F(000); calc. density / *g/cm³*	4; 1320; 2.170
Wavelength / *Å*	0.71073
Crystal size / *mm*	$0.370 \times 0.024 \times 0.022$
Theta range for data collection / °	3.004 to 27.499
Limiting indices	$-11 \le h \le 11, -17 \le k \le 17, -23 \le l \le 22$
Reflections collected / unique	24733 / 4930
Completeness to $\vartheta = 25.242$	99.1 %
R_{int}	11.48 %
Absorption coefficient / *mm⁻¹*	6.425
Refinement method	Full-matrix least-squares on F^2
Data / restrains / parameters	4930 / 0 / 182
R indices (all data) R_1 ; wR_2	0.1006; 0.0808
R indices [$I > 4\sigma(I)$] R_1 ; wR_2	0.0422; 0.0691 (for 3011 reflections)
Godness-of-fit for F^2	1.000
Largest diff. peak and hole / e^-/A^3	0.869 and -1.022

Table A.38: Fractional coordinates ($\cdot\ 10^4$) and equivalent isotropic displacement parameter U_{eq} ($\mathring{A}^2 \cdot 10^3$) for the independent atoms in the structure of [Sr(en)$_4$](Te$_3$).

	Wyck.	*x*	*y*	*z*	U_{eq}
Te(1)	4*e*	4563(1)	1411(1)	6345(1)	32(1)
Te(2)	4*e*	5384(1)	3175(1)	7004(1)	27(1)
Te(3)	4*e*	7454(1)	4085(1)	6222(1)	27(1)
Sr(1)	4*e*	5818(1)	2743(1)	3499(1)	22(1)
N(1)	4*e*	7442(6)	1049(4)	3342(3)	31(2)
N(2)	4*e*	7028(6)	1960(4)	4813(3)	31(2)
N(3)	4*e*	8658(6)	3447(5)	3431(3)	33(2)
N(4)	4*e*	6429(6)	4555(4)	4110(3)	27(1)
N(5)	4*e*	3734(6)	3087(4)	4477(3)	28(1)
N(6)	4*e*	3680(6)	1335(4)	3481(3)	29(1)
N(7)	4*e*	5846(6)	2540(4)	1973(3)	30(2)
N(8)	4*e*	3719(6)	3746(4)	2644(3)	28(1)
C(1)	4*e*	8381(8)	824(6)	4048(4)	38(2)
C(2)	4*e*	7526(8)	921(5)	4722(4)	32(2)
C(3)	4*e*	9031(7)	4189(5)	4020(4)	28(2)
C(4)	4*e*	7873(7)	4986(5)	3988(4)	32(2)
C(5)	4*e*	2418(8)	2515(5)	4252(4)	35(2)
C(6)	4*e*	2780(8)	1456(5)	4119(4)	32(2)
C(7)	4*e*	4937(8)	3278(5)	1517(4)	32(2)
C(8)	4*e*	4510(8)	4116(5)	2021(4)	29(2)

Table A.39: Anisotropic displacement parameters U_{ij} / Å^2 · 10^3 for the independent atoms in the structure of [Sr(en)$_4$](Te$_3$).

	U_{11}	U_{22}	U_{33}	U_{23}	U_{13}	U_{12}
Te(1)	38(1)	31(1)	27(1)	-3(1)	8(1)	-7(1)
Te(2)	28(1)	29(1)	24(1)	-2(1)	5(1)	-1(1)
Te(3)	27(1)	27(1)	29(1)	1(1)	6(1)	1(1)
Sr(1)	21(1)	25(1)	20(1)	0(1)	1(1)	0(1)
N(1)	33(3)	32(4)	28(4)	2(3)	5(3)	-3(3)
N(2)	30(3)	34(4)	28(4)	1(3)	4(3)	0(3)
N(3)	25(3)	41(4)	34(4)	0(3)	2(3)	-2(3)
N(4)	24(3)	34(4)	23(4)	-2(3)	-2(3)	2(3)
N(5)	23(3)	36(4)	26(4)	-3(3)	3(3)	4(3)
N(6)	29(3)	29(3)	26(4)	-10(3)	-2(3)	-2(3)
N(7)	27(3)	36(4)	25(4)	-8(3)	-2(3)	-3(3)
N(8)	33(3)	31(4)	20(3)	4(3)	2(3)	3(3)
C(1)	46(5)	28(5)	39(5)	-1(4)	4(4)	9(4)
C(2)	42(5)	29(4)	24(4)	6(3)	-1(3)	5(4)
C(3)	28(4)	22(4)	34(5)	-1(3)	5(3)	-9(3)
C(4)	34(4)	32(5)	31(5)	-3(4)	2(3)	-5(4)
C(5)	33(4)	37(5)	34(5)	0(4)	6(3)	-5(3)
C(6)	35(4)	25(4)	35(5)	1(3)	3(4)	-5(3)
C(7)	50(5)	23(4)	23(5)	7(3)	4(4)	-3(3)
C(8)	30(4)	28(4)	26(4)	3(3)	-7(3)	-4(3)

Table A.40: Selected bond lengths for [Sr(en)$_4$](Te$_3$).

Atoms 1, 2	Distance / Å	Atoms 1, 2	Distance / Å
Te(1)-Te(2)	2.7346(7)	N(2)-C(2)	1.493(9)
Te(2)-Te(3)	2.7377(7)	N(3)-C(3)	1.466(9)
Sr(1)-N(8)	2.687(5)	N(4)-C(4)	1.473(8)
Sr(1)-N(2)	2.697(6)	N(5)-C(5)	1.449(8)
Sr(1)-N(7)	2.721(5)	N(6)-C(6)	1.468(9)
Sr(1)-N(4)	2.721(5)	N(7)-C(7)	1.486(9)
Sr(1)-N(6)	2.724(5)	N(8)-C(8)	1.465(8)
Sr(1)-N(5)	2.730(5)	C(1)-C(2)	1.495(10)
Sr(1)-N(1)	2.760(6)	C(3)-C(4)	1.507(10)
Sr(1)-N(3)	2.766(5)	C(5)-C(6)	1.497(10)
Sr(1)-C(8)	3.337(7)	C(7)-C(8)	1.519(10)
N(1)-C(1)	1.477(9)		

Table A.41: Selected bond angles for [Sr(en)$_4$](Te$_3$).

Atoms 1, 2, 3	Angle / °	Atoms 1, 2, 3	Angle / °
Te(1)-Te(2)-Te(3)	110.52(2)	N(2)-C(2)-C(1)	110.9(6)
C(1)-N(1)-Sr(1)	111.0(4)	N(3)-C(3)-C(4)	110.7(6)
C(2)-N(2)-Sr(1)	112.4(4)	N(4)-C(4)-C(3)	109.8(6)
C(3)-N(3)-Sr(1)	111.0(4)	N(5)-C(5)-C(6)	111.6(6)
C(4)-N(4)-Sr(1)	116.8(4)	N(6)-C(6)-C(5)	112.1(6)
C(5)-N(5)-Sr(1)	109.9(4)	N(7)-C(7)-C(8)	110.2(6)
C(6)-N(6)-Sr(1)	111.3(4)	N(8)-C(8)-C(7)	111.1(6)
C(7)-N(7)-Sr(1)	114.4(4)	N(8)-C(8)-Sr(1)	51.7(3)
C(8)-N(8)-Sr(1)	103.0(4)	C(7)-C(8)-Sr(1)	87.3(4)
N(1)-C(1)-C(2)	110.9(6)		

A.1.9 [Eu(NH$_3$)$_9$]$_2$(Te$_4$)$_3$

Table A.42: Crystal data and structure refinement for [Eu(NH$_3$)$_9$]$_2$(Te$_4$)$_3$.

Empirical formula	Eu$_2$ H$_{54}$ N$_{18}$ Te$_{12}$
Formula weight / *g/mol*	2141.73
Temperature / *K*	123(3)
Crystal system; Space group	Triclinic; $P\bar{1}$
Lattice constants / Å	$a = 10.6034(3)$ $\alpha = 90.256(2)°$
	$b = 13.3138(2)$ $\beta = 104.4930(10)°$
	$c = 16.5630(5)$ $\gamma = 90.493(2)°$
Volume / Å^3	2263.68(10)
Z; F(000); calc. density / *g/cm^3*	2; 1860 ;3.142
Wavelength / Å	0.71073
Crystal size / *mm*	$0.086 \times 0.054 \times 0.016$
Theta range for data collection / °	2.957 to 27.550
Limiting indices	$-13 \leq h \leq 13$, $-17 \leq k \leq 16$, $-21 \leq l \leq 21$
Reflections collected / unique	36702 / 10341
Completeness to $\vartheta = 25.242$	99.6 %
R$_{int}$	11.89 %
Absorption coefficient / *mm^{-1}*	10.347
Refinement method	Full-matrix least-squares on F^2
Data / restrains / parameters	10341 / 0 / 309
R indices (all data) R_1 ; wR_2	0.1063; 0.1487
R indices [$I > 4\sigma(I)$] R_1 ; wR_2	0.0569; 0.1264 (for 6672 reflections)
Godness-of-fit for F^2	0.989
Largest diff. peak and hole / *e$^-$/A^3*	3.060 and -2.807

Table A.43: Fractional coordinates ($\cdot\ 10^4$) and equivalent isotropic displacement parameter U_{eq} ($\text{Å}^2 \cdot 10^3$) for the independent atoms in the structure of $[Eu(NH_3)_9]_2(Te_4)_3$.

	Wyck.	x	y	z	U_{eq}
Eu(1)	2*i*	2547(1)	10116(1)	2529(1)	20(1)
Eu(2)	2*i*	2373(1)	5029(1)	7451(1)	20(1)
N(1)	2*i*	2447(12)	8124(8)	2412(9)	34(3)
N(2)	2*i*	3125(12)	9396(9)	4017(8)	33(3)
N(3)	2*i*	4725(11)	9338(8)	2382(8)	28(3)
N(4)	2*i*	4453(12)	11173(10)	3511(8)	34(3)
N(5)	2*i*	3618(11)	11411(8)	1714(8)	26(3)
N(6)	2*i*	1597(12)	11348(9)	3455(8)	29(3)
N(7)	2*i*	799(10)	11321(9)	1639(8)	28(3)
N(8)	2*i*	346(10)	9396(8)	2649(8)	23(3)
N(9)	2*i*	1945(12)	9520(9)	988(8)	29(3)
N(10)	2*i*	482(14)	6070(12)	6488(10)	53(4)
N(11)	2*i*	1378(11)	6357(9)	8272(9)	33(3)
N(12)	2*i*	3335(12)	6300(8)	6602(8)	30(3)
N(13)	2*i*	4193(12)	6206(9)	8395(8)	33(3)
N(14)	2*i*	4566(11)	4304(8)	7366(8)	26(3)
N(15)	2*i*	2989(11)	4401(8)	8964(8)	26(3)
N(16)	2*i*	2331(13)	3040(9)	7426(9)	37(3)
N(17)	2*i*	1859(13)	4347(9)	5945(8)	35(3)
N(18)	2*i*	194(11)	4270(8)	7595(9)	30(3)
Te(1)	2*i*	6156(1)	2915(1)	9378(1)	28(1)
Te(2)	2*i*	8441(1)	3900(1)	9377(1)	29(1)
Te(3)	2*i*	7980(1)	5893(1)	8971(1)	27(1)
Te(4)	2*i*	7253(1)	6142(1)	7272(1)	25(1)
Te(5)	2*i*	6413(1)	8147(1)	4351(1)	41(1)
Te(6)	2*i*	5401(1)	6554(1)	5022(1)	47(1)
Te(7)	2*i*	2906(1)	6133(1)	4107(1)	41(1)
Te(8)	2*i*	1088(1)	7320(1)	4541(1)	37(1)
Te(9)	2*i*	2299(1)	8836(1)	7183(1)	31(1)
Te(10)	2*i*	2963(1)	9094(1)	8882(1)	30(1)
Te(11)	2*i*	3427(1)	11085(1)	9325(1)	30(1)

Te(12)	2*i*	1162(1)	12033(1)	9379(1)	27(1)

Table A.44: Anisotropic displacement parameters U_{ij} / Å^2 · 10^3 for the independent atoms in the structure of [Eu(NH$_3$)$_9$]$_2$(Te$_4$)$_3$.

	U_{11}	U_{22}	U_{33}	U_{23}	U_{13}	U_{12}
Eu(1)	19(1)	20(1)	24(1)	1(1)	9(1)	1(1)
Eu(2)	20(1)	22(1)	22(1)	2(1)	10(1)	2(1)
N(1)	33(7)	32(7)	40(9)	-1(6)	16(7)	-4(6)
N(2)	25(7)	35(7)	40(9)	0(6)	12(6)	1(5)
N(3)	30(7)	24(6)	35(8)	8(5)	17(6)	7(5)
N(4)	25(7)	52(8)	30(8)	-8(6)	13(6)	-10(6)
N(5)	28(7)	13(6)	39(8)	-2(5)	11(6)	-3(5)
N(6)	34(7)	36(7)	17(7)	-1(5)	7(6)	3(5)
N(7)	15(6)	35(7)	36(8)	9(6)	12(6)	8(5)
N(8)	16(6)	29(6)	23(7)	-6(5)	4(5)	3(5)
N(9)	34(7)	29(7)	29(8)	-2(5)	16(6)	-8(5)
N(10)	41(9)	85(12)	41(10)	21(9)	23(8)	23(8)
N(11)	18(6)	34(7)	47(9)	2(6)	11(6)	8(5)
N(12)	28(7)	26(7)	32(8)	8(5)	3(6)	6(5)
N(13)	33(7)	36(7)	28(8)	0(6)	7(6)	-4(5)
N(14)	22(6)	24(6)	33(8)	1(5)	9(6)	-3(5)
N(15)	24(6)	20(6)	34(8)	9(5)	6(6)	1(5)
N(16)	39(8)	35(7)	43(9)	-11(6)	21(7)	-4(6)
N(17)	44(8)	34(7)	24(8)	3(6)	6(6)	-11(6)
N(18)	27(7)	29(7)	35(8)	2(6)	12(6)	4(5)
Te(1)	30(1)	27(1)	30(1)	4(1)	13(1)	7(1)
Te(2)	25(1)	32(1)	32(1)	3(1)	9(1)	7(1)
Te(3)	26(1)	26(1)	29(1)	-5(1)	9(1)	-1(1)
Te(4)	25(1)	23(1)	31(1)	0(1)	12(1)	0(1)
Te(5)	41(1)	50(1)	30(1)	-5(1)	5(1)	17(1)

Te(6)	47(1)	64(1)	33(1)	12(1)	16(1)	26(1)
Te(7)	64(1)	29(1)	32(1)	0(1)	13(1)	1(1)
Te(8)	35(1)	41(1)	36(1)	9(1)	8(1)	-8(1)
Te(9)	24(1)	27(1)	44(1)	-3(1)	14(1)	0(1)
Te(10)	26(1)	27(1)	40(1)	6(1)	13(1)	5(1)
Te(11)	25(1)	34(1)	32(1)	-4(1)	11(1)	-5(1)
Te(12)	30(1)	25(1)	28(1)	-2(1)	13(1)	-4(1)

Table A.45: Selected bond lengths for $[Eu(NH_3)_9]_2(Te_4)_3$.

Atoms 1, 2	Distance / Å	Atoms 1, 2	Distance / Å
Eu(1)-N(8)	2.569(11)	Eu(2)-N(11)	2.612(12)
Eu(1)-N(2)	2.578(13)	Eu(2)-N(10)	2.637(14)
Eu(1)-N(9)	2.590(12)	Eu(2)-N(16)	2.649(12)
Eu(1)-N(3)	2.604(11)	Eu(2)-N(13)	2.653(12)
Eu(1)-N(6)	2.615(12)	Te(1)-Te(2)	2.7460(14)
Eu(1)-N(5)	2.615(11)	Te(2)-Te(3)	2.7574(13)
Eu(1)-N(7)	2.624(11)	Te(3)-Te(4)	2.7470(15)
Eu(1)-N(4)	2.644(12)	Te(5)-Te(6)	2.7317(18)
Eu(1)-N(1)	2.658(11)	Te(6)-Te(7)	2.7511(18)
Eu(2)-N(14)	2.561(11)	Te(7)-Te(8)	2.7324(16)
Eu(2)-N(12)	2.566(11)	Te(9)-Te(10)	2.7432(16)
Eu(2)-N(15)	2.573(12)	Te(10)-Te(11)	2.7548(14)
Eu(2)-N(17)	2.575(13)	Te(11)-Te(12)	2.7429(14)
Eu(2)-N(18)	2.581(11)		

Table A.46: Selected bond angles for $[Eu(NH_3)_9]_2(Te_4)_3$.

Atoms 1, 2, 3	Angle / °	Atoms 1, 2, 3	Angle / °
Te(1)-Te(2)-Te(3)	110.55(4)	Te(8)-Te(7)-Te(6)	112.77(5)
Te(4)-Te(3)-Te(2)	111.13(4)	Te(9)-Te(10)-Te(11)	111.70(5)
Te(5)-Te(6)-Te(7)	110.32(5)	Te(12)-Te(11)-Te(10)	110.98(4)

A.1.10 [Ba(NH$_3$)$_8$](Te$_4$)

Table A. 47: Crystal data and structure refinement for [Ba(NH$_3$)$_8$](Te$_4$).

Empirical formula	Ba$_2$ H$_{48}$ N$_{16}$ Te$_8$
Formula weight / *g/mol*	1568.02
Temperature / *K*	123(3)
Crystal system; Space group	Monoclinic; *P* 2$_1$/*c*
Lattice constants / Å	*a* = 11.3006(4)
	b = 25.5827(10) *β* = 90.023(2)°
	c = 13.5640(5)
Volume / Å^3	3921.4(3)
Z; F(000); calc. density / *g/cm^3*	4; 2752; 2.656
Wavelength / Å	0.71073
Crystal size / *mm*	0.296 × 0.134 × 0.024
Theta range for data collection / °	2.993 to 27.619
Limiting indices	-14 ≤ *h* ≤ 14, -33 ≤ *k* ≤ 33, -17 ≤ *l* ≤ 17
Reflections collected / unique	16341 / 8727
Completeness to ϑ = 25.242	96.4 %
R$_{int}$	5.77 %
Absorption coefficient / *mm^{-1}*	7.847
Refinement method	Full-matrix least-squares on F^2
Data / restrains / parameters	8727 / 0 / 253
R indices (all data) R_1 ; wR_2	0.1063; 0.1963
R indices [$I > 4\sigma(I)$] R_1 ; wR_2	0.0678; 0.1743 (for 6053 reflections)
Godness-of-fit for F^2	1.027
Largest diff. peak and hole / *e$^-$/A^3*	4.902 and -1.678

Table A. 48: Fractional coordinates ($\cdot\ 10^4$) and equivalent isotropic displacement parameter U_{eq} ($\text{Å}^2 \cdot 10^3$) for the independent atoms in the structure of $[Ba(NH_3)_8](Te_4)$.

	Wyck.	*x*	*y*	*z*	U_{eq}
Ba(1)	4*e*	7479(1)	6281(1)	5164(1)	28(1)
N(1)	4*e*	7532(18)	6812(6)	7058(13)	42(4)
N(2)	4*e*	9122(17)	5488(7)	5953(14)	44(5)
N(3)	4*e*	9864(16)	6754(7)	5207(17)	49(5)
N(4)	4*e*	8764(15)	5781(7)	3579(14)	38(4)
N(5)	4*e*	7457(17)	7198(6)	4014(12)	39(4)
N(6)	4*e*	5828(14)	5780(7)	3833(14)	34(4)
N(7)	4*e*	5151(15)	6788(8)	5352(14)	40(5)
N(8)	4*e*	6062(15)	5511(7)	6199(14)	37(4)
Ba(2)	4*e*	2479(1)	8759(1)	4270(1)	27(1)
N(9)	4*e*	2489(18)	8248(6)	2358(12)	39(4)
N(10)	4*e*	2535(13)	7826(5)	5389(11)	26(3)
N(11)	4*e*	124(18)	8239(7)	4069(14)	44(5)
N(12)	4*e*	813(16)	9278(7)	5616(16)	45(5)
N(13)	4*e*	1081(16)	9518(8)	3130(15)	48(5)
N(14)	4*e*	3788(16)	9232(7)	5884(14)	40(5)
N(15)	4*e*	4094(13)	9501(7)	3305(16)	43(5)
N(16)	4*e*	4871(15)	8268(7)	4263(13)	37(5)
Te(1)	4*e*	2621(1)	5650(1)	5499(1)	29(1)
Te(2)	4*e*	2240(1)	5852(1)	3552(1)	32(1)
Te(3)	4*e*	2567(1)	6894(1)	3225(1)	30(1)
Te(4)	4*e*	4802(1)	6989(1)	2447(1)	28(1)
Te(5)	4*e*	7642(1)	5646(1)	-1149(1)	34(1)
Te(6)	4*e*	7295(1)	5812(1)	809(1)	36(1)
Te(7)	4*e*	7568(1)	6853(1)	1211(1)	33(1)
Te(8)	4*e*	9805(1)	6969(1)	1989(1)	28(1)

Table A.49: Anisotropic displacement parameters U_{ij} / Å^2 · 10^3 for the independent atoms in the structure of [Ba(NH$_3$)$_8$](Te$_4$).

	U_{11}	U_{22}	U_{33}	U_{23}	U_{13}	U_{12}
Ba(1)	21(1)	31(1)	30(1)	0(1)	-2(1)	-2(1)
N(1)	45(11)	35(9)	45(11)	0(8)	-11(10)	0(9)
N(2)	53(13)	45(11)	34(11)	-3(9)	-14(9)	4(10)
N(3)	26(10)	39(10)	82(16)	-11(10)	-11(10)	9(8)
N(4)	29(10)	46(11)	39(11)	-8(9)	-3(8)	0(8)
N(5)	39(11)	50(10)	27(9)	6(7)	-3(8)	17(10)
N(6)	16(8)	40(10)	46(11)	-4(8)	-4(7)	4(7)
N(7)	18(9)	58(12)	43(11)	-14(9)	-3(8)	10(8)
N(8)	32(10)	44(11)	35(11)	8(8)	7(8)	12(8)
Ba(2)	22(1)	32(1)	28(1)	0(1)	-4(1)	1(1)
N(9)	50(12)	36(8)	31(10)	-1(7)	1(10)	0(9)
N(10)	19(8)	29(7)	29(9)	5(6)	-16(7)	-9(7)
N(11)	61(13)	41(10)	30(10)	3(8)	-20(10)	3(10)
N(12)	28(10)	43(11)	63(14)	-18(10)	-4(9)	-12(8)
N(13)	36(11)	58(13)	48(13)	17(10)	-12(9)	5(10)
N(14)	43(11)	33(10)	44(12)	-1(8)	-19(9)	-5(8)
N(15)	7(8)	43(11)	80(16)	7(10)	11(8)	1(7)
N(16)	29(10)	49(11)	33(10)	-28(8)	-4(8)	25(8)
Te(1)	28(1)	30(1)	28(1)	1(1)	-1(1)	-2(1)
Te(2)	32(1)	35(1)	29(1)	2(1)	-2(1)	-9(1)
Te(3)	26(1)	33(1)	30(1)	5(1)	-1(1)	1(1)
Te(4)	25(1)	33(1)	26(1)	2(1)	-3(1)	-5(1)
Te(5)	29(1)	33(1)	40(1)	-1(1)	-2(1)	-1(1)
Te(6)	33(1)	41(1)	35(1)	8(1)	-5(1)	-8(1)
Te(7)	26(1)	46(1)	28(1)	-5(1)	-5(1)	4(1)
Te(8)	23(1)	34(1)	27(1)	1(1)	3(1)	-3(1)

Table A.50: Selected bond lengths for [Ba(NH$_3$)$_8$](Te$_4$).

Atoms 1, 2	Distance / Å	Atoms 1, 2	Distance / Å
Ba(1)-N(5)	2.816(16)	Ba(2)-N(12)	2.940(19)
Ba(1)-N(4)	2.893(18)	Ba(2)-N(15)	2.940(17)
Ba(1)-N(6)	2.895(16)	Ba(2)-N(13)	2.941(17)
Ba(1)-N(8)	2.901(18)	Ba(2)-N(16)	2.981(15)
Ba(1)-N(1)	2.906(17)	Ba(2)-N(11)	2.99(2)
Ba(1)-N(7)	2.944(16)	Te(1)-Te(2)	2.7260(19)
Ba(1)-N(2)	2.951(18)	Te(2)-Te(3)	2.7279(17)
Ba(1)-N(3)	2.956(18)	Te(3)-Te(4)	2.7490(19)
Ba(2)-N(10)	2.829(13)	Te(5)-Te(6)	2.718(2)
Ba(2)-N(9)	2.904(16)	Te(6)-Te(7)	2.7347(19)
Ba(2)-N(14)	2.906(17)	Te(7)-Te(8)	2.7552(19)

Table A.51: Selected bond angles for [Ba(NH$_3$)$_8$](Te$_4$).

Atoms 1, 2, 3	Angle / °	Atoms 1, 2, 3	Angle / °
Te(1)-Te(2)-Te(3)	108.75(6)	Te(5)-Te(6)-Te(7)	109.30(6)
Te(2)-Te(3)-Te(4)	105.84(6)	Te(6)-Te(7)-Te(8)	106.54(6)

A.1.11 [Ca(en)₄](Te₄)·0.5en

Table A.52: Crystal data and structure refinement for [Ca(en)₄](Te₄)·0.5en.

Empirical formula	$C_9 H_{32} Ca N_9 Te_4$
Formula weight / *g/mol*	816.91
Temperature / *K*	123(3)
Crystal system; Space group	Orthorhombic; *Pbca*
Lattice constants / *Å*	$a = 16.7867(4)$
	$b = 17.0564(7)$
	$c = 17.1660(7)$
Volume / *Å³*	4915.0(3)
Z; F(000); calc. density / *g/cm³*	8; 3016;2.208
Wavelength / *Å*	0.71073
Crystal size / *mm*	$0.066 \times 0.054 \times 0.030$
Theta range for data collection / °	2.921 to 27.435
Limiting indices	$-21 \leq h \leq 21, -22 \leq k \leq 22, -22 \leq l \leq 22$
Reflections collected / unique	10437 / 5568
Completeness to $\vartheta = 25.242$	99.6 %
R_{int}	7.21 %
Absorption coefficient / *mm⁻¹*	4.920
Refinement method	Full-matrix least-squares on F^2
Data / restrains / parameters	5568 / 0 / 223
R indices (all data) R_1 ; wR_2	0.1153; 0.0976
R indices [$I > 4\sigma(I)$] R_1 ; wR_2	0.0438; 0.0803 (for 3094 reflections)
Godness-of-fit for F^2	0.966
Largest diff. peak and hole / e^- /A^3	1.557 and -1.268

Table A.53: Fractional coordinates ($\cdot\ 10^4$) and equivalent isotropic displacement parameter U_{eq} ($\text{Å}^2 \cdot 10^3$) for the independent atoms in the structure of [Ca(en)$_4$](Te$_4$)·0.5en.

	Wyck.	*x*	*y*	*z*	U_{eq}
Te(1)	8*c*	8187(1)	5758(1)	5664(1)	33(1)
Te(2)	8*c*	8574(1)	7280(1)	5116(1)	34(1)
Te(3)	8*c*	8360(1)	8245(1)	6387(1)	43(1)
Te(4)	8*c*	6928(1)	8996(1)	6422(1)	35(1)
Ca(1)	8*c*	6324(1)	6381(1)	8310(1)	21(1)
N(1)	8*c*	5480(4)	5328(4)	9067(4)	36(2)
N(2A)	8*c*	6290(30)	5090(20)	7660(20)	28(4)
C(2A)	8*c*	6072(16)	4427(14)	8180(13)	46(8)
N(2B)	8*c*	6052(15)	5117(15)	7491(13)	28(4)
C(2B)	8*c*	5377(9)	4663(7)	7815(7)	31(4)
N(3)	8*c*	7348(4)	5864(4)	9255(4)	33(1)
N(5)	8*c*	4897(4)	6809(4)	7963(4)	37(2)
N(6)	8*c*	6200(4)	6875(4)	6872(3)	33(2)
N(7)	8*c*	6824(4)	7807(4)	8454(4)	37(2)
N(8)	8*c*	5873(4)	7045(4)	9599(4)	34(2)
C(1)	8*c*	5434(6)	4581(5)	8641(5)	49(3)
C(3)	8*c*	8007(6)	5513(8)	8831(7)	75(4)
N(4A)	8*c*	7780(6)	6344(7)	7706(6)	33(1)
C(4A)	8*c*	8369(7)	5995(9)	8237(7)	45(4)
N(4B)	8*c*	7590(17)	6001(17)	7677(16)	33(1)
C(4B)	8*c*	8040(20)	5430(20)	8163(19)	45(4)
C(5)	8*c*	4932(7)	7321(8)	7268(6)	89(5)
C(6)	8*c*	5400(5)	7074(6)	6657(5)	51(3)
C(7)	8*c*	6259(5)	8266(5)	8929(5)	41(2)
C(8)	8*c*	6137(5)	7867(5)	9704(5)	39(2)
N(9)	8*c*	5855(4)	5248(4)	5695(4)	41(2)
C(9)	8*c*	5029(5)	5189(5)	5408(5)	39(2)

Table A.54: Anisotropic displacement parameters U_{ij} / Å^2 · 10^3 for the independent atoms in the structure of [Ca(en)$_4$](Te$_4$)·0.5en.

	U_{11}	U_{22}	U_{33}	U_{23}	U_{13}	U_{12}
Te(1)	29(1)	35(1)	33(1)	-11(1)	-1(1)	1(1)
Te(2)	31(1)	33(1)	38(1)	3(1)	-2(1)	3(1)
Te(3)	44(1)	32(1)	52(1)	-9(1)	-19(1)	6(1)
Te(4)	41(1)	32(1)	32(1)	1(1)	2(1)	1(1)
Ca(1)	24(1)	25(1)	16(1)	0(1)	1(1)	6(1)
N(1)	29(4)	49(5)	29(4)	-2(3)	-1(3)	-4(3)
N(2A)	43(15)	34(5)	7(9)	-3(6)	-12(6)	5(9)
C(2A)	60(20)	45(16)	35(14)	-11(11)	14(13)	-20(13)
N(2B)	43(15)	34(5)	7(9)	-3(6)	-12(6)	5(9)
C(2B)	37(10)	17(7)	38(9)	-4(6)	1(7)	-9(6)
N(3)	31(3)	38(4)	29(3)	8(3)	3(2)	0(3)
N(5)	38(5)	50(5)	24(4)	6(3)	5(3)	15(4)
N(6)	32(4)	44(5)	23(4)	-8(3)	-2(3)	5(3)
N(7)	44(5)	44(5)	24(4)	-1(3)	14(3)	-15(4)
N(8)	30(4)	38(4)	34(4)	2(3)	2(3)	4(3)
C(1)	60(7)	44(6)	43(6)	1(5)	-6(5)	-23(5)
C(3)	38(7)	112(10)	75(8)	51(7)	17(6)	32(6)
N(4A)	31(3)	38(4)	29(3)	8(3)	3(2)	0(3)
C(4A)	21(8)	73(11)	41(7)	13(7)	11(5)	2(6)
N(4B)	31(3)	38(4)	29(3)	8(3)	3(2)	0(3)
C(4B)	21(8)	73(11)	41(7)	13(7)	11(5)	2(6)
C(5)	69(8)	143(12)	55(7)	28(8)	13(6)	66(8)
C(6)	37(6)	80(8)	35(5)	30(5)	0(4)	-8(5)
C(7)	43(6)	27(5)	52(6)	-6(4)	0(4)	-2(4)
C(8)	37(5)	50(6)	31(5)	-11(4)	3(4)	0(4)
N(9)	39(5)	56(5)	28(4)	-7(4)	-10(3)	4(4)
C(9)	33(5)	52(6)	32(5)	-7(4)	-9(4)	2(4)

Table A.55: Selected bond lengths for [Ca(en)$_4$](Te$_4$)·0.5en. Symmetry transformations used to generate equivalent atoms: #1 -x+1, -y+1, -z+1.

Atoms 1, 2	Distance / Å	Atoms 1, 2	Distance / Å
Te(1)-Te(2)	2.8374(8)	N(2B)-C(2B)	1.48(3)
Te(2)-Te(3)	2.7565(8)	C(2B)-C(1)	1.428(15)
Te(3)-Te(4)	2.7249(8)	N(3)-C(3)	1.453(11)
Ca(1)-N(2A)	2.46(4)	N(5)-C(5)	1.479(12)
Ca(1)-N(4B)	2.47(3)	N(6)-C(6)	1.434(11)
Ca(1)-N(3)	2.523(6)	N(7)-C(7)	1.476(10)
Ca(1)-N(5)	2.574(7)	N(8)-C(8)	1.482(10)
Ca(1)-N(7)	2.583(7)	C(3)-C(4B)	1.16(3)
Ca(1)-N(8)	2.599(7)	C(3)-C(4A)	1.444(15)
Ca(1)-N(2B)	2.61(2)	N(4A)-C(4A)	1.471(15)
Ca(1)-N(6)	2.616(6)	N(4B)-C(4B)	1.49(4)
Ca(1)-N(1)	2.632(7)	C(5)-C(6)	1.376(12)
Ca(1)-N(4A)	2.654(11)	C(7)-C(8)	1.508(12)
N(1)-C(1)	1.471(11)	N(9)-C(9)	1.475(10)
N(2A)-C(2A)	1.49(5)	C(9)-C(9)#1	1.547(15)
C(2A)-C(1)	1.36(2)		

Table A.56: Selected bond angles for [Ca(en)$_4$](Te$_4$)·0.5en. Symmetry transformations used to generate equivalent atoms: #1 -x+1, -y+1, -z+1.

Atoms 1, 2, 3	Angle / °	Atoms 1, 2, 3	Angle / °
Te(3)-Te(2)-Te(1)	104.71(2)	C(2B)-C(1)-N(1)	114.4(9)
Te(4)-Te(3)-Te(2)	114.39(3)	C(4B)-C(3)-N(3)	125.4(19)
C(1)-N(1)-Ca(1)	112.0(5)	C(4A)-C(3)-N(3)	116.1(10)
C(2A)-N(2A)-Ca(1)	115(2)	C(4A)-N(4A)-Ca(1)	112.8(7)
C(1)-C(2A)-N(2A)	113(3)	C(3)-C(4A)-N(4A)	112.6(10)
C(2B)-N(2B)-Ca(1)	111.3(15)	C(4B)-N(4B)-Ca(1)	111.0(19)
C(1)-C(2B)-N(2B)	111.9(11)	C(3)-C(4B)-N(4B)	117(3)
C(3)-N(3)-Ca(1)	109.9(5)	C(6)-C(5)-N(5)	117.2(9)
C(5)-N(5)-Ca(1)	108.5(6)	C(5)-C(6)-N(6)	114.2(8)
C(6)-N(6)-Ca(1)	113.2(5)	N(7)-C(7)-C(8)	109.6(7)

C(7)-N(7)-Ca(1)	110.1(5)	N(8)-C(8)-C(7)	111.2(7)
C(8)-N(8)-Ca(1)	115.4(5)	N(9)-C(9)-C(9)#1	112.9(9)
C(2A)-C(1)-N(1)	114.6(12)		

A.1.12 [Yb(NH₃)₈]₄(Te₂₀)(Te₃)₂·4NH₃

Table A.57: Crystal data and structure refinement for [Yb(NH₃)₈]₄(Te₂₀)(Te₃)₂·4NH₃.

Empirical formula	$Yb_2 Te_{13} N_{18} H_{54}$
Formula weight / *g/mol*	2311.49
Temperature / *K*	123
Crystal system; Space group	Monoclinic ; $P\,2_1/c$
Lattice constants / *Å*	$a = 14.8371(4)$
	$b = 20.2111(6)$; $\beta = 87.547(2)$
	$c = 14.6159(4)$
Volume / *Å³*	4378.9(2)
Z; F(000); calc. density / *g/cm³*	6 ; 5.259
Wavelength / *Å*	0.71073
Crystal size / *mm*	$0.075 \times 0.043 \times 0.014$
Theta range for data collection / °	2.927 to 27.441
Limiting indices	$-19 \le h \le 19$; $-26 \le k \le 26$; $-18 \le l \le 18$
Reflections collected / unique	58471 / 9833
Completeness to $\vartheta = 25.242$	99.3 %
R_{int}	11.40 %
Absorption coefficient / *mm⁻¹*	19.137
Refinement method	Full-matrix least-squares on F^2
Data / restrains / parameters	9833 / 0 / 315
R indices (all data) R_1 ; wR_2	0.0696 ; 0.1230
R indices [$I > 4\sigma(I)$] R_1 ; wR_2	0.0475 ; 0.1121 (for 7425 reflections)
Godness-of-fit for F^2	1.005
Largest diff. peak and hole / e^-/A^3	2.167 and -4.314

Table A.58: Fractional coordinates ($\cdot 10^4$) and equivalent isotropic displacement parameter U_{eq} ($\text{Å}^2 \cdot 10^3$) for the independent atoms in the structure of [Yb(NH$_3$)$_8$]$_4$(Te$_{20}$)(Te$_3$)$_2$·4NH$_3$.

	Wyck.	*x*	*y*	*z*	U_{eq}
Yb(1)	4e	559(1)	6749(1)	7692(1)	17(1)
N(9)	4e	1594(6)	5816(4)	7605(6)	22(2)
N(10)	4e	197(6)	6088(4)	6355(6)	24(2)
N(11)	4e	775(6)	7417(4)	6314(6)	24(2)
N(12)	4e	-1029(6)	7041(5)	7506(6)	25(2)
N(13)	4e	289(6)	7889(4)	8274(7)	30(2)
N(14)	4e	832(5)	6747(4)	9320(6)	23(2)
N(15)	4e	2092(5)	7207(4)	7730(7)	25(2)
N(16)	4e	-308(6)	5827(4)	8425(6)	23(2)
Yb(2)	4e	5502(1)	8759(1)	7859(1)	17(1)
N(1)	4e	5531(6)	8154(4)	6400(7)	26(2)
N(2)	4e	6910(5)	8108(4)	7729(6)	24(2)
N(3)	4e	6486(6)	9515(4)	6948(7)	27(2)
N(4)	4e	6480(6)	9325(4)	8964(7)	27(2)
N(5)	4e	4554(5)	9479(4)	8835(7)	25(2)
N(6)	4e	5464(6)	8002(5)	9180(6)	28(2)
N(7)	4e	4551(6)	9418(4)	6854(7)	28(2)
N(8)	4e	4093(6)	8122(4)	7846(7)	24(2)
Te(1)	4e	1688(1)	1847(1)	10074(1)	24(1)
Te(2)	4e	2144(1)	3167(1)	10081(1)	27(1)
Te(3)	4e	1072(1)	3772(1)	8858(1)	29(1)
Te(4)	4e	6247(1)	1218(1)	8816(1)	21(1)
Te(5)	4e	4947(1)	1300(1)	7427(1)	22(1)
Te(6)	4e	3412(1)	1509(1)	8603(1)	22(1)
Te(7)	4e	2506(1)	380(1)	7837(1)	20(1)
Te(8)	4e	1670(1)	-7(1)	9467(1)	24(1)
Te(9)	4e	2263(1)	-1314(1)	9650(1)	21(1)
Te(10)	4e	3319(1)	-2292(1)	5333(1)	22(1)
Te(11)	4e	3321(1)	-1060(1)	4465(1)	22(1)
Te(12)	4e	1934(1)	-304(1)	5338(1)	24(1)
Te(13)	4e	1789(1)	-908(1)	6999(1)	27(1)

N(17)	4e	523(7)	4557(5)	6747(7)	31(2)	
N(18)	4e	5829(6)	9330(4)	4907(6)	26(2)	

Table A.59: Anisotropic displacement parameters U_{ij} / Å^2 · 10^3 for the independent atoms in the structure of [Yb(NH$_3$)$_8$]$_4$(Te$_{20}$)(Te$_3$)$_2$·4NH$_3$.

	U_{11}	U_{22}	U_{33}	U_{23}	U_{13}	U_{12}
Yb(1)	11(1)	22(1)	18(1)	0(1)	-1(1)	0(1)
N(9)	17(4)	29(5)	19(5)	-8(4)	3(3)	-4(4)
N(10)	20(5)	28(5)	25(5)	-4(4)	4(4)	-5(4)
N(11)	22(5)	28(5)	21(5)	-1(4)	-5(4)	0(4)
N(12)	19(5)	38(5)	18(5)	4(4)	-1(4)	2(4)
N(13)	20(5)	30(5)	41(6)	-5(4)	-6(4)	-3(4)
N(14)	13(4)	30(5)	25(5)	0(4)	-2(4)	0(3)
N(15)	15(4)	29(5)	31(6)	-2(4)	3(4)	2(3)
N(16)	16(4)	24(4)	28(6)	-4(4)	-5(4)	-3(3)
Yb(2)	12(1)	22(1)	19(1)	1(1)	-2(1)	0(1)
N(1)	16(4)	32(5)	30(6)	-8(4)	-3(4)	1(4)
N(2)	15(4)	33(5)	25(5)	-5(4)	-2(4)	5(3)
N(3)	27(5)	24(4)	29(6)	3(4)	-7(4)	0(4)
N(4)	25(5)	31(5)	24(5)	-6(4)	-3(4)	-5(4)
N(5)	11(4)	32(5)	30(6)	-3(4)	3(4)	4(3)
N(6)	17(5)	43(5)	24(6)	5(4)	-5(4)	-3(4)
N(7)	25(5)	33(5)	26(6)	4(4)	-7(4)	-2(4)
N(8)	17(4)	26(5)	29(6)	0(4)	3(4)	-1(3)
Te(1)	17(1)	35(1)	22(1)	1(1)	-2(1)	-1(1)
Te(2)	18(1)	36(1)	27(1)	-3(1)	-1(1)	-4(1)
Te(3)	24(1)	32(1)	32(1)	-3(1)	-5(1)	0(1)
Te(4)	17(1)	23(1)	23(1)	0(1)	2(1)	-1(1)
Te(5)	19(1)	29(1)	19(1)	0(1)	0(1)	-3(1)

Te(6)	18(1)	25(1)	23(1)	0(1)	-3(1)	-2(1)
Te(7)	15(1)	24(1)	22(1)	0(1)	-2(1)	1(1)
Te(8)	20(1)	28(1)	24(1)	1(1)	0(1)	3(1)
Te(9)	14(1)	28(1)	22(1)	0(1)	-1(1)	-2(1)
Te(10)	14(1)	29(1)	23(1)	-3(1)	0(1)	-1(1)
Te(11)	17(1)	26(1)	23(1)	0(1)	-1(1)	-1(1)
Te(12)	20(1)	27(1)	26(1)	-3(1)	-1(1)	2(1)
Te(13)	28(1)	27(1)	27(1)	-4(1)	6(1)	-7(1)
N(17)	34(5)	33(5)	25(6)	4(4)	-4(4)	-6(4)
N(18)	29(5)	30(5)	19(5)	1(4)	-2(4)	-2(4)

Table A.60: Selected bond lengths for $[Yb(NH_3)_8]_4(Te_{20})(Te_3)_2 \cdot 4NH_3$. Symmetry transformations used to generate equivalent atoms: #1 -x+1, -y, -z+2.

Atoms 1, 2	Distance / Å	Atoms 1, 2	Distance / Å
Yb(1)-N(9)	2.430(8)	Yb(2)-N(4)	2.494(9)
Yb(1)-N(14)	2.430(9)	Te(1)-Te(2)	2.7526(10)
Yb(1)-N(11)	2.434(9)	Te(2)-Te(3)	2.7318(11)
Yb(1)-N(10)	2.445(9)	Te(4)-Te(5)	2.8634(10)
Yb(1)-N(12)	2.456(9)	Te(4)-Te(9)#1	3.2226(10)
Yb(1)-N(15)	2.458(8)	Te(5)-Te(6)	2.8267(10)
Yb(1)-N(16)	2.480(8)	Te(6)-Te(7)	2.8973(9)
Yb(1)-N(13)	2.484(9)	Te(7)-Te(8)	2.7512(10)
Yb(2)-N(5)	2.440(8)	Te(7)-Te(13)	3.0849(10)
Yb(2)-N(8)	2.457(8)	Te(8)-Te(9)	2.8012(9)
Yb(2)-N(1)	2.458(9)	Te(9)-Te(4)#1	3.2226(10)
Yb(2)-N(6)	2.462(9)	Te(10)-Te(11)	2.7949(10)
Yb(2)-N(3)	2.464(9)	Te(11)-Te(12)	2.8245(9)
Yb(2)-N(7)	2.470(9)	Te(12)-Te(13)	2.7180(11)
Yb(2)-N(2)	2.470(8)		

Table A.61: Selected bond angles for $[Yb(NH_3)_8]_4(Te_{20})(Te_3)_2\cdot4NH_3$. Symmetry transformations used to generate equivalent atoms: #1 $-x+1$, $-y$, $-z+2$.

Atoms 1, 2, 3	Angle / °	Atoms 1, 2, 3	Angle / °
Te(3)-Te(2)-Te(1)	106.33(3)	Te(6)-Te(7)-Te(13)	172.48(3)
Te(5)-Te(4)-Te(9)#1	173.20(3)	Te(7)-Te(8)-Te(9)	102.63(3)
Te(6)-Te(5)-Te(4)	97.29(3)	Te(8)-Te(9)-Te(4)#1	103.76(3)
Te(5)-Te(6)-Te(7)	91.25(3)	Te(10)-Te(11)-Te(12)	106.87(3)
Te(8)-Te(7)-Te(6)	95.09(3)	Te(13)-Te(12)-Te(11)	100.87(3)
Te(8)-Te(7)-Te(13)	87.34(3)	Te(12)-Te(13)-Te(7)	87.74(3)

A.1.13 [Eu(en)$_4$]Te$_6$

Table A.62: Crystal data and structure refinement for [Eu(en)$_4$]Te$_6$.

Empirical formula	C$_8$ H$_{32}$ Eu N$_8$ Te$_6$
Formula weight / *g/mol*	1157.97
Temperature / *K*	123(3)
Crystal system; Space group	Monoclinic; *C*2/*c*
Lattice constants / Å	*a* = 11.4252(3)
	b = 28.7635(9); *β* = 127.350(1)°
	c = 9.5547(3)
Volume / Å^3	2496.08(13)
Z; F(000); calc. density / *g/cm^3*	4; 2044 ;3.081
Wavelength / Å	0.71073
Crystal size / *mm*	0.176 × 0.086 × 0.024
Theta range for data collection / °	3.033 to 29.938
Limiting indices	-16 ≤ *h* ≤ 15, -40 ≤ *k* ≤ 40, -13 ≤ *l* ≤ 13
Reflections collected / unique	13988 / 3543
Completeness to ϑ = 25.242	98.6 %
R$_{int}$	9.70 %
Absorption coefficient / *mm^{-1}*	9.395
Refinement method	Full-matrix least-squares on F^2
Data / restrains / parameters	3543 / 0 / 107
R indices (all data) R_1 ; wR_2	0.1101; 0.2965
R indices [*I* > 4σ(*I*)] R_1 ; wR_2	0.0962; 0.2858 (for 2952 reflections)
Godness-of-fit for F^2	1.093
Largest diff. peak and hole / *e$^-$/A^3*	6.233 and -8.871

Table A.63: Fractional coordinates ($\cdot\ 10^4$) and equivalent isotropic displacement parameter U_{eq} ($\text{Å}^2 \cdot 10^3$) for the independent atoms in the structure of [Eu(en)$_4$]Te$_6$.

	Wyck.	*x*	*y*	*z*	U_{eq}
Eu(1)	4*e*	5000	3740(1)	2500	19(1)
Te(1)	4*e*	5000	4230(1)	7500	23(1)
Te(2)	8*f*	1661(1)	4238(1)	5398(2)	22(1)
Te(3)	8*f*	565(2)	3366(1)	4598(4)	57(1)
Te(4)	4*e*	0	3200(1)	7500	53(1)
N(2)	8*f*	6020(20)	3410(6)	5490(30)	28(4)
N(4)	8*f*	6980(20)	4073(7)	2370(20)	27(4)
N(3)	8*f*	6360(20)	4428(7)	4610(20)	28(4)
N(1)	8*f*	3510(20)	3030(6)	2310(20)	29(4)
C(4)	8*f*	7560(20)	4525(7)	3280(30)	25(4)
C(3)	8*f*	7800(20)	4509(7)	5020(30)	25(4)
C(2)	8*f*	5410(30)	2961(7)	5460(30)	31(5)
C(1)	8*f*	3760(30)	2964(9)	3970(30)	37(5)

Table A.64: Anisotropic displacement parameters U_{ij} / $\text{Å}^2 \cdot 10^3$ for the independent atoms in the structure of [Eu(en)$_4$]Te$_6$.

	U_{11}	U_{22}	U_{33}	U_{23}	U_{13}	U_{12}
Eu(1)	26(1)	16(1)	15(1)	0	12(1)	0
Te(1)	32(1)	22(1)	19(1)	0	18(1)	0
Te(2)	21(1)	24(1)	21(1)	1(1)	12(1)	-1(1)
Te(3)	32(1)	24(1)	114(2)	-18(1)	44(1)	-9(1)
Te(4)	49(2)	21(1)	28(1)	0	-8(1)	0
N(2)	37(10)	17(7)	34(9)	-8(7)	23(8)	-1(7)
N(4)	29(9)	34(9)	13(7)	2(6)	10(7)	5(7)
N(3)	40(10)	34(9)	19(7)	-4(7)	23(8)	-1(8)
N(1)	33(9)	17(7)	26(8)	-4(6)	13(8)	-2(7)
C(4)	29(10)	17(8)	33(10)	-1(7)	21(9)	1(7)
C(3)	24(9)	18(8)	23(9)	0(7)	9(8)	-6(7)
C(2)	38(12)	23(9)	14(8)	9(7)	6(8)	0(8)
C(1)	37(13)	36(12)	36(12)	7(10)	21(11)	-7(10)

Table A.65: Selected bond lengths for [Eu(en)$_4$]Te$_6$. Symmetry transformations used to generate equivalent atoms: #1 -x+1, y, -z+$^1/_2$ #2 -x+1, y, -z+$^3/_2$.

Atoms 1, 2	Distance / Å	Atoms 1, 2	Distance / Å
Eu(1)-N(4)	2.52(2)	Te(1)-Te(2)	3.0483(13)
Eu(1)-N(4)#1	2.52(2)	Te(2)-Te(3)	2.696(2)
Eu(1)-N(2)#1	2.527(19)	N(2)-C(2)	1.46(3)
Eu(1)-N(2)	2.527(19)	N(4)-C(4)	1.48(3)
Eu(1)-N(3)#1	2.569(18)	N(3)-C(3)	1.46(3)
Eu(1)-N(3)	2.569(18)	N(1)-C(1)	1.45(3)
Eu(1)-N(1)	2.590(19)	C(4)-C(3)	1.52(3)
Eu(1)-N(1)#1	2.590(19)	C(2)-C(1)	1.53(3)
Te(1)-Te(2)#2	3.0483(13)		

Table A.66: Selected bond angles for [Eu(en)$_4$]Te$_6$. Symmetry transformations used to generate equivalent atoms: #1 -x+1, y, -z+$^1/_2$ #2 -x+1, y, -z+$^3/_2$.

Atoms 1, 2, 3	Angle / °	Atoms 1, 2, 3	Angle / °
Te(2)#2-Te(1)-Te(2)	179.16(8)	C(1)-N(1)-Eu(1)	110.1(13)
Te(3)-Te(2)-Te(1)	111.11(7)	N(4)-C(4)-C(3)	109.5(16)
C(2)-N(2)-Eu(1)	114.9(13)	N(3)-C(3)-C(4)	106.9(16)
C(4)-N(4)-Eu(1)	113.7(13)	N(2)-C(2)-C(1)	108.5(17)
C(3)-N(3)-Eu(1)	112.2(12)	N(1)-C(1)-C(2)	109(2)

A.1.14 [Ca(en)₄]₂(As₄Te₆)

Table A.67: Crystal data and structure refinement for [Ca(en)₄]₂(As₄Te₆).

Empirical formula	$C_8 H_{32} As_2 Ca N_8 Te_3$
Formula weight / *g/mol*	813.13
Temperature / *K*	123(2)
Crystal system; Space group	Orthorhombic; *Pbca*
	a = 17.1043(5)
Lattice constants / *Å*	b = 16.4652(6)
	c = 17.3352(5)
Volume / *Å³*	4882.0(3)
Z; F(000); calc. density / *g/cm³*	8; 3024 ; 2.213
Wavelength / *Å*	0.71073
Crystal size / *mm*	$0.070 \times 0.056 \times 0.052$
Theta range for data collection / °	2.930 to 27.510
Limiting indices	$-22 \leq h \leq 22, -21 \leq k \leq 21, -22 \leq l \leq 22$
Reflections collected / unique	10566 / 5590
Completeness to $\vartheta = 25.242$	99.7 %
R_{int}	8.93 %
Absorption coefficient / *mm⁻¹*	6.469
Refinement method	Full-matrix least-squares on F^2
Data / restrains / parameters	5590 / 0 / 200
R indices (all data) R_1 ; wR_2	0.1207; 0.0817
R indices [$I > 4\sigma(I)$] R_1 ; wR_2	0.0421; 0.0657 (for 2913 reflections)
Godness-of-fit for F^2	0.922
Largest diff. peak and hole / e^-/A^3	0.975 and -1.171

Table A.68: Fractional coordinates ($\cdot\ 10^4$) and equivalent isotropic displacement parameter U_{eq} ($\text{Å}^2 \cdot 10^3$) for the independent atoms in the structure of $[Ca(en)_4]_2(As_4Te_6)$.

	Wyck.	*x*	*y*	*z*	U_{eq}
Te(1)	8*c*	4238(1)	5545(1)	4061(1)	24(1)
Te(2)	8*c*	2540(1)	5602(1)	5493(1)	28(1)
Te(3)	8*c*	4302(1)	5032(1)	7437(1)	26(1)
As(1)	8*c*	4009(1)	5882(1)	5524(1)	24(1)
As(2)	8*c*	4232(1)	4533(1)	6039(1)	23(1)
Ca(1)	8*c*	3031(1)	2258(1)	8180(1)	23(1)
N(1)	8*c*	4099(4)	2754(4)	7239(4)	36(2)
N(2)	8*c*	3643(4)	1099(4)	7332(3)	29(2)
N(3)	8*c*	2461(4)	3628(4)	7649(3)	31(2)
N(4)	8*c*	1940(3)	2064(4)	7168(3)	29(2)
N(5)	8*c*	3706(3)	3443(4)	8936(3)	28(2)
N(6)	8*c*	4049(4)	1759(4)	9173(4)	38(2)
N(7)	8*c*	2026(4)	2516(4)	9257(4)	29(2)
N(8)	8*c*	2334(3)	928(4)	8669(4)	29(2)
C(1)	8*c*	4629(4)	2101(5)	6979(5)	30(2)
C(2)	8*c*	4139(4)	1403(5)	6703(4)	28(2)
C(3)	8*c*	1998(5)	3521(6)	6935(5)	36(2)
C(4)	8*c*	1476(5)	2808(5)	7025(5)	36(2)
C(5)	8*c*	4393(4)	3174(5)	9394(5)	33(2)
C(6)	8*c*	4231(5)	2371(5)	9764(4)	35(2)
C(7)	8*c*	1806(5)	1792(6)	9686(4)	36(2)
C(8)	8*c*	1618(4)	1094(6)	9132(4)	33(2)

Table A. 69: Anisotropic displacement parameters U_{ij} / Å^2 · 10^3 for the independent atoms in the structure of [Ca(en)$_4$]$_2$(As$_4$Te$_6$).

	U_{11}	U_{22}	U_{33}	U_{23}	U_{13}	U_{12}
Te(1)	26(1)	25(1)	22(1)	1(1)	0(1)	4(1)
Te(2)	23(1)	34(1)	26(1)	2(1)	1(1)	2(1)
Te(3)	32(1)	24(1)	22(1)	-2(1)	3(1)	-2(1)
As(1)	25(1)	24(1)	22(1)	-1(1)	2(1)	2(1)
As(2)	27(1)	22(1)	21(1)	-2(1)	1(1)	0(1)
Ca(1)	25(1)	21(1)	22(1)	0(1)	-1(1)	1(1)
N(1)	47(5)	23(4)	37(4)	5(4)	4(3)	4(4)
N(2)	31(4)	25(4)	30(4)	7(3)	-5(3)	-3(3)
N(3)	34(4)	28(4)	30(4)	-2(4)	1(3)	-5(4)
N(4)	35(4)	27(4)	24(3)	-3(3)	0(3)	-2(3)
N(5)	27(4)	39(5)	17(3)	6(3)	1(3)	2(3)
N(6)	42(4)	34(5)	38(4)	-2(4)	-14(3)	-1(4)
N(7)	30(4)	22(4)	35(4)	-2(3)	4(3)	-6(3)
N(8)	32(4)	22(4)	33(4)	5(3)	-7(3)	3(3)
C(1)	26(4)	30(6)	32(5)	-3(4)	4(4)	3(4)
C(2)	29(5)	34(5)	21(4)	4(4)	-3(4)	4(4)
C(3)	32(5)	34(6)	44(5)	13(5)	-19(4)	-3(4)
C(4)	26(5)	38(6)	44(5)	11(5)	-11(4)	7(4)
C(5)	29(4)	34(6)	35(5)	-11(5)	-5(4)	-1(4)
C(6)	45(5)	35(6)	26(4)	-8(4)	-14(4)	8(5)
C(7)	44(5)	41(6)	25(4)	-4(5)	10(4)	-6(5)
C(8)	26(4)	40(6)	31(5)	7(5)	3(4)	-4(4)

Table A.70: Selected bond lengts for [Ca(en)$_4$]$_2$(As$_4$Te$_6$). Symmetry transformations used to generate equivalent atoms: #1 -x+1, -y+1, -z+1.

Atoms 1, 2	Distance / Å	Atoms 1, 2	Distance / Å
Te(1)-As(1)	2.6256(9)	N(1)-C(1)	1.476(10)
Te(1)-As(2)#1	2.6266(9)	N(2)-C(2)	1.470(9)
Te(2)-As(1)	2.5553(9)	N(3)-C(3)	1.479(9)
Te(3)-As(2)	2.5614(9)	N(4)-C(4)	1.480(10)
As(1)-As(2)	2.4234(12)	N(5)-C(5)	1.487(9)
Ca(1)-N(7)	2.573(6)	N(6)-C(6)	1.469(10)
Ca(1)-N(4)	2.580(6)	N(7)-C(7)	1.454(10)
Ca(1)-N(1)	2.582(6)	N(8)-C(8)	1.489(9)
Ca(1)-N(6)	2.584(6)	C(1)-C(2)	1.501(11)
Ca(1)-N(5)	2.617(7)	C(3)-C(4)	1.483(11)
Ca(1)-N(3)	2.624(7)	C(5)-C(6)	1.496(11)
Ca(1)-N(2)	2.627(7)	C(7)-C(8)	1.531(11)
Ca(1)-N(8)	2.634(7)		

Table A.71: Selected bond lengts for [Ca(en)$_4$]$_2$(As$_4$Te$_6$). Symmetry transformations used to generate equivalent atoms: #1 -x+1, -y+1, -z+1.

Atoms 1, 2, 3	Angle / °	Atoms 1, 2, 3	Angle / °
As(1)-Te(1)-As(2)#1	102.87(3)	C(6)-N(6)-Ca(1)	112.9(5)
As(2)-As(1)-Te(2)	89.83(3)	C(7)-N(7)-Ca(1)	114.0(5)
As(2)-As(1)-Te(1)	98.02(4)	C(8)-N(8)-Ca(1)	113.2(5)
Te(2)-As(1)-Te(1)	95.10(3)	N(1)-C(1)-C(2)	108.2(6)
As(1)-As(2)-Te(3)	93.60(4)	N(2)-C(2)-C(1)	110.3(6)
As(1)-As(2)-Te(1)#1	100.21(3)	N(3)-C(3)-C(4)	109.1(7)
Te(3)-As(2)-Te(1)#1	91.78(3)	N(4)-C(4)-C(3)	110.5(6)
C(1)-N(1)-Ca(1)	113.4(5)	N(5)-C(5)-C(6)	110.2(6)
C(2)-N(2)-Ca(1)	113.4(5)	N(6)-C(6)-C(5)	110.3(6)
C(3)-N(3)-Ca(1)	112.9(5)	N(7)-C(7)-C(8)	110.5(6)
C(4)-N(4)-Ca(1)	113.5(5)	N(8)-C(8)-C(7)	107.6(6)
C(5)-N(5)-Ca(1)	113.2(5)		

A.1.15 [Sr(en)$_4$]$_2$(As$_4$Te$_6$)

Table A.72: Crystal data and structure refinement for [Sr(en)$_4$]$_2$(As$_4$Te$_6$).

Empirical formula	C$_8$ H$_{32}$ As$_2$ Sr N$_8$ Te$_3$
Formula weight / *g/mol*	860.67
Temperature / *K*	123(2)
Crystal system; Space group	Orthorhombic; *Pbca*
Lattice constants / *Å*	a = 17.2116(2)
	b = 16.3773(3)
	c = 17.6420(3)
Volume / *Å³*	4972.92(14)
Z; F(000); calc. density / *g/cm³*	8; 3168 ; 2.299
Wavelength / *Å*	0.71073
Crystal size / *mm*	0.244 × 0.120 × 0.062
Theta range for data collection / °	2.069 to 30.083
Limiting indices	-23 ≤ h ≤ 24, -23 ≤ k ≤ 23, -24 ≤ l ≤ 24
Reflections collected / unique	56562 / 7302
Completeness to $\vartheta = 25.242$	99.9 %
R$_{int}$	13.44 %
Absorption coefficient / *mm⁻¹*	8.267
Refinement method	Full-matrix least-squares on F^2
Data / restrains / parameters	7302 / 0 / 200
R indices (all data) R_1 ; wR_2	0.0555; 0.1212
R indices [$I > 4\sigma(I)$] R_1 ; wR_2	0.0448; 0.1143 (for 6025 reflections)
Godness-of-fit for F^2	1.044
Largest diff. peak and hole / e^-/A^3	2.480 and -2.299

Table A.73: Fractional coordinates ($\cdot\ 10^4$) and equivalent isotropic displacement parameter U_{eq} ($\text{Å}^2 \cdot 10^3$) for the independent atoms in the structure of $[Sr(en)_4]_2(As_4Te_6)$.

	Wyck.	x	y	z	U_{eq}
Te(1)	8c	4241(1)	5543(1)	4086(1)	20(1)
Te(2)	8c	2555(1)	5626(1)	5494(1)	24(1)
Te(3)	8c	4315(1)	4993(1)	7410(1)	21(1)
As(1)	8c	4018(1)	5879(1)	5524(1)	19(1)
As(2)	8c	4239(1)	4520(1)	6028(1)	19(1)
Sr(1)	8c	2999(1)	2221(1)	8171(1)	19(1)
N(1)	8c	4125(3)	2723(3)	7189(3)	33(1)
N(2)	8c	3657(2)	1018(2)	7287(2)	26(1)
N(3)	8c	2397(2)	3650(2)	7595(2)	27(1)
N(4)	8c	1847(3)	2050(3)	7139(2)	29(1)
N(5)	8c	3701(2)	3467(2)	8938(2)	26(1)
N(6)	8c	4043(3)	1778(3)	9238(3)	38(1)
N(7)	8c	1948(2)	2472(3)	9294(2)	27(1)
N(8)	8c	2257(2)	845(2)	8699(2)	24(1)
C(1)	8c	4632(3)	2057(3)	6953(3)	28(1)
C(2)	8c	4157(3)	1348(3)	6678(3)	27(1)
C(3)	8c	1962(3)	3522(3)	6898(3)	38(1)
C(4)	8c	1414(3)	2803(3)	6983(3)	36(1)
C(5)	8c	4366(3)	3213(4)	9395(3)	35(1)
C(6)	8c	4208(4)	2426(4)	9802(3)	41(1)
C(7)	8c	1732(3)	1711(3)	9702(3)	30(1)
C(8)	8c	1558(3)	1034(3)	9150(3)	29(1)

Table A.74: Anisotropic displacement parameters U_{ij} / $\text{Å}^2 \cdot 10^3$ for the independent atoms in the structure of $[Sr(en)_4]_2(As_4Te_6)$.

	U_{11}	U_{22}	U_{33}	U_{23}	U_{13}	U_{12}
Te(1)	21(1)	19(1)	20(1)	0(1)	0(1)	4(1)
Te(2)	19(1)	27(1)	25(1)	1(1)	1(1)	2(1)
Te(3)	27(1)	17(1)	20(1)	-2(1)	3(1)	-3(1)
As(1)	20(1)	15(1)	21(1)	-1(1)	1(1)	1(1)
As(2)	22(1)	15(1)	20(1)	-1(1)	1(1)	0(1)
Sr(1)	21(1)	15(1)	20(1)	0(1)	-1(1)	0(1)
N(1)	38(2)	22(2)	39(2)	2(2)	7(2)	0(2)
N(2)	32(2)	19(2)	27(2)	-1(2)	0(2)	-3(2)
N(3)	26(2)	17(2)	38(2)	-3(2)	0(2)	-2(2)
N(4)	34(2)	20(2)	33(2)	-1(2)	-6(2)	-2(2)
N(5)	35(2)	17(2)	25(2)	1(1)	0(2)	-2(2)
N(6)	44(3)	25(2)	46(3)	-2(2)	-21(2)	6(2)
N(7)	31(2)	20(2)	32(2)	-4(2)	2(2)	1(2)
N(8)	27(2)	17(2)	28(2)	0(1)	-6(2)	-2(2)
C(1)	23(2)	22(2)	38(3)	-1(2)	4(2)	-1(2)
C(2)	33(3)	23(2)	26(2)	-4(2)	-1(2)	0(2)
C(3)	42(3)	31(3)	40(3)	12(2)	-16(2)	-7(2)
C(4)	33(3)	26(2)	47(3)	10(2)	-8(2)	-4(2)
C(5)	33(3)	32(3)	41(3)	-6(2)	-6(2)	-7(2)
C(6)	54(4)	30(3)	37(3)	-1(2)	-23(3)	3(2)
C(7)	37(3)	27(2)	26(2)	2(2)	4(2)	2(2)
C(8)	33(3)	21(2)	32(2)	0(2)	-2(2)	-1(2)

Table A.75: Selected bond lengths for [Sr(en)$_4$]$_2$(As$_4$Te$_6$). Symmetry transformations used to generate equivalent atoms: #1 -x+1, -y+1, -z+1.

Atoms 1, 2	Distance / Å	Atoms 1, 2	Distance / Å
Te(1)-As(1)	2.6244(5)	N(1)-C(1)	1.458(6)
Te(1)-As(2)#1	2.6251(5)	N(2)-C(2)	1.480(6)
Te(2)-As(1)	2.5530(5)	N(3)-C(3)	1.456(6)
Te(3)-As(2)	2.5618(5)	N(4)-C(4)	1.468(7)
As(1)-As(2)	2.4257(6)	N(5)-C(5)	1.461(7)
Sr1-N(6)	2.701(4)	N(6)-C(6)	1.482(7)
Sr1-N(4)	2.707(4)	N(7)-C(7)	1.488(6)
Sr1-N(7)	2.714(4)	N(8)-C(8)	1.475(7)
Sr1-N(1)	2.727(4)	C(1)-C(2)	1.500(7)
Sr1-N(5)	2.731(4)	C(3)-C(4)	1.516(7)
Sr1-N(8)	2.752(4)	C(5)-C(6)	1.500(8)
Sr1-N(3)	2.754(4)	C(7)-C(8)	1.506(7)
Sr1-N(2)	2.756(4)		

Table A.76: Selected bond angles for [Sr(en)$_4$]$_2$(As$_4$Te$_6$). Symmetry transformations used to generate equivalent atoms: #1 -x+1, -y+1, -z+1.

Atoms 1, 2, 3	Angle / °	Atoms 1, 2, 3	Angle / °
As(1)-Te(1)-As(2)#1	103.181(17)	C(6)-N(6)- Sr1	113.8(3)
As(2)-As(1)-Te(2)	90.78(2)	C(7)-N(7)- Sr1	113.2(3)
As(2)-As(1)-Te(1)	97.973(19)	C(8)-N(8)- Sr1	112.9(3)
Te(2)-As(1)-Te(1)	95.182(17)	N(1)-C(1)-C(2)	110.2(4)
As(1)-As(2)-Te(3)	94.565(19)	N(2)-C(2)-C(1)	111.4(4)
As(1)-As(2)-Te(1)#1	99.44(2)	N(3)-C(3)-C(4)	110.4(4)
Te(3)-As(2)-Te(1)#1	91.949(17)	N(4)-C(4)-C(3)	110.8(5)
C(1)-N(1)- Sr1	112.4(3)	N(5)-C(5)-C(6)	111.5(4)
C(2)-N(2)- Sr1	112.9(3)	N(6)-C(6)-C(5)	109.1(4)
C(3)-N(3)- Sr1	112.5(3)	N(7)-C(7)-C(8)	110.7(4)
C(4)-N(4)- Sr1	114.3(3)	N(8)-C(8)-C(7)	110.0(4)
C(5)-N(5)- Sr1	114.0(3)		

A.1.16 [Eu(en)$_4$]$_2$(As$_4$Se$_6$)

Table A.77: Crystal data and structure refinement for [Eu(en)$_4$]$_2$(As$_4$Se$_6$).

Empirical formula	C$_8$ H$_{32}$ As$_2$ Eu N$_8$ Se$_3$
Formula weight / *g/mol*	779.09
Temperature / *K*	123(2)
Crystal system; Space group	Orthorhombic; *Pbca*
Lattice constants / *Å*	a = 16.7023(2)
	b = 15.7065(2)
	c = 17.2823(2)
Volume / *Å^3*	4533.75(10)
Z; F(000); calc. density / *g/cm^3*	8; 2936 ; 2.283
Wavelength / *Å*	0.71073
Crystal size / *mm*	0.120 × 0.080 × 0.070
Theta range for data collection / °	2.954 to 27.492
Limiting indices	-21 ≤ h ≤ 21, -20 ≤ k ≤ 20, -22 ≤ l ≤ 22
Reflections collected / unique	9867 / 5196
Completeness to ϑ = 25.242	99.7 %
R$_{int}$	2.78 %
Absorption coefficient / *mm^{-1}*	10.488
Refinement method	Full-matrix least-squares on F^2
Data / restrains / parameters	5196 / 0 / 327
R indices (all data) R_1 ; wR_2	0.0436; 0.0549
R indices [$I > 4\sigma(I)$] R_1 ; wR_2	0.0263; 0.0510 (for 4064 reflections)
Godness-of-fit for F^2	0.999
Largest diff. peak and hole / *e $^-$/A^3*	0.758 and -0.975

Table A.78: Fractional coordinates ($\cdot\ 10^4$) and equivalent isotropic displacement parameter U_{eq} ($\text{Å}^2 \cdot 10^3$) for the independent atoms in the structure of $[Eu(en)_4]_2(As_4Se_6)$.

	Wyck.	*x*	*y*	*z*	U_{eq}
Se(1)	8*c*	5714(1)	4942(1)	7321(1)	20(1)
As(1)	8*c*	5711(1)	4508(1)	6029(1)	17(1)
Se(2)	8*c*	4257(1)	4495(1)	5900(1)	19(1)
As(2)	8*c*	4016(1)	4108(1)	4556(1)	17(1)
Se(3)	8*c*	2634(1)	4314(1)	4556(1)	22(1)
Eu(1)	8*c*	7051(1)	2184(1)	8149(1)	17(1)
N(1)	8*c*	7773(2)	731(2)	8693(2)	22(1)
N(2)	8*c*	8143(2)	2433(2)	9284(2)	26(1)
N(3)	8*c*	8223(2)	1989(2)	7100(2)	25(1)
N(4)	8*c*	7648(2)	3667(2)	7545(2)	23(1)
N(5)	8*c*	5896(2)	2652(2)	7148(2)	26(1)
N(6)	8*c*	6390(2)	893(2)	7288(2)	23(1)
N(7)	8*c*	6370(2)	3531(2)	8898(2)	22(1)
N(8)	8*c*	5974(3)	1784(2)	9254(2)	32(1)
C(1)	8*c*	8499(2)	916(3)	9151(2)	23(1)
C(2)	8*c*	8329(3)	1649(3)	9702(2)	28(1)
C(3)	8*c*	8666(3)	2782(3)	6923(3)	30(1)
C(4)	8*c*	8095(3)	3509(3)	6820(2)	29(1)
C(5)	8*c*	5370(2)	1944(3)	6929(2)	25(1)
C(6)	8*c*	5864(2)	1192(3)	6660(2)	23(1)
C(7)	8*c*	5680(3)	3306(3)	9386(3)	27(1)
C(8)	8*c*	5840(3)	2478(3)	9807(3)	30(1)

Table A.79: Anisotropic displacement parameters U_{ij} / Å^2 · 10^3 for the independent atoms in the structure of [Eu(en)$_4$]$_2$(As$_4$Se$_6$).

	U_{11}	U_{22}	U_{33}	U_{23}	U_{13}	U_{12}
Se(1)	25(1)	20(1)	15(1)	-1(1)	-3(1)	1(1)
As(1)	20(1)	17(1)	15(1)	-1(1)	-1(1)	1(1)
Se(2)	19(1)	23(1)	16(1)	0(1)	0(1)	-4(1)
As(2)	16(1)	18(1)	16(1)	-1(1)	-1(1)	-1(1)
Se(3)	16(1)	30(1)	21(1)	1(1)	0(1)	-1(1)
Eu(1)	18(1)	17(1)	15(1)	0(1)	1(1)	0(1)
N(1)	24(2)	24(2)	20(2)	-1(2)	2(2)	-2(2)
N(2)	30(2)	22(2)	27(2)	-4(2)	-4(2)	0(2)
N(3)	28(2)	21(2)	27(2)	-1(2)	5(2)	2(2)
N(4)	26(2)	23(2)	21(2)	-4(2)	0(2)	3(2)
N(5)	28(2)	18(2)	32(2)	2(2)	-5(2)	-2(2)
N(6)	27(2)	18(2)	25(2)	2(2)	2(2)	-1(2)
N(7)	22(2)	24(2)	18(2)	2(2)	-2(2)	1(2)
N(8)	43(2)	20(2)	34(2)	0(2)	14(2)	-4(2)
C(1)	20(2)	21(2)	28(2)	2(2)	-3(2)	0(2)
C(2)	30(2)	32(3)	21(2)	0(2)	-6(2)	-1(2)
C(3)	25(2)	26(2)	37(3)	4(2)	12(2)	-1(2)
C(4)	35(2)	27(3)	24(2)	10(2)	11(2)	0(2)
C(5)	23(2)	23(2)	28(2)	3(2)	-2(2)	-3(2)
C(6)	23(2)	20(2)	25(2)	-5(2)	-2(2)	-1(2)
C(7)	24(2)	29(3)	28(2)	-3(2)	5(2)	1(2)
C(8)	36(3)	23(2)	30(2)	-1(2)	12(2)	-5(2)

Table A.80: Selected bond lengths for [Eu(en)$_4$]$_2$(As$_4$Se$_6$). Symmetry transformations used to generate equivalent atoms: #1 -x+1, -y+1, -z+1.

Atoms 1, 2	Distance / Å	Atoms 1, 2	Distance / Å
Se(1)-As(1)	2.3349(5)	N(1)-C(1)	1.479(5)
As(1)-Se(2)	2.4402(5)	N(2)-C(2)	1.459(6)
As(1)-As(2)#1	2.4407(5)	N(3)-C(3)	1.480(5)
Se(2)-As(2)	2.4335(5)	N(4)-C(4)	1.478(5)
As(2)-Se(3)	2.3307(5)	N(5)-C(5)	1.468(5)
Eu(1)-N(3)	2.686(4)	N(6)-C(6)	1.473(5)
Eu(1)-N(5)	2.693(3)	N(7)-C(7)	1.472(5)
Eu(1)-N(8)	2.696(4)	N(8)-C(8)	1.466(6)
Eu(1)-N(2)	2.707(3)	C(1)-C(2)	1.520(6)
Eu(1)-N(7)	2.727(3)	C(3)-C(4)	1.496(6)
Eu(1)-N(4)	2.740(4)	C(5)-C(6)	1.511(6)
Eu(1)-N(1)	2.747(3)	C(7)-C(8)	1.513(6)
Eu(1)-N(6)	2.748(3)		

Table A.81: Selected bond angles for [Eu(en)$_4$]$_2$(As$_4$Se$_6$). Symmetry transformations used to generate equivalent atoms: #1 -x+1, -y+1, -z+1.

Atoms 1, 2, 3	Angle / °	Atoms 1, 2, 3	Angle / °
Se(1)-As(1)-Se(2)	95.269(18)	C(6)-N(6)-Eu(1)	113.7(2)
Se(1)-As(1)-As(2)#1	97.806(18)	C(7)-N(7)-Eu(1)	114.3(3)
Se(2)-As(1)-As(2)#1	98.931(18)	C(8)-N(8)-Eu(1)	113.0(3)
As(2)-Se(2)-As(1)	104.706(18)	N(1)-C(1)-C(2)	109.2(3)
Se(3)-As(2)-Se(2)	97.431(18)	N(2)-C(2)-C(1)	111.7(3)
Se(3)-As(2)-As(1)#1	93.512(18)	N(3)-C(3)-C(4)	110.4(4)
Se(2)-As(2)-As(1)#1	98.215(18)	N(4)-C(4)-C(3)	110.4(3)
C(1)-N(1)-Eu(1)	112.3(2)	N(5)-C(5)-C(6)	110.2(3)
C(2)-N(2)-Eu(1)	112.3(3)	N(6)-C(6)-C(5)	110.4(3)
C(3)-N(3)-Eu(1)	114.1(3)	N(7)-C(7)-C(8)	110.1(3)
C(4)-N(4)-Eu(1)	111.3(3)	N(8)-C(8)-C(7)	110.7(4)
C(5)-N(5)-Eu(1)	112.8(2)		

A.1.17 [Ca(en)₄](As₂Se₆)

Table A.82: Crystal data and structure refinement for [Ca(en)₄](As₂Se₆).

Empirical formula	$C_8 H_{32} As_2 Ca N_8 Se_6$
Formula weight / *g/mol*	904.09
Temperature / *K*	123(2)
Crystal system; Space group	Monoclinic; *C* 2/*c*
Lattice constants / *Å*	a = 22.6915(8)
	b = 10.0484(3) β = 128.281(2)
	c = 14.3506(5)
Volume / *Å³*	2568.56(16)
Z; F(000); calc. density / *g/cm³*	4; 1704 ; 2.338
Wavelength / *Å*	0.71073
Crystal size / *mm*	$0.156 \times 0.086 \times 0.070$
Theta range for data collection / °	3.354 to 27.502
Limiting indices	$-28 \leq h \leq 29, -13 \leq k \leq 12, -18 \leq l \leq 18$
Reflections collected / unique	4361 / 2682
Completeness to $\vartheta = 25.242$	93.4 %
R_{int}	4.50 %
Absorption coefficient / *mm⁻¹*	11.315
Refinement method	Full-matrix least-squares on F^2
Data / restrains / parameters	2682 / 0 / 115
R indices (all data) R_1 ; wR_2	0.0550; 0.1163
R indices [$I > 4\sigma(I)$] R_1 ; wR_2	0.0429; 0.1104 (for 2186 reflections)
Godness-of-fit for F^2	1.052
Largest diff. peak and hole / e^-/A^3	1.029 and -0.976

Table A.83: Fractional coordinates ($\cdot$ 10^4) and equivalent isotropic displacement parameter U_{eq} ($\text{Å}^2 \cdot 10^3$) for the independent atoms in the structure of $[Ca(en)_4](As_2Se_6)$.

	Wyck.	x	y	z	U_{eq}
Se(1)	8*f*	1463(1)	8343(1)	4491(1)	20(1)
Se(2)	8*f*	2615(1)	9116(1)	6217(1)	20(1)
Se(3)	8*f*	4439(1)	7700(1)	8373(1)	21(1)
As(1)	8*f*	3248(1)	6989(1)	6867(1)	20(1)
Ca(1)	4*e*	5000	2150(2)	7500	16(1)
N(4)	8*f*	4380(3)	4078(5)	7804(5)	31(1)
N(3)	8*f*	4413(3)	1405(5)	8484(4)	20(1)
N(1)	8*f*	4163(3)	200(5)	6170(4)	26(1)
N(2)	8*f*	3909(3)	2883(5)	5322(5)	29(1)
C(3)	8*f*	3785(4)	2296(6)	8104(6)	29(1)
C(4)	8*f*	4063(4)	3719(6)	8410(6)	29(1)
C(2)	8*f*	3304(4)	1853(7)	4695(6)	33(2)
C(1)	8*f*	3644(3)	503(6)	4890(5)	28(1)

Table A.84: Anisotropic displacement parameters U_{ij} / $\text{Å}^2 \cdot 10^3$ for the independent atoms in the structure of $[Ca(en)_4](As_2Se_6)$.

	U_{11}	U_{22}	U_{33}	U_{23}	U_{13}	U_{12}
Se(1)	17(1)	19(1)	18(1)	0(1)	8(1)	1(1)
Se(2)	19(1)	21(1)	18(1)	-3(1)	10(1)	-2(1)
Se(3)	19(1)	22(1)	15(1)	-1(1)	7(1)	-2(1)
As(1)	18(1)	19(1)	16(1)	1(1)	8(1)	-2(1)
Ca(1)	18(1)	14(1)	15(1)	0	11(1)	0
N(4)	51(4)	21(3)	25(3)	9(2)	25(3)	13(2)
N(3)	25(3)	15(2)	24(3)	0(2)	18(2)	3(2)
N(1)	30(3)	24(3)	23(3)	-1(2)	16(2)	-4(2)
N(2)	34(3)	25(3)	23(3)	5(2)	16(3)	12(2)
C(3)	27(3)	31(4)	33(4)	3(3)	21(3)	6(3)
C(4)	39(4)	28(3)	26(3)	7(3)	23(3)	14(3)
C(2)	16(3)	52(4)	22(3)	1(3)	8(3)	6(3)
C(1)	24(3)	36(4)	24(3)	-14(3)	16(3)	-11(3)

Table A.85: Selected bond lengths for $[Ca(en)_4](As_2Se_6)$. Symmetry transformations used to generate equivalent atoms: #1 $-x+1/2$, $-y+3/2$, $-z+1$ #2 $-x+1$, y, $-z+3/2$.

Atoms 1, 2	Distance / Å	Atoms 1, 2	Distance / Å
Se(1)-Se(2)	2.3557(8)	Ca(1)-N(4)#2	2.585(5)
Se(1)-As(1)#1	2.4343(8)	Ca(1)-N(2)#2	2.618(5)
Se(2)-As(1)	2.4162(8)	Ca(1)-N(2)	2.618(5)
Se(3)-As(1)	2.2916(8)	N(4)-C(4)	1.477(8)
Ca(1)-N(1)	2.569(5)	N(3)-C(3)	1.471(7)
Ca(1)-N(1)#2	2.569(5)	N(1)-C(1)	1.474(7)
Ca(1)-N(3)#2	2.582(5)	N(2)-C(2)	1.495(8)
Ca(1)-N(3)	2.582(5)	C(3)-C(4)	1.514(9)
Ca(1)-N(4)	2.585(5)	C(2)-C(1)	1.499(9)

Table A.86: Selected bond angles for $[Ca(en)_4](As_2Se_6)$. Symmetry transformations used to generate equivalent atoms: #1 $-x+1/2$, $-y+3/2$, $-z+1$ #2 $-x+1$, y, $-z+3/2$.

Atoms 1, 2, 3	Angle / °	Atoms 1, 2, 3	Angle / °
Se(2)-Se(1)-As(1)#1	102.33(3)	C(1)-N(1)-Ca(1)	114.9(4)
Se(1)-Se(2)-As(1)	96.96(3)	C(2)-N(2)-Ca(1)	111.1(4)
Se(3)-As(1)-Se(2)	99.22(3)	N(3)-C(3)-C(4)	109.5(5)
Se(3)-As(1)-Se(1)#1	92.98(3)	N(4)-C(4)-C(3)	109.1(5)
Se(2)-As(1)-Se(1)#1	101.70(3)	N(2)-C(2)-C(1)	109.9(5)
C(4)-N(4)-Ca(1)	115.5(3)	N(1)-C(1)-C(2)	109.9(5)
C(3)-N(3)-Ca(1)	109.3(3)		

A.1.18 [Ca(en)₄]₂(As₂Se₇O)

Table A.87: Crystal data and structure refinement for [Ca(en)₄]₂(As₂Se₇O).

Empirical formula	$C_{16} H_{64} As_2 Ca_2 N_{16} O Se_7$
Formula weight / *g/mol*	1279.55
Temperature / *K*	123(3)
Crystal system; Space group	Orthorhombic; *Iba*2
Lattice constants / *Å*	$a = 16.6561(3)$
	$b = 31.2220(5)$
	$c = 16.5018(3)$
Volume / $Å^3$	8581.5(3)
Z; F(000); calc. density / g/cm^3	8; 4992; 1.981
Wavelength / *Å*	0.71073
Crystal size / *mm*	$0.290 \times 0.150 \times 0.084$
Theta range for data collection / °	3.135 to 27.500
Limiting indices	$-21 \leq h \leq 21, -21 \leq k \leq 21, -40 \leq l \leq 40$
Reflections collected / unique	27266 / 7787
Completeness to $\vartheta = 25.242$	99.7 %
R_{int}	12.62 %
Absorption coefficient / mm^{-1}	7.771
Refinement method	Full-matrix least-squares on F^2
Data / restrains / parameters	7787 / 1 / 399
R indices (all data) R_1 ; wR_2	0.0640; 0.1480
R indices [$I > 4\sigma(I)$] R_1 ; wR_2	0.0546; 0.1438 (for 8405 reflections)
Godness-of-fit for F^2	1.097
Largest diff. peak and hole / e^-/A^3	2.327 and -1.897
Absolute structure parameter	0.52(3)

Table A.88: Fractional coordinates ($\cdot\ 10^4$) and equivalent isotropic displacement parameter U_{eq} ($\text{Å}^2 \cdot 10^3$) for the independent atoms in the structure of $[Ca(en)_4]_2(As_2Se_7O)$.

	Wyck.	*x*	*y*	*z*	U_{eq}
As(1)	8*c*	6343(1)	3831(1)	2901(1)	24(1)
As(2)	8*c*	8428(1)	3967(1)	5126(1)	34(1)
Se(1)	8*c*	5006(1)	3783(1)	3199(1)	34(1)
Se(2)	8*c*	6855(1)	4500(1)	3002(1)	33(1)
Se(3)	8*c*	6685(1)	3487(1)	1731(1)	28(1)
Se(4)	8*c*	6794(1)	3392(1)	4009(1)	32(1)
Se(5)	8*c*	8185(1)	3459(1)	4030(1)	35(1)
Se(7)	8*c*	8270(1)	3592(1)	6324(1)	45(1)
Se(8)	8*c*	9801(1)	3943(1)	4818(1)	46(1)
O(1)	8*c*	8072(6)	4536(3)	5046(6)	28(2)
Ca(1)	4*a*	5000	5000	5464(2)	21(1)
N(1)	8*c*	6165(8)	5520(5)	5771(8)	40(3)
N(2)	8*c*	5732(7)	5255(4)	4172(8)	31(3)
N(3)	8*c*	5871(7)	4349(4)	5142(7)	28(2)
N(4)	8*c*	5693(8)	4673(4)	6769(7)	30(3)
C(1)	8*c*	6404(10)	5773(6)	5003(11)	45(4)
C(2)	8*c*	6469(10)	5504(6)	4324(12)	44(4)
C(3)	8*c*	6062(9)	4097(5)	5851(9)	30(3)
C(4)	8*c*	6323(10)	4374(5)	6549(10)	36(3)
Ca(2)	8*c*	5766(2)	2420(1)	6487(2)	25(1)
N(5)	8*c*	4752(7)	2668(4)	7575(8)	31(3)
N(6)	8*c*	5144(8)	1778(4)	7326(8)	32(3)
N(7)	8*c*	6281(8)	1706(4)	5842(7)	32(3)
N(8)	8*c*	6843(8)	2541(4)	5391(8)	33(3)
N(9)	8*c*	5114(8)	3052(4)	5706(8)	34(3)
N(10)	8*c*	4671(7)	2167(4)	5523(9)	37(3)
N(11)	8*c*	6418(7)	3125(4)	7069(8)	28(2)
N(12)	8*c*	6902(7)	2279(4)	7498(8)	32(3)
C(5)	8*c*	4672(11)	2343(5)	8242(10)	40(4)
C(6)	8*c*	4541(10)	1908(5)	7920(12)	44(4)

C(7)	8c	6659(9)	1787(5)	5048(9)	36(3)
C(8)	8c	7241(9)	2131(5)	5086(10)	36(3)
C(9)	8c	4559(8)	2921(5)	5061(9)	31(3)
C(10)	8c	4126(9)	2526(5)	5293(10)	36(3)
C(11)	8c	6890(9)	3044(5)	7804(10)	37(3)
C(12)	8c	7407(9)	2649(5)	7661(10)	34(3)
Ca(3)	4b	10000	5000	2425(3)	28(1)
N(13)	8c	9001(10)	4776(6)	3467(11)	59(5)
N(14)	8c	9223(11)	5661(5)	2990(12)	62(4)
N(15)	8c	10847(18)	5717(8)	1806(14)	119(12)
N(16)	8c	11000(12)	4799(6)	1284(12)	70(5)
C(13)	8c	8840(17)	5160(7)	3975(14)	73(7)
C(14)	8c	8559(10)	5536(6)	3501(12)	44(4)
C(15)	8c	11402(10)	5551(6)	1214(13)	46(4)
C(16)	8c	11686(13)	5111(7)	1260(15)	63(6)

Table A.89: Anisotropic displacement parameters U_{ij} / $\text{Å}^2 \cdot 10^3$ for the independent atoms in the structure of $[Ca(en)_4]_2(As_2Se_7O)$.

	U_{11}	U_{22}	U_{33}	U_{23}	U_{13}	U_{12}
As(1)	27(1)	26(1)	20(1)	-3(1)	-3(1)	5(1)
As(2)	36(1)	37(1)	30(1)	0(1)	-3(1)	-9(1)
Se(1)	28(1)	37(1)	39(1)	-12(1)	0(1)	3(1)
Se(2)	42(1)	25(1)	33(1)	-3(1)	1(1)	-2(1)
Se(3)	34(1)	28(1)	24(1)	-7(1)	1(1)	4(1)
Se(4)	37(1)	32(1)	26(1)	2(1)	-6(1)	-2(1)
Se(5)	35(1)	40(1)	31(1)	-7(1)	-7(1)	10(1)
Se(7)	32(1)	72(1)	31(1)	17(1)	6(1)	12(1)
Se(8)	32(1)	57(1)	49(1)	16(1)	-2(1)	-12(1)
O(1)	29(5)	23(5)	31(6)	7(4)	0(4)	1(4)
Ca(1)	24(2)	17(2)	22(2)	0	0	1(1)
N(1)	42(7)	51(8)	26(7)	4(6)	-8(6)	-8(6)
N(2)	27(6)	35(6)	30(7)	2(5)	2(5)	2(5)

N(3)	31(6)	34(6)	19(6)	-2(5)	2(5)	5(5)
N(4)	44(7)	32(6)	16(5)	1(5)	-1(5)	-3(5)
C(1)	32(8)	56(10)	47(11)	2(8)	3(7)	-10(7)
C(2)	36(9)	53(10)	44(10)	20(8)	-5(7)	-10(7)
C(3)	35(7)	31(7)	25(7)	3(6)	-7(6)	2(6)
C(4)	37(8)	45(9)	28(8)	3(6)	-8(6)	3(6)
Ca(2)	23(1)	29(1)	23(1)	3(1)	2(1)	0(1)
N(5)	30(6)	36(7)	27(6)	3(5)	4(5)	4(5)
N(6)	30(6)	39(7)	25(6)	1(5)	6(5)	2(5)
N(7)	32(6)	35(6)	27(7)	-4(5)	-5(5)	6(5)
N(8)	32(7)	35(7)	32(7)	10(5)	-3(5)	4(5)
N(9)	41(7)	34(6)	27(6)	-1(5)	-7(6)	7(5)
N(10)	32(6)	35(7)	43(8)	-2(6)	-7(6)	2(5)
N(11)	28(6)	26(6)	31(6)	3(5)	-2(5)	2(5)
N(12)	32(6)	34(6)	31(7)	2(5)	-2(5)	8(5)
C(5)	50(9)	38(8)	33(8)	-1(7)	4(7)	-8(7)
C(6)	49(9)	43(9)	40(9)	-6(8)	7(8)	-1(7)
C(7)	35(8)	53(9)	19(7)	8(6)	-3(6)	10(7)
C(8)	29(7)	51(9)	28(8)	8(7)	-5(6)	5(7)
C(9)	31(7)	36(8)	25(8)	-4(6)	-10(6)	3(6)
C(10)	34(8)	34(7)	40(9)	-6(6)	-15(6)	12(6)
C(11)	37(8)	41(8)	33(9)	0(7)	-6(7)	2(6)
C(12)	33(7)	35(8)	33(8)	5(6)	-2(6)	-2(6)
Ca(3)	28(2)	21(2)	35(2)	0	0	-2(2)
N(13)	53(9)	60(10)	66(11)	24(8)	15(8)	2(8)
N(14)	80(12)	48(9)	58(10)	-5(8)	6(10)	-8(8)
N(15)	170(30)	106(18)	76(15)	57(14)	71(17)	90(18)
N(16)	78(13)	69(12)	63(12)	-8(10)	11(10)	-9(10)
C(13)	112(19)	55(12)	51(12)	-27(10)	-30(13)	37(12)
C(14)	29(8)	48(10)	55(11)	-17(8)	0(7)	-3(7)
C(15)	37(9)	46(10)	56(12)	-6(8)	-3(8)	-7(7)
C(16)	60(12)	70(14)	60(14)	6(11)	-2(10)	-21(10)

Table A.90: Selected bond lengths for [Ca(en)$_4$]$_2$(As$_2$Se$_7$O). Symmetry transformations used to generate equivalent atoms: #1 -x+1, -y+1, z #2 -x+2, -y+1, z.

Atoms 1, 2	Distance / Å	Atoms 1, 2	Distance / Å
As(1)-Se(2)	2.2644(19)	Ca(2)-N(11)	2.634(12)
As(1)-Se(3)	2.2820(19)	Ca(2)-N(6)	2.647(13)
As(1)-Se(1)	2.286(2)	N(5)-C(5)	1.50(2)
As(1)-Se(4)	2.405(2)	N(6)-C(6)	1.46(2)
As(2)-O(1)	1.879(9)	N(7)-C(7)	1.48(2)
As(2)-Se(7)	2.311(2)	N(8)-C(8)	1.53(2)
As(2)-Se(8)	2.344(2)	N(9)-C(9)	1.467(19)
As(2)-Se(5)	2.439(2)	N(10)-C(10)	1.492(18)
Se(4)-Se(5)	2.327(2)	N(11)-C(11)	1.47(2)
Ca(1)-N(3)	2.554(11)	N(12)-C(12)	1.45(2)
Ca(1)-N(3)#1	2.554(11)	C(5)-C(6)	1.48(2)
Ca(1)-N(1)#1	2.580(13)	C(7)-C(8)	1.45(2)
Ca(1)-N(1)	2.580(13)	C(9)-C(10)	1.48(2)
Ca(1)-N(2)	2.582(12)	C(11)-C(12)	1.52(2)
Ca(1)-N(2)#1	2.582(12)	Ca(3)-N(13)#2	2.493(16)
Ca(1)-N(4)#1	2.648(12)	Ca(3)-N(13)	2.493(16)
Ca(1)-N(4)	2.648(12)	Ca(3)-N(16)#2	2.590(19)
N(1)-C(1)	1.54(2)	Ca(3)-N(16)	2.590(19)
N(2)-C(2)	1.47(2)	Ca(3)-N(14)	2.610(17)
N(3)-C(3)	1.447(18)	Ca(3)-N(14)#2	2.610(17)
N(4)-C(4)	1.45(2)	Ca(3)-N(15)#2	2.84(3)
C(1)-C(2)	1.40(3)	Ca(3)-N(15)	2.84(3)
C(3)-C(4)	1.50(2)	N(13)-C(13)	1.49(3)
Ca(2)-N(10)	2.546(13)	N(14)-C(14)	1.44(2)
Ca(2)-N(12)	2.560(13)	N(15)-C(15)	1.44(3)
Ca(2)-N(8)	2.575(13)	N(16)-C(16)	1.50(3)
Ca(2)-N(5)	2.582(12)	C(13)-C(14)	1.49(3)
Ca(2)-N(9)	2.596(12)	C(15)-C(16)	1.45(3)
Ca(2)-N(7)	2.615(12)		

Table A.91: Selected bond angles for $[Ca(en)_4]_2(As_2Se_7O)$.

Atoms 1, 2, 3	Angle / °	Atoms 1, 2, 3	Angle / °
Se(2)-As(1)-Se(3)	113.73(8)	C(6)-N(6)-Ca(2)	114.2(10)
Se(2)-As(1)-Se(1)	114.28(7)	C(7)-N(7)-Ca(2)	110.9(9)
Se(3)-As(1)-Se(1)	113.24(8)	C(8)-N(8)-Ca(2)	114.3(9)
Se(2)-As(1)-Se(4)	110.65(8)	C(9)-N(9)-Ca(2)	114.3(9)
Se(3)-As(1)-Se(4)	107.34(7)	C(10)-N(10)-Ca(2)	111.2(9)
Se(1)-As(1)-Se(4)	95.96(8)	C(11)-N(11)-Ca(2)	112.2(9)
O(1)-As(2)-Se(7)	120.2(3)	C(12)-N(12)-Ca(2)	114.3(9)
O(1)-As(2)-Se(8)	108.8(3)	C(6)-C(5)-N(5)	111.7(14)
Se(7)-As(2)-Se(8)	106.27(9)	N(6)-C(6)-C(5)	113.3(14)
O(1)-As(2)-Se(5)	120.7(3)	C(8)-C(7)-N(7)	111.9(14)
Se(7)-As(2)-Se(5)	106.63(9)	C(7)-C(8)-N(8)	110.2(12)
Se(8)-As(2)-Se(5)	88.84(8)	N(9)-C(9)-C(10)	110.6(13)
Se(5)-Se(4)-As(1)	105.69(7)	C(9)-C(10)-N(10)	113.3(13)
Se(4)-Se(5)-As(2)	103.57(7)	N(11)-C(11)-C(12)	108.4(13)
C(1)-N(1)-Ca(1)	110.8(9)	N(12)-C(12)-C(11)	110.2(12)
C(2)-N(2)-Ca(1)	114.6(10)	C(13)-N(13)-Ca(3)	106.5(15)
C(3)-N(3)-Ca(1)	112.9(9)	C(14)-N(14)-Ca(3)	111.9(11)
C(4)-N(4)-Ca(1)	111.0(9)	C(15)-N(15)-Ca(3)	106.3(15)
C(2)-C(1)-N(1)	111.7(15)	C(16)-N(16)-Ca(3)	110.6(14)
C(1)-C(2)-N(2)	112.7(15)	C(14)-C(13)-N(13)	113.3(17)
N(3)-C(3)-C(4)	111.7(12)	N(14)-C(14)-C(13)	106.3(17)
N(4)-C(4)-C(3)	110.7(12)	N(15)-C(15)-C(16)	120.9(19)
C(5)-N(5)-Ca(2)	111.5(9)	C(15)-C(16)-N(16)	111.4(18)

A.1.19 [Ca(en)₃(H₂O)₂]As₂Se₄

Table A.92: Single crystal data and refinement for [Ca(en)$_3$(H$_2$O)$_2$]As$_2$Se$_4$.

Empirical formula	C$_6$ H$_{28}$ As$_2$ Ca N$_6$ O$_2$ Se$_4$
Formula weight / *g/mol*	722.10
Temperature / *K*	123(3)
Crystal system; Space group	Hexagonal; *P*6$_1$22
Lattice constants / *Å*	a = 9.8708(3)
	c = 40.2274(12)
Volume / *Å^3*	3394.4(2)
Z; F(000); calc. density / *g/cm^3*	6; 2064; 2.120
Wavelength / *Å*	0.71073
Crystal size / *mm*	$0.170 \times 0.114 \times 0.100$
Theta range for data collection / °	3.128 to 34.945
Limiting indices	-15 ≤ h ≤ 15, -13 ≤ k ≤ 13, -49 ≤ l ≤ 64
Reflections collected / unique	10538 / 4300
Completeness to ϑ = 25.242	91.3 %
R$_{int}$	5.67 %
Absorption coefficient / *mm^{-1}*	9.623
Refinement method	Full-matrix least-squares on F^2
Data / restrains / parameters	4300 / 0 / 111
R indices (all data) R_1 ; wR_2	0.0584; 0.0741
R indices [$I > 4\sigma(I)$] R_1 ; wR_2	0.0376; 0.0689 (for 3378 reflections)
Godness-of-fit for F^2	0.963
Largest diff. peak and hole / *e $^-$/A^3*	0.671 and -0.716
Absolute structure parameter	0.03(2)

Table A.93: Fractional coordinates ($\cdot\ 10^4$) and equivalent isotropic displacement parameter U_{eq} ($\mathring{A}^2 \cdot 10^3$) for the independent atoms in the structure of $[Ca(en)_3(H_2O)_2]As_2Se_4$.

	Wyck.	*x*	*y*	*z*	U_{eq}
As(1)	12*c*	2694(1)	1733(1)	6270(1)	16(1)
Se(3)	6*a*	552(1)	552(1)	6667	19(1)
Se(2)	6*b*	771(1)	386(1)	5833	19(1)
Se(1)	12*c*	4012(1)	354(1)	6308(1)	21(1)
Ca(1)	6*b*	-728(1)	4636(1)	5833	16(1)
N(3)	12*c*	1816(5)	4714(5)	6037(1)	28(1)
O(1)	12*c*	-1567(5)	2312(5)	6238(1)	49(1)
N(1)	12*c*	-69(5)	6401(5)	6355(1)	26(1)
N(2)	12*c*	-3172(5)	4522(5)	6093(1)	30(1)
C(1)	12*c*	-1477(6)	6130(6)	6536(2)	30(1)
C(3)	12*c*	3235(6)	6276(6)	5999(2)	37(2)
C(2)	12*c*	-2743(7)	5910(7)	6303(2)	32(2)
C(2A)	12*c*	-2770(60)	4770(60)	6512(15)	32(2)

Table A.94: Anisotropic displacement parameters U_{ij} / $\mathring{A}^2 \cdot 10^3$ for the independent atoms in the structure of $[Ca(en)_3(H_2O)_2]As_2Se_4$.

	U_{11}	U_{22}	U_{33}	U_{23}	U_{13}	U_{12}
As(1)	20(1)	16(1)	13(1)	0(1)	0(1)	10(1)
Se(3)	21(1)	21(1)	15(1)	-2(1)	2(1)	11(1)
Se(2)	21(1)	23(1)	12(1)	-1(1)	0	10(1)
Se(1)	22(1)	23(1)	23(1)	3(1)	3(1)	14(1)
Ca(1)	16(1)	17(1)	14(1)	0(1)	0	8(1)
N(3)	33(2)	24(2)	31(3)	-4(2)	-8(2)	18(2)
O(1)	34(2)	45(2)	64(4)	17(2)	3(2)	18(2)
N(1)	24(2)	25(2)	22(3)	-2(2)	2(2)	7(2)
N(2)	24(2)	31(2)	30(3)	-5(2)	0(2)	11(2)
C(1)	28(2)	29(2)	30(4)	-4(2)	8(2)	12(2)
C(3)	23(2)	31(3)	59(5)	-17(3)	-11(2)	16(2)

C(2)	36(3)	34(3)	32(4)	-9(3)	1(3)	23(3)
C(2A)	36(3)	34(3)	32(4)	-9(3)	1(3)	23(3)

Table A.95: Selected bond lengths for [Ca(en)$_3$(H$_2$O)$_2$]As$_2$Se$_4$. Symmetry transformations used to generate equivalent atoms: #1 x, x-y+1, $-z$+$^7/_6$ #2 y, x, $-z$+$^4/_3$ #3 x, x-y, $-z$+$^7/_6$.

Atoms 1, 2	Distance / Å	Atoms 1, 2	Distance / Å
As(1)-Se(1)	2.3108(6)	Ca(1)-N(3)	2.606(4)
As(1)-Se(3)	2.4312(6)	Ca(1)-N(3)#1	2.606(4)
As(1)-Se(2)	2.4359(6)	N(3)-C(3)	1.484(6)
Ca(1)-N(2)	2.580(4)	N(1)-C(1)	1.470(6)
Ca(1)-N(2)#1	2.580(4)	N(2)-C(2)	1.479(7)
Ca(1)-O(1)	2.589(5)	N(2)-C(2A)	1.72(6)
Ca(1)-O(1)#1	2.589(5)	C(1)-C(2A)	1.31(5)
Ca(1)-N(1)	2.594(4)	C(1)-C(2)	1.489(8)
Ca(1)-N(1)#1	2.594(4)	C(3)-C(3)#1	1.496(13)

Table A.96: Selected bond angles for [Ca(en)$_3$(H$_2$O)$_2$]As$_2$Se$_4$. Symmetry transformations used to generate equivalent atoms: #1 x, x-y+1, $-z$+$^7/_6$ #2 y, x, $-z$+$^4/_3$ #3 x, x-y, $-z$+$^7/_6$.

Atoms 1, 2, 3	Angle / °	Atoms 1, 2, 3	Angle / °
Se(1)-As(1)-Se(3)	106.57(2)	C(2)-N(2)-Ca(1)	111.2(3)
Se(1)-As(1)-Se(2)	103.90(2)	C(2A)-N(2)-Ca(1)	104.3(17)
Se(3)-As(1)-Se(2)	87.594(19)	C(2A)-C(1)-N(1)	120(2)
As(1)#2-Se(3)-As(1)	95.16(3)	N(1)-C(1)-C(2)	111.3(5)
As(1)#3-Se(2)-As(1)	95.11(3)	N(3)-C(3)-C(3)#1	110.3(4)
C(3)-N(3)-Ca(1)	113.1(3)	N(2)-C(2)-C(1)	109.0(4)
C(1)-N(1)-Ca(1)	112.5(3)	C(1)-C(2A)-N(2)	105(4)

A.1.20 [Sr(en)₃(H₂O)₂]As₂Se₄

Table A.97: Single crystal data and refinement for [Sr(en)$_3$(H$_2$O)$_2$]As$_2$Se$_4$.

Empirical formula	C$_6$ H$_{28}$ As$_2$ Sr N$_6$ O$_2$ Se$_4$
Formula weight / *g/mol*	722.10
Temperature / *K*	123(3)
Crystal system; Space group	Hexagonal; *P*6$_1$22
Lattice constants / Å	*a* = 9.9512(3)
	c = 40.1420(11)
Volume / *Å³*	3442.6(2)
Z; F(000); calc. density / *g/cm³*	6; 2172; 2.227
Wavelength / Å	0.71073
Crystal size / *mm*	0.320 × 0.114 × 0.094
Theta range for data collection / °	3.116 to 27.600
Limiting indices	-12 ≤ *h* ≤ 12, -12 ≤ *k* ≤ 12, -52 ≤ *l* ≤ 52
Reflections collected / unique	22295 / 2644
Completeness to ϑ = 25.242	99.6 %
R$_{int}$	9.20 %
Absorption coefficient / *mm⁻¹*	11.564
Refinement method	Full-matrix least-squares on F^2
Data / restrains / parameters	2644 / 0 / 111
R indices (all data) R_1 ; wR_2	0.0328; 0.0629
R indices [*I* > 4σ(*I*)] R_1 ; wR_2	0.0273; 0.0610 (for 2402 reflections)
Godness-of-fit for F^2	1.078
Largest diff. peak and hole / *e⁻/A³*	0.510 and -0.395
Absolute structure parameter	-0.03(2)

Table A.98: Fractional coordinates ($\cdot$ 10^4) and equivalent isotropic displacement parameter U_{eq} ($\text{Å}^2 \cdot 10^3$) for the independent atoms in the structure of $[Sr(en)_3(H_2O)_2]As_2Se_4$.

	Wyck.	x	y	z	U_{eq}
As(1)	12*c*	-953(1)	1669(1)	3729(1)	21(1)
Se(1)	12*c*	-3616(1)	303(1)	3692(1)	28(1)
Se(2)	6*b*	-366(1)	366(1)	4167	25(1)
Se(3)	6*a*	0	506(1)	3333	24(1)
Sr(1)	6*b*	5370(1)	4630(1)	4167	21(1)
N(3)	12*c*	2835(6)	4759(6)	3961(1)	35(1)
C(3)	12*c*	3018(8)	6316(8)	3998(2)	50(2)
O(1)	12*c*	7873(7)	6214(7)	4559(2)	57(1)
C(1)	12*c*	7664(8)	6173(9)	3445(2)	42(2)
N(1)	12*c*	6545(7)	6433(6)	3620(1)	38(1)
N(2)	12*c*	7685(7)	4426(7)	3867(1)	41(1)
C(2)	12*c*	8656(13)	5833(14)	3668(3)	43(2)
C(2)	12*c*	7550(20)	4680(20)	3479(4)	43(2)

Table A.99: Anisotropic displacement parameters U_{ij} / $\text{Å}^2 \cdot 10^3$ for the independent atoms in the structure of $[Sr(en)_3(H_2O)_2]As_2Se_4$.

	U_{11}	U_{22}	U_{33}	U_{23}	U_{13}	U_{12}
As(1)	21(1)	21(1)	18(1)	0(1)	1(1)	7(1)
Se(1)	20(1)	29(1)	33(1)	-2(1)	1(1)	11(1)
Se(2)	30(1)	30(1)	17(1)	1(1)	1(1)	16(1)
Se(3)	23(1)	27(1)	20(1)	2(1)	3(1)	12(1)
Sr(1)	22(1)	22(1)	21(1)	-2(1)	-2(1)	11(1)
N(3)	26(2)	31(3)	43(3)	8(2)	-4(2)	11(2)
C(3)	29(3)	45(4)	85(5)	24(4)	3(3)	24(3)
O(1)	60(3)	50(3)	65(4)	-14(3)	-19(3)	30(3)

C(1)	46(4)	43(4)	42(4)	4(3)	14(3)	26(3)
N(1)	46(3)	39(3)	32(3)	6(2)	14(2)	25(3)
N(2)	38(3)	48(3)	51(3)	7(3)	6(3)	31(3)
C(2)	33(5)	40(5)	53(6)	10(5)	13(4)	16(4)
C(2)	33(5)	40(5)	53(6)	10(5)	13(4)	16(4)

Table A.100: Selected bond lengths for [Sr(en)$_3$(H$_2$O)$_2$]As$_2$Se$_4$. Symmetry transformations used to generate equivalent atoms: #1 -y+1, -x+1, -z+$^5/_6$ #2 -y+2, -x+2, -z+$^5/_6$ #3 -x+2, -x+y+1, -z+$^2/_3$.

Atoms 1, 2	Distance / Å	Atoms 1, 2	Distance / Å
As(1)-Se(2)	2.3078(11)	Sr(1)-O(1)#1	2.716(7)
As(1)-Se(3)	2.4313(11)	Sr(1)-N(3)	2.726(6)
As(1)-Se(1)	2.4353(11)	Sr(1)-N(3)#1	2.727(6)
Sr(1)-N(2)	2.710(7)	N(1)-C(1)	1.419(13)
Sr(1)-N(2)#1	2.710(7)	N(2)-C(2)	1.446(13)
Sr(1)-N(1)#1	2.709(7)	N(3)-C(3)	1.461(11)
Sr(1)-N(1)	2.709(7)	C(1)-C(2)	1.514(16)
Sr(1)-O(1)	2.716(7)	C(3)-C(3)#1	1.56(3)

Table A.101: Selected bond angles for [Sr(en)$_3$(H$_2$O)$_2$]As$_2$Se$_4$. Symmetry transformations used to generate equivalent atoms: #1 -y+1, -x+1, -z+$^5/_6$ #2 -y+2, -x+2, -z+$^5/_6$ #3 -x+2, -x+y+1, -z+$^2/_3$.

Atoms 1, 2, 3	Angle / °	Atoms 1, 2, 3	Angle / °
Se(2)-As(1)-Se(3)		C(2)-N(2)-Sr(1)	
Se(2)-As(1)-Se(1)		C(3)-N(3)-Sr(1)	
Se(3)-As(1)-Se(1)		N(1)-C(1)-C(2)	
As(1)-Se(1)-As(1)#2		N(2)-C(2)-C(1)	
As(1)#3-Se(3)-As(1)		N(3)-C(3)-C(3)#1	
C(1)-N(1)-Sr(1)			

A.1.21 [Eu(NH₃)₈][Cu(S₄)₂]·NH₃

Table A.102: Single crystal data and refinement for [Eu(NH$_3$)$_8$][Cu(S$_4$)$_2$]·NH$_3$.

Empirical formula	Cu Eu H$_{27}$ N$_9$ S$_8$
Formula weight / *g/mol*	636.25
Temperature / *K*	123(3)
Crystal system; Space group	Tetragonal; $I\bar{4}$
Lattice constants / *Å*	$a = 10.0716(1)$
	$c = 9.8677(2)$
Volume / *Å³*	1000.95(3)
Z; F(000); calc. density / *g/cm³*	2, 628 ; 2.111
Wavelength / *Å*	0.71073
Crystal size / *mm*	$0.146 \times 0.100 \times 0.080$
Theta range for data collection / °	4.047 to 27.449
Limiting indices	$-13 \le h \le 12, -13 \le k \le 13, -12 \le l \le 12$
Reflections collected / unique	9337 / 1148
Completeness to $\vartheta = 25.242$	99.6 %
R$_{int}$	7.56 %
Absorption coefficient / *mm⁻¹*	5.005
Refinement method	Full-matrix least-squares on F^2
Data / restrains / parameters	1148 / 0 / 52
R indices (all data) R_1 ; wR_2	0.0166; 0.0353
R indices [$I > 4\sigma(I)$] R_1 ; wR_2	0.0166; 0.0353 (for 1147 reflections)
Godness-of-fit for F^2	1.178
Largest diff. peak and hole / e^-/A^3	0.410 and -0.403
Absolute structure parameter	-0.02431

Table A.103: Fractional coordinates ($\cdot\ 10^4$) and equivalent isotropic displacement parameter U_{eq} ($\text{Å}^2 \cdot 10^3$) for the independent atoms in the structure of $[Eu(NH_3)_8][Cu(S_4)_2]\cdot NH_3$.

	Wyck.	x	y	z	U_{eq}
Eu(1)	2a	5000	5000	5000	12(1)
N(1)	8g	3942(5)	3739(5)	3047(4)	18(1)
N(2)	8g	3493(4)	3202(5)	5971(4)	19(1)
Cu(1)	2c	0	5000	2500	17(1)
S(3)	8g	-186(1)	3977(1)	5843(1)	19(1)
S(1)	8g	587(1)	3337(1)	4018(1)	18(1)
N(4)	4e	5000	5000	337(7)	24(2)

Table A.104: Anisotropic displacement parameters U_{ij} / $\text{Å}^2 \cdot 10^3$ for the independent atoms in the structure of $[Eu(NH_3)_8][Cu(S_4)_2]\cdot NH_3$.

	U_{11}	U_{22}	U_{33}	U_{23}	U_{13}	U_{12}
Eu(1)	12(1)	12(1)	11(1)	0	0	0
N(1)	21(3)	15(3)	17(2)	1(2)	1(2)	1(2)
N(2)	22(3)	16(2)	18(2)	0(2)	-2(2)	0(2)
Cu(1)	19(1)	19(1)	12(1)	0	0	0
S(3)	20(1)	24(1)	13(1)	3(1)	1(1)	1(1)
S(1)	19(1)	19(1)	15(1)	1(1)	1(1)	2(1)
N(4)	34(10)	28(9)	9(5)	0	0	-16(9)

Table A.105: Selected bond lengths for $[Eu(NH_3)_8][Cu(S_4)_2]\cdot NH_3$. Symmetry transformations used to generate equivalent atoms: #1 $-y+1, x, -z+1$ #2 $y, -x+1, -z+1$ #3 $-x+1, -y+1, z$ #4 $y-\frac{1}{2}, -x+\frac{1}{2}, -z+\frac{1}{2}$ #5 $-x, -y+1, z$ #6 $-y+\frac{1}{2}, x+\frac{1}{2}, -z+\frac{1}{2}$ #7 $y, -x+1, -z$.

Atoms 1, 2	Distance / Å	Atoms 1, 2	Distance / Å
Eu(1)-N(1)	2.542(4)	Cu(1)-S(1)	2.3236(13)
Eu(1)-N(1)#1	2.542(4)	Cu(1)-S(1)#4	2.3236(13)
Eu(1)-N(1)#2	2.542(4)	Cu(1)-S(1)#5	2.3236(13)
Eu(1)-N(1)#3	2.542(4)	Cu(1)-S(1)#6	2.3236(13)
Eu(1)-N(2)	2.550(4)	S(3)-S(1)	2.0650(16)

Eu(1)-N(2)#3	2.550(4)	S(3)-S(3)#5	2.094(3)
Eu(1)-N(2)#2	2.550(4)	N(4)-N(4)#7	0.664(14)
Eu(1)-N(2)#1	2.550(4)		

Table A.106: Selected bond angles for $[Eu(NH_3)_8][Cu(S_4)_2] \cdot NH_3$. Symmetry transformations used to generate equivalent atoms: #1 $-y+1, x, -z+1$ #2 $y, -x+1, -z+1$ #3 $-x+1, -y+1, z$ #4 $y-^1/_2, -x+^1/_2, -z+^1/_2$ #5 $-x, -y+1, z$ #6 $-y+^1/_2, x+^1/_2, -z+^1/_2$ #7 $y, -x+1, -z$.

Atoms 1, 2, 3	Angle / °	Atoms 1, 2, 3	Angle / °
S(1)-Cu(1)-S(1)#4	114.56(3)	S(1)#4-Cu(1)-S(1)#6	99.72(6)
S(1)-Cu(1)-S(1)#5	99.72(6)	S(1)#5-Cu(1)-S(1)#6	114.56(3)
S(1)#4-Cu(1)-S(1)#5	114.56(3)	S(1)-S(3)-S(3)#5	103.89(6)
S(1)-Cu(1)-S(1)#6	114.56(3)	S(3)-S(1)-Cu(1)	103.96(6)

A.1.22 [Er(NH₃)₈][Cu(S₄)₂]·NH₃

Table A.107: Single crystal data and refinement for [Er(NH$_3$)$_8$][Cu(S$_4$)$_2$]·NH$_3$.

Empirical formula	Cu Er H$_{27}$ N$_9$ S$_8$
Formula weight / *g/mol*	651.57
Temperature / *K*	123(3)
Crystal system; Space group	Tetragonal; $I\bar{4}$
Lattice constants / $\mathring{A}$	a = 10.0096(3)
	c = 9.8212(3)
Volume / $\mathring{A}^3$	984.01(7)
Z; F(000); calc. density / *g/cm^3*	2, 638 ; 2.111
Wavelength / $\mathring{A}$	0.71073
Crystal size / *mm*	$0.146 \times 0.100 \times 0.080$
Theta range for data collection / °	4.072 to 27.498
Limiting indices	$-13 \leq h \leq 12$, $-12 \leq k \leq 12$, $-12 \leq l \leq 12$
Reflections collected / unique	3611 / 1083
Completeness to ϑ = 25.242	99.4 %
R$_{int}$	15.92 %
Absorption coefficient / *mm^{-1}*	6.168
Refinement method	Full-matrix least-squares on F^2
Data / restrains / parameters	1083 / 0 / 49
R indices (all data) R_1 ; *wR$_2$*	0.0465; 0.1219
R indices [$I > 4\sigma(I)$] R_1 ; *wR$_2$*	0.0460; 0.1215 (for 1068 reflections)
Godness-of-fit for F^2	1.178
Largest diff. peak and hole / *e$^-$/A^3*	1.468 and -1.406
Absolute structure parameter	-0.012(19)

Table A.108: Fractional coordinates ($\cdot\ 10^4$) and equivalent isotropic displacement parameter U_{eq} ($\text{Å}^2 \cdot 10^3$) for the independent atoms in the structure of $[Er(NH_3)_8][Cu(S_4)_2] \cdot NH_3$.

	Wyck.	x	y	z	U_{eq}
Cu(1)	2c	0	5000	7500	16(1)
S(1)	8g	605(3)	3331(3)	5980(3)	15(1)
S(2)	8g	-181(3)	3971(3)	4151(3)	17(1)
Er(1)	2a	5000	5000	5000	10(1)
N(1)	8g	3527(12)	3217(10)	4061(10)	17(2)
N(2)	8g	6031(10)	6250(11)	6924(10)	17(2)
N(3)	4e	5000	5000	9620(20)	78(11)

Table A.109: Anisotropic displacement parameters U_{ij} / $\text{Å}^2 \cdot 10^3$ for the independent atoms in the structure of $[Er(NH_3)_8][Cu(S_4)_2] \cdot NH_3$.

	U_{11}	U_{22}	U_{33}	U_{23}	U_{13}	U_{12}
Cu(1)	21(1)	21(1)	7(1)	0	0	0
S(1)	18(1)	18(2)	11(1)	-1(1)	-1(1)	2(1)
S(2)	15(2)	26(2)	11(1)	-2(1)	0(1)	0(1)
Er(1)	12(1)	12(1)	7(1)	0	0	0
N(1)	25(5)	11(4)	16(5)	-4(4)	1(4)	0(4)
N(2)	13(5)	20(5)	17(5)	2(4)	-7(4)	-7(4)
N(3)	150(40)	34(16)	54(17)	0	0	10(20)

Table A.110: Selected bond lengths for $[Er(NH_3)_8][Cu(S_4)_2] \cdot NH_3$. Symmetry transformations used to generate equivalent atoms: #1 $-y+\frac{1}{2}, x+\frac{1}{2}, -z+\frac{3}{2}$ #2 $-x, -y+1, z$ #3 $y-\frac{1}{2}, -x+\frac{1}{2}, -z+\frac{3}{2}$ #4 $-y+1, x, -z+1$ #5 $y, -x+1, -z+1$ #6 $-x+1, -y+1, z$ #7 $y, -x+1, -z+2$.

Atoms 1, 2	Distance / Å	Atoms 1, 2	Distance / Å
Cu(1)-S(1)	2.321(3)	Er(1)-N(2)#5	2.490(10)
Cu(1)-S(1)#1	2.321(3)	Er(1)-N(2)#6	2.490(10)
Cu(1)-S(1)#2	2.321(3)	Er(1)-N(1)	2.492(11)
Cu(1)-S(1)#3	2.321(3)	Er(1)-N(1)#6	2.492(11)

S(1)-S(2)	2.062(4)	Er(1)-N(1)#4	2.492(11)
S(2)-S(2)#2	2.092(7)	Er(1)-N(1)#5	2.492(11)
Er(1)-N(2)	2.490(10)	N(3)-N(3)#7	0.75(4)
Er(1)-N(2)#4	2.490(10)		

Table A.111: Selected bond angles for $[Er(NH_3)_8][Cu(S_4)_2] \cdot NH_3$. Symmetry transformations used to generate equivalent atoms: #1 $-y+^1/_2, x+^1/_2, -z+^3/_2$ #2 $-x, -y+1, z$ #3 $y-^1/_2, -x+^1/_2, -z+^3/_2$ #4 $-y+1, x, -z+1$ #5 $y, -x+1, -z+1$ #6 $-x+1, -y+1, z$ #7 $y, -x+1, -z+2$.

Atoms 1, 2, 3	Angle / °	Atoms 1, 2, 3	Angle / °
S(1)-Cu(1)-S(1)#1	114.45(8)	S(1)#1-Cu(1)-S(1)#3	99.92(14)
S(1)-Cu(1)-S(1)#2	99.92(14)	S(1)#2-Cu(1)-S(1)#3	114.45(8)
S(1)#1-Cu(1)-S(1)#2	114.45(8)	S(2)-S(1)-Cu(1)	103.73(15)
S(1)-Cu(1)-S(1)#3	114.45(8)	S(1)-S(2)-S(2)#2	103.87(14)

A.1.23 [Eu(NH$_3$)$_9$][Ag(Se$_4$)$_2$]·2NH$_3$

Table A.112: Single crystal data and refinement for [Eu(NH$_3$)$_9$][Ag(Se$_4$)$_2$]·2NH$_3$.

Empirical formula	Ag Eu H$_{33}$ N$_{11}$ Se$_8$
Formula weight / *g/mol*	1078.88
Temperature / *K*	123(3)
Crystal system; Space group	Tetragonal; $P\bar{4}n2$
Lattice constants / Å	$a = 15.2120(7)$
	$c = 11.2754(6)$
Volume / Å^3	2609.2(3)
Z; F(000); calc. density / *g/cm^3*	4; 1968; 2.746
Wavelength / Å	0.71073
Crystal size / *mm*	$0.024 \times 0.028 \times 0.060$
Theta range for data collection / °	2.994 to 27.494
Limiting indices	$-19 \leq h \leq 19$, $-19 \leq k \leq 19$, $-14 \leq l \leq 13$
Reflections collected / unique	27912 / 3003
Completeness to $\vartheta = 25.242$	99.7 %
R$_{int}$	20.00 %
Absorption coefficient / *mm^{-1}*	14.300
Refinement method	Full-matrix least-squares on F^2
Data / restrains / parameters	3003 / 0 / 103
R indices (all data) R_1 ; wR_2	0.1364; 0.1583
R indices [$I > 4\sigma(I)$] R_1 ; wR_2	0.0684; 0.1418 (for 2872 reflections)
Godness-of-fit for F^2	1.072
Largest diff. peak and hole / *e$^-$/A^3*	2.051 and -1.235
Absolute structure parameter	0.02(3)

Table A.113: Fractional coordinates ($\cdot$ 10^4) and equivalent isotropic displacement parameter U_{eq} ($\text{Å}^2 \cdot 10^3$) for the independent atoms in the structure of $[Eu(NH_3)_9][Ag(Se_4)_2] \cdot 2NH_3$.

	Wyck.	*x*	*y*	*z*	U_{eq}
Eu(1)	4*f*	2767(1)	7767(1)	7500	31(1)
N(1)	8*i*	2880(20)	6176(13)	6710(20)	57(8)
N(2)	8*i*	4207(15)	7171(16)	8350(20)	43(6)
N(3)	4*f*	3929(13)	8929(13)	7500	28(7)
N(4)	8*i*	2723(16)	8688(14)	9430(20)	40(6)
N(5)	8*i*	2497(16)	6644(18)	9260(30)	52(7)
Ag(1)	4*g*	2659(1)	7660(1)	2500	36(1)
Se(1)	8*i*	2617(2)	6073(2)	3547(3)	33(1)
Se(2)	8*i*	4107(2)	5682(2)	3456(3)	34(1)
Se(3)	8*i*	4495(2)	6096(2)	1503(3)	36(1)
Se(4)	8*i*	4252(2)	7615(2)	1523(3)	37(1)
N(6)	8*i*	3990(20)	10331(18)	5960(30)	81(11)

Table A.114: Anisotropic displacement parameters U_{ij} / Å^2 $\cdot$ 10^3 for the independent atoms in the structure of $[Eu(NH_3)_9][Ag(Se_4)_2] \cdot 2NH_3$.

	U_{11}	U_{22}	U_{33}	U_{23}	U_{13}	U_{12}
Eu(1)	31(1)	31(1)	31(1)	-1(1)	1(1)	11(1)
N(1)	120(20)	13(12)	39(16)	-7(12)	4(17)	-3(13)
N(2)	40(14)	56(16)	34(15)	15(14)	5(12)	18(12)
N(3)	35(10)	35(10)	15(14)	1(12)	-1(12)	-1(13)
N(4)	49(16)	26(13)	45(15)	-2(12)	12(14)	3(11)
N(5)	38(15)	64(18)	55(18)	-6(16)	5(13)	-7(13)
Ag(1)	35(1)	35(1)	38(2)	-1(1)	1(1)	13(1)
Se(1)	28(1)	30(1)	40(2)	-3(2)	4(2)	6(1)
Se(2)	29(2)	30(2)	44(2)	2(2)	-1(2)	5(1)
Se(3)	29(2)	37(2)	41(2)	-3(2)	0(2)	4(1)
Se(4)	34(2)	31(2)	45(2)	6(2)	2(2)	5(1)
N(6)	100(30)	40(17)	100(30)	27(16)	-40(20)	-41(17)

Table A.115: Selected bond lengths for [Eu(NH$_3$)$_9$][Ag(Se$_4$)$_2$]·2NH$_3$. Symmetry transformations used to generate equivalent atoms: #1 y-$\frac{1}{2}$, x+$\frac{1}{2}$, -z+$\frac{3}{2}$ #2 y-$\frac{1}{2}$, x+$\frac{1}{2}$, -z+$\frac{1}{2}$.

Atoms 1, 2	Distance / Å	Atoms 1, 2	Distance / Å
Eu(1)-N(3)	2.50(3)	Eu(1)-N(5)	2.65(3)
Eu(1)-N(2)	2.56(2)	Ag(1)-Se(4)	2.662(3)
Eu(1)-N(2)#1	2.56(2)	Ag(1)-Se(4)#2	2.662(3)
Eu(1)-N(1)#1	2.58(2)	Ag(1)-Se(1)#2	2.687(3)
Eu(1)-N(1)	2.58(2)	Ag(1)-Se(1)	2.687(3)
Eu(1)-N(4)	2.59(2)	Se(1)-Se(2)	2.345(3)
Eu(1)-N(4)#1	2.59(2)	Se(2)-Se(3)	2.365(4)
Eu(1)-N(5)#1	2.65(3)	Se(3)-Se(4)	2.341(4)

Table A.116: Selected bond angles for [Eu(NH$_3$)$_9$][Ag(Se$_4$)$_2$]·2NH$_3$. Symmetry transformations used to generate equivalent atoms: #1 y-$\frac{1}{2}$, x+$\frac{1}{2}$, -z+$\frac{3}{2}$ #2 y-$\frac{1}{2}$, x+$\frac{1}{2}$, -z+$\frac{1}{2}$.

Atoms 1, 2, 3	Angle / °	Atoms 1, 2, 3	Angle / °
Se(4)-Ag(1)-Se(4)#2	102.54(16)	Se(1)#2-Ag(1)-Se(1)	98.62(15)
Se(4)-Ag(1)-Se(1)#2	129.42(9)	Se(2)-Se(1)-Ag(1)	100.69(13)
Se(4)#2-Ag(1)-Se(1)#2	100.41(8)	Se(1)-Se(2)-Se(3)	102.39(15)
Se(4)-Ag(1)-Se(1)	100.41(8)	Se(4)-Se(3)-Se(2)	102.34(15)
Se(4)#2-Ag(1)-Se(1)	129.42(9)	Se(3)-Se(4)-Ag(1)	99.95(13)

A.1.24 [Yb(NH$_3$)$_8$](AuSe$_5$S$_7$)·NH$_3$

Table A.117: Single crystal data and refinement for [Yb(NH$_3$)$_8$](AuSe$_5$S$_7$)·NH$_3$.

Empirical formula	Au H$_{27}$ N$_9$ S$_7$ Se$_5$ Yb
Formula weight / *g/mol*	1142.53
Temperature / *K*	123(2)
Crystal system; Space group	Triclinic; $\overline{1}$
Lattice constants / *Å*	a = 9.1610(3); α = 87.445(2)°
	b = 9.5272(2); β = 84.318(1)°
	c = 15.4891(5); γ = 67.723(2)°
Volume / *Å^3*	1244.79(7)
Z; F(000); calc. density / *g/cm^3*	2; 1042; 3.048
Wavelength / *Å*	0.71073
Crystal size / *mm*	0.246 × 0.094 × 0.080
Theta range for data collection / °	3.052 to 27.537
Limiting indices	-11 ≤ h ≤ 11, -12 ≤ k ≤ 12, -20 ≤ l ≤ 20
Reflections collected / unique	8805 / 5245
Completeness to ϑ = 25.242	93.3 %
R$_{int}$	10.71 %
Absorption coefficient / *mm^{-1}*	17.392
Refinement method	Full-matrix least-squares on F^2
Data / restrains / parameters	5245 / 0 / 220
R indices (all data) R_1 ; wR_2	0.0633; 0.1718
R indices [I > 4σ(I)] R_1 ; wR_2	0.0588; 0.1681 (for 4787 reflections)
Godness-of-fit for F^2	1.049
Largest diff. peak and hole / *e$^-$/A^3*	3.346 and -5.152

Table A.118: Fractional coordinates ($\cdot \, 10^4$) and equivalent isotropic displacement parameter U_{eq} ($\text{Å}^2 \cdot 10^3$) for the independent atoms in the structure of $[Yb(NH_3)_8](AuSe_5S_7) \cdot NH_3$.

	Wyck.	*x*	*y*	*z*	U_{eq}
Au(1)	1*b*	10000	0	5000	14(1)
Au(2)	1*h*	5000	5000	5000	15(1)
Se(1)	2*i*	7543(2)	4221(2)	5639(1)	28(1)
Se(2)	2*i*	9576(2)	2707(2)	4712(1)	24(1)
Se(3)	2*i*	3587(2)	6425(2)	6322(1)	25(1)
Se(4)	2*i*	7626(2)	830(2)	5981(1)	43(1)
S(1)	2*i*	7365(4)	-1171(4)	6578(2)	12(1)
S(2)	2*i*	9026(3)	-1829(3)	7573(2)	8(1)
S(3)	2*i*	7537(4)	-1473(4)	8733(2)	20(1)
S(4)	2*i*	6743(4)	721(4)	9162(2)	19(1)
Se(5)	2*i*	5443(3)	6388(3)	7209(2)	56(1)
S(5)	2*i*	5290(4)	4942(4)	8277(3)	24(1)
S(6)	2*i*	3825(4)	6280(4)	9274(2)	20(1)
S(7)	2*i*	1498(4)	6896(4)	8996(2)	15(1)
Yb(1)	2*i*	1489(1)	2176(1)	8054(1)	12(1)
N(1)	2*i*	2053(16)	507(15)	6791(9)	27(3)
N(2)	2*i*	3639(15)	-202(14)	8416(9)	24(3)
N(3)	2*i*	3915(14)	2443(14)	7356(8)	20(2)
N(4)	2*i*	2665(13)	2925(13)	9214(7)	15(2)
N(5)	2*i*	715(16)	4172(15)	6923(8)	25(3)
N(6)	2*i*	-554(14)	4383(14)	8822(8)	21(2)
N(7)	2*i*	-1052(14)	2131(14)	7682(8)	21(2)
N(8)	2*i*	591(14)	874(13)	9223(7)	18(2)
N(9)	2*i*	3709(17)	1912(17)	5345(9)	30(3)

Table A.119: Anisotropic displacement parameters U_{ij} / Å^2 · 10^3 for the independent atoms in the structure of [Yb(NH$_3$)$_8$](AuSe$_5$S$_7$)·NH$_3$.

	U_{11}	U_{22}	U_{33}	U_{23}	U_{13}	U_{12}
Au(1)	14(1)	14(1)	13(1)	0(1)	-3(1)	-5(1)
Au(2)	18(1)	13(1)	15(1)	0(1)	1(1)	-7(1)
Se(1)	27(1)	26(1)	29(1)	-1(1)	-3(1)	-7(1)
Se(2)	23(1)	21(1)	26(1)	1(1)	-1(1)	-7(1)
Se(3)	27(1)	22(1)	25(1)	-2(1)	1(1)	-8(1)
Se(4)	41(1)	47(1)	41(1)	1(1)	-1(1)	-16(1)
S(1)	15(1)	14(1)	8(1)	2(1)	-1(1)	-6(1)
S(2)	13(1)	5(1)	5(1)	0(1)	2(1)	-3(1)
S(3)	20(2)	20(2)	18(2)	5(1)	0(1)	-7(1)
S(4)	14(1)	23(2)	20(2)	0(1)	-1(1)	-8(1)
Se(5)	59(1)	53(1)	59(1)	-10(1)	8(1)	-28(1)
S(5)	15(2)	14(2)	42(2)	-6(1)	-3(1)	-4(1)
S(6)	20(2)	19(2)	23(2)	1(1)	-6(1)	-11(1)
S(7)	16(1)	10(1)	19(2)	2(1)	-2(1)	-5(1)
Yb(1)	12(1)	10(1)	14(1)	0(1)	0(1)	-5(1)
N(1)	28(7)	25(7)	29(7)	-11(5)	-2(5)	-10(5)
N(2)	21(6)	14(6)	35(7)	-4(5)	-7(5)	-4(5)
N(3)	20(6)	20(6)	22(6)	-4(5)	3(5)	-13(5)
N(4)	19(5)	13(5)	14(5)	0(4)	-1(4)	-7(4)
N(5)	27(6)	21(6)	27(6)	2(5)	-2(5)	-9(5)
N(6)	15(5)	21(6)	24(6)	-4(5)	-1(4)	-4(5)
N(7)	17(5)	18(6)	29(6)	-2(5)	-5(5)	-8(5)
N(8)	23(6)	17(6)	17(5)	3(4)	-1(4)	-10(5)
N(9)	32(7)	38(8)	29(7)	2(6)	-4(6)	-23(6)

Table A.120: Selected bond lengths for [Yb(NH$_3$)$_8$](AuSe$_5$S$_7$)·NH$_3$. Symmetry transformations used to generate equivalent atoms: #1 -x+2, -y, -z+1 #2 -x+1, -y+1, -z+1.

Atoms 1, 2	Distance / Å	Atoms 1, 2	Distance / Å
Au(1)-Se(4)	2.411(2)	S(3)-S(4)	2.053(5)
Au(1)-Se(4)#1	2.411(2)	Se(5)-S(5)	2.133(5)
Au(1)-Se(2)#1	2.4843(15)	S(5)-S(6)	2.068(5)
Au(1)-Se(2)	2.4843(15)	S(6)-S(7)	2.070(5)
Au(2)-Se(1)#2	2.4571(16)	Yb(1)-N(8)	2.402(11)
Au(2)-Se(1)	2.4571(16)	Yb(1)-N(4)	2.445(11)
Au(2)-Se(3)#2	2.4704(15)	Yb(1)-N(2)	2.459(12)
Au(2)-Se(3)	2.4704(15)	Yb(1)-N(1)	2.465(12)
Se(1)-Se(2)	2.286(2)	Yb(1)-N(7)	2.469(12)
Se(3)-Se(5)	2.279(3)	Yb(1)-N(3)	2.471(11)
Se(4)-S(1)	2.165(4)	Yb(1)-N(5)	2.474(13)
S(1)-S(2)	2.177(4)	Yb(1)-N(6)	2.477(12)
S(2)-S(3)	2.104(4)		

Table A.121: Selected bond angles for [Yb(NH$_3$)$_8$](AuSe$_5$S$_7$)·NH$_3$. Symmetry transformations used to generate equivalent atoms: #1 -x+2, -y, -z+1 #2 -x+1, -y+1, -z+1.

Atoms 1, 2, 3	Angle / °	Atoms 1, 2, 3	Angle / °
Se(4)-Au(1)-Se(4)#1	180.0	Se(3)#2-Au(2)-Se(3)	180.0
Se(4)-Au(1)-Se(2)#1	91.53(6)	Se(2)-Se(1)-Au(2)	111.15(8)
Se(4)#1-Au(1)-Se(2)#1	88.47(6)	Se(1)-Se(2)-Au(1)	109.92(7)
Se(4)-Au(1)-Se(2)	88.47(6)	Se(5)-Se(3)-Au(2)	107.64(9)
Se(4)#1-Au(1)-Se(2)	91.53(6)	S(1)-Se(4)-Au(1)	107.68(12)
Se(2)#1-Au(1)-Se(2)	180.0	Se(4)-S(1)-S(2)	104.23(16)
Se(1)#2-Au(2)-Se(1)	180.0	S(3)-S(2)-S(1)	103.10(17)
Se(1)#2-Au(2)-Se(3)#2	90.90(5)	S(4)-S(3)-S(2)	112.9(2)
Se(1)-Au(2)-Se(3)#2	89.10(5)	S(5)-Se(5)-Se(3)	106.32(15)
Se(1)#2-Au(2)-Se(3)	89.10(5)	S(6)-S(5)-Se(5)	108.2(2)
Se(1)-Au(2)-Se(3)	90.90(5)	S(5)-S(6)-S(7)	108.6(2)

A.1.25 [Yb(NH$_3$)$_8$](AuS$_4$Se$_6$)

Table A.122: Single crystal data and refinement for [Yb(NH$_3$)$_8$](AuS$_4$Se$_6$).

Empirical formula	Au H$_{24}$ N$_8$ S$_4$ Se$_6$ Yb
Formula weight / *g/mol*	1108.28
Temperature / *K*	123(2)
Crystal system; Space group	Monoclinic, *C* 2
Lattice constants / *Å*	*a* = 15.9560(7)
	b = 9.7517(3); *β* = 115.597(2)°
	c = 15.7527(7)
Volume / *Å³*	2210.53(16)
Z; F(000); calc. density / *g/cm³*	4; 1988; 3.330
Wavelength / *Å*	0.71073
Crystal size / *mm*	0.160 × 0.034 × 0.014
Theta range for data collection / °	3.037 to 27.472
Limiting indices	-20 ≤ h ≤ 20, -12 ≤ k ≤ 12, -20 ≤ l ≤ 20
Reflections collected / unique	11698 / 4487
Completeness to ϑ = 25.242	98.3 %
R$_{int}$	9.26 %
Absorption coefficient / *mm⁻¹*	21.092
Refinement method	Full-matrix least-squares on F^2
Data / restrains / parameters	4487 / 1 / 175
R indices (all data) R_1 ; wR_2	0.0816; 0.1860
R indices [$I > 4\sigma(I)$] R_1 ; wR_2	0.0601; 0.1699 (for 3561 reflections)
Godness-of-fit for F^2	1.080
Largest diff. peak and hole / e^-/A^3	4.224 and -2.827
Absolute structure parameter	0.49(3)

Table A.123: Fractional coordinates ($\cdot$ 10^4) and equivalent isotropic displacement parameter U_{eq} ($\text{Å}^2 \cdot 10^3$) for the independent atoms in the structure of [Yb(NH$_3$)$_8$](AuS$_4$Se$_6$).

	Wyck.	*x*	*y*	*z*	U_{eq}
Au(1)	2a	5000	6155(2)	10000	19(1)
S(1)	4c	6283(4)	6105(7)	8522(4)	11(1)
S(2)	4c	6783(4)	8150(7)	8595(4)	14(1)
Se(1)	4c	3280(2)	6064(4)	9387(2)	25(1)
Se(5)	4c	4849(3)	6096(5)	8376(2)	42(1)
Se(2)	4c	2684(2)	5964(5)	7765(2)	40(1)
Au(2)	2b	0	8106(2)	5000	25(1)
Se(3)	4c	2313(3)	8198(5)	7250(2)	45(1)
Se(4)	4c	706(2)	8195(4)	6746(2)	33(1)
Se(6)	4c	1529(3)	8239(5)	5031(3)	56(1)
S(4)	4c	1330(4)	7986(6)	3552(4)	10(1)
S(5)	4c	1745(4)	5879(6)	3467(4)	10(1)
Yb(1)	2b	0	3212(2)	5000	17(1)
N(1)	4c	-913(17)	1910(30)	5728(17)	26(4)
N(2)	4c	-1102(16)	1750(30)	3751(16)	25(4)
N(3)	4c	-211(17)	4510(30)	3592(17)	25(4)
N(4)	4c	1420(17)	4590(30)	5450(17)	26(4)
Yb(2)	2a	10000	6204(2)	10000	19(1)
N(5)	4c	8509(17)	4980(30)	9514(17)	27(5)
N(6)	4c	9840(20)	4720(30)	8688(16)	32(6)
N(7)	4c	8916(17)	7620(30)	8716(15)	28(6)
N(8)	4c	10947(17)	7540(30)	9345(16)	26(5)

Table A.124: Anisotropic displacement parameters U_{ij} / $Å^2 \cdot 10^3$ for the independent atoms in the structure of $[Yb(NH_3)_8](AuS_4Se_6)$.

	U_{11}	U_{22}	U_{33}	U_{23}	U_{13}	U_{12}
Au(1)	24(1)	15(1)	18(1)	0	8(1)	0
S(1)	18(3)	4(3)	16(3)	1(2)	12(2)	0(3)
S(2)	16(3)	14(3)	15(3)	0(2)	11(2)	3(2)
Se(1)	26(2)	23(2)	25(1)	-1(1)	11(1)	-2(1)
Se(5)	54(2)	36(2)	39(2)	-4(2)	23(2)	-3(2)
Se(2)	39(2)	44(2)	28(2)	-7(2)	5(1)	2(2)
Au(2)	34(1)	14(1)	19(1)	0	4(1)	0
Se(3)	50(2)	42(2)	28(2)	2(2)	3(2)	-18(2)
Se(4)	47(2)	19(2)	23(1)	1(1)	7(1)	0(2)
Se(6)	62(3)	48(2)	56(3)	-4(2)	22(2)	-5(2)
S(4)	16(2)	5(2)	10(2)	0(2)	8(2)	-3(2)
S(5)	16(2)	5(2)	10(2)	0(2)	8(2)	-3(2)
Yb(1)	22(1)	14(1)	18(1)	0	10(1)	0
N(1)	30(10)	32(11)	28(9)	-1(8)	25(8)	-1(8)
N(2)	27(9)	24(10)	30(9)	1(7)	16(8)	-10(7)
N(3)	27(9)	24(10)	30(9)	1(7)	16(8)	-10(7)
N(4)	30(10)	32(11)	28(9)	-1(8)	25(8)	-1(8)
Yb(2)	25(1)	14(1)	17(1)	0	10(1)	0
N(5)	25(13)	27(14)	21(12)	-5(10)	3(10)	-2(11)
N(6)	64(19)	13(13)	21(13)	-3(10)	20(13)	3(12)
N(7)	39(15)	34(15)	12(10)	10(10)	11(10)	11(11)
N(8)	38(14)	15(12)	22(12)	-2(9)	10(11)	-2(10)

Table A.125: Selected bond lengths for $[Yb(NH_3)_8](AuS_4Se_6)$. Symmetry transformations used to generate equivalent atoms: #1 $-x+1$, y, $-z+2$ #2 $-x$, y, $-z+1$ #3 $-x+2$, y, $-z+2$.

Atoms 1, 2	Distance / Å	Atoms 1, 2	Distance / Å
Au(1)-Se(5)#1	2.465(3)	Yb(1)-N(3)	2.45(2)
Au(1)-Se(5)	2.465(3)	Yb(1)-N(2)	2.45(2)

Au(1)-Se(1)	2.486(3)	Yb(1)-N(2)#2	2.45(2)
Au(1)-Se(1)#1	2.486(3)	Yb(1)-N(4)#2	2.46(2)
S(1)-S(2)	2.132(9)	Yb(1)-N(4)	2.46(2)
S(1)-Se(5)	2.197(6)	Yb(1)-N(1)#2	2.55(2)
Se(1)-Se(2)	2.312(4)	Yb(1)-N(1)	2.55(2)
Se(2)-Se(3)	2.311(5)	Yb(2)-N(6)	2.44(2)
Au(2)-Se(6)	2.423(5)	Yb(2)-N(6)#3	2.44(2)
Au(2)-Se(6)#2	2.423(5)	Yb(2)-N(7)	2.44(2)
Au(2)-Se(4)#2	2.482(3)	Yb(2)-N(7)#3	2.44(2)
Au(2)-Se(4)	2.482(3)	Yb(2)-N(5)	2.47(3)
Se(3)-Se(4)	2.334(5)	Yb(2)-N(5)#3	2.47(3)
Se(6)-S(4)	2.224(7)	Yb(2)-N(8)	2.53(2)
S(4)-S(5)	2.180(8)	Yb(2)-N(8)#3	2.53(2)
Yb(1)-N(3)#2	2.45(2)		

Table A.126: Selected bond angles for $[Yb(NH_3)_8](AuS_4Se_6)$. Symmetry transformations used to generate equivalent atoms: #1 -x+1, y, -z+2 #2 -x, y, -z+1 #3 -x+2, y, -z+2.

Atoms 1, 2, 3	Angle / °	Atoms 1, 2, 3	Angle / °
Se(5)#1-Au(1)-Se(5)	177.3(2)	Se(6)-Au(2)-Se(6)#2	173.8(3)
Se(5)#1-Au(1)-Se(1)	89.93(11)	Se(6)-Au(2)-Se(4)#2	89.50(13)
Se(5)-Au(1)-Se(1)	89.97(11)	Se(6)#2-Au(2)-Se(4)#2	90.28(13)
Se(5)#1-Au(1)-Se(1)#1	89.97(11)	Se(6)-Au(2)-Se(4)	90.28(13)
Se(5)-Au(1)-Se(1)#1	89.93(11)	Se(6)#2-Au(2)-Se(4)	89.50(13)
Se(1)-Au(1)-Se(1)#1	175.89(19)	Se(4)#2-Au(2)-Se(4)	175.97(19)
S(2)-S(1)-Se(5)	111.0(3)	Se(2)-Se(3)-Se(4)	101.29(19)
Se(2)-Se(1)-Au(1)	106.80(13)	Se(3)-Se(4)-Au(2)	106.48(15)
S(1)-Se(5)-Au(1)	105.1(2)	S(4)-Se(6)-Au(2)	106.6(2)
Se(3)-Se(2)-Se(1)	105.56(19)	S(5)-S(4)-Se(6)	105.0(3)

A.1.26 [Ca(en)$_4$](AuTe$_5$)$_2$

Table A.127: Single crystal data and refinement for [Ca(en)$_4$](AuTe$_5$)$_2$.

Empirical formula	C$_8$ H$_{32}$ Au$_2$ Ca N$_8$ Te$_{10}$
Formula weight / *g/mol*	1950.43
Temperature / *K*	123(2)
Crystal system; Space group	Triclinic; $\overline{1}$
Lattice constants / Å	$a = 9.4108(7)$; $\alpha = 87.035(5)°$
	$b = 9.4927(7)$; $\beta = 77.389(4)°$
	$c = 19.7263(13)$; $\gamma = 77.790(3)°$
Volume / Å^3	1680.8(2)
Z; F(000); calc. density / *g/cm^3*	2; 1668; 3.854
Wavelength / Å	0.71073
Crystal size / *mm*	$0.124 \times 0.064 \times 0.010$
Theta range for data collection / °	3.041 to 27.666
Limiting indices	$-12 \leq h \leq 12$, $-12 \leq k \leq 12$, $-25 \leq l \leq 25$
Reflections collected / unique	17683 / 7038
Completeness to $\vartheta = 25.242$	92.1 %
R$_{int}$	10.71 %
Absorption coefficient / *mm^{-1}*	17.392
Refinement method	Full-matrix least-squares on F^2
Data / restrains / parameters	7038 / 0 / 248
R indices (all data) R_1 ; wR_2	0.1572; 0.2796
R indices [$I > 4\sigma(I)$] R_1 ; wR_2	0.1194; 0.2640 (for 5027 reflections)
Godness-of-fit for F^2	1.175
Largest diff. peak and hole / e^-/A^3	4.197 and -3.684

Table A.128: Fractional coordinates ($\cdot$ 10^4) and equivalent isotropic displacement parameter U_{eq} ($\text{Å}^2 \cdot 10^3$) for the independent atoms in the structure of $[Ca(en)_4](AuTe_5)_2$.

	Wyck.	*x*	*y*	*z*	U_{eq}
Au(1)	1f	5000	10000	5000	22(1)
Au(2)	1g	10000	5000	5000	21(1)
Te(1)	2i	1987(3)	7476(3)	6167(1)	26(1)
Te(2)	2i	4715(3)	7257(3)	5267(2)	27(1)
Te(3)	2i	7644(3)	9012(3)	4207(1)	26(1)
Te(4)	2i	8108(3)	6039(3)	4201(1)	26(1)
Te(5)	2i	10110(3)	7721(3)	5257(2)	27(1)
Au(3)	1c	10000	5000	0	19(1)
Au(4)	1d	5000	0	0	19(1)
Te(6)	2i	10842(4)	2852(3)	831(2)	21(1)
Te(8)	2i	7273(4)	2201(4)	1140(2)	21(1)
Te(7)	2i	7331(3)	4368(3)	160(2)	19(1)
Te(9)	2i	7671(3)	-159(3)	315(2)	20(1)
Te(10)	2i	3862(3)	2409(3)	736(2)	20(1)
Au(5)	2i	5481(11)	4933(12)	-2(5)	15(2)
Au(6)	2i	9539(11)	52(12)	4(6)	13(2)
Te(11)	2i	7910(20)	2186(18)	822(10)	8(3)
Te(12)	2i	5000(20)	2682(18)	748(9)	12(3)
Te(13)	2i	8438(17)	4758(16)	-345(8)	5(3)
Te(14)	2i	7480(20)	4860(20)	-321(11)	22(4)
Te(15)	2i	11240(20)	2825(18)	1158(10)	10(3)
Te(16)	2i	12180(30)	2690(20)	1147(11)	27(5)
Te(17)	2i	7930(20)	-658(18)	-161(9)	11(3)
Te(18)	2i	7010(20)	-590(20)	-142(11)	22(4)
Te(19)	2i	8870(30)	2050(20)	823(11)	25(4)
Te(20)	2i	5930(20)	2520(20)	721(10)	20(4)
Ca(1)	2i	3586(10)	7567(9)	2507(4)	27(2)
N(1)	2i	5880(40)	6960(40)	1470(20)	37(9)
N(2)	2i	5930(50)	6320(50)	2930(20)	47(10)

N(3)	2*i*	2590(40)	5970(40)	3506(19)	33(8)
N(4)	2*i*	3360(50)	9020(40)	3610(20)	38(9)
N(5)	2*i*	4680(40)	9930(40)	2210(20)	37(9)
N(6)	2*i*	3230(50)	5170(50)	2110(20)	48(11)
N(8)	2*i*	780(50)	8740(50)	2780(20)	43(10)
C(5)	2*i*	4770(50)	10550(50)	2870(20)	35(10)
C(6)	2*i*	2160(60)	4350(60)	2630(30)	47(12)
C(7)	2*i*	970(60)	8470(60)	1630(30)	46(12)
C(8)	2*i*	210(70)	9380(70)	2210(30)	61(16)
N(7)	2*i*	2420(50)	8300(50)	1440(20)	56(12)
C(1)	2*i*	7280(70)	6690(70)	1770(30)	60(15)
C(2)	2*i*	7020(60)	5680(60)	2390(30)	47(12)
C(3)	2*i*	2890(70)	4450(60)	3300(30)	58(15)
C(4)	2*i*	3410(60)	10620(60)	3390(30)	52(13)

Table A.129: Anisotropic displacement parameters U_{ij} / Å^2 · 10^3 for the independent atoms in the structure of [Ca(en)$_4$](AuTe$_5$)$_2$.

	U_{11}	U_{22}	U_{33}	U_{23}	U_{13}	U_{12}
Au(1)	20(1)	17(1)	29(1)	2(1)	-7(1)	-5(1)
Au(2)	18(1)	18(1)	29(1)	-1(1)	-6(1)	-5(1)
Te(1)	30(1)	23(1)	29(1)	0(1)	-6(1)	-12(1)
Te(2)	23(1)	19(1)	41(2)	3(1)	-9(1)	-7(1)
Te(3)	22(1)	23(1)	33(2)	2(1)	-7(1)	-5(1)
Te(4)	25(1)	19(1)	33(2)	-1(1)	-9(1)	-2(1)
Te(5)	24(1)	20(1)	39(2)	-3(1)	-7(1)	-6(1)
Au(3)	13(1)	19(1)	25(1)	-2(1)	-6(1)	-2(1)
Au(4)	13(1)	19(1)	25(1)	3(1)	-6(1)	-5(1)
Te(6)	11(2)	20(2)	31(2)	3(1)	-4(1)	-3(1)
Te(8)	17(2)	25(2)	25(2)	2(1)	-8(2)	-9(1)
Te(7)	11(1)	19(2)	29(2)	-1(1)	-7(1)	-6(1)
Te(9)	15(2)	18(2)	30(2)	4(1)	10(1)	-7(1)
Te(10)	14(2)	18(2)	28(2)	1(1)	-8(1)	-2(1)

Au(5)	9(5)	23(6)	12(5)	0(4)	-1(5)	-4(5)
Au(6)	12(5)	13(5)	17(5)	-1(4)	-8(5)	-5(5)
Ca(1)	31(4)	26(4)	27(4)	-1(3)	-8(3)	-10(3)

Table A.130: Selected bond lengths for [Ca(en)$_4$](AuTe$_5$)$_2$. Symmetry transformations used to generate equivalent atoms: #1 -x+1, -y+2, -z+1 #2 -x+2, -y+1, -z+1 #3 x-1, y, z #4 -x+2, -y+1, -z #5 -x+1, -y, -z #6 x+1, y, z #7 -x+1, -y+1, -z #8 -x+2, -y, -z.

Atoms 1, 2	Distance / Å	Atoms 1, 2	Distance / Å
Au(1)-Te(3)	2.643(3)	Te(11)-Te(12)	2.72(3)
Au(1)-Te(3)#1	2.643(3)	Te(12)-Te(16)#3	2.60(3)
Au(1)-Te(2)	2.687(3)	Te(13)-Te(15)#4	2.76(2)
Au(1)-Te(2)#1	2.687(3)	Te(13)-Te(16)#4	2.85(3)
Au(2)-Te(4)#2	2.637(3)	Te(14)-Te(16)#4	2.80(3)
Au(2)-Te(4)	2.637(3)	Te(14)-Te(15)#4	2.98(3)
Au(2)-Te(5)	2.685(3)	Te(15)-Te(19)	2.71(3)
Au(2)-Te(5)#2	2.685(3)	Te(15)-Te(17)#8	2.79(2)
Te(1)-Te(5)#3	2.751(4)	Te(15)-Te(18)#8	2.96(3)
Te(1)-Te(2)	2.758(4)	Te(16)-Te(18)#8	2.75(3)
Te(3)-Te(4)	2.764(4)	Te(16)-Te(17)#8	2.84(3)
Au(3)-Te(6)#4	2.648(4)	Te(19)-Te(20)	2.76(3)
Au(3)-Te(6)	2.648(4)	Ca(1)-N(6)	2.55(4)
Au(3)-Te(7)	2.653(3)	Ca(1)-N(3)	2.56(4)
Au(3)-Te(7)#4	2.653(3)	Ca(1)-N(2)	2.56(4)
Au(4)-Te(10)#5	2.667(3)	Ca(1)-N(8)	2.59(4)
Au(4)-Te(10)	2.667(3)	Ca(1)-N(4)	2.59(4)
Au(4)-Te(9)#5	2.691(3)	Ca(1)-N(7)	2.58(5)
Au(4)-Te(9)	2.691(3)	Ca(1)-N(1)	2.62(4)
Te(6)-Te(10)#6	2.750(4)	Ca(1)-N(5)	2.64(4)
Te(8)-Te(9)	2.750(5)	N(1)-C(1)	1.53(7)
Te(8)-Te(7)	2.751(5)	N(2)-C(2)	1.38(6)
Au(5)-Te(12)	2.60(2)	N(3)-C(3)	1.47(7)
Au(5)-Te(20)	2.64(2)	N(4)-C(4)	1.56(6)

Au(5)-Te(12)#7	2.65(2)	N(5)-C(5)	1.48(6)
Au(5)-Te(14)#7	2.68(2)	N(6)-C(6)	1.57(6)
Au(5)-Te(13)	2.687(19)	N(8)-C(8)	1.41(7)
Au(6)-Te(19)	2.44(2)	C(5)-C(4)	1.45(7)
Au(6)-Te(19)#8	2.62(2)	C(6)-C(3)	1.63(8)
Au(6)-Te(11)	2.64(2)	C(7)-N(7)	1.31(7)
Au(6)-Te(17)#8	2.65(2)	C(7)-C(8)	1.43(8)
Au(6)-Te(18)	2.65(2)	C(1)-C(2)	1.52(8)

Table A.131: Selected bond lengths for [Ca(en)$_4$](AuTe$_5$)$_2$. Symmetry transformations used to generate equivalent atoms: #1 -*x*+1, -*y*+2, -*z*+1 #2 -*x*+2, -*y*+1, -*z*+1 #3 *x*-1, *y*, *z* #4 -*x*+2, -*y*+1, -*z* #5 -*x*+1, -*y*, -*z* #6 *x*+1, *y*, *z* #7 -*x*+1, -*y*+1, -*z* #8 -*x*+2, -*y*, -*z*.

Atoms 1, 2, 3	Angle / °	Atoms 1, 2, 3	Angle / °
Te(3)-Au(1)-Te(3)#1	180.0	Au(6)#8-Au(6)-Te(19)	92.7(15)
Te(3)-Au(1)-Te(2)	88.41(8)	Te(17)-Au(6)-Te(19)	115.2(9)
Te(3)#1-Au(1)-Te(2)	91.59(8)	Au(6)#8-Au(6)-Te(11)	112.2(16)
Te(3)-Au(1)-Te(2)#1	91.59(8)	Te(17)-Au(6)-Te(11)	96.0(8)
Te(3)#1-Au(1)-Te(2)#1	88.41(8)	Te(19)#8-Au(6)-Te(11)	179.1(8)
Te(2)-Au(1)-Te(2)#1	180.00(11)	Au(6)#8-Au(6)-Te(18)	159.1(17)
Te(4)#2-Au(2)-Te(4)	180.0	Te(19)-Au(6)-Te(18)	106.9(8)
Te(4)#2-Au(2)-Te(5)	91.58(8)	Te(19)#8-Au(6)-Te(18)	91.8(7)
Te(4)-Au(2)-Te(5)	88.42(8)	Te(11)-Au(6)-Te(18)	87.6(7)
Te(4)#2-Au(2)-Te(5)#2	88.42(8)	Te(17)#8-Au(6)-Te(18)	179.1(8)
Te(4)-Au(2)-Te(5)#2	91.58(8)	Te(19)-Te(11)-Te(20)	174(2)
Te(5)-Au(2)-Te(5)#2	180.0	Te(20)-Te(11)-Au(6)	109.8(10)
Te(5)#3-Te(1)-Te(2)	101.52(12)	Te(19)-Te(11)-Te(12)	177(2)
Au(1)-Te(2)-Te(1)	104.46(10)	Au(6)-Te(11)-Te(12)	112.0(7)
Au(1)-Te(3)-Te(4)	107.97(11)	Te(20)-Te(12)-Au(5)	83.8(18)
Au(2)-Te(4)-Te(3)	108.42(11)	Te(16)#3-Te(12)-Au(5)	112.0(9)
Au(2)-Te(5)-Te(1)#6	105.09(11)	Te(16)#3-Te(12)-Te(11)	157.7(10)
Te(6)#4-Au(3)-Te(6)	180.0	Au(5)-Te(12)-Te(11)	86.8(7)
Te(6)#4-Au(3)-Te(7)	88.40(10)	Au(5)#7-Te(12)-Te(11)	106.2(7)
Te(6)-Au(3)-Te(7)	91.60(10)	Te(13)-Te(14)-Au(5)	163(2)

Te(6)#4-Au(3)-Te(7)#4	91.60(10)	Te(16)-Te(15)-Te(19)	151(2)
Te(6)-Au(3)-Te(7)#4	88.40(10)	Te(18)-Te(17)-Au(6)	152(2)
Te(7)-Au(3)-Te(7)#4	180.0	Te(11)-Te(19)-Au(6)	93.3(19)
Te(10)#5-Au(4)-Te(10)	180.0	Te(11)-Te(19)-Te(15)	152(2)
Te(10)#5-Au(4)-Te(9)#5	91.36(10)	Au(6)-Te(19)-Te(15)	113.9(10)
Te(10)-Au(4)-Te(9)#5	88.64(10)	Au(6)#8-Te(19)-Te(15)	95.1(8)
Te(10)#5-Au(4)-Te(9)	88.64(10)	Au(6)-Te(19)-Te(20)	91.3(8)
Te(10)-Au(4)-Te(9)	91.36(10)	Au(6)#8-Te(19)-Te(20)	110.1(9)
Te(9)#5-Au(4)-Te(9)	180.0	Te(15)-Te(19)-Te(20)	153.5(10)
Au(3)-Te(6)-Te(10)#6	109.87(13)	Te(12)-Te(20)-Te(11)	171(2)
Te(9)-Te(8)-Te(7)	100.88(15)	Te(12)-Te(20)-Au(5)	77.6(18)
Au(3)-Te(7)-Te(8)	105.29(13)	Te(11)-Te(20)-Au(5)	106.6(10)
Au(4)-Te(9)-Te(8)	104.37(13)	Te(12)-Te(20)-Te(19)	172(2)
Au(4)-Te(10)-Te(6)#3	105.15(13)	Au(5)-Te(20)-Te(19)	105.3(8)
Au(5)#7-Au(5)-Te(14)	160.2(18)	C(1)-N(1)-Ca(1)	108(3)
Au(5)#7-Au(5)-Te(12)	83.4(15)	C(2)-N(2)-Ca(1)	111(3)
Te(14)-Au(5)-Te(12)	111.5(9)	C(3)-N(3)-Ca(1)	112(3)
Au(5)#7-Au(5)-Te(20)	102.0(16)	C(4)-N(4)-Ca(1)	108(3)
Te(14)-Au(5)-Te(20)	93.2(9)	C(5)-N(5)-Ca(1)	108(3)
Te(12)-Au(5)-Te(20)	18.6(5)	C(6)-N(6)-Ca(1)	117(3)
Au(5)#7-Au(5)-Te(13)	165.7(16)	C(8)-N(8)-Ca(1)	115(3)
Te(12)-Au(5)-Te(13)	107.6(6)	C(4)-C(5)-N(5)	112(4)
Te(20)-Au(5)-Te(13)	89.1(6)	N(6)-C(6)-C(3)	96(4)
Te(12)#7-Au(5)-Te(13)	91.5(6)	N(7)-C(7)-C(8)	118(5)
Te(14)#7-Au(5)-Te(13)	179.0(8)	N(7)-C(7)-Ca(1)	48(3)
Au(5)#7-Au(5)-Te(20)#7	61.0(14)	C(8)-C(7)-Ca(1)	84(3)
Te(14)-Au(5)-Te(20)#7	103.5(9)	N(8)-C(8)-C(7)	106(5)
Te(12)-Au(5)-Te(20)#7	144.4(6)	C(7)-N(7)-Ca(1)	110(4)
Te(20)-Au(5)-Te(20)#7	163.0(4)	C(2)-C(1)-N(1)	107(5)
Te(14)#7-Au(5)-Te(20)#7	71.4(7)	N(2)-C(2)-C(1)	113(5)
Te(13)-Au(5)-Te(20)#7	107.7(6)	N(3)-C(3)-C(6)	109(4)
Au(6)#8-Au(6)-Te(17)	150.6(18)	C(5)-C(4)-N(4)	106(4)

A.1.27 [Yb(NH₃)₈](AuSe₄)₃

Table A.132: Single crystal data and refinement for [Yb(NH$_3$)$_8$](AuSe$_4$)$_3$.

Empirical formula	Au$_3$ H$_{24}$ N$_8$ Se$_{12}$ Yb
Formula weight / *g/mol*	1847.73
Temperature / *K*	123
Crystal system; Space group	Trigonal; R$\overline{3}$
Lattice constants / *Å*	a = 15.9319(4)
	c = 8.7617(2)
Volume / *Å³*	1925.99(11)
Z; F(000); calc. density / *g/cm³*	3; 2385; 4.779
Wavelength / *Å*	0.71073
Crystal size / *mm*	$0.068 \times 0.046 \times 0.038$
Theta range for data collection / °	3.759 to 27.514
Limiting indices	$-20 \leq h \leq 20$; $-20 \leq k \leq 20$; $-11 \leq l \leq 11$
Reflections collected / unique	11992 / 989
Completeness to ϑ = 25.242	99.7 %
R$_{int}$	7.44 %
Absorption coefficient / *mm⁻¹*	37.709
Refinement method	Full-matrix least-squares on F^2
Data / restrains / parameters	989 / 0 / 42
R indices (all data) R_1 ; *wR*$_2$	0.0313 ; 0.0569
R indices [$I > 4\sigma(I)$] R_1 ; *wR*$_2$	0.0243 ; 0.0549 (for 846 reflections)
Godness-of-fit for F^2	1.107
Largest diff. peak and hole / e^-/A^3	1.290 and -1.716

Table A.133: Fractional coordinates ($\cdot$ 10^4) and equivalent isotropic displacement parameter U_{eq} ($\text{Å}^2 \cdot 10^3$) for the independent atoms in the structure of $[Yb(NH_3)_8](AuSe_4)_3$.

	Wyck.	*x*	*y*	*z*	U_{eq}
Au(1)	9*d*	8333	6667	1667	14(1)
Se(1)	18*f*	7944(1)	5641(1)	3968(1)	18(1)
Se(2)	18*f*	9294(1)	6056(1)	5523(1)	17(1)
Yb(1)	3*b*	6667	3333	8333	16(1)
N(1)	6*c*	6667	3333	5537(11)	28(2)
N(2)	18*f*	6627(7)	4782(6)	7514(9)	60(3)

Table A.134: Anisotropic displacement parameters U_{ij} / $\text{Å}^2 \cdot 10^3$ for the independent atoms in the structure of $[Yb(NH_3)_8](AuSe_4)_3$.

	U_{11}	U_{22}	U_{33}	U_{23}	U_{13}	U_{12}
Au(1)	14(1)	17(1)	13(1)	2(1)	1(1)	9(1)
Se(1)	17(1)	21(1)	17(1)	6(1)	2(1)	10(1)
Se(2)	20(1)	17(1)	15(1)	0(1)	-2(1)	11(1)
Yb(1)	18(1)	18(1)	12(1)	0	0	9(1)
N(1)	29(4)	29(4)	25(5)	0	0	15(2)
N(2)	106(8)	46(5)	50(5)	0(4)	10(5)	55(5)

Table A.135: Selected bond lengths for $[Yb(NH_3)_8](AuSe_4)_3$. Symmetry transformations used to generate equivalent atoms: #1 $-x+^5/_3$, $-y+^4/_3$, $-z+^1/_3$ #2 $x-y+^1/_3$, $x-^1/_3$, $-z+^2/_3$ #3 $-x+y+^4/_3$, $-x+^5/_3$, $z-^1/_3$ #4 $x-y+^1/_3$, $x-^1/_3$, $-z+^5/_3$ #5 $y+^1/_3$, $-x+y+^2/_3$, $-z+^5/_3$ #6 $-x+y+1$, $-x+1$, z #7 $-y+1$, $x-y$, z #8 $-x+^4/_3$, $-y+^2/_3$, $-z+^5/_3$ #9 $-y+^5/_3$, $x-y+^1/_3$, $z+^1/_3$.

Atoms 1, 2	Distance / Å	Atoms 1, 2	Distance / Å
Au(1)-Se(1)	2.4717(6)	Yb(1)-N(2)#6	2.447(7)
Au(1)-Se(1)#1	2.4718(6)	Yb(1)-N(2)#7	2.447(8)
Au(1)-Se(2)#2	2.4900(6)	Yb(1)-N(2)	2.447(7)
Au(1)-Se(2)#3	2.4901(6)	Yb(1)-N(2)#8	2.448(7)
Se(1)-Se(2)	2.3441(9)	Yb(1)-N(1)	2.450(10)
Yb(1)-N(2)#4	2.447(7)	Yb(1)-N(1)#8	2.450(10)
Yb(1)-N(2)#5	2.447(8)		

Table A.136: Selected bond angles for [Yb(NH$_3$)$_8$](AuSe$_4$)$_3$. Symmetry transformations used to generate equivalent atoms: #1 $-x+^5/_3$, $-y+^4/_3$, $-z+^1/_3$ #2 $x-y+^1/_3$, $x-^1/_3$, $-z+^2/_3$ #3 $-x+y+^4/_3$, $-x+^5/_3$, $z-^1/_3$ #4 $x-y+^1/_3$, $x-^1/_3$, $-z+^5/_3$ #5 $y+^1/_3$, $-x+y+^2/_3$, $-z+^5/_3$ #6 $-x+y+1$, $-x+1$, z #7 $-y+1$, $x-y$, z #8 $-x+^4/_3$, $-y+^2/_3$, $-z+^5/_3$ #9 $-y+^5/_3$, $x-y+^1/_3$, $z+^1/_3$.

Atoms 1, 2, 3	Angle / °	Atoms 1, 2, 3	Angle / °
Se(1)-Au(1)-Se(1)#1	180.0	N(2)#4-Yb(1)-N(2)#8	111.77(18)
Se(1)-Au(1)-Se(2)#2	89.87(2)	N(2)#5-Yb(1)-N(2)#8	111.77(17)
Se(1)#1-Au(1)-Se(2)#2	90.13(2)	N(2)#6-Yb(1)-N(2)#8	68.23(17)
Se(1)-Au(1)-Se(2)#3	90.13(2)	N(2)#7-Yb(1)-N(2)#8	68.23(17)
Se(1)#1-Au(1)-Se(2)#3	89.87(2)	N(2)-Yb(1)-N(2)#8	180.0
Se(2)#2-Au(1)-Se(2)#3	180.0	N(2)#4-Yb(1)-N(1)	107.06(19)
Se(2)-Se(1)-Au(1)	113.31(3)	N(2)#5-Yb(1)-N(1)	107.06(19)
Se(1)-Se(2)-Au(1)#9	111.30(3)	N(2)#6-Yb(1)-N(1)	72.94(19)
N(2)#4-Yb(1)-N(2)#5	111.77(17)	N(2)#7-Yb(1)-N(1)	72.94(19)
N(2)#4-Yb(1)-N(2)#6	180.0(4)	N(2)-Yb(1)-N(1)	72.94(19)
N(2)#5-Yb(1)-N(2)#6	68.23(17)	N(2)#8-Yb(1)-N(1)	107.06(19)
N(2)#4-Yb(1)-N(2)#7	68.23(18)	N(2)#4-Yb(1)-N(1)#8	72.94(19)
N(2)#5-Yb(1)-N(2)#7	180.0	N(2)#5-Yb(1)-N(1)#8	72.94(19)
N(2)#6-Yb(1)-N(2)#7	111.77(17)	N(2)#6-Yb(1)-N(1)#8	107.06(19)
N(2)#4-Yb(1)-N(2)	68.23(17)	N(2)#7-Yb(1)-N(1)#8	107.06(19)
N(2)#5-Yb(1)-N(2)	68.23(17)	N(2)-Yb(1)-N(1)#8	107.06(19)
N(2)#6-Yb(1)-N(2)	111.77(18)	N(2)#8-Yb(1)-N(1)#8	72.94(19)
N(2)#7-Yb(1)-N(2)	111.77(17)	N(1)-Yb(1)-N(1)#8	180.0

A.2 Used computer programs

Software	Function	Programmer	Year
Diamond 4	Visualization of crystal structures	Crystal Impact	2016
Find It	Data base for inorganic crystal structures	Fachinformationszentrum Karlsruhe	2016
Microsoft Office	Text editing	Microsoft	2016
WinGX 2014.1	Program shell for programs used for crystal structure analysis	L.J. Farrugia	2014
Shelx	Solution and refinement of crystal structures	G.M. Sheldrick	1998
ChemDraw	Chemical formula editing	PerkinElmer Informatics	2017
Platon	Supporting program for crystal structure solution and refinement	A.L. Spek	2014
Paint	Graphic editing	Microsoft	2008
ConQuest	Data base for organic crystal structures	Cambridge Crystallographic Data Center	2021

A.3 EDX spectra

[Eu(en)₄]Te₆
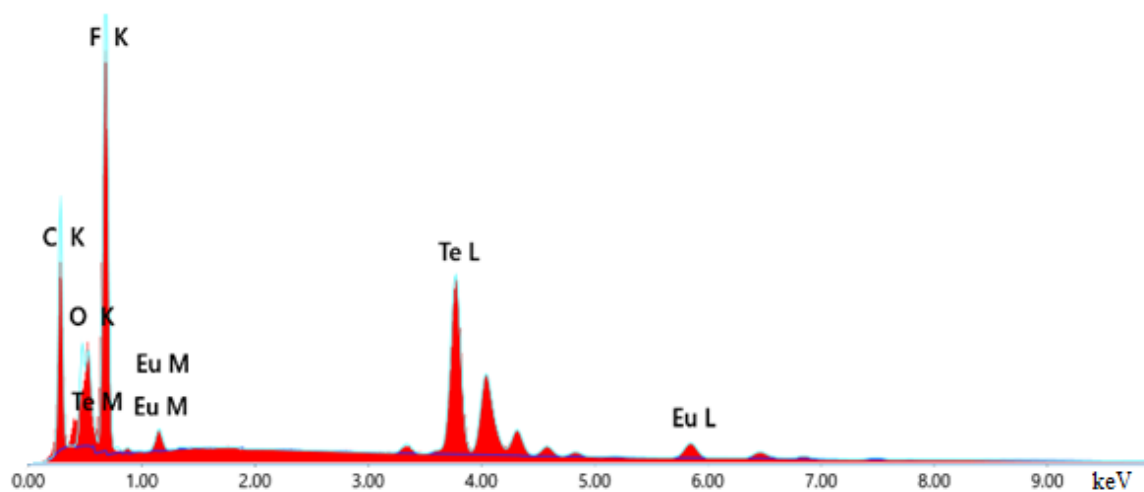
Figure A.1: EDX spectrum (Spot 1) of a crystal of the compound [Eu(en)₄]Te₆.
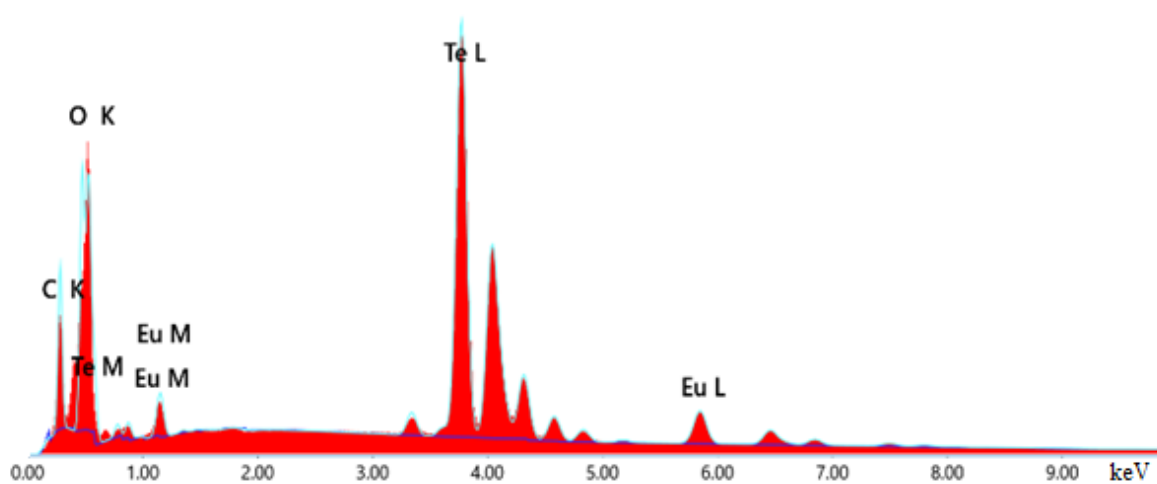
Figure A.2: EDX spectrum (Spot 2) of a crystal of the compound [Eu(en)₄]Te₆.
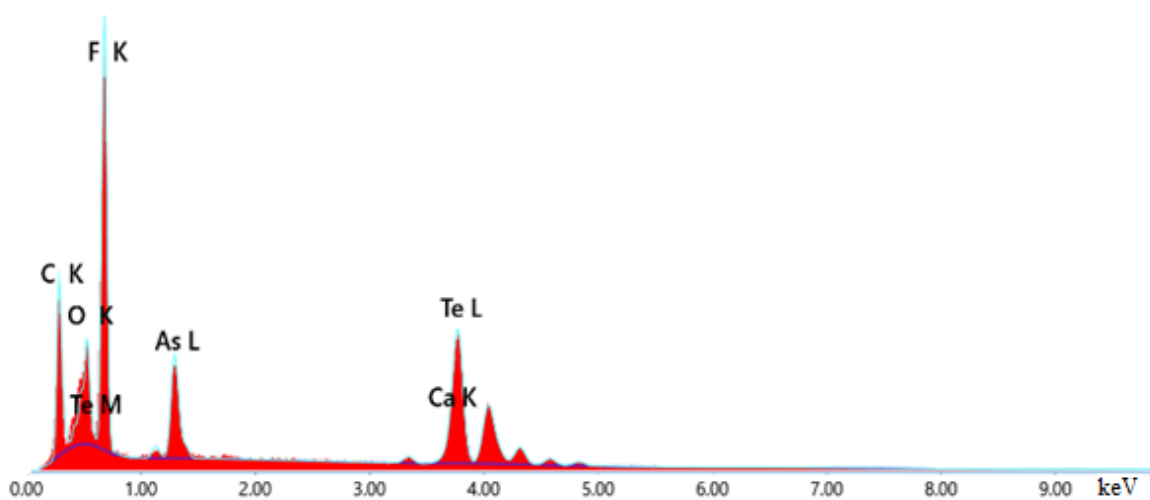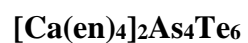
[Ca(en)₄]₂As₄Te₆

Figure A.3: EDX spectrum of a crystal of the compound [Ca(en)$_4$]$_2$As$_4$Te$_6$.
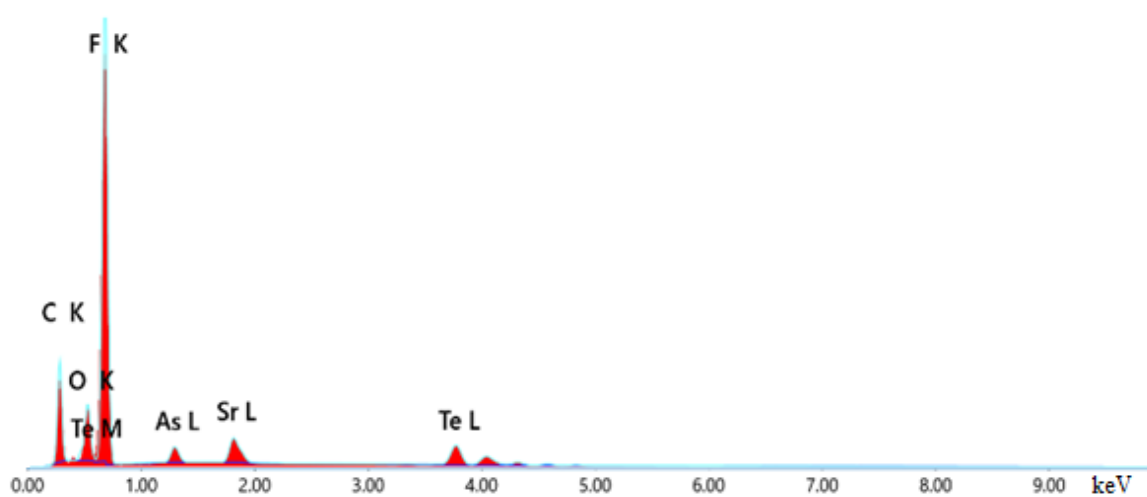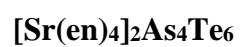
[Sr(en)₄]₂As₄Te₆

Figure A.4: EDX spectrum of a crystal of the compound [Sr(en)$_4$]$_2$As$_4$Te$_6$.
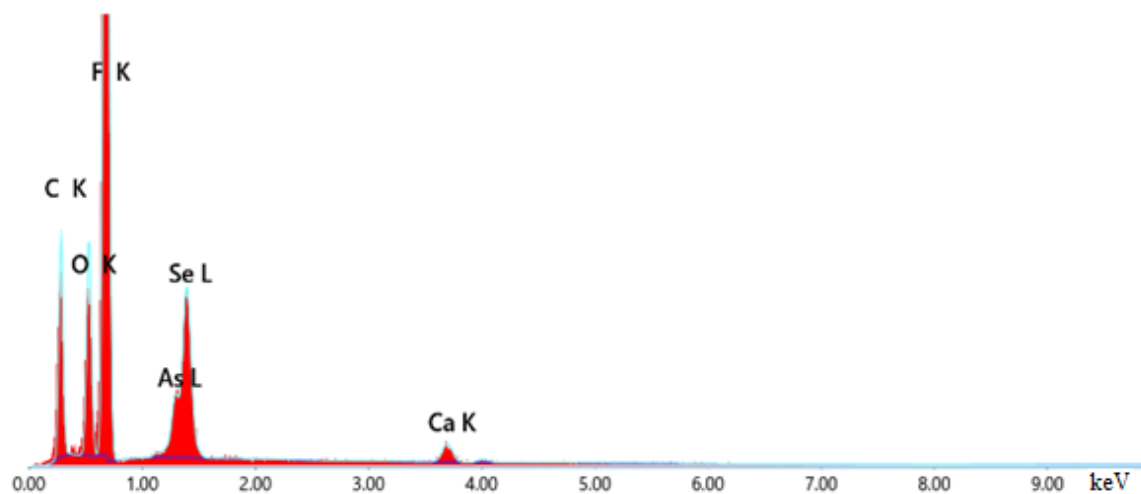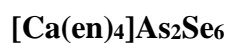
[Ca(en)₄]As₂Se₆

Figure A.5: EDX spectrum of a crystal of the compound [Ca(en)₄]As₂Se₆.
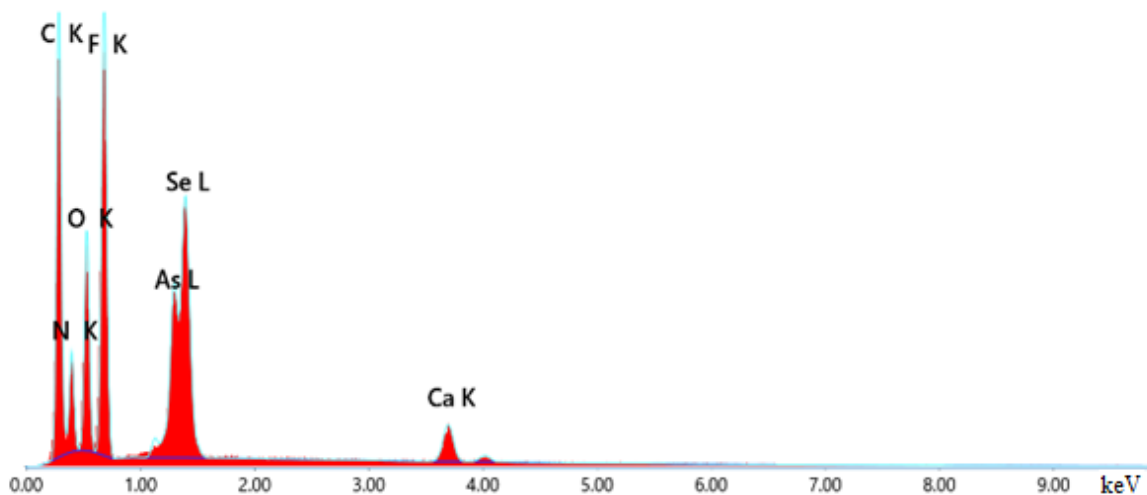
[Ca(en)₃(H₂O)₂]As₂Se₄

Figure A.6: EDX spectrum of a crystal of the compound [Ca(en)₃(H₂O)₂]As₂Se₄.
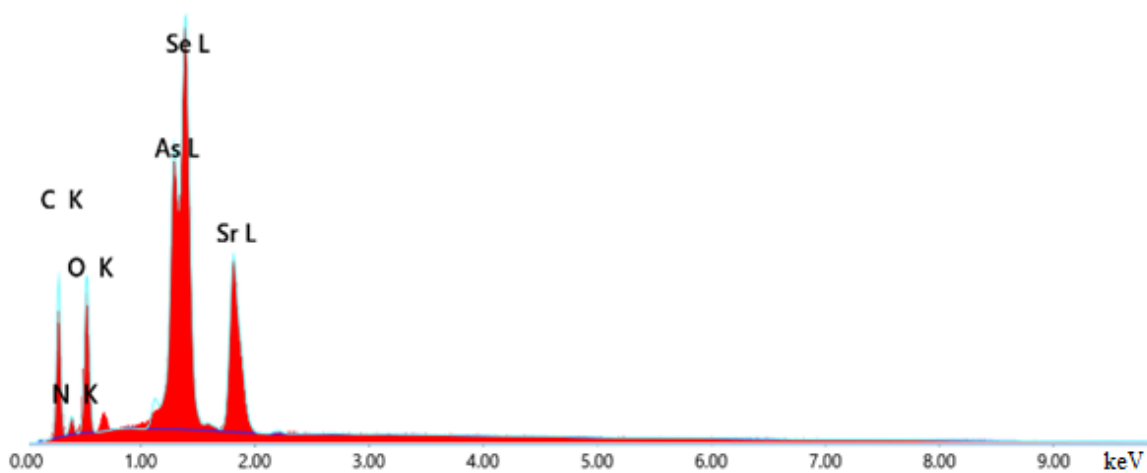
[Sr(en)₃(H₂O)₂]As₂Se₄

Figure A.7: EDX spectrum of a crystal of the compound [Sr(en)$_3$(H$_2$O)$_2$]As$_2$Se$_4$.
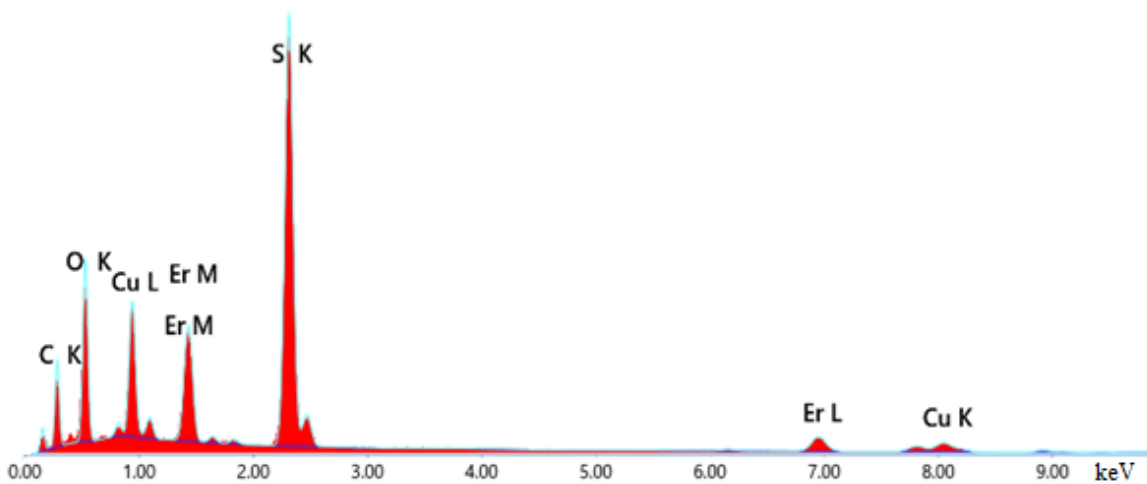
[Er(NH₃)₈][Cu(S₄)₂]·NH₃

Figure A.8: EDX spectrum of a crystal of the compound [Er(NH$_3$)$_8$][Cu(S$_4$)$_2$]·NH$_3$.

[Eu(NH₃)₉][Ag(Se₄)₂]·2NH₃
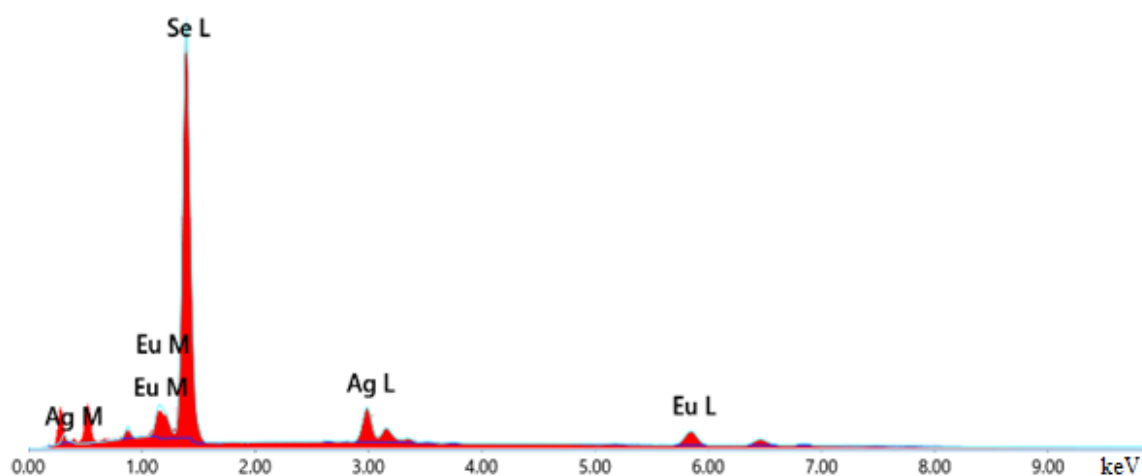
$[Eu(NH_3)_9][Ag(Se_4)_2]\cdot 2NH_3$

Figure A.9: EDX spectrum of a crystal of the compound $[Eu(NH_3)_9][Ag(Se_4)_2]\cdot 2NH_3$.
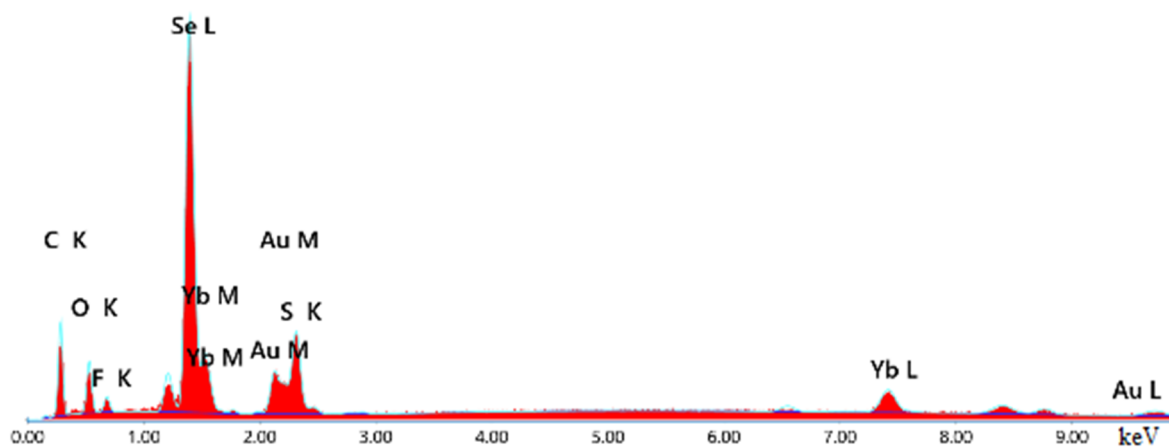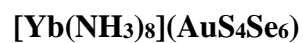
[Yb(NH₃)₈](AuS₄Se₆)

$[Yb(NH_3)_8](AuS_4Se_6)$

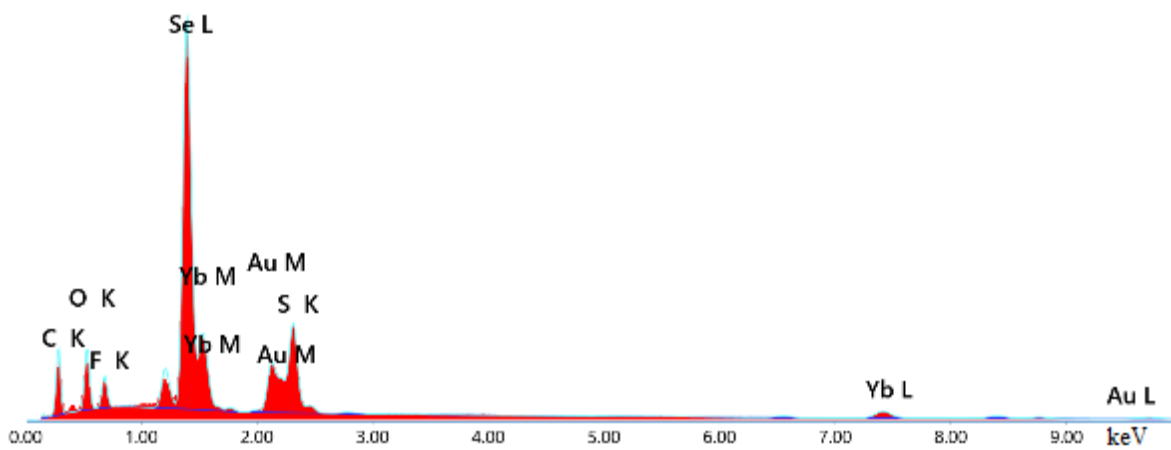**Figure A.10**: EDX spectrum (Spot 1) of a crystal of the compound $[Yb(NH_3)_8](AuS_4Se_6)$.
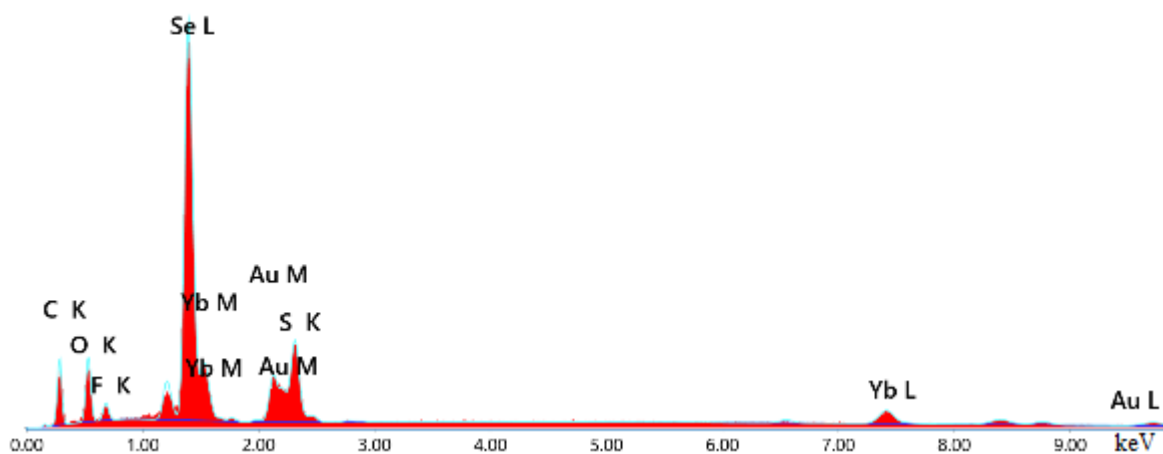
Figure A.11: EDX spectrum (Spot 2) of a crystal of the compound $[Yb(NH_3)_8](AuS_4Se_6)$.
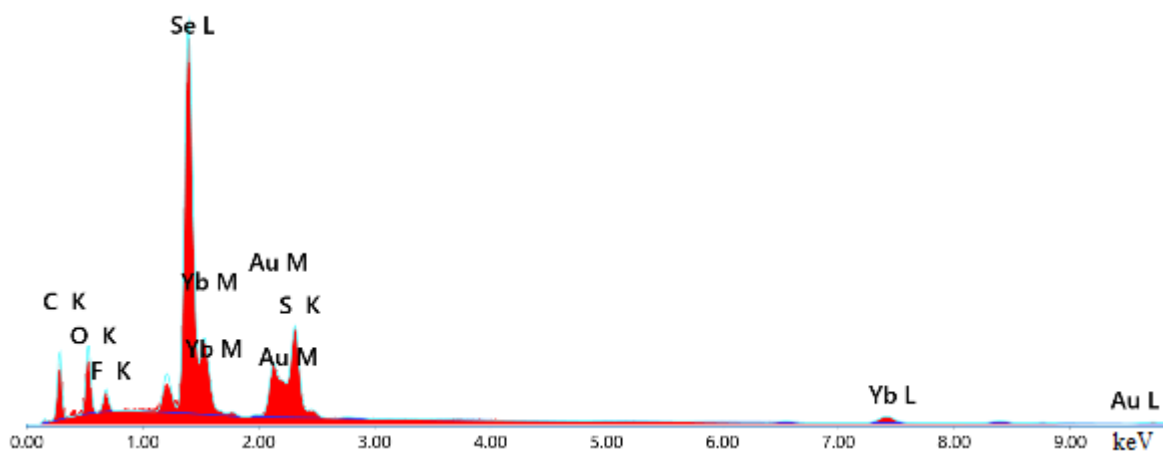
Figure A.12: EDX spectrum (Spot 3) of a crystal of the compound $[Yb(NH_3)_8](AuS_4Se_6)$.

Figure A.13: EDX spectrum (Spot 4) of a crystal of the compound [Yb(NH$_3$)$_8$](AuS$_4$Se$_6$).
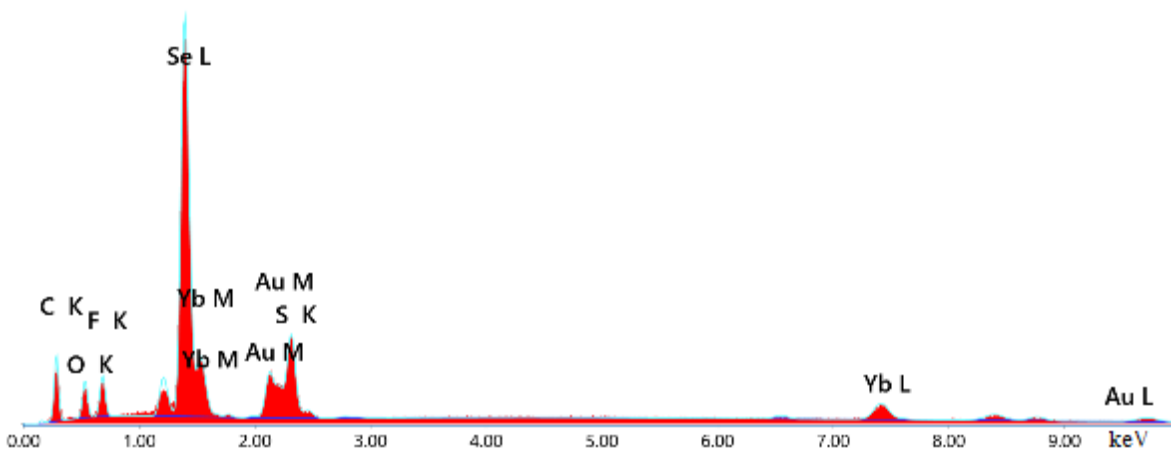
Figure A.14: EDX spectrum (Spot 5) of a crystal of the compound [Yb(NH$_3$)$_8$](AuS$_4$Se$_6$).

A.4 Used chemicals

| Chemical	Producer	Treatment before use
Europium	smart-elements GmbH	No further treatment
Samarium	Stock of the working group	No further treatment
Erbium	Stock of the working group	No further treatment
Ytterbium	Stock of the working group	No further treatment
Calcium	Stock of the working group	No further treatment
Strontium	Stock of the working group	No further treatment
Barium	Stock of the working group	Mechanic removal of the oxide layer
Sulfur	Riedel de Haën	No further treatment
Selenium	Merck KGaA	Sublimation
Tellurium	Merck KGaA	Sublimation
Arsenic	Stock of the working group	No further treatment
Sodium	Merck KGaA	Mechanic removal of the oxide layer
Ammonia	Air Liquide	Dried with sodium
Ethylene diamine	Stock of the working group	Distilled over CaH_2
Copper	Stock of the working group	No further treatment
Silver	Sigma-Aldrich	No further treatment
Gold	Gold containing scraps of the working group	Recylcing procedure explained in chapter 2.1

A.5 X-ray powder diffraction pattern
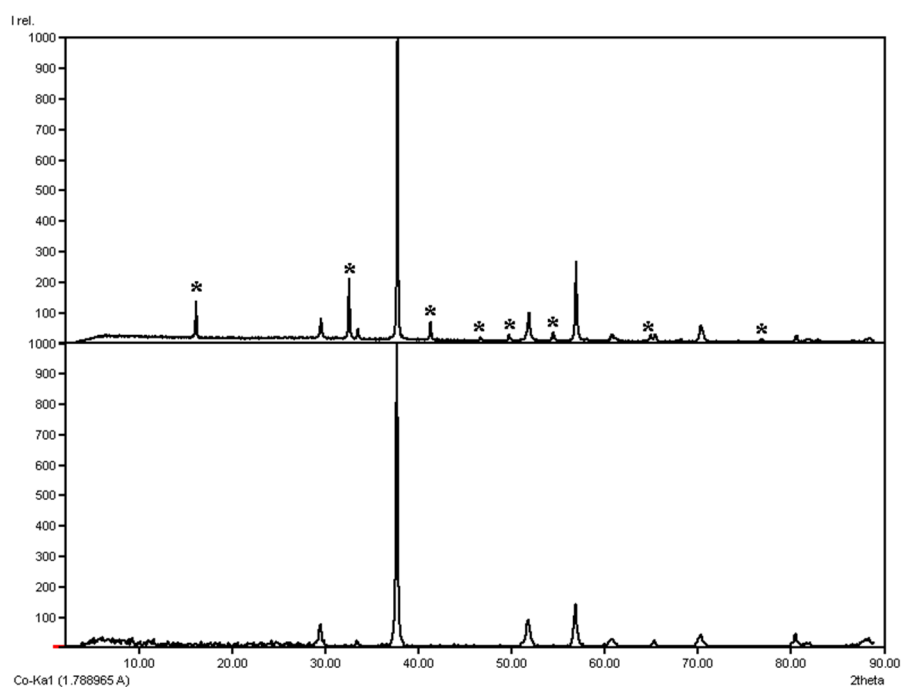
Figure A.15: X-ray powder diffraction pattern of the used arsenic before (top) and after the purification with ammonia solution. The marked reflections originate from As_2O_3.
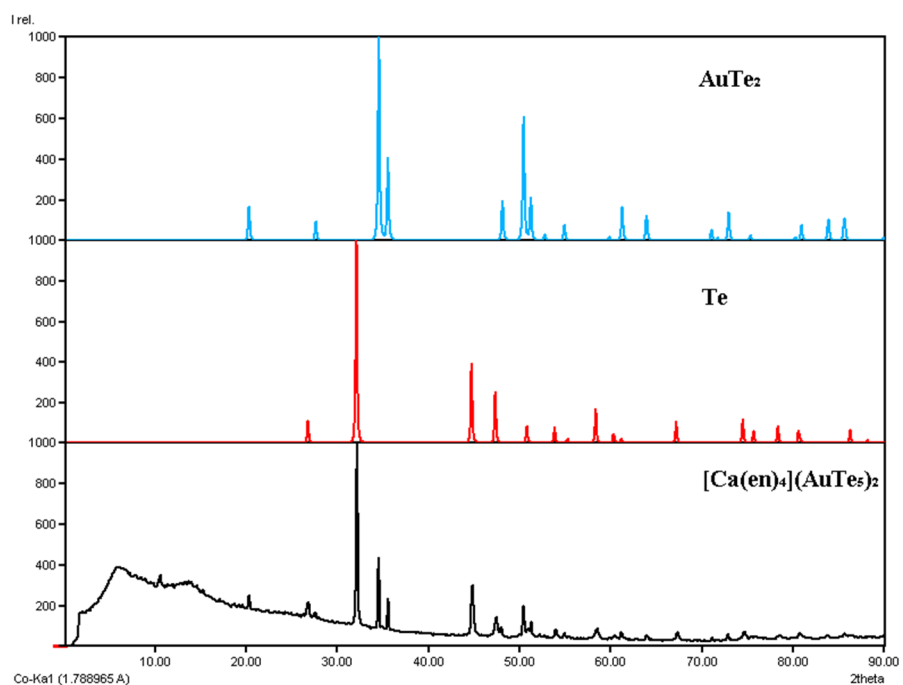

Figure A. 16: X-ray diffraction pattern of crystals with the composition $[Ca(en)_4](AuTe_5)_2$ after they were washed with ethanol and dried.

Bibliography

[1] T. Nilges, S. Lange, M. Bawohl, J. M. Deckwart, M. Janssen, H.-D. Wiemhöfer, R. Decourt, B. Chevalier, J. Vannahme, H. Eckert et al., *Nat. Mater.* **2009**, *8*, 101.

[2] Q. Zhang, C. D. Malliakas, M. G. Kanatzidis, *Inorg. Chem.* **2009**, *48*, 10910.

[3] N. Gobeltz, B. Ledé, K. Raulin, A. Demortier, J.-P. Lelieur, *Microporous Mesoporous Mat.* **2011**, *141*, 214.

[4] A. Joannis, *Ann. Chim. Phys.* **1906**, 75.

[5] E. Zintl, J. Goubean, W. Dullenkopf, *Z. Phys. Chem.* **1931**, *154A*, 1.

[6] E. Zintl, H. Kaiser, *Z. Anorg. Allg. Chem.* **1933**, *211*, 113.

[7] F. Laves in *Die Naturwissenschaften* (Ed.: F. Süffert), Springer Berlin Heidelberg, Berlin, Heidelberg, **1941**, pp. 244–256.

[8] W. Klemm, E. Busmann, *Z. Anorg. Allg. Chem.* **1963**, *319*, 297.

[9] H. Schäfer, B. Eisenmann, W. Müller, *Angew. Chem.* **1973**, *85*, 742.

[10] K.-H. Lii, R. C. Haushalter, *J. Solid State Chem.* **1987**, *67*, 374.

[11] B. Eisenmann, A. Hofmann, *Z. Kristallogr. - Cryst. Mater.* **1991**, *197*, 149.

[12] D. Kummer, L. Diehl, *Angew. Chem.* **1970**, *82*, 881.

[13] T. Kottke, D. Stalke, *J. Appl. Crystallogr.* **1993**, *26*, 615.

[14] N. Korber, A. Fleischmann, *J. Chem. Soc., Dalton Trans.* **2001**, 383.

[15] L. Diehl, K. Khodadadeh, D. Kummer, J. Strähle, *Chem. Ber.* **1976**, *109*, 3404.

[16] R. Hauptmann, T. F. Fässler, *Z. Anorg. Allg. Chem.* **2002**, *628*, 1500.

[17] C. Suchentrunk, N. Korber, *New J. Chem.* **2006**, *30*, 1737.

[18] G. Dhanaraj, K. Byrappa, V. Prasad, M. Dudley (Eds.) *Springer Handbooks*, Springer Berlin Heidelberg, Berlin, Heidelberg, **2010**.

[19] A. Rabenau, *Angew. Chem.* **1985**, *97*, 1017.

[20] G. Demazeau, *J. Mater. Sci.* **2008**, *43*, 2104.

[21] A. R. von Hippel (Ed.) *Artech House microwave library*, Artech House, Boston, London, **1995**.

[22] H. W. Xiang, *J. Phys. Chem. Ref. Data* **2004**, *33*, 1005.

[23]   R. Juza, H. Jacobs, *Angew. Chem. Int. Ed. Engl.* **1966**, *5*, 247.

[24]   D. Ehrentraut, *Technology of Gallium Nitride Crystal Growth*, Springer Berlin / Heidelberg, Berlin, Heidelberg, **2010**.

[25]   L. Glasser, *J. Chem. Educ.* **2009**, *86*, 1457.

[26]   P. Linstrom, *NIST Chemistry WebBook, NIST Standard Reference Database 69*, National Institute of Standards and Technology, **1997**.

[27]   STOE & Cie GmbH, *WinXPOW v1.05. Program for Controlling the Powder Diffractometer*, Darmstadt, **1999**.

[28]   Crystal Impact, *Match! Program for Phase Identifiction from Powder Diffractograms*, **2016**.

[29]   B. Nonius, *Collect. Data collection software*, Netherlands, **1999**.

[30]   A. J. M. Duisenberg, R. W. W. Hooft, A. M. M. Schreurs, J. Kroon, *J Appl Crystallogr* **2000**, *33*, 893.

[31]   Z. Otwinowski, W. Minor, *Meth. Enzymol.* **1997**, *276*, 307.

[32]   G. M. Sheldrick, *Acta Crystallogr. Sect. A* **2015**, *71*, 3.

[33]   A. L. Spek, *J. Appl. Crystallogr.* **2003**, *36*, 7.

[34]   L. J. Farrugia, *J. Appl. Crystallogr.* **2012**, *45*, 849.

[35]   G. Bergerhoff, M. Berndt, K. Brandenburg, *J. Res. Natl. Inst. Stand. Technol.* **1996**, *101*, 221.

[36]   M. Llunel, D. Casanova, J. Cirera, P. Alemany, S. Alvarez, *SHAPE. Program for the Stereochemical Analysis*, **2013**.

[37]   M. Pinsky, D. Avnir, *Inorg. Chem.* **1998**, *37*, 5575.

[38]   D. Casanova, M. Llunell, P. Alemany, S. Alvarez, *Chemistry* **2005**, *11*, 1479.

[39]   A. Ruiz-Martínez, D. Casanova, S. Alvarez, *J. Chem. Soc. Dalton Trans.* **2008**, 2583.

[40]   K. Fischer, *Angew. Chem.* **1935**, *48*, 394.

[41]   B. E. Warren, J. T. Burwell, *J. Chem. Phys.* **1935**, *3*, 6.

[42]   F. L. Boschke (Ed.) *Top. Curr. Chem.*, *Vol. 102*, **1982**.

[43]   A. J. Bradley, *Philos. Mag.* **1924**, *48*, 477.

[44]   P. Böttcher, J. Getzschmann, R. Keller, *Z. Anorg. Allg. Chem.* **1993**, *619*, 476.

[45]   M. G. Kanatzidis, N. C. Baenziger, D. Coucouvanis, *Inorg. Chem.* **1983**, *22*, 290.

[46]   V. Müller, A. Ahle, G. Frenzen, B. Neumüller, K. Dehnicke, D. Fenske, *Z. Anorg. Allg. Chem.* **1993**, *619*, 1247.

[47]   F. Dornhaus, M. Bolte, M. Wagner, H.-W. Lerner, *Z. Anorg. Allg. Chem.* **2007**, *633*, 425.

[48]   V. Müller, C. Grebe, U. Müller, K. Dehnicke, *Z. Anorg. Allg. Chem.* **1993**, *619*, 416.

[49]   W. S. Sheldrick, M. Wachhold, *Chem. Commun.* **1996**, 607.

[50]   A. Assoud, J. Xu, H. Kleinke, *Inorg. Chem.* **2007**, *46*, 9906.

[51]   R. C. L. M. Slater, *Acta Crystallogr.* **1959**, *12*, 187.

[52]   L. S. Bartell, M. J. Rothman, C. S. Ewig, J. R. van Wazer, *J. Chem. Phys.* **1980**, *73*, 367.

[53]   G. C. Pimentel, *J. Chem. Phys.* **1951**, *19*, 446.

[54]   R. E. Rundle, *J. Am. Chem. Soc.* **1947**, *69*, 1327.

[55]   R. E. Rundle, *J. Am. Chem. Soc.* **1949**, *17*, 671.

[56]   A. Assoud, S. Derakhshan, N. Soheilnia, H. Kleinke, *Chem. Mater.* **2004**, *16*, 4193.

[57]   D. M. Smith, L. C. Roof, M. A. Ansari, J. M. McConnachie, J. C. Bollinger, M. A. Pell, R. J. Salm, J. A. Ibers, *Inorg. Chem.* **1996**, *35*, 4999.

[58]   O. Kysliak, M. Marcus, T. Bredow, J. Beck, *Inorg. Chem.* **2013**, *52*, 8327.

[59]   Y. Lu, J. A. Ibers, *Inorg. Chem.* **1991**, *30*, 3317.

[60]   S. A. Sunshine, J. A. Ibers, *Acta Crystallogr. Sect. C* **1987**, *43*, 1019.

[61]   M. Julien-Pouzol, S. Jaulmes, F. Alapini, *Acta Crystallogr. Sect. B* **1977**, *33*, 2270.

[62]   K. Anderko, K. Schubert, *Int. J. Mater. Res.* **1954**, *54*, 371.

[63]   K. Stöwe, *J. Solid State Chem.* **2000**, *149*, 123.

[64]   I. Schewe-Miller, P. Böttcher, *J. Alloys Compd.* **1992**, *183*, 98.

[65]   R. E. Peierls, *Quantum theory of solids*, Clarendon Press, Oxford, **2001**.

[66]   I. Schewe, P. Böttcher, *Z. Naturforsch. B* **1990**, *45*, 417.

[67]   T. Doert, R. Cardoso-Gil, P. Böttcher, *Z. Anorg. Allg. Chem.* **1999**, *625*, 2160.

[68]   D. Y. Valentine, O. B. Cavin, H. L. Yakel, *Acta Crystallogr. Sect. B* **1977**, *33*, 1389.

[69]   H. Böhm, H.-G. v. Schnering, *Z. Kristallogr. - Cryst. Mater.* **1985**, *171*, 41.

[70]   P. Böttcher, U. Kretschmann, *Z. Anorg. Allg. Chem.* **1985**, *523*, 145.

[71]   A. E. C. Palmqvist, B. B. Iversen, E. Zanghellini, M. Behm, G. D. Stucky, *Angew. Chem. Int. Ed. Engl.* **2004**, *43*, 700.

[72]   S. S. Rudel, T. Graubner, A. J. Karttunen, F. Kraus, *Z. Anorg. Allg. Chem.* **2020**, *646*, 1396.

[73]   D. M. Young, G. L. Schimek, J. W. Kolis, *Inorg. Chem.* **1996**, *35*, 7620.

[74]   N. Wiberg, *Inorganic Chemistry*, De Gruyter Inc, Berlin/Boston, **2008**.

[75]   D. S. Thompson, E. E. Hazen, J. S. Waugh, *J. Phys. Chem.* **1966**, *44*, 2954.

[76]   D. S. Thompson, M. J. Stone, J. S. Waugh, *J. Phys. Chem.* **1966**, *70*, 934.

[77]   P. Dubois, J. P. Lelieur, G. Lepoutre, *Inorg. Chem.* **1989**, *28*, 195.

[78]   T. Chivers, C. Lau, *Inorg. Chem.* **1982**, *21*, 453.

[79]   H. Föppl, E. Busmann, F.-K. Frorath, *Z. Anorg. Allg. Chem.* **1962**, *314*, 12.

[80]   J. Woo Park, J. Tae Kim, S. Man Koo, C. G. Kim, Y. S. Kim, *Polyhedron* **2000**, *19*, 2547.

[81]   J. M. McConnachie, M. A. Ansari, J. C. Bollinger, R. J. Salm, J. A. Ibers, *Inorg. Chem.* **1993**, *32*, 3201.

[82]   H. A. Tasman, K. H. Boswijk, *Acta Crystallogr.* **1955**, *8*, 59.

[83]   W. S. Sheldrick, M. Wachhold, *Coord. Chem. Rev.* **1998**, *176*, 211.

[84]   A. Kromm, T. van Almsick, W. S. Sheldrick, *Z. Naturforsch. B* **2010**, *65*, 918.

[85]   W. S. Sheldrick, *J. Chem. Soc., Dalton Trans.* **2000**, 3041.

[86]   M. G. Kanatzidis, *Chem. Mater.* **1990**, *2*, 353.

[87]   J. Li, Z. Chen, R.-J. Wang, D. M. Proserpio, *Coord. Chem. Rev.* **1999**, *190-192*, 707.

[88]   W. S. Sheldrick, M. Wachhold, *Angew. Chem.* **1997**, *109*, 214.

[89]   V. Vater, W. S. Sheldrick, *Z. Naturforsch. B* **1997**, *52*, 1119.

[90]   H. Sommer, R. Hoppe, *Z. Anorg. Allg. Chem.* **1977**, *430*, 199.

[91]   H.Y.-P. Hong, J. C. Mikkelsen, G. W. Roland, *Mater. Res. Bull.* **1974**, *9*, 365.

[92]   D.-X. Jia, Q.-X. Zhao, J. Dai, Y. Zhang, Q.-Y. Zhu, *Z. Anorg. Allg. Chem.* **2006**, *632*, 349.

[93]   W. S. Sheldrick, J. Kaub, *Z. Naturforsch. B* **1985**, *40*, 19.

[94]   W. S. Sheldrick, J. Kaub, *Z. Naturforsch. B* **1985**, *40*, 1020.

[95]   T. van Almsick, W. S. Sheldrick, *Acta Crystallogr. Sect. E* **2006**, *62*, i41-i43.

[96]   B. Siewert, U. Müller, *Z. Anorg. Allg. Chem.* **1992**, *609*, 82.

[97]   W. Czado, U. Müller, *Z. Anorg. Allg. Chem.* **1998**, *624*, 239.

[98]   B. Siewert, U. Müller, *Z. Anorg. Allg. Chem.* **1991**, *595*, 211.

[99]   D. M. Smith, M. A. Pell, J. A. Ibers, *Inorg. Chem.* **1998**, *37*, 2340.

[100]   K. Wendel, U. Müller, *Z. Anorg. Allg. Chem.* **1995**, *621*, 979.

[101]   C. H. E. Belin, M. M. Charbonnel, *Inorg. Chem.* **1982**, *21*, 2504.

[102]   B. Eisenmann, R. Zagler, *Z. Naturforsch. B* **1987**, *42*, 1079.

[103]   D. M. Smith, C.-W. Park, J. A. Ibers, *Inorg. Chem.* **1996**, *35*, 6682.

[104]   E. J. Porter, G. M. Sheldrick, *J. Chem. Soc., A* **1971**, 3130.

[105]   M. Palazzi, S. Jaulmes, *Acta Crystallogr. Sect. B* **1977**, *33*, 908.

[106]   B. Eisenmann, H. Schfer, *Z. Anorg. Allg. Chem.* **1979**, *456*, 87.

[107]   W. S. Sheldrick, H.-J. Husler, *Z. Anorg. Allg. Chem.* **1988**, *561*, 139.

[108]   H.-J. Häusler, *Dissertation*, Universität Kaiserslautern, **1987**.

[109] W. S. Sheldrick, J. Kaub, *Z. Anorg. Allg. Chem.* **1986**, *535*, 179.

[110] T. van Almsick, W. S. Sheldrick, *Z. Anorg. Allg. Chem.* **2006**, *632*, 1409.

[111] A. Kromm, W. S. Sheldrick, *Z. Anorg. Allg. Chem.* **2008**, *634*, 2948.

[112] C. J. Warren, R. C. Haushalter, A. B. Bocarsly, *Chem. Mater.* **1994**, *6*, 780.

[113] W. S. Sheldrick, J. Kaub, *Z. Naturforsch. B* **1985**, *40*, 571.

[114] A. L. Allred, E. G. Rochow, *J. Inorg. Nucl. Chem.* **1958**, *5*, 264.

[115] J. Zhao, J. Liang, Y. Pan, Y. Zhang, D. Jia, *Monatsh. Chem.* **2011**, *142*, 1203.

[116] M. A. Ansari, J. A. Ibers, S. C.O'Neal, W. T. Pennington, J. W. Kolis, *Polyhedron* **1992**, *11*, 1877.

[117] W. Bronger, A. Donike, D. Schmitz, *Z. Anorg. Allg. Chem.* **1998**, *624*, 553.

[118] J. R. Sootsman, D. Y. Chung, M. G. Kanatzidis, *Angew. Chem. Int. Ed. Engl.* **2009**, *48*, 8616.

[119] L. D. Gulay, M. R. Huch, I. D. Olekseyuk, J. Stępień-Damm, A. Pietraszko, *J. Alloys Compd.* **2007**, *428*, 139.

[120] F. Q. Huang, Y. Yang, C. Flaschenriem, J. A. Ibers, *Inorg. Chem.* **2001**, *40*, 1397.

[121] C. J. Warren, D. M. Ho, A. B. Bocarsly, R. C. Haushalter, *J. Am. Chem. Soc.* **1993**, *115*, 6416.

[122] W. Bronger, H. U. Kathage, *J. Alloys Compd.* **1992**, *184*, 87.

[123] W. J. Peer, J. J. Lagowski, *J. Am. Chem. Soc.* **1978**, *100*, 6260.

[124] M. G. Kanatzidis, Y. Park, *J. Am. Chem. Soc.* **1989**, *111*, 3767.

[125] M. G. Kanatzidis, S. P. Huang, *J. Am. Chem. Soc.* **1989**, *111*, 760.

[126] R. C. Haushlater, *Angew. Chem.* **1985**, *97*, 412.

[127] S. P. Huang, M. G. Kanatzidis, *Inorg. Chem.* **1991**, *30*, 3572.

[128] K. O. Klepp, C. Weithaler, M. Sing, *J. Alloys Compd.* **1998**, *269*, 92.

[129] K. O. Klepp, W. Bronger, *J. Less-common Met.* **1987**, *128*, 65.

[130] K.-J. Range, F. Rau, M. Zabel, W. Bronger, U. Kathage, G. Auffermann, *J. Alloys Compd.* **1994**, *205*, 271.

[131] Y. Park, M. G. Kanatzidis, *Angew. Chem. Int. Ed. Engl.* **1990**, *29*, 914.

[132] E. A. Axtell, J.-H. Liao, M. G. Kanatzidis, *Inorg. Chem.* **1998**, *37*, 5583.

[133] Y. Park, M. G. Kanatzidis, *J. Alloys Compd.* **1997**, *257*, 137.

[134] T. K. Reynolds, M. A. McGuire, F. J. DiSalvo, *J. Solid State Chem.* **2004**, *177*, 2998.

[135] J. Getzschmann, E. Rönsch, P. Böttcher, *Z. Kristallogr. - N. Cryst. Struct.* **1997**, *212*.

[136] S. P. Huang, M. G. Kanatzidis, *Inorg. Chem.* **1991**, *30*, 1455.

[137] Y. Park, M. G. Kanatzidis, *Angew. Chem.* **1990**, *102*, 945.

[138] A. Rabenau, H. Rau, G. Rosenstein, *J. Less-common Met.* **1970**, *21*, 395.

[139] C. R. Landvogt, *Dissertation*, Universität Bonn, **2017**.

[140] G. Krämer, M. Jansen, *J. Solid State Chem.* **1995**, *118*, 247.

[141] C. Graf, A. Assoud, O. Mayasree, H. Kleinke, *Molecules* **2009**, *14*, 3115.

[142] E. Hashem, J. A. Platts, F. Hartl, G. Lorusso, M. Evangelisti, C. Schulzke, R. J. Baker, *Inorg. Chem.* **2014**, *53*, 8624.

[143] S. M. de Sio, R. E. Wilson, *Inorg. Chem.* **2014**, *53*, 1750.

[144] C. A. Coulson, G. R. Lester, *J. Chem. Soc.* **1956**, *0*, 3650.

[145] R. Countryman, W. S. McDonald, *J. Inorg. Nucl. Chem.* **1971**, *33*, 2213.

[146] R. B. King, *Molecules* **2020**, *25*.

Danksagung

Zuallererst möchte ich mich bei meinem Doktorvater Herrn Prof. Dr. Johannes Beck für die Betreuung während der gesamten Studienzeit, die hilfreichen Anregungen, die Forschung betreffenden Freiheiten und vor allem für das spannende Thema der Synthesen in flüssigem Ammoniak bedanken.

Mein Dank geht auch an Herrn Prof. Dr. Robert Glaum für die Übernahme des Korreferats. Des Weiteren geht mein Dank an die übrigen Mitglieder der Prüfungskommission.

Ein besonderer Dank geht an Dr. Jörg Daniels für die Messungen von Einkristallen und die Unterstützung bei der Kristallsuche unter Tieftemperaturbedingungen. Neben dem Fachlichen möchte ich mich auch für die weniger fachlichen Ratschläge bedanken.

Bei Dr. Ralf Weisbarth und Dr. Wilfried Assenmacher bedanke ich mich für die EDX-Messungen und Erstgenanntem auch für sein gutes Auge, was Vereinfachen und Ableiten von Strukturen angeht.

Der größte Dank geht an meine Eltern, ohne deren Unterstützung in jeglicher Hinsicht, ein Studium und eine anschließende Promotion nicht denkbar gewesen wären – danke für Alles!

Genauso hätte ich mein Studium nicht ohne die Herren Simon Steiner, Sebastian Spicher und Patrick Rössel durchgestanden – danke für die schöne Zeit.

Bedanken möchte ich mich auch bei (Captain) Klaus Armbruster für die Einführung an der Ammoniakanlage und die Hilfe bei Handgriffen und Techniken aller Art.

Norbert Wagner, Simone Weisbarth und Volker Bendisch möchte ich für die technische Unterstützung, Stickstoffversorgung und Bereitstellung von Chemikalien danken. Meinen Bachelor- und Masteranden Celine Schönewald, Jo Siebenaller und Annika Schmitz möchte ich für die tatkräftige synthetische Unterstützung danken.

Danke auch an den Rest des ganzen AK's, der neben fachlicher Unterstützung auch immer für gemeinsame Aktivitäten und Ausflüge zu haben war. Frederick Hermann möchte ich besonders für die gemeinsamen und sehr abwechslungsreichen Stunden an der Ammoniakanlage danken.

Da es auch ein Lebe außerhalb der Chemie gibt, möchte ich mich noch bei meinen Freunden Vera, Till, Basti und Tim für die offenen Ohren und die nötigen Ablenkungen außerhalb der Universität bedanken.

Zu guter Letzt möchte ich meiner Freundin Elisa Müller für die Unterstützung und Motivation, sowie das Ertragen meiner Person, wenn es mal nicht so lief wie es sollte, danken.